AN INVESTIGATION OF THE DYNAMIC CHARACTERISTICS OF A BOLTED-ROTOR SYSTEM

AHMAD AZLAN MAT ISA

Doctor of Philosophy

ASTON UNIVERSITY

November 2001

Aston University

An Investigation of the Dynamic Characteristics of a Bolted-Rotor System

Ahmad Azlan Mat Isa

Doctor of Philosophy
November 2001

Summary

A Jeffcott rotor consists of a disc at the centre of an axle supported at its end by bearings. A bolted Jeffcott rotor is formed by two discs, each with a shaft on one side. The discs are held together by spring loaded bolts near the outer edge. When the rotor turns there is tendency for the discs to separate on one side. This effect is more marked if the rotor is unbalanced especially at resonance speeds.

The equations of motion of the system have been developed with four degrees of freedom to include the rotor and bearing movements in the respective axes. These equations which include non-linear terms caused by the rotor opening, are subjected to external force such from rotor imbalance. A simulation model based on these equations was created using SIMULINK.

An experimental test rig was used to characterise the dynamic features. Rotor discs open at a lateral displacement of the rotor of 0.8 mm. This is the threshold value used to show the change of stiffness from high stiffness to low stiffness. The experimental results, which measure the vibration amplitude of the rotor, show the dynamic behaviour of the bolted rotor due to imbalance.

Close agreement of the experimental and theoretical results from time histories, waterfall plots, pseudo-phase plots and rotor orbit plot, indicated the validity of the model and existence of the non-linear jump phenomenon.

Keywords: Bolted rotor; Non-linearities; Rotordynamics; Whirling

Acknowledgements

The author wishes to express his deep gratitude and appreciation to Dr. J. E. T. Penny the main supervisor who provided valuable guidance and encouragement throughout the project. The author also would like to thank Dr. S.D. Garvey, co-supervisor, for his advise and useful discussions.

The author would also like to express his deepest gratitude to his colleague Mr A. Glendenning for his assistance, technicians Mr. J. Jeffs, Mr. P. Pizer, Mr. A. Evitts and Mr. J. Forden for their fruitful support throughout the course of his stay at Aston University.

The author is grateful to Universiti Teknologi MARA, Malaysia for the financial support provided for this project.

Special thanks are due to his wife (Rukiah Mohamad), son (Abdullah) and two daughters (Aisyah and Asma') for their love, patience and support during the course of this work. Without them this thesis would not be completed.

List of Contents

Chapter Seven :
EXPERIMENTAL RESULTS

Chapter Eight :
DISCUSSION

Chapter Nine :
CONCLUSIONS AND FURTHER WORK

LISTS OF FIGURES

LISTS OF TABLES

Chapter One

INTRODUCTION

1.0 INTRODUCTION

Over the last century, the use of rotating machinery has become increasingly important with the demand for powerful machinery from industry. Development and improvement in the driving mechanism such as alternating motors and generators and more recently with the gas turbine, many new and more difficult problems that require more attention are encountered. The operating speeds in machines have increased rapidly over that period. The demand for accurate predictions of the dynamic properties of machines has become more important than ever. With the ever-increasing number of studies to understand the dynamic behaviour and properties of the rotating machinery, the knowledge is branched into a new area of dynamics known as rotordynamics (Dimarogonas and Paipetis, 1983).

Researchers in the early development of rotordynamics focused on the obvious basic problem, which was to eliminate or reduce resonance. This common problem is associated with the condition of the rotating machinery and with imperfect balance. With greater sophistication in design, greater speed and higher endurance, other related problems become more significant. These include among others the effect of large deflections, fluid interaction, cracked rotors, rubbing and

interaction with static components, flexible supports and foundations. Obviously this demanded more accurate models to predict the behaviour of each associated problem before including it in the overall model. The improved reliability of rotors has been, and still is a primary concern for researchers and designers. Over the years they have examined the dynamic behaviour in order to explore all possible means to improve rotating machinery performance with the aim of achieving the highest reliability at minimum cost. To improve the reliability of the system it is important to keep the dynamic response level to a minimum. Suppressing the vibration level can only be carried out once the mechanics of the various behaviours are thoroughly understood and the means of reducing it are developed.

One of the problems encountered in fabricating mechanical components is maintaining homogeneity of the material used. Inhomogeneity can be associated with the material used or to the design employed (i.e. geometric inhomogeneity). For various reasons, such as ease of fabrication, ease of transportation and modularity of design, machines consist of smaller components that are joined together. Therefore, a joint is one form of inhomogeneity which is always present due to the nature of the component design. In rotordynamics there are numerous possibilities where system inhomogeneties appear. For example, in bearings there are interaction between the moving and stationary components, where a small clearance is always present. In gas turbines, the rotor is often made up of one or more components bolted together to form a single rotor. There are a number of studies dedicated to coupling. However, these studies focus on the misalignment problems (Xu and Marangoni, 1994). The effect of the joint itself has been neglected. Since the effect of joints can substantially influence the dynamic behaviour of

rotating machinery therefore, the purpose of this work was to investigate the dynamic behaviour of the rotor with the presence of a joint.

1.1 AIM OF RESEARCH

The purpose of this research is to study the dynamic properties of a bolted rotor. The bolted rotor here consists of a simple two piece disc bolted together forming a single rotor.

The main objectives of the study are outlined as follows:

1. To conduct a literature survey of past research of dynamic properties of bolted rotors. Since the subject has been neglected the survey tries to link to other related studies.

2. To study the behaviour of a modified Jeffcott rotor. This rotor was used to model a rotor with a disc bolted together forming a single rotor disc. A mechanism for the joint effect is proposed and modelled to determine the effect as the rotor is run through the critical speed.

3. To carry out simulation work using the model to observe the response due to unbalance with increase in the shaft rotation speed. The displacement and velocity of the various positions are determined using the parameter input based upon properties of the actual rotor.

4. To explore the rotor stability and to determine the system stability corresponding to imbalance response.

5. To carry out an experimental works to verify the theoretical findings. Broadly, it can be achieved by a specially designed test rig and instrumentation which could measure the various displacements at the indicated positions.

1.2 OUTLINE OF THE THESIS

This thesis consists of nine chapters. The present chapter serves as an introduction to bolted rotor and outlines the overall research programme.

The rest of the chapters are as follows:

Chapter 2 critically reviews available literature relevant to the subject being investigated. Although there is an enormous amount of literature available, only those which closely matched the topic are presented. The small order model used for the non-linear and the cracked rotor model are presented.

Chapter 3 deals with the joint as a common source of non-linearity in the structure. The appearance of non-linearity in structure and in relation to a bolted rotor is discussed. A proposed model for the system is also presented.

Chapter 4 describes a detailed presentation of the simulation model and algorithms chosen to solve the ordinary differential equations, i.e. to run the simulation. The limitation of the simulation is also discussed.

Chapter 5 presents the detail of the simulation results including the results due to unbalance. The results of the spectral map, orbits and

whirl are presented from the simulated results. The stability plot of the run-up is also presented.

The experimental work is outlined in Chapter 6. The development and the construction of the test rig are discussed. The instrumentation and data acquisition employed is also described. Modal characteristics of the system are presented.

The experimental results are presented in chapter 7. The run-up results are compared with the run-down results. Other related results are also presented. These include the balancing results, modal test results, and the post-processing results where the orbits, the spectral maps and the pseudo-phase plots are also computed.

Chapter 8 discusses comprehensively the experimental and simulation results.

Finally chapter 9 draws conclusions and provides recommendations for further work in this area.

Chapter Two

LITERATURE REVIEW

2.0 INTRODUCTION

A vast amount of literature has been written on the subject of rotordynamics. Among others, it deals with the problems of mathematical modelling, determination of critical speeds, imbalance response, fault diagnosis techniques and non-linear modelling. All these topics have been investigated and reported separately. The aim of all this study is to understand dynamic behaviour of rotors so that a more predictive and reliable rotating machinery system can be designed, constructed and operated safely. The requirement for increasingly reliable rotating machinery system is now more important and continues to grow constantly. This is largely due to consistent demand in the power generation and transportation industries. Along with the progress that has been made in engineering and materials science, rotating machinery is lighter and is operated at higher speed, and very often is required to operate continuously for long periods of time.

Rotordynamics analysis has proven to be important in designing and in troubleshooting of operating rotors. It can help in accomplishing the objectives of predicting the critical speeds, calculating corrective balance masses and its locations, predicting amplitudes of synchronous vibrations, predicting threshold speeds and vibration frequency or dynamic instability. Understanding of all this related knowledge is vital for the successful performance of a reliable rotor system. The phenomenon of bending vibrations and critical speeds of rotating shafts are perhaps the most common problem in design and maintenance of the rotating machinery (Rao 1983). With the ever-increasing importance of the study of rotordynamics, research starts to diversify into various areas whereby the need to specialise into certain areas of rotordynamics become more significant.

In this study the intention is to develop the link between the overall aspect of the rotordynamics design to the specific problem of bolted rotors. Except for certain special applications, most rotors are not built from a single piece, however the subject has been neglected, mainly for two reasons. Firstly, the subject is difficult to analyse and, secondly, the effect is of secondary as compared to other more demanding problems. Since the subject of study is new it is very difficult to obtain a single piece of literature specifically written on the subject. Therefore, the approach adopted is to study the literature of related problems, such as cracked rotor and other non-linear problems. Furthermore, the effect of the bolted joints will only be significant when the amplitude of vibration is relatively large. Since a simple modelling procedure is used in the analysis it is useful to

include the overall aspect of modelling before a model is produced for the study.

2.1 MODELLING OF ROTORDYNAMICS

2.1.1 Linear Model

Understanding the principles of rotordynamics is important for engineers and scientists particularly those who are involved in the transportation and power-generation industries and other fields which employ high-speed machines. With the continuously increasing speed of rotating machinery, the needs for accurate prediction and simulation has long been a necessity. These needs have become increasingly more important with the demand for higher power-to-weight ratios along with increased need for reliability and safety. Hence, the issue of reliable and accurate modelling becomes an important factor in the analysis of the rotordynamics system. The development of accurate models relate back to an understanding of the basic principle of each individual components or generalised components of the system. A relatively good model is essential to predict accurately the dynamic behaviour of the system. Past limitations in computational capabilities and difficulties in understanding complex physical systems have resulted in most rotordynamics models being developed from simplified linearised models.

Nelson (1994) discussed aspects of rotordynamics modelling ranging from small order model systems to large order complex systems in a historical review. In a more extensive review Nelson (1998), pointed

out that the first model related to rotordynamics was published by Rankine in 1869. With all the shortcomings due to its simplistic nature it was not capable of predicting correctly the dynamic characteristics of rotors. This model however, became the basis for further development in the subject. Over the following decades, additional information on the scientific principles has been discovered. The dynamic behaviour of rotors can now be predicted with greater accuracy. Among the famous contributors in this area are: Foppl, Stodola and Hozler in Germany, Jeffcott, Smith and Robertson in United Kingdom and, Newkirk and Kimball in the United States. By the mid 1930s the main mechanisms of the subject were well understood.

The rigid rotating disk is the distinguishing feature of any rotordynamic models. It originated with an analysis presented by Foppl of a turbine developed by the Swedish engineer de Laval (Dimarogonas, 1996). This simple rotor model consists of a rigid disk centrally supported on a massless shaft with rigid bearings. It is generally called the *Laval Rotor*. The same model is also frequently referred to as the *Jeffcott Rotor* in honour of work done by Jeffcott (1919) using a similar configuration. The Jeffcott model became the fundamental model of a rotor-bearing system and it is widely used as a tool for mathematical modelling of the system. It is then expanded to explain other related effects on the rotor bearing-system vibration such as damping and support flexibility.

Modelling of complex rotor systems first requires that the system be discretized to obtain a model of manageable order. To achieve a model that retains the essential characteristics of a real system, the

modelling process requires sound engineering judgement and experience. Typical discrete components include rigid disks, shaft segments, bearings, dampers, seals and couplings. The models developed were mainly linear models although some of the discrete components involved exhibit non-linear characteristics. This is due to the fact that linearization of the problem frequently gives sufficient information to understand the problem. The complexity of rotor models can range from relatively simple to highly complicated. The complexity depends on the level of model sophistication and detail required for a particular analysis. This decision should be based on the objectives of the analysis and experience within the specific system.

The developments of digital computer technology have revolutionised the analysis of rotor systems. With the increase in speed and capacity of computers, computational techniques and strategies for analysing rotor systems have been developed in parallel with the creation of the various physical and mathematical models which were introduced to study rotor system mechanisms.

Present rotating machinery designs call for higher speed, performance, and reliability within compact configurations. Increased modelling and analysis accuracy is required in turn to assist in the enhancement of efficient design, testing, manufacturing, and monitoring of these systems. As the speed and power requirement increase, the possibility of significant effects from non-linearities also increases.

2.1.2 Non-linear Model

In general the early stages of rotordynamics analysis satisfactory results were obtained using highly idealised linear models. As demand grew for more accurate simulations with more complex models the linearized model became inadequate to generate all the information required. The rotating assemblies of most rotor systems can be quite accurately be idealised as linear systems. There are a number of valid procedures for obtaining a set of governing equations for the assemblies. The strongly non-linear character of a rotordynamic system is usually contained in the interconnecting mechanisms between the rotating assemblies and the support or fixed structure. These include clearances and non-linearity of rolling and magnetic bearings, rubbing with stator, and built-up rotating assemblies, rubbing of seals and rotor blades, aerodynamic and other fluid interaction effects. Fluid film bearings and/or dampers are frequently utilised in engine designs as a mean of altering vibration levels. Many of these mechanisms are strongly non-linear and can have a significant effect on the dynamic characteristics of the system. Ongoing research will continue to improve the understanding of the behaviour of these mechanisms and this information is essential to provide an accurate simulation of the overall rotordynamics system.

Increase in the rotating speed of rotors and the demand for more accurate simulations, increases the complexity of the models. Although linear models still provide satisfactory results within the linear range, this model is no longer adequate to represent the physical system. Therefore, the need for non-linear models arises

when they are related to problems where non-linear effects cannot be excluded.

The use of non-linear terms in a rotordynamic model was only introduced in early 1950s. Yamamoto's (1954) work was amongst the earliest on such models. He studied the subharmonic oscillation caused by ball bearings using the Jeffcott rotor. Since then he also had investigated various kinds of non-linear vibrations phenomena. Some of the non-linear phenomema were discussed by Tondl (1965) in his book on rotordynamics. These studies were conducted primarily to gain a better understanding of non-linear systems.

Ishida (1994) made a comprehensive review of non-linear effects in rotordynamics systems. Various non-linearities are mentioned either as occurring in the restoring forces or as damping forces. These non-linearities are due to various causes such as clearance in bearings, squeeze film dampers, oil films in journal bearings, magnetic forces, seals, friction and stiffening effect in shaft deflection. Results from these kind of non-linear effects in rotor systems emerge as phenomena such as subharmonic oscillations, summed and differential harmonic oscillations, chaotic motions, jump phenomena and limit cycles.

As mentioned earlier, bearing clearance is one of the causes of non-linear phenomenon in rotor bearing systems. Many studies were carried out using small order models to gain greater insight into the contributions made by this non-linear term. An experimental study carried out by Bently (1974) has shown clearly the existence of subharmonic whirling motion with a system having bearing

clearance. He further interpreted his findings in terms of approximate analytical results for both linear parametric-excitation phenomena, as modelled by the Mathieu equation, and non-linear subharmonic motion modelled by Duffing's equation (Nayfeh and Mook, 1979). The use of approximate analytical method to study the occurrence of subharmonics had been attempted by many researchers. Childs (1982) used the perturbation technique and Choi and Noah (1987) used the Harmonic Balance Method (HBM) along with a Discrete Fourier Transform (DFT) procedure. The presence of higher subharmonic (up to 9th order) was shown by Ehrich (1988) using numerical integration in a high speed system with bearing clearance. Childs (1983) also observed the subsynchronous (aperiodic) whirling motion using a numerical simulation. Kim and Noah (1990) used a modified Jeffcott model to study the occurrence of a periodic whirling motion as well as subharmonics using bifurcation theory. Nevertheless, the understanding of the underlying structure of the non-synchronous whirling behaviour of rotor systems is far from being complete.

The other non-linear effect commonly studied is the rotor-stator rub situation. Rubs can make a rotor unstable because the friction force due to the interaction tends to drive the rotor into a backward whirl. This will result in the rotor will perform a backward whirl with increasing radial deflection. There are many causes of rub. Rubbing could be due to mass imbalance, misalignment of the rotor or defective bearings. Muszynska (1989) made a comprehensive review of the subject. Most moving components in intermittent contact with each other have severe non-linearity effects. primarily from discontinuous stiffness. This can occur in mechanical linkages,

impact oscillators, gears and also bearing clearance. This can result in chaotic motions (Gonsalves et. al. 1995).

Another non-linear effect commonly present in rotordynamics is non-linear restoring forces. The conditions that give rise to non-periodic motions of a Jeffcott rotor in the presence of non-linear restoring forces was examined and identified by Adiletta et. al. (1996a,b). They analysed the effect of a non-linear restoring force by designing a special rotor using flexible piano wire with the rotor positioned in the middle of the plane. By making appropriate assumptions and simplifications, the equations of motion are reduced to a pair of Duffing equations. Ishida et al. (1996) made a study of a continuous rotor in which gyroscopic moments, rotatory inertia and geometric non-linearities were considered. Transverse shear effects however were ignored in their model.

Among the recent developments in research in rotordynamics are an understanding of the behaviour of cracked rotors and the non-linearity effect acting on the rotors. These two approaches closely resemble the theoretical and practical considerations of the bolted rotors. This is due to the fact that for a bolted rotor with transverse deflection above the limit of the restoring moment it resembles the cracked rotor. The bolted joint exhibits non-linear properties however tight the bolted connection is clamped.

2.2 CRACKED ROTOR MODEL

A cracked rotor is a known phenomenon which happens mainly due to propagation of fatigue cracks caused by the rotating dynamic force

in machinery. Initiations of cracks frequently appear in rotating shaft disk units because of manufacturing flaws or defects in the material (Dimarogonas and Paipetis, 1983). Under fatigue load operating conditions, the cracks may start to propagate. Most failures in rotating machinery are caused by operating in these adverse service conditions over a period of time. For this reason, methods of early detection and localisation of the cracks have been the subject of investigation.

With the existence of cracks in the shaft, the dynamic properties change. This is due to the fact that the shaft, now with the presence of cracks, has a stiffness that is not homogenous. Apart from the problem associated with the propagating of the crack with time, which must be stopped, the shaft now becomes asymmetric. However, another interesting characteristic of a cracked shaft is that it is a symmetrical shaft when the crack closes and asymmetrical shaft when the crack opens. The dynamics of asymmetric shaft is known to exhibit destabilising effects. Many researches have discovered the existence of backward whirling between the two critical speeds (Kang et. al. (1992). Dynamics of rotors can be strongly affected by several asymmetric properties with destabilising effects such as rotors with different stiffness, damping and moments of inertia properties in two mutually perpendicular planes.

The influence of a transverse crack on a rotating shaft was first observed in the late 1960s in connection with the possibility of crack identification on a large steam turbine (Dimarogonas and Paipetis 1983). Since then, many techniques have been developed for off-line crack monitoring such as ultrasonic detection or acoustic emission

and, more importantly, on-line detection. This is more difficult to be carried out due the effect of gravity, which causes the crack to alternately open and close through a cycle. This effect is known as the crack breathing.

Wauer [1990] did a review study on the dynamic behaviour of cracked rotors. The survey summarises the cracked rotor model, including cracked static structures, and finding different detection approaches to diagnose fracture damage. Since a crack influences the stiffness of the rotor and the stiffness influences the dynamic behaviour of the system, vibration monitoring as a means of detecting crack initiation and propagation becomes an important instrument. Gasch (1993) studied the stability behaviour of a rotating shaft with crack and the force vibrations due to imbalance as well as the crack. With the assumption of weight dominance (i.e. the vibration is small such that the equation can be linearised), he showed that there is a range of instability as the depth of the crack increases.

Most of the cracked rotor models are based on rotors containing one or more transverse cracks. Generally, the assumption is made that the mass and damping values are not affected by the crack. Therefore the influence of the crack only concerns the stiffness of the rotor element. Most of the researchers derived the crack breathing based on fracture mechanics (Jun et. al. 1992, Dimarogonas et. al. 1983). In the vibrational behaviour of a cracked rotor, two predominant features are noted, namely the existence of second and higher harmonics and the increase in the amplitude of the harmonic with the increase in crack depth. Sekhar and Prabu (1994) made use of the relationship between bending stress in a crack and backward

whirl as a possible diagnostic tool for monitoring the crack growth. They show that with the increase of crack depth the critical speeds split into two critical speeds and backward whirl being noticed between these two speeds.

Among the earliest cracked rotor model was the one developed by Gasch (1976), wherein he used a step function as the representation of the changes in stiffness. The opening of crack was characterised by a decrease in stiffness, and the closed crack has the same stiffness as the undamaged rotor. The depth or the shape of the crack did not become the criteria for the stiffness of the crack when it opened and therefore the breathing of the crack was only modelled with changes between two stiffness quantities. Inspired by this work, Mayes (1979) used a similar method with a rotor stiffness value that was piecewise constant. This allowed the vibrational behaviour of an anisotropy rotor to be described by a switching anisotropy at two points for one rotation. By computing the switching points and assembling the solutions for the piecewise anisotropy rotor, the resulting vibrational behaviour was found. Later Mayes and Davies (1984) used a finite element model to find the vibrational response of a rotor with a transverse crack. They studied experimentally the effect of a transverse crack on the dynamics of a multi-rotor, multi-bearing system. They found that the dynamic behaviour of a cracked shaft was similar to the slotted shaft with additional excitation due to crack opening and closing and, with the exception of a large crack, they developed a method of reducing the section diameter required for a model.

Grabowski (1980) improved the model developed by Mayes by assumming the area above the horizontal diameter of the crack as the contact zone under weight dominant conditions. Modal analysis showed a strong dependence of the dynamic response on the crack position and a relatively weak dependence of the vibration of the cracked shaft upon the unbalance. To calculate the resulting stiffness values, the moments of area in the crack plane were used by computing numerically to include the area of the undamaged section of the rotor and the area of the closed crack. This resulting area had a different centre of gravity than the original rotor centre of gravity; however this difference was negligible.

Another model, proposed by Bachschmid (1984), was based on Grabowski's model. In this model the closed part was a function of the bending stresses in the plane. By an iterative procedure the displacements of the rotor at different locations were computed, and the function of an axis with zero axial stresses in the crack plane was derived under the assumption of a linear stress field. Afterwards the moments of inertia in the crack plane in the two main inertia axes were calculated, yielding the stiffness for this displacement configuration. The main difference from the other modelling techniques is that the stiffness behaviour of the breathing crack is determined by the dynamical displacement of the rotor. Thus this model is not limited to unbalance or weight dominant conditions.

The model by Mayes and Davies (1983) assumed round shaped crack and areas of contact. Their computational model used the minimum and maximum stiffness values of the rotor with an open crack. The

assumption made for the breathing of the crack and the changing of stiffness was by a sinusoidal function.

Dimarongonas and Papadopoulos (1983) used linear elastic crack mechanics to model stiffness characteristics of the cracked rotor. They divided the rotors segment into a packet of cracked plates, which were oriented parallel to the rotor axes. For each plate they used known stress-intensity-factors (SIF) to calculate local elasticity coefficients, which depend on the crack depth. Thus the elasticity matrix for the plates packet could be determined. Together with the elasticity coefficients of the uncracked system the elasticity coefficients of the cracked rotor element could be computed. It was used later by other researchers to identify the crack position and crack depth (Tsai and Wong, 1996).

2.3 BOLTED ROTORS

A significant proportion of all of the rotating machines in operation have rotors which are either bolted or laminated construction. Gas turbines and small steam turbines frequently comprise a set of discs clamped together by either a single central bolt or a small number of bolts on a small pitch circle diameter. The roots of the turbine blades are trapped between adjacent discs. Most electrical machines (except permanent magnet machines) have a solid forged or fabricated shaft onto which a stack of laminations is fitted. The dynamics of such rotors are potentially quite different from the dynamics of a solid rotor of similar dimensions.

As demonstrated in many studies (Nayak ,1972, Soom, 1992) the dynamic behaviour of bolted structures is significantly different from that of a solid structure. It has also been shown that the behaviour varies with the amount of deformation occurring in the structure. Dunne and Heppenstall (1991) demonstrated the variation of the natural frequency with the variation of axial load. However, their analysis was restricted to free-free modal analysis of the bolted shaft with a central bolt, which was represented by rings compressed together by a long central bolt.

The known effect of a joint in a structure is that it reduces the stiffness and it behaves in a non-linear manner. In rotating machinery it alters the transverse vibration characteristic. This characteristic is an important parameter for the correct prediction of the whirling speed.

As mentioned earlier, although there have been many papers written on simple rotors describing various phenomena, there is hardly any literature on bolted rotors. Klompas (1983) discussed the effect of anomalous rotor joints, as he names it. His model was treated similar to a coupling, whereby he studied the effect of the variable position of a cantilevered rotor attached at the extremity of a gas turbine. The mechanism was visualised and verified as a linear model or linearised model where the perturbing moments were impressed into rotor joints to simulate specific characteristics, which did not conform to an axisymmetric elastic assumption of the model. The theoretical work on transverse rotor cracks did cover some aspect of the mechanism which may be encountered in a mechanical joint.

From an experiment using a bolted disk to represent a cracked rotor, Tamura et al. (1988) observed that when the crack was large the amplitude at the resonance was relatively higher. He also observed the existence of resonance at sub-multiples of the critical speed. Although he achieved his objective of proving the unstable effect of a cracked rotor this interesting feature might also be contributed by the bolted assembly that he was using.

Rigid flange couplings are usually used to join two machine components. These couplings are arranged between the two intermediate bearings to support the rotors. If only one intermediate bearing is provided, the coupling is arranged as close as possible to it (Simon, 1992). Limited accuracy in the alignment of a coupling is a source of vibration excitation. An exact alignment of the adjoining individual rotors is not possible; small offsets of the rotor centre-lines (radial offset) and angular deviations due to out-of-squareness of the coupling flanges will always remain. When the coupling halves are forced together by bolting, rotation of the shaft will produce a rotating pair of forces caused by radial offset and a rotating pair of bending moments caused by out-of squareness, the rotation frequencies of these pairs being equal to the rotational frequency of the shaft. These rotating pairs of forces and bending moments will excite vibration in the complete structure.

2.4 STABILITY IN ROTORDYNAMICS

Stability plays an important role in the design of rotordynamic systems. Stability is the dynamic characteristic of a given system

such that the motion decays with time (stable) or grows with respect to time (unstable). Generally, an unstable system is of little practical use. Rotordynamic instability is manifested by the shaft whirl at frequencies other than the shaft speed. In rotating machinery subsynchronous frequencies are associated with instabilities. Large amplitude subsynchronous vibration does not occur frequently, but when it does it is much more destructive and more difficult to cure than the imbalance problem (Vance, 1989).

Three general aspects of the rotordynamic instabilities have been recognized (Ehrich, 1993). They are:

1. The effect of the cross-coupling stiffness coefficient which yields tangential reaction forces normal to the radial displacement and in the direction of the shaft rotation. There are many sources of the cross-coupling stiffness such as hydrodynamic bearings, seal rubs (dry friction whip), torquewhirl, impeller dynamics and propeller flutter. Gyroscopic moments are another example of cross-coupled forces although they are moments instead of force and inertia induced rather than by an external force on the rotor

2. The sensitivity of rotors to destabilising forces increases with the rotor flexibility. This means that the instability is amplified close to the resonance of the system.

3. Instability can also occur if a system has a low damping. However, this is only applicable to external damping since internal damping is actually a potential source of destabilizing forces and is to be avoided.

In rotordynamics, most motions have an inherent periodicity related to the rotor speed. This characteristic lends itself well to study using Fourier analysis, which is the most widely used approach for the vibratory analysis of rotating machinery. Although the information obtained is very useful in diagnosing rotordynamics problems, very little insight into the stability characteristics of the system is obtained (Flowers et al. 1998).

The introduction of machines operating at higher speeds has inspired the analyses of stability in rotordynamics. Among the pioneer researchers dealing with this problem were Newkirk (1924), who analysed instability problems associated with the bearing effect. He also identified instabilities due to dry friction, while Kimball (1924) gave basic results for internal damping in the shafts.

There are three existing methods of stability assessment: Liapunov-based, numerical and analytical.

Firstly, consider the use of Liapunov functions to provide conservative bounds on the values of the parameters that yields stable solutions (Jordon and Smith, 1979). The method is based on the premise that system energy does not increase near an equilibrium state and as such Liapunov's ideas can be seen as extensions to the general energy concept. One applies the method by examining the properties of Liapunov functions from knowledge of the whole system rather than the solutions. The rules for finding suitable Liapunov functions

are complex, but can be applied fairly straightforwardly to certain, relatively simple, practical problems.

Secondly, numerical methods typically solve for the state transition matrix through integration of the governing system equations. The transition matrix can be obtained by first transforming the equations of motion to state form and then integrating numerically over a period of time. Using this state transition matrix the Floquet eigenvalue is computed (Hsu 1974). The indication of system stability is when all the eigenvalues are less than unity: the system is unstable if one or more eigenvalue is greater than unity. The limiting stable case is when the eigenvalue is one. Gasch (1993) and Hu and Huang (1998) used this technique for determination of stability of cracked rotors. The advantage of this numerical approach is that an accurate prediction of stability can be obtained even when the periodic coefficients are large.

The third method available for stability determination is by analytical methods. The Harmonic Balance Method can be combined with a perturbation expansion or with boundary tracing to provide stability information (Wu et. al 1995). Other combinations such as the averaging method and perturbation methods have also been used (Hsu 1963,1965). Other usable analytical methods include Struble's asymptotic approximation method, the averaging method (including the method of harmonic balance), the Linstedt-Poincare and also the multiple scales perturbation technique. These methods, and others, are potentially capable of successfully treating parametric and non-linear problems. However, there may be certain drawbacks to particular individual applications.

2.5 CONCLUSION

In this chapter a brief overview of the existing models used in rotordynamics were discussed. It is assumed that the analysis of a bolted rotor can be based on an extension of the analysis of a cracked rotor with non-linear stiffness. Cracked rotors have the asymmetrical stiffness that is consistent and independent of the position of the unbalance. However, the stiffness of a bolted rotor depends on the position of the unbalance or the magnitude of deflection. Non-linear analysis of a rotor-dynamic system is also discussed and methods of determining the bounds of stability are outlined.

Chapter Three

THEORETICAL BACKGROUND AND MATHEMATICAL MODEL

3.0 INTRODUCTION

In this chapter, the main task is to present a model of a joint, and apply it to a bolted rotor. The theoretical background on the analysis of non-linearity is laid out. Equations of motion for a bolted rotor with four degrees of freedom are presented and a non-linear term is incorporated. From these equations the dynamic response of the system to the external excitation, imbalance force and an impulse can be determined.

3.1 THEORETICAL BACKGROUND

3.1.1 Modelling of Non-linear Structures

In many engineering applications, accurate mathematical models are required in order to predict the effects of structural modifications or to correct undesirably high levels of response. The precise derivation of a mathematical model can only be achieved firstly by choosing the right model assumptions and then selecting the right technique to solve the problem. Table 3.1 summarises briefly the different dynamic response characteristics of linear and non-linear systems. The first

step is to check the presence of any non-linear behaviour, so that linear or non-linear classification can be determined. Then the choice must be made either to describe the system by an analytical model or by a discrete model. The last step is the application of the appropriate linear or non-linear analysis.

	Linear Systems	Non-linear system
Frequency response	Continuous response with no points of instability	Discontinuous response resulting in jump phenomenon for increasing or decreasing frequencies
Frequency amplitude dependence	Resonant frequency independent of amplitude	Resonance frequency as a function of amplitude
Sub/Ultra Harmonic Response	None	Possible
Internal Resonance	None	Possible

Table 3.1: Characteristics of linear and non-linear systems (Benhafsi, 1993)

A good derivation of a non-linear model can be obtained by studying all information available about the particular non-linearity. Usually, the source of non-linearity and its classification provide a basic understanding of the non-linearity involved. The source of the non-linearity can be due to many different mechanisms. For example, the stiffness of springs exhibit non-linear characteristics (Watanabe and Sato, 1988).

Other examples of non-linearities commonly encountered are at the boundaries of a system where non-linearities can occur although the system itself is linear. A beam that is clamped at one end and has a clearance on the other is an example of such a system (Murakami and Sato, 1990).

Although there are large numbers of non-linearities generated by different mechanisms, it is possible to classify non-linearities into a global non-linear behaviour, such as material properties (Rice and Xu, 1996), and a local non-linear behaviour, such as localised non-linear springs (Watanabe and Sato, 1988). Many of the localised non-linear phenomena are due to a non-linear interaction, taking place between two connecting parts. A real mechanical structure usually consists of many components which are connected together through different joints such as bolted joints (Gaul *et al*, 1994), riveted joints, welded joints, adhesive joints or any other clamping mechanism (Sanliturk and Ewins, 1996). Although the joints are very easily identified on the structure, a mathematical model of the joint is usually difficult to obtain (Bohlen and Gaul, 1987). One way of obtaining a mathematical model of the joint is by finding the relationship between an external excitation force applied and the response (Burdekin *et al*, 1978).

The model validation of a joint is done by correlating the analytical model with dynamic test data, since most structural non-linearities cannot be predicted from geometrical information alone and therefore must be measured. Furthermore, the more information known about the non-linearities, the better will be the analytical model derived (Haslinger, 1995).

Once the structure is classified as non-linear, it becomes necessary to choose which kind of model is to be used to represent its dynamic behaviour. The dynamic behaviour of the structure can be represented by an analytical model or by a discretised model. Although analytical models can give accurate solutions, for complicated structures it is extremely difficult to find the solutions. Therefore discrete approximate models are usually used instead. Three different models can be used for discretisation of structures.They are spatial models, modal models and response models. Although any of the models can be used to represent a structure, there is usually one model that is more appropriate than the others for the representation (Jazequel et al 1990).

3.1.2 Non-linearity in Rotordynamics

The rotating assemblies of most rotor systems can be quite accurately idealised as linear systems, and there are a number of procedures to obtain the governing equation for the assemblies. The strongly non-linear components of a rotordynamic system are usually contained in mechanisms that interconnect the rotating assemblies with the support structure or with each other. Typical mechanisms include clearances (Choi and Noah, 1992) and non-linearity of rolling and magnetic bearings (Krigerman and Gottlieb 1998), rubbing in splines and built-up rotating assemblies, rubbing in seals and rotor blades, and other fluid interaction effects. Fluid film bearings and/or dampers are frequently utilised in machine design as a means of altering vibration levels. Many of these mechanisms are strongly non-linear and can significantly effect the dynamic characteristics of the system.

Significant advancements have been made to accurately define these mechanisms, both experimentally and analytically. Ehrich (1995) characterised the non-linerities frequently encountered in high speed rotating machinery into two distinct categories:

i. Non-linearity consisting of systematic hardening or softening for the increase in amplitude of motion along radial direction with a stiffness characteristic that is isotropic or axisymmetric. The unique non-linear effect for the stiffening system is the `rightward leaning' resonance peak which results in the amplitude jump phenomena and hysteresis in amplitude during acceleration and deceleration of the rotor system.

ii. Stiffening, which takes place locally at the point of contact, and the stiffness characteristic is anisotropy when the rotor is eccentrically placed within a stiffer motion-limiting stator. The vibration motion is asychronous with the rotational frequency of the unbalance, with a number of unique subcritical and supercritical pseudo-resonant peaks.

The bolted rotor system can be categorised in the first group since it comprises an isotropic shaft with a softening effect.

3.2 MODELING OF THE BOLTED ROTOR

Abstract representation of the physical system is critical to enable the successful results to be produced from the model. Full representation with the inclusion of the whole dynamic effect of the system can result in the model being too complicated. Hence, simplification will avoid the unnecessary computation for components, which are less significant. Since a modified *Jeffcott* model was used for analysis, the

rotor-bearing system was assumed to be a simply supported beam with a lumped mass rotating discs being bolted together and the shaft was represented as massless shaft. The lumped mass consists of the mass of the bolted disc and part of the shaft mass. The bearing stiffness was considered as asymmetric with small mass.

3.2.1 Model of restoring force

The restoring forces of the system consist of the restoring forces from the shaft, bearing and its support, and the joint. Therefore the stiffness coefficient is the equivalent spring constant resulting from the series connection of the shaft, bearing and bearing-support stiffness. However, the force of particular interest in this study is the restoring force acting between the two rotor disc halves. The force is dependent on the shaft deflection and is intermittent between linear and non-linear as the deflection exceeds the threshold value of the restoring force. In the force computation the following assumption are made, and their validity was explored in detail as:

- Opening of the gap is assumed above a threshold value. The threshold value depends on the clamping force on the rotor. The greater the clamping force applied the larger is the threshold deflection value. However, when the deflection exceeds the threshold value then the restoring force changes to the stiffness of the joint which is much lower than the shaft stiffness.

- The restoring force is consistent throughout the surface and is similar in all directions. This assumption was made to facilitate the analysis since the micro effect on both surfaces of the rotor are assumed to be consistent and the applied force exerted by the

clamping spring is the same in all directions. In effect the stiffness is initially isotropic.

- The transformations from shaft stiffness to joint stiffness are abrupt. After the threshold value, the stiffness of the joint become dominant since it is much smaller than the shaft stiffness. However, the shaft stiffness portion still contributes some force to the deflection.

- The effect of surface roughness is negligible. A good surface finish will minimised the effect of the stiffness.

- The bearing and support pedestal also contribute to the overall stiffness of the system. However the stiffness is anisotropy due to the support flexibility in the horizontal position.

In a very simple, preliminary model, the axial force is assumed to be proportional to the shaft deflection.

The value of the force can only be measured from the deflection of the center part of the rotor. Since the purpose of this study was to look into the effect of the joint on the behaviour of the rotor, other effects on the maximum deflection amplitude such as stator-rub was not considered.

3.2.2 Model of damping of the system

The system damping is relatively low because the shaft is made of a relatively rigid material. However, the effect of the joint on damping is significant. In this model the damping of the system is also

considered to vary with the deflection of the shaft. The value of the damping can be determined by using the logarithmic decrement method. Before the shaft opens, the damping factor is assumed negligible, however when the joint opens a damping factor is included. This is due to the fact that initially the shaft is considered to be solid. However, when the joint starts to open the damping value increases. The expected increase in the damping value is inversely proportional to the stiffness of the shaft. Since there is an intermittent open and closure of the joint, then the value of the damping also varies with this action.

3.2.3 Gyroscopic effect

The gyroscopic moment also contributes to the system equations of motion. Due to the fact that the discs are placed at the center position of the shaft the gyroscopic effect is negligible. However, when the discs open up then the effect becomes more significant and its effect needs to be included in the system equations. Since the gyroscopic moment depends on the disc spin and the disc rotation (nutation), the computation of the rotation of the disc is arrived at by multiplying it with the geometrical value of the system. The system is modelled with two degrees of freedom, therefore the displacements must be converted into force by dividing by the distance from the center to the bearing.

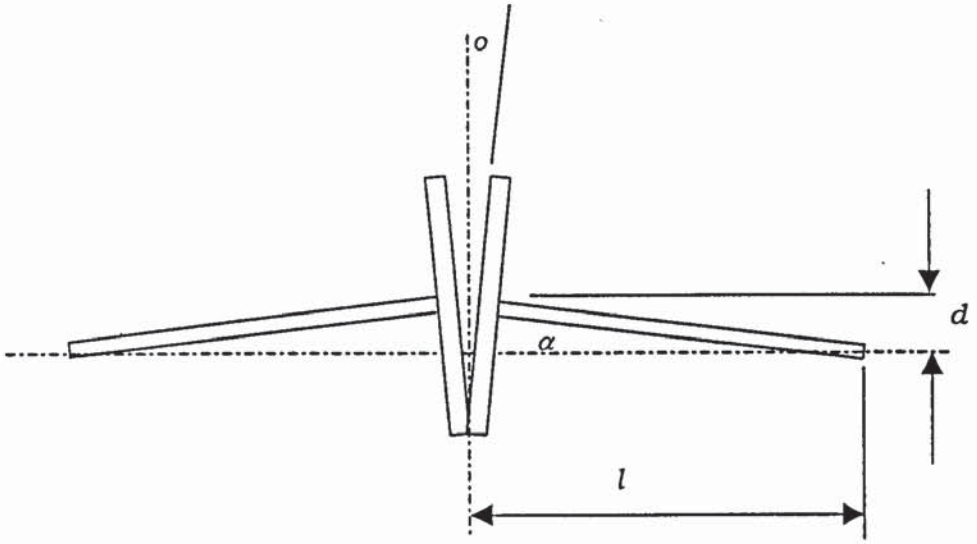

Figure 3.1: Condition when the disc is opening.

The assumption made that the shaft remains straight and the disc does not flex at the position of the disc opening is due to the change in stiffness. The small angle of rotation, α, when the rotor disc center is deflected by an amount ,*d*, is shown in Figure 3.1. *D* is the diameter of the disc and the angle *o* defines as the opening of the disc. Thus, we have

For the shaft:

$$\alpha = d/(l/2) = 2d/l \tag{3.1}$$

For the disc:

$$\alpha = o/D \tag{3.2}$$

Equating the equations:

$$o = \frac{2dD}{l} \tag{3.3}$$

Therefore the opening rate can be obtained from the deflection in the x and y directions such that:

$$\dot{o} = \frac{2\dot{d}D}{l} \tag{3.4}$$

The gyroscopic moment can therefore be expressed as:

$$M_{\xi} = J_p \omega \dot{o}_{\xi} = -J_p \omega (2D\dot{\eta}/l) \ , \ M_{\eta} = J_p \omega \dot{o}_{\eta} = J_p \omega (2D\dot{\xi}/l) \tag{3.5}$$

Converting into force by dividing (3.3) by the half rotor length we have:

$$F_{\xi} = -J_p \omega (4D\dot{\eta}/l^2) \ , \ F_{\eta} = J_p \omega (4D\dot{\xi}/l^2) \tag{3.6}$$

3.3 EQUATIONS OF MOTION

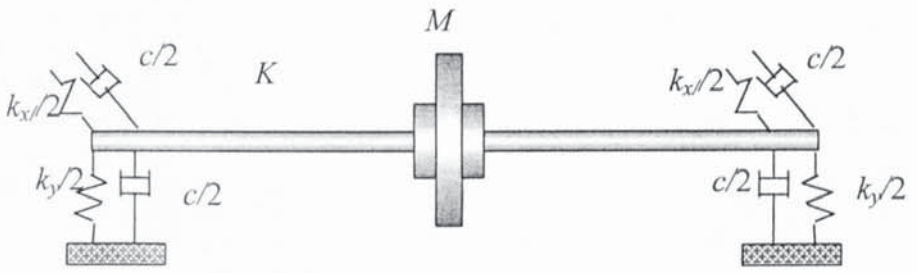

Figure 3.2. Schematic diagram of the rotor-bearing system.

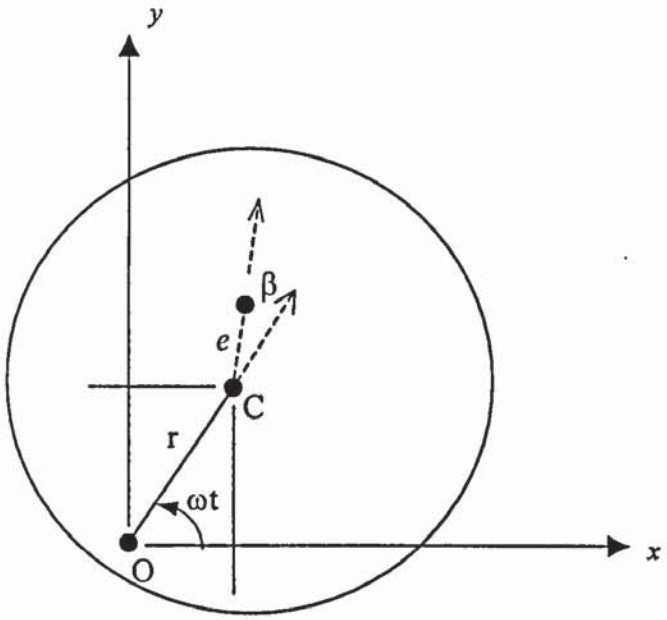

Figure 3.3. Schematic diagram showing the axes

Consider a *Jeffcott* rotor (shown in Figure 3.2) carrying an unbalanced disc at the mid-span mounted on a massless shaft. Since the disc is located at the mid-span the gyroscopic or rotary inertia are neglected. The mass of the shaft is neglected compared with that of the disc and the stiffness of the bearings is high compared with that of the shaft.

By assuming the shaft is axisymmetric, the equations of motion for the rotor may be written, in the fixed co-ordinates system with reference to Figure 3.3 as (Lee 1993):

$$m\frac{d^2}{dt^2}(x + e\cos(\omega t + \beta)) = -kx$$

$$m\frac{d^2}{dt^2}(y + e\sin(\omega t + \beta)) = -ky - mg \qquad (3.7)$$

Where m is the mass of the rotor, k is the stiffness of the rotor, e is the unbalance radius, ω is the spin speed, β is the angle between the unbalance mass and reference axis and g is the gravitational acceleration.

The above equation (3.7) can be simplified as:

$$\begin{bmatrix} m & 0 \\ 0 & m \end{bmatrix}\begin{bmatrix} \ddot{x} \\ \ddot{y} \end{bmatrix}+\begin{bmatrix} k & 0 \\ 0 & k \end{bmatrix}\begin{bmatrix} x \\ y \end{bmatrix}=me\omega^2\begin{bmatrix} \cos(\omega t+\beta) \\ \sin(\omega t+\beta) \end{bmatrix}+\begin{bmatrix} 0 \\ -mg \end{bmatrix} \tag{3.8}$$

If m_b is the mass of the bearing, C_b is the damping value, k_{bx} and k_{by} are the stiffnesses of the bearing and foundation combined in the x and y directions, as shown in Figure 3.4, additional equations must be added to equation (3.8). The system becomes a 4 degree of freedom problem. The mass of the bearing is an approximate value since it cannot be determined accurately. This is necessary to include the effect of damping from the bearing, since it is assumed the rotor-shaft system damping is negligible. By including the gyroscopic matrix as well, the equations becomes:

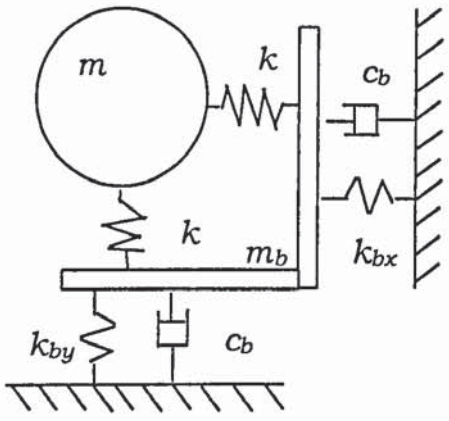

Figure 3.4: Schematic diagram of the rotor-bearing system

$$\begin{bmatrix} m & 0 & 0 & 0 \\ 0 & m & 0 & 0 \\ 0 & 0 & m_h & 0 \\ 0 & 0 & 0 & m_h \end{bmatrix} \begin{bmatrix} \ddot{x} \\ \ddot{y} \\ \ddot{x}_h \\ \ddot{y}_h \end{bmatrix} + \begin{bmatrix} 0 & g & 0 & 0 \\ -g & 0 & 0 & 0 \\ 0 & 0 & c_h & 0 \\ 0 & 0 & 0 & c_h \end{bmatrix} \begin{bmatrix} \dot{x} \\ \dot{y} \\ \dot{x}_h \\ \dot{y}_h \end{bmatrix} + \begin{bmatrix} k & 0 & -k & 0 \\ 0 & k & 0 & -k \\ -k & 0 & k+k_{hx} & 0 \\ 0 & -k & 0 & k+k_{hy} \end{bmatrix} \begin{bmatrix} x \\ y \\ x_h \\ y_h \end{bmatrix} =$$

$$\begin{bmatrix} me\omega^2 \cos(\omega t + \beta) \\ me\omega^2 \sin(\omega t + \beta) - mg \\ 0 \\ 0 \end{bmatrix}$$

(3.9)

or in matrix notation as:

$$\mathbf{M}\ddot{\mathbf{r}} + (\mathbf{C} + \mathbf{G})\dot{\mathbf{r}} + \mathbf{K}\mathbf{r} = \mathbf{F} \qquad (3.10)$$

where

$$\mathbf{r} = \begin{bmatrix} x \\ y \\ x_h \\ y_h \end{bmatrix}$$

where,

M= mass matrix

C= damping matrix

G= gyroscopic matrix

K= stiffness matrix

F = external force matrix

The motion of the bolted rotor is much easier to describe in rotating rather than fixed co-ordinates. This is due to the assumption that the stiffness of the system is dependent on the shaft deflection. The change of stiffness is assumed to follow the direction of the rotation of

the unbalance force. Transforming equation (3.9) into rotating co-ordinates using the transformation unit vector in the fixed and rotating co-ordinates as shown in Figure 3.5, we have:

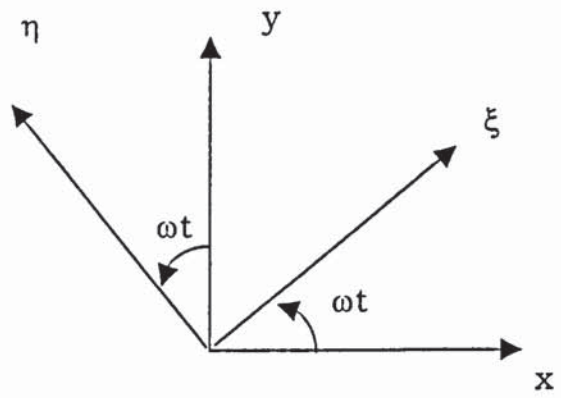

Figure 3.5. Vectors in fixed and rotating co-ordinates.

$$\begin{bmatrix} x \\ y \\ x_h \\ y_h \end{bmatrix} = \begin{bmatrix} \cos\omega t & -\sin\omega t & 0 & 0 \\ \sin\omega & \cos\omega t & 0 & 0 \\ 0 & 0 & \cos\omega t & -\sin\omega \\ 0 & 0 & \sin\omega & \cos\omega t \end{bmatrix} \begin{bmatrix} \xi \\ \eta \\ \xi_h \\ \eta_h \end{bmatrix} \tag{3.11}$$

or

$$\mathbf{r} = \mathbf{T}\zeta \tag{3.12}$$

where

$$\mathbf{T} = \begin{bmatrix} \cos\omega t & -\sin\omega t & 0 & 0 \\ \sin\omega & \cos\omega t & 0 & 0 \\ 0 & 0 & \cos\omega t & -\sin\omega \\ 0 & 0 & \sin\omega & \cos\omega t \end{bmatrix} \quad \text{and } \zeta = \begin{bmatrix} \xi \\ \eta \\ \xi_h \\ \eta_h \end{bmatrix} \tag{3.13}$$

Therefore from (3.8) we have:

$$\begin{aligned} \mathbf{r} &= \mathrm{T}\zeta \\ \dot{\mathbf{r}} &= \mathrm{T}\dot{\zeta} + \dot{\mathrm{T}}\zeta \\ \ddot{\mathbf{r}} &= \mathrm{T}\ddot{\zeta} + 2\dot{\mathrm{T}}\dot{\zeta} + \ddot{\mathrm{T}}\zeta \end{aligned} \tag{3.14}$$

where

$$\dot{\mathrm{T}} = \begin{bmatrix} -\omega\sin\omega t & -\omega\cos\omega t & 0 & 0 \\ \omega\cos\omega t & -\omega\sin\omega t & 0 & 0 \\ 0 & 0 & -\omega\sin\omega t & -\omega\cos\omega t \\ 0 & 0 & \omega\cos\omega t & -\omega\sin\omega t \end{bmatrix}$$

$$\ddot{\mathrm{T}} = \begin{bmatrix} -\omega^2\cos\omega t & \omega^2\sin\omega t & 0 & 0 \\ -\omega^2\sin\omega t & -\omega^2\cos\omega t & 0 & 0 \\ 0 & 0 & -\omega^2\cos\omega t & \omega^2\sin\omega t \\ 0 & 0 & -\omega^2\sin\omega t & -\omega^2\cos\omega t \end{bmatrix} = -\omega\mathbf{T} \tag{3.15}$$

Substituting (3.14) into (3.10) we have:

$$\mathbf{M}(\mathrm{T}\ddot{\zeta} + 2\dot{\mathrm{T}}\dot{\zeta} + \ddot{\mathrm{T}}\zeta) + (\mathbf{C}+\mathbf{G})(\mathrm{T}\dot{\zeta} + \dot{\mathrm{T}}\zeta) + \mathbf{K}\mathrm{T}\zeta = \mathbf{F} \tag{3.16}$$

multiplying by the transpose of **T** equation (3.16) becomes:

$$\mathrm{T}'\mathbf{M}(\mathrm{T}\ddot{\zeta} + 2\dot{\mathrm{T}}\dot{\zeta} + \ddot{\mathrm{T}}\zeta) + \mathrm{T}'(\mathbf{C}+\mathbf{G})(\mathrm{T}\dot{\zeta} + \dot{\mathrm{T}}\zeta) + \mathrm{T}'\mathbf{K}\mathrm{T}\zeta = \mathrm{T}'\mathbf{F} \tag{3.17}$$

Therefore, the stiffness matrix in the rotating axis is:

$\mathrm{K}_r = \mathrm{T}'\mathbf{K}\mathrm{T}$ or

$$\mathbf{K}_r = \begin{bmatrix} k & 0 & -k & 0 \\ 0 & k & 0 & -k \\ -k & 0 & k + k_{hx}\cos^2\omega t + k_{hy}\sin^2\omega t & -(k_{hx} - k_{hy})\cos\omega t \sin\omega t \\ 0 & -k & -(k_{hx} - k_{hy})\cos\omega t \sin\omega t & k + k_{hx}\sin^2\omega t + k_{hy}\cos^2\omega t \end{bmatrix} \quad (3.18)$$

In the bolted rotor another important parameter is the change in the stiffness of the system. This happens when it undergoes a deflection above the threshold value where the stiffness changes to a much lower value due to the opening of the bolted joint (shown in Figure 3.1). This gives a load deflection relation essentially as shown in Figure 3.6.

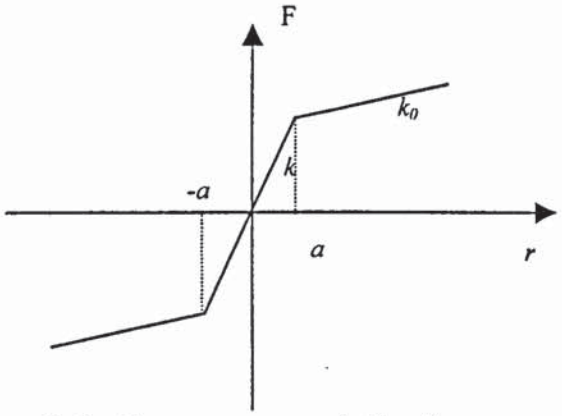

Figure 3.6: Force versus deflection curve

From equation (3.17), the restoring force component can be represented as follows:

$$\mathrm{K}_r\zeta = \begin{bmatrix} k & 0 & -k & 0 \\ 0 & k & 0 & -k \\ -k & 0 & k + k_{hx}\cos^2\omega t + k_{hy}\sin^2\omega t & -(k_{hx} - k_{hy})\cos\omega t \sin\omega t \\ 0 & -k & -(k_{hx} - k_{hy})\cos\omega t \sin\omega t & k + k_{hx}\sin^2\omega t + k_{hy}\cos^2\omega t \end{bmatrix} \begin{bmatrix} \xi \\ \eta \\ \xi_h \\ \eta_h \end{bmatrix} \text{ or}$$

$$\mathrm{K}_r\zeta = \begin{bmatrix} F_1 \\ F_2 \\ F_3 \\ F_3 \end{bmatrix}$$

The value of F_1 and F_2 are represented by Figure 3.6. The restoring force of the system can be represented as:

$$F_1 = k(\xi - \xi_h) - \Delta(k - k_a)(\xi - \xi_h)(1 - a/\bar{r})$$

$$F_2 = k(\eta - \eta_h) - \Delta(k - k_a)(\eta - \eta_h)(1 - a/\bar{r}) \qquad (3.19)$$

where

$$\bar{r} = \sqrt{(\xi - \xi_h)^2 + (\eta - \eta_h)^2}$$

$\Delta = 0$, for $|\bar{r}| \le |a|$ and $\Delta = 1$, for $|\bar{r}| > |a|$

$\Delta = 0$, for $|\bar{r}| \le |a|$ and $\Delta = 1$, for $|\bar{r}| > |a|$

a is the threshold in x-direction and y-direction.

3.4. MODEL USING FINITE ELEMENT METHOD (FEM)

To make sure that the above model is giving an accurate representation of the system, I analysed the system using the finite

element technique. Finite element method has been used widely in rotordynamic. It has been possible to predict the natural frequencies, the mass and the stiffness of the system accurately using finite element method. As shown in previous section, due to the nature of the problem the above representation can be can be reduced to 4 degrees of freedom. To find out whether the model used was an accurate model, a comparison was made using a full finite element model and a reduced model which is equivalent to the above model.

As the system is system is symmetrical, only one half was considered. The boundary conditions used for the analysis consists of the pin joint at the bearing and a constraint with zero slope at the disc. The full finite element model was carried out using 7 element with 8 node. The elements utilised are shown in Figure 3.7. where bearing type 4 represents a short bearing and bearing type 8 represents a pseudo-bearing that allows deflection only.

Figure 3.7: Finite element model

The Guyan reduction technique (Friswell *at el* 2000) was used to reduce the number of degree of freedom to the required number. This

technique allowed the selection of the required degrees of freedom and elimination of unwanted degrees of freedom.

In the Guyan reduction (Guyan, 1965), the second order form of the system where the deflection and force vectors, **q** and **f**, and the mass and stiffness matrices, **M** and **K**, are re-ordered and partitioned into separate quantities relating to master (retained) and slave (discarded) degrees of freedom. Assuming that no force is applied to the slave degrees of freedom and the damping is negligible the equation of motion of the structure becomes

$$\begin{bmatrix} \mathbf{M}_{mm} & \mathbf{M}_{ms} \\ \mathbf{M}_{sm} & \mathbf{M}_{ss} \end{bmatrix} \begin{Bmatrix} \ddot{\mathbf{q}} \\ \ddot{\mathbf{q}} \end{Bmatrix} + \begin{bmatrix} \mathbf{K}_{mm} & \mathbf{K}_{ms} \\ \mathbf{K}_{sm} & \mathbf{K}_{ss} \end{bmatrix} \begin{Bmatrix} \mathbf{q} \\ \mathbf{q} \end{Bmatrix} = \begin{bmatrix} \mathbf{f}_m \\ 0 \end{bmatrix}$$

The subscripts *m* and *s* relate to the master and slave co-ordinates respectively. By neglecting the inertia terms in the second set of equations the slave degrees of freedom may be eliminated so that;

$$\begin{Bmatrix} \mathbf{q} \\ \mathbf{q} \end{Bmatrix} = \begin{bmatrix} \mathbf{I} \\ -\mathbf{K}_{ss}^{-1}\mathbf{K}_{sm} \end{bmatrix} \mathbf{q}_m = \mathbf{T}_s \mathbf{q}_m$$

where **Ts** denotes the static transformation between the full displacement vector and the master co-ordinates.

Using Guyan reduction the number of nodes was reduced to four. Checking the natural frequency with and without Guyan reduction shows that the natural frequency of the first critical speed are the same in both directions.

From this it can be deduced that the above above formulation is not far away from the accurate model. For the full model the natural frequency are: 28.5 Hz and 27.5 Hz with shaft stiffness of 68300 N/m and mass of 0.3 kg and 2.7328 kg for the bearing and the disc mass. For the model with Guyan reduction the natural frequency in horzontal direction and vertical directions are 27.5 Hz and 28.5 Hz respectively. Hence it can be deduced that the model are an accurate representation. Furthermore, as shown in the Campbell diagram (Genta 1995) below in Figure 3.8. it was proved that the gyroscopic effects were minimum.

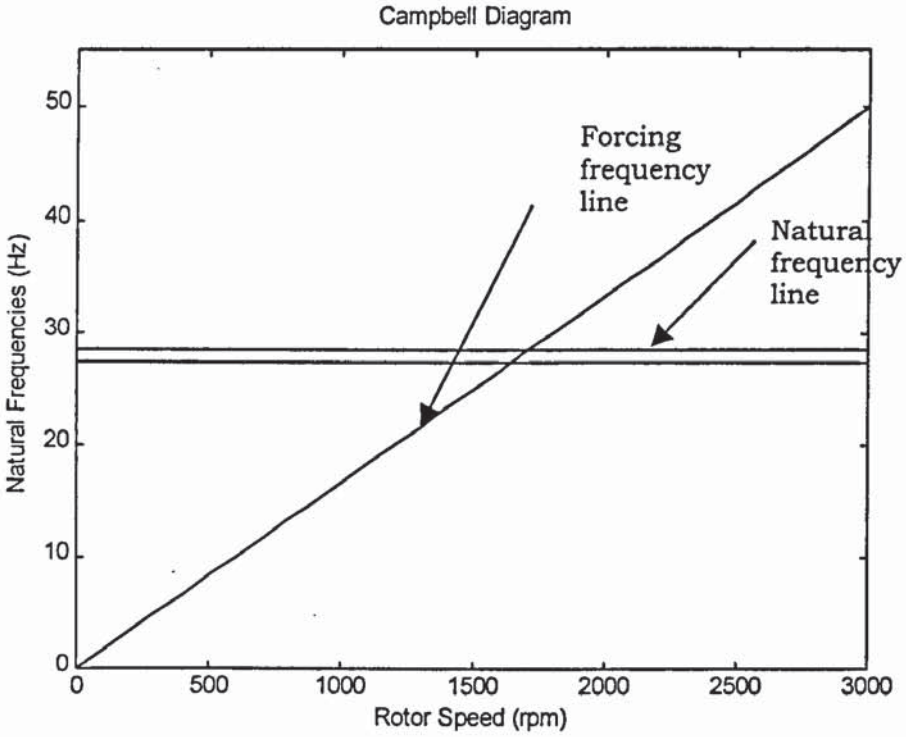

Figure 3.8: Campbell diagram

3.5 CONCLUSION

The effect of a bolted rotor is discussed in the context of the non-linear effect of the joint in general. The effect of the joint in the rotor is discussed. The general equations of motion of the bolted rotor are derived. The non-linear effect on stiffness of the rotor was discussed. Since, a simple Jeffcott rotor is used, the equations derived result in a rotor system using only four-degrees of freedom. Finally a finite element model using Guyan reduction was used to ascertain the model used was an accurate model.

Chapter Four

NUMERICAL SIMULATION

4.0 INTRODUCTION

The purpose of this chapter is to present an effective algorithm to solve the equations of motion of a bolted rotor. Since the problem involves a non-linear term a direct solution cannot be obtained and the use of a simulation package is described. The numerical simulation technique chosen is also discussed.

4.1 PROBLEM INTERPRETATION

A definite solution in close form for the problem at hand does not exist due to its complexity. This is largely due to the intermittent and non-linear characteristics of the jointed part of the rotor. Although in practice the existence of more than one joints is common, such as in a gas turbine, where the root of the turbine discs are compressed together by a central bolt or several bolts on a small pitch circle diameter (PCD), here the focus is on a simpler problem of a rotor with a single joint. Although other problems might arise due to construction, such as joint misalignment, shaft bowing and uneven circumferential joint face, it is assumed in the analysis that these

problems are insignificant. A modified *Jeffcott* rotor was modelled with a disc that was bolted together.

During large deflections of the rotor, the lateral movement is resisted by the restoring force of the bolts and the compression of the joint, hence the joint changes the dynamic properties of the system. It is known that the properties of a joint are different from the solid material due to the interface of the joint and these properties depend entirely on the normal force at the interface. However, when the joint partially opens due to external excitation the dynamic behaviour totally changes. The opening of the gap between the rotor discs makes the problem more difficult to analyse. This is because the stiffness of the system when the joint starts to open consists of the shaft stiffness, joint stiffness (surface roughness and interface material properties), bolt stiffness and axial bearing stiffness.

4.2. NUMERICAL SIMULATION

Simulation is a popular technique used today with the recent improvements in computer speed and memory size. Simulation has many advantages, one of which is that the physical system is not required and the influence of changes in parameters on the system can easily be accommodated early in the design stage. This can eliminate the cost of building the physical system before its optimum performance is known. However, simulation is only an effective technique of solving a problem when the physical system can be correctly modelled. Therefore, a precise understanding of the physical system behaviour is required before an effective model can be developed. Once the model has been correctly produced, changing the

parameters only requires changes in the inputs values. In the actual physical system modifications require a very tedious and time-consuming process. Apart from that, an input to the simulation can also be from experimental results or from a previous analysis of the system. Other important advantages of simulation is the possibility of extracting data from any point of reference, to check the validity of each stage of the system, which in some cases might not be possible experimentally.

In order to fulfil this purpose, a valid mathematical model of the system must be formulated first to accurately reproduce similar results to the measured data from a test rig. Once the model has been validated, it can be used to conduct parametic studies with confidence for a certain range of the parameters. Thus, the mathematical model to be developed should be able to predict accurately the dynamic behaviour of the bolted-rotor system.

4.3 SIMULINK : SIMULATION PACKAGE

In this study the numerical work was carried out using the MATLAB toolbox SIMULINK. The main reasons for selecting this software package for modelling are (i) it supports non-linear systems modelling (ii) it is designed for modelling, simulating and analysing dynamical systems and (iii) it is widely available. It is commonly used in control system design, communication system design, and other simulation applications.

The features included in the package enables simulation models to be developed with minimum effort and hence, a faster and more efficient

simulation process can be achieved. SIMULINK provides an interactive tool, which makes modelling and simulation operation itself relatively simple.

SIMULINK enables the user to build graphical block diagrams to represent the simulation model, simulate a dynamic system, evaluate system performance, and refine the design in a quick and simple process. Built as a MATLAB toolbox, SIMULINK shares all the benefits of MATLAB capabilities in analysis and design tools software. Its versatile features enable a model to be represented in a very simple way, avoiding the needs to write long programming language scripts. The representation of a model is similar to the flow diagram as outline in the simulation flow diagram. SIMULINK is designed to support both linear and non-linear systems modelling. Apart from that, a SIMULINK model can be run in continuous time, sampled time or a combination of the two. The sampling rate of the system can be also multi-rate, i.e. have different parts that are sampled or updated at different rates.

4.3.1 Building model with SIMULINK

SIMULINK provides a graphical user interface (GUI) to facilitate the modelling process. This enables the model to be built by means of block diagrams, constructed from the block library or user created blocks, by means of click and drag mouse operations. This has the advantage, previously stated, of eliminating the requirement to formulate the equations in a programing language and therefore the time wastage involved in getting the program running properly.

SIMULINK includes a comprehensive block library of sinks, sources, linear and non-linear components, and connectors. There is also a facility to customise and create user-defined blocks.

Each library block contains many sub-blocks that can be used to create the simulation model. The parameter of the particular block is changed by modifying the value in the dialog box for each sub-block. The lines with arrows connecting blocks represent the signal flow. Each signal line can carry a scalar or vector signal. Apart from that, the signal line can be branched to feed more than one blocks. Vector lines and scalar lines can be differentiated in the flow diagram by using the wide vector command, which highlights the vector lines and represents them with a number to indicate the vector size.

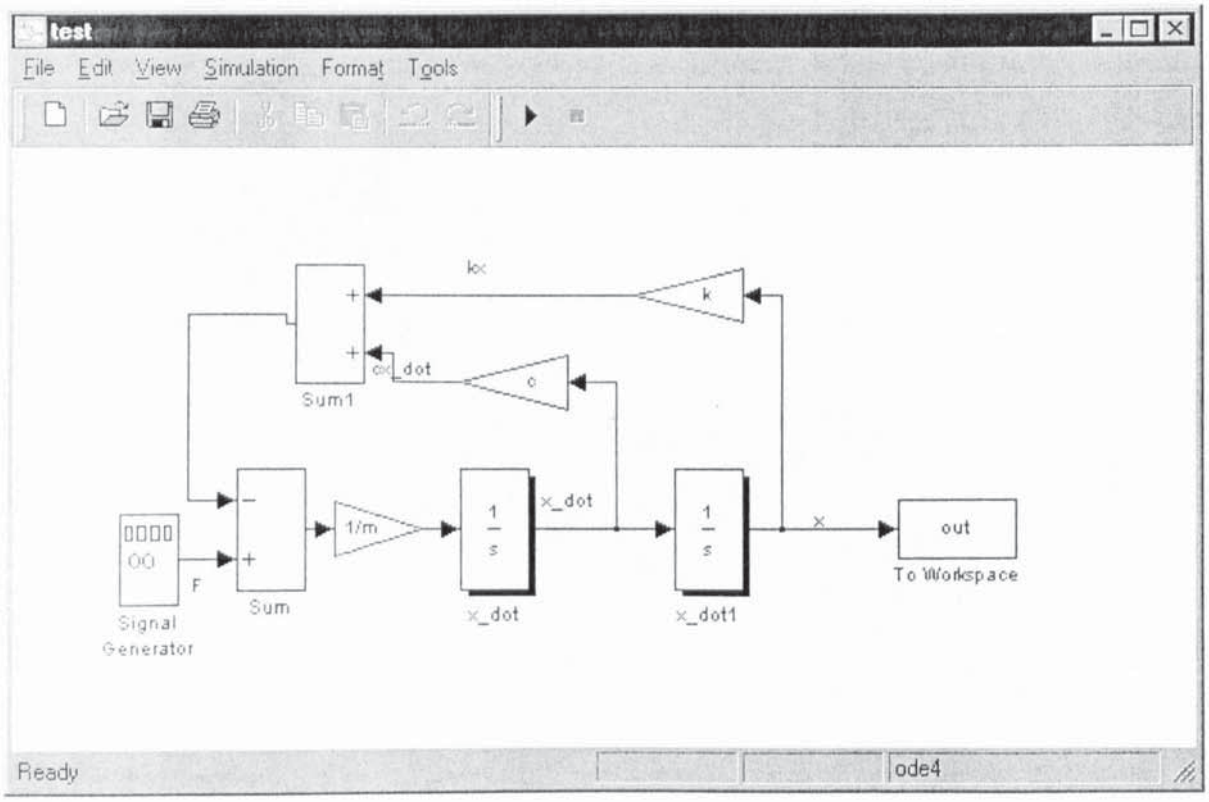

Figure 4.1: Simulation model (Second order system: $M\ddot{x}+C\dot{x}+Kx=F$)

As an example, to draw the flow diagram in SIMULINK to simulate the equation $M\ddot{x} + C\dot{x} + Kx = F(t)$, the equation first be written in the form:

$$\ddot{x} = \frac{1}{M}(F(t) - C\dot{x} - Kx) \qquad (4.1)$$

The flow diagram for (4.1) is shown in Figure 4.1. Two integrators were used to obtain the velocity and displacement. The velocity and displacement can be tapped from the flow line of the diagram using simulated scope or workspace. The values of *M*, *C*, *K* and *F* are fed in from the MATLAB window or using M-file. Slight modification to the diagram is required for more than one degree of freedom as shown in Figure 4.2. Here we are simulating $\ddot{\mathbf{x}} = \mathbf{M}^{-1}(\mathbf{F}(t) - \mathbf{C}\dot{\mathbf{x}} - \mathbf{K}\mathbf{x})$. In Figure 4.2 the blocks matrix gain, matrix gain1 and matrix gain2 represent the matrices **C**, **K**, and $\mathbf{M}^{-1}$ respectively.

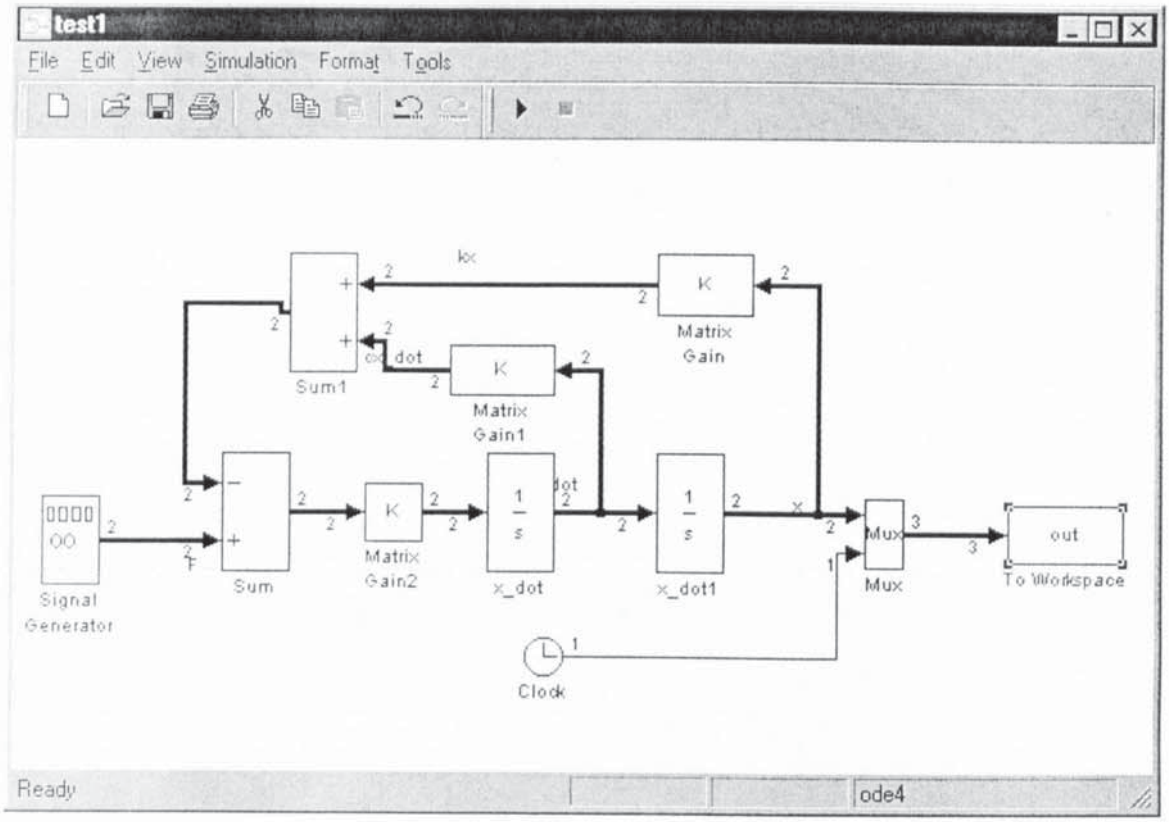

Figure 4.2. Simulation model of 2 DOF (second order system).

4.3.2 Creating sub-systems

SIMULINK allows models to be created in a hierarchical manner, so models can be built using both top-down and bottom-up approaches. With the increase in size and complexity of a model, the flow diagram can look awkward. Sub-systems are the means to simplify the model into an organised and presentable form. Using sub-systems has these advantages:

- It helps to reduce the number of blocks displayed in the model window.

- It keeps functionally related blocks together.

- It enables the establishment of a hierarchical block diagram, where a subsystem is on one layer and the blocks that make up the systems are in another layer.

4.3.3 Masking of Customised Blocks

Another important and powerful feature that SIMULINK has is the ability to customise dialog boxes and icons for subsystem. This is called masking and its advantages are:

- Reducing the dialog box of a subsystem into single masked dialog box. This avoids the need to open each block dialog box in the subsystem.

- Providing a more descriptive and helpful user interface by defining a dialog box with own block description, parameter field labels and helps text.

- Defining the commands that compute variables whose values depend on block parameters.

- Creating a block icon that depicts the subsystem's purpose.

- Preventing unintended modification of subsystems by hiding some or all of their contents behind a customised interface.

4.3.4 Running a simulation model

There are two ways of running the simulation model: either by using SIMULINK command menu or from the MATLAB command window.

SIMULINK menu commands are commonly used during the development and refinement of the model. Its interactive nature allows modification to the model, displaying the output at any point and also changing parameters easily during the simulation process. The important difference between the two methods of running a simulation is that using SIMULINK menu, the operations can be performed interactively while the simulation is running. The changes that can be made while the simulation is running are:

- Modification to the parameters, which include the simulation time, the step size and the solver.
- Display an output at any point by tapping the line and using Scope.
- Simulating another system simultaneously.
- Changing certain parameters of the block.

Another method of running the simulation is by entering the simulation commands in the MATLAB command window or from the M-file, which enables the simulation to run unattended. An analysis of the simulation can be performed by changing parameters randomly and executing the simulations in a loop. The output from the model can be displayed in various ways such as by using a scope, a workspace of file, or it can be analysed in the MATLAB window using MATLAB functions.

4.3.5 Solvers

Simulation of dynamic system involves the numerical integration of sets of ordinary differential equations (ODEs). SIMULINK provides a number of solvers for the simulation of such equations, which is part of the MATLAB command. No single method simulates every type of model accurately and efficiently because of the diversity of dynamic system behaviour. The important considerations for obtaining fast and accurate results depend on the selection of an appropriate method and careful adoption of the simulation parameters. Performance of the simulation in terms of speed and accuracy varies for different models and conditions.

There is the choice between the fixed-step solvers and variable-step solvers. The variable-step solvers can modify their step size during simulation whereas the fixed-step solvers maintain the same step. The difference between the two is that variable-step solvers provide error control and zero crossing detection whereas the other does not.

4.4 SIMULATION MODEL OF THE BOLTED ROTOR

The SIMULINK block flow diagram representing the bolted rotor is constructed based on the equations of motion developed previously. Rewriting the equations given in (3.17), we have:

$$\mathbf{T'M}(\mathbf{T}\ddot{\zeta}+2\mathbf{T}\dot{\zeta}+\mathbf{T}\ddot{\zeta})+\mathbf{T'}(\mathbf{C}+\mathbf{G})(\mathbf{T}\dot{\zeta}+\mathbf{T}\dot{\zeta})+\mathbf{T'KT}\zeta=\mathbf{T'F} \qquad (4.2)$$

Figure 4.3 shows the SIMULINK model of the above equations of motion. To transform equation (4.2) into SIMULINK model, the

equation was first described into a first order differential equation. There are four (4) degrees of freedom involved in the equation and the equations are divided into two (2) sets of sub-systems for integration. The integrator represent the rotor system and the bearing and foundation. In each sub-system, there are two (2) sets of integrators for the velocities and displacements, representing both the vertical and horizontal directions. The output vectors therefore consists of the two (2) sets of velocities and two (2) sets of accelerations and along with the inputs from the unbalance in the vertical and horizontal directions in the rotor system equations. In the bearing and foundations component the vector output consists of four (4) sets of outputs representing the two (2) sets of velocities and two (2) sets of displacements of the bearing and foundation. The advantage of this arrangement is that it minimises the inter-crossing of the vector line and the flow of the vector can easily be understood.

Sub-systems for the stiffness force and damping force components are created in each direction by multiplying with a multiplier which are the values of the stiffness and the damping. However, the damping value of the rotor system is negligible, hence the damping coefficient is set to zero. On the other hand, the value of the bearing

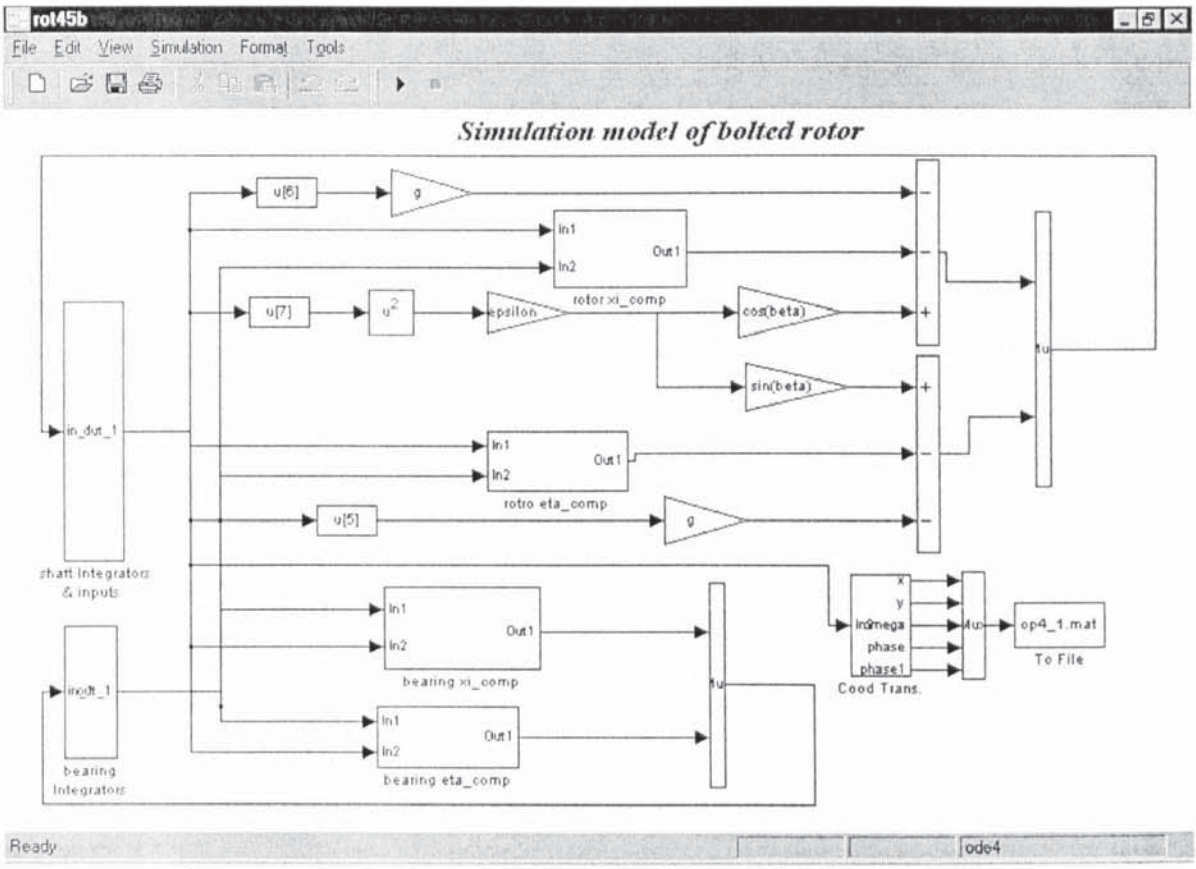

Figure 4.3: SIMULINK model of the bolted rotor system

damping is set to the damping ratio of 0.0068. This value is estimated using a logarithmic decrement method on the test rig as shown in appendix A4.5. The stiffness of the shaft is estimated using simply supported beams theory initially. However, the experimental results as in section 7.1 shows that the stiffness value is higher. Therefore, fixed-pinned boundaries were used (Appendix A1.2.3). The stiffness used was 90 000 N/m and it is considered to be isotropic. The bearing stiffnesses are different in the vertical and horizontal directions. The value are taken as 1.35 GN/m and 1.85 GN/m in the horizontal and vertical direction respectively.

The introduction of the non-linear term to the system is incorporated in the stiffness force by introducing a switching function which allows the change of stiffness from higher stiffness (90 000 N/m) to lower stiffness (40 000 N/m). It is included in both directions as a function of displacement. Figure 4.4 shows the model of the non-linear component. All the components of the flow signal are combined into vectors by MUX block and re-connected to the integrator. The desired output parameters from the system: - either velocities or displacement can be obtained by tapping the signal flow line and storing it into a file. This data can be processed by using MATLAB.

The magnitudes of displacements and velocities in rotating axis can be transformed into fixed axis by using the transformation equation (as in equation 3.11). Figure 4.4 shows the SIMULINK model representing the stiffness change due to the softening effect of the joint. Details of other parts of the SIMULINK model are given in the Appendix E.

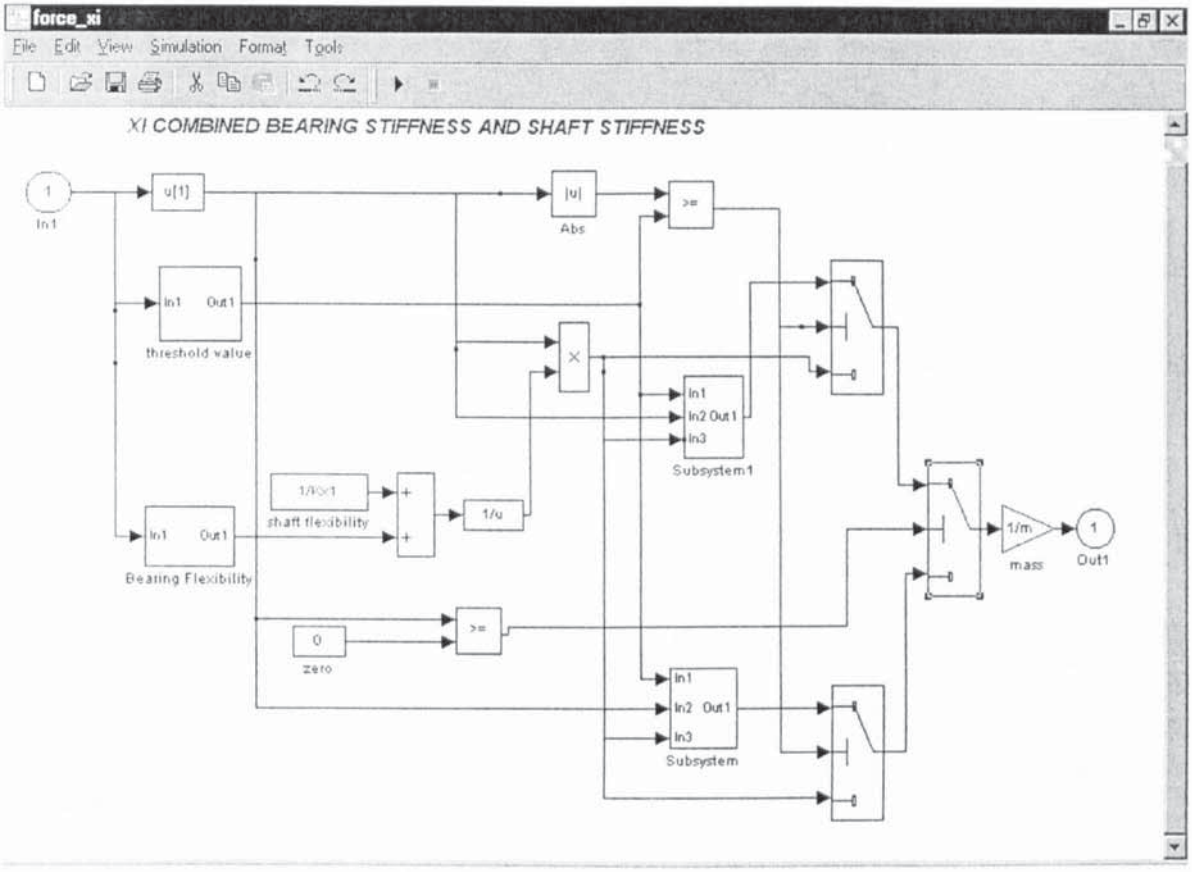

Figure 4.4. Sub-system of the non-linear stiffness component

4.5 INPUT VALUE TO SIMULINK MODEL

The input parameters required for the simulation model are based on the equations of motion of the rotor. The values used for this simulation are set to be the same as the design of the test rig. The input parameters are the mass, damping coefficient, linear shaft stiffness value and opening stiffness value and input due to unbalance of the rotor. The value of imbalance is varied to determine the state of the rotor when the abrupt changes in stiffness from higher stiffness to lower stiffness are encountered. Since the mass is considered as a lumped mass, the value is taken as 2.5kg. The damping is initially assumed to be zero as the worst condition would

occur when the value of damping is zero. Then the value is increased to determine the effect of the damping on the rotor. From these values, the natural frequency of the system is calculated to be about 27.3 Hz. Therefore, the simulations range is varied from 20 Hz to 35 Hz.

4.6 TIME DOMAIN ANALYSIS

In this study, the differential equations of motion have been developed in Chapter 3 and a solution of these equations can readily be obtained using SIMULINK. Since the mathematical model is described in terms of second order differential equations, the time-domain integration method is frequently used to solve the second order differential equations with deterministic excitation.

The equation is a stiff equation particularly when the amplitudes are above that threshold value. SIMULINK offers the stiff solver for variable step size integration. However, the simulation was carried out in the fixed step size. Fixed-step size was used so that an equally space data was produced for further analysis. There is no different in solvers performance with fixed-step size integration although the simulation rate is greatly reduced and memory storage is large. With error tolerance used that is 0.001 the results produce are consistent for Adams (ode2), Gear(ode3) and Runge-Kutta(ode4) methods.

The solver chosen in this study was the Runge-Kutta method. This is a very well known method that can be applied to non-linear equations with reasonable precision. The basic idea behind Runge-Kutta integration method is to find the solution for equilibrium equation at

discrete time steps. The method involves reducing a second order differential equation into a pair of first-order differential equations.

The procedure of the integration method is that by assigning an initial value $\{z\}_n$ for a starting time value of t_n, the approximate solution $\{z\}_{n+1}$ at the final point t_{n+1} or at some discrete list of points stepped by stepsize intervals dt can be found. In the Runge-Kutta method, the solution is propagated over the interval dt from $\{z\}_n$ to $\{z\}_{n+1}$ by combining the information from several smaller steps, each one involving the evaluation on the right side of equation (4.3). Then the solution for the next step interval is treated in an identical manner. The fact that no prior behaviour of the solution is required in its propagation allows any point along the trajectory of ordinary differential equations to be used as an initial point. The classical fourth order Runge-Kutta formula is by far the most frequently used. In each step the derivative is evaluated four times, once at the initial point, twice at intermediate trial points and once at a trial endpoint. From these derivatives the final function value is calculated as shown in equation (4.3).

$$\{z_n\} = \{z\}_n + \frac{h}{6}\{a_1\} + \frac{h}{3}\{a_2\} + \frac{h}{3}\{a_3\} + \frac{h}{6}\{a_4\} \qquad (4.3)$$

Where

$\{a_1\} = \{f(t_n, \{z_n\})\}$

$\{a_2\} = \{f(t_n + \frac{h}{2}, \{z_n + \frac{k_1}{2}\})\}$

$\{a_3\} = \{f(t_n + \frac{h}{2}, \{z_n + \frac{k_2}{2}\})\}$

$\{a_4\} = \{f(t_n + h, \{z_n + a_3\})\}$

h= step increment

4.7 FREQUENCY DOMAIN ANALYSIS

The steady-state dynamic response of a multi-degree of freedom, non-linear system can be determined by numerical integration of the equations of motion. SIMULINK produces the output in the time domain. However, the frequency response of the system at steady state can be extracted using the Fast Fourier Transfrom (FFT) function in MATLAB. These results can be saved into a separate file. Once the simulation is completed the values can be retrieved and plotted individually or plotted together forming a spectral maps plot. This plot exhibits the spectra as the speed of the rotor is increased through the speed range of interest.

The Discrete Fourier Transform (DFT) is discussed in many books (Lindfield and Penny, 1995, Brigham, 1988, Ramirez, 1985). The pre-requisite of using the function is that the data points are equispaced with an even number points. The relationship between the point the data points and its time (y,t) can be given in a finite set of sine and cosine functions as:

$$y = \frac{1}{n}\left(A_0 + \sum_{k=1}^{m-1} \{A_k \cos(2\pi kt/T) + B_k \sin(2\pi kt/T)\} + A_m \cos(2\pi mt/T) \right) \qquad (4.4)$$

where r=0,1,2,...,n-1,m=n/2 and T is the range of the data. The coefficients A_0, A_m, A_k and B_k (where k=1,2,....,m-1) must be determined. With n data values and n unknowns, the coefficients of the data can be used to fit the equation exactly.

If Δf be the frequency increment and f_{max} be the maximum frequency, then

$$\Delta f = 1/T \tag{4.5}$$

and

$$f_{max} = m\Delta f = (n/2)\Delta f = n/(2T) \tag{4.6}$$

The data values are equally spaced in the range T and t_r may be expressed as

$$t_r = rT/n, \; r = 0, 1, 2 \ldots . n\text{-}1 \tag{4.7}$$

letting Δt be the sampling interval, then

$$\Delta t = T/n \tag{4.8}$$

Substituting (4.7) into (4.4) we obtain

$$y_r = \frac{1}{n}\left(A_0 + \sum_{k=1}^{m-1} \{A_k \cos(2\pi kr/n) + B_k \sin(2\pi kr/n)\} + A_m \cos(\pi r) \right) \tag{4.9}$$

where r=0,1,2,....,n-1.

To develop the basic FFT algorithm one restriction must be placed on the data. The data must be equispaced and the number of points must be an integer power of 2.

MATLAB provides the function FFT to determine the DFT of a sequence of data values using the FFT algorithm.

4.8 STABILITY ANALYSIS

In a well defined velocity ranges a rotor can develop an unstable behaviour. The behaviour of rotor is considered stable when the amplitude of vibration in normal operation does not exceed a value that is considered acceptable. Muszynska (1984) states that a rotor is stable at a required rotational speed, when this motion is not accompanied by other modes of vibrations or the vibrations amplitude does not exceed an acceptable value. There is a source of energy, the centrifugal field in rotors in some cases, that can cause an unbounded growth in the amplitude of vibrations (Genta 1995).

The stability of the system can be determined using Poincare's mapping technique (Thompson 1986). The study condenses the behaviour of three-dimensional trajectories to a mapping of a two-dimensional surface. Thus the stability properties of the map reflect the stability properties of the flow.

The Poincare plot for the simulated data of the rotor are shown from Figure 5.19 to Figure 5.38.

4.9 CONCLUSION

The simulation model for the bolted rotor has been developed using SIMULINK from the equations of motion presented in the previous chapter. The important features of SIMULINK have been described to

show the simplicity of modelling using SIMULINK. Simple example of second order system has been used to illustrate the capabilities of SIMULINK. The construction of the bolted rotor model was also illustrated and the non-linear component was successfully modelled with SIMULINK. Finally the aspect of rotordynamic stability was also discussed.

Chapter Five

SIMULATION RESULTS

5.0 INTRODUCTION

In this chapter the simulation results of the response of the bolted rotor when it is run through the critical speed are presented. The numerical simulation was developed using SIMULINK which has been discussed in the previous chapter. In the development of the simulation model, to simplify the analysis of the system many assumptions are made. These assumptions are based on limitations of the model and the practical limitations of the test rig. Since the simulation model was used to model the test rig, all the input parameters were obtained from the test rig. The system considered was single plane system and four degrees of freedom were sufficient to model the system

The first stage in running the simulation was to make sure that it was working correctly by running test cases with simple systems or known systems. This process allowed syntax errors and logical errors in the simulation model to be rectified. Once this model ran successfully the actual data for the physical model can then be used.

5.1 SIMULATION TEST CASES

The test cases used in the simulation were to ensure that the simulation model was giving desired responses. The first stage of the simulation work was to model a linear, second order, single degree of freedom system acted on by a harmonic unbalance external force. The equation has an analytical solution which can be readily obtained (Dimorogonas, 1996). The model was run using the fourth-order Runge-Kutta solver with speed increments of 0.5 Hz from 20 Hz to 35 Hz with step size of 0.001. The amplitude of the response was extracted and saved as a data file. The result was compared with an analytical solution using the same input parameters.

As shown in Figure 5.1.the response was plotted against increasing speed. With a damping ratio of 0.01, there is a very small error between the response from the numerical simulation and from the analytical value. The results shows that with correct selection of the numerical parameters and method the response gave a good approximation to the actual response.

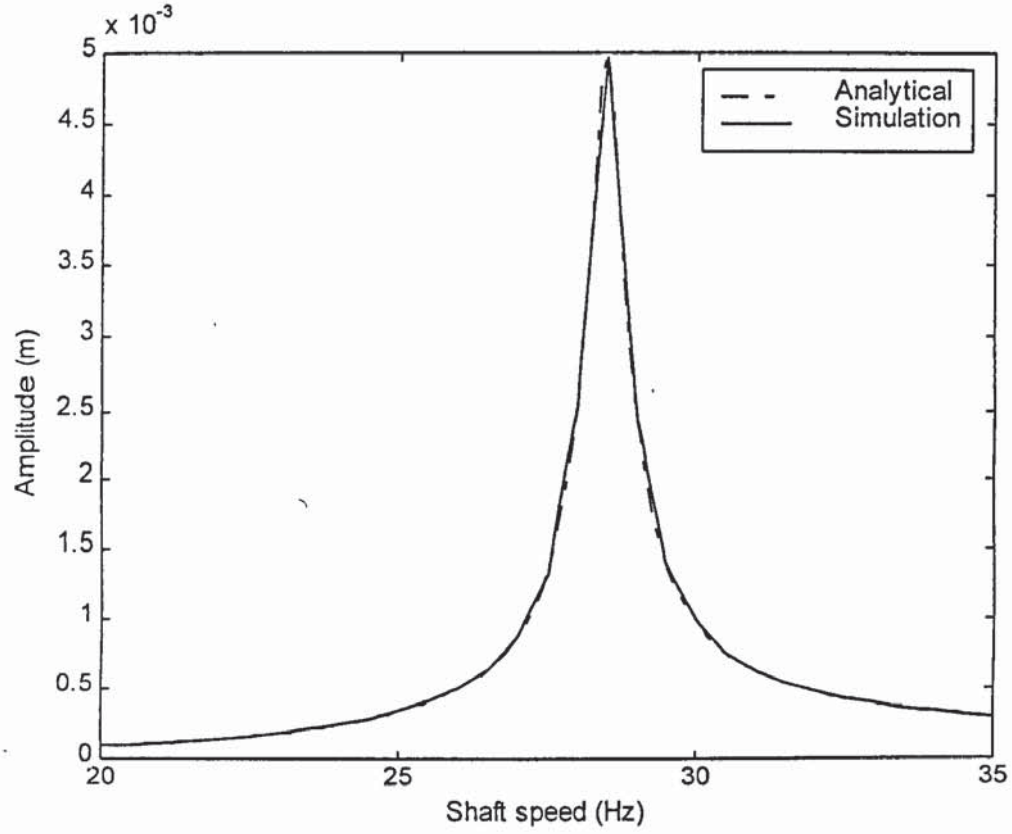

Figure 5.1: Rotor amplitude due to unbalance response without any change in stiffness.

5.2 BOLTED ROTOR-NUMERICAL RESULTS

In order to establish the influence of the bolted disc on the rotor response, an unbalance excitation was applied as the forcing function to the simulation model. The speed of the rotor was allowed to increase from 20 Hz to 35 Hz, corresponding to the speed close to the first natural frequency of the system. The simulation model developed was based on the non-linear four degree of freedom system which was

discussed in Chapter 3. The non-linear term become effective after the critical value of deflection was reached. The threshold value indicates that the joint stiffness become dominant and the rotor disc starts to open. The threshold value used in the simulation was obtained from the force-deflection test carried out on the test rig. This value was taken as 0.75 mm in both the vertical and horizontal directions. The simulation parameters are shown in Table 5.1.

Rotor disc mass	2.5 kg
Shaft stiffness, K	70000N/m
Bearing stiffness (horizontal)	3.5e6N/m
Bearing stiffness (vertical)	7.5e6N/m
Bearing damping ratio	0.05
Bearing mass	0.3 kg

Table 5.1: Simulation parameters

The numerical integration solver employed was ode45 which is Runge-Kutta fourth-order method with fixed step size of 0.001. Initially a continuous input was applied to the model by using the model chirp function in the SIMULINK library with some modification. This enables the continuous run-up responses through the speed range to be determined. Continuous time histories were obtained from this input. This is shown in Figure 5.2. The amplitude in the x and y directions are the same except for the phase difference of 90°. Figure 5.3 shows the plot of the phase angle with increasing time. Following this, a discrete input was applied to the model where the speed incremental was carried out in a loop. At each speed the model was run until it reached a steady state condition before the response was

recorded. The response is shown in Figure 5.4 with different unbalance values of 0.001mm ($3.8x10^{-6}$ kg-m) , 0.01m($3.8x10^{-5}$ kg-m), 0.05mm ($19x10^{-5}$kg-m) and 0.1 mm($3.8x10^{-4}$kg-m). Figure 5.5 shows the same response using an unbalance value of 0.05 mm. This discrete input was preferred because it was much easier to analyse the data by using the Fast Fourier Transform (FFT), and to produce the orbits and the Poincare plot. It has the advantage of using less memory because at each speed increment the output data can be stored in a data file.

The DFT of the simulation results with an unbalance value of 0.05 mm was obtained at an increasing speed from 20 Hz (1200 rpm) to 35 Hz (2100 rpm) in increments of 0.5 Hz (30 Hz), correspond to the experimental run-up. The DFT was carried out using 1024 points, corresponding to 1.024 seconds of data. The frequency increment used therefore was 0.9765 Hz and the maximum frequency was 512 Hz.

In order to understand what happens during the run-up stage, the FFT amplitudes were plotted with respect to increasing speed and frequency. This plot is known as the spectra plot or waterfall plot and shown in Figure 5.6. Another form of representation was by using a contour plot, where the peak of the amplitude was shown in contour line, (see Figure 5.7). Both of these plots were created using the MATLAB plotting facility. These two plots show the existence of other frequencies other than the speed of the rotor.

The responses at different speeds are shown in Figure 5.8 to Figure 5.17. They represent the frequency spectrum and shaft centre line

deflection orbit at the speed stated. The shaft orbits were plotted using simulation data over 15 cycles. This is to ensure that sufficient data were used to represent the complete loop, especially after exceeding the threshold value where the rotor stiffness changes.

Figure 5.18 shows a section of the signal in the x and y directions during run-up after the jump at 27 Hz. There is a phase difference of 90° between the two signals. There is a complete cycle of opening, closing and back to opening every 0.8 sec.

Periodic motions of the system can be represented by closed orbits in the phase space. However, to make a comparison with the experimental data, pseudo phase plots were plotted using the simulated data. The pseudo phase plot is the plot of x_i versus x_{i+1}, where x_{i+1} are the points taken at a delayed time of T from x_i where T is the period of the cycle. The pseudo phase plots at the corresponding rotor speed are shown in from Figure 5.19 to Figure 5.38 for the x and y directions. These results are discussed in Chapter 7.

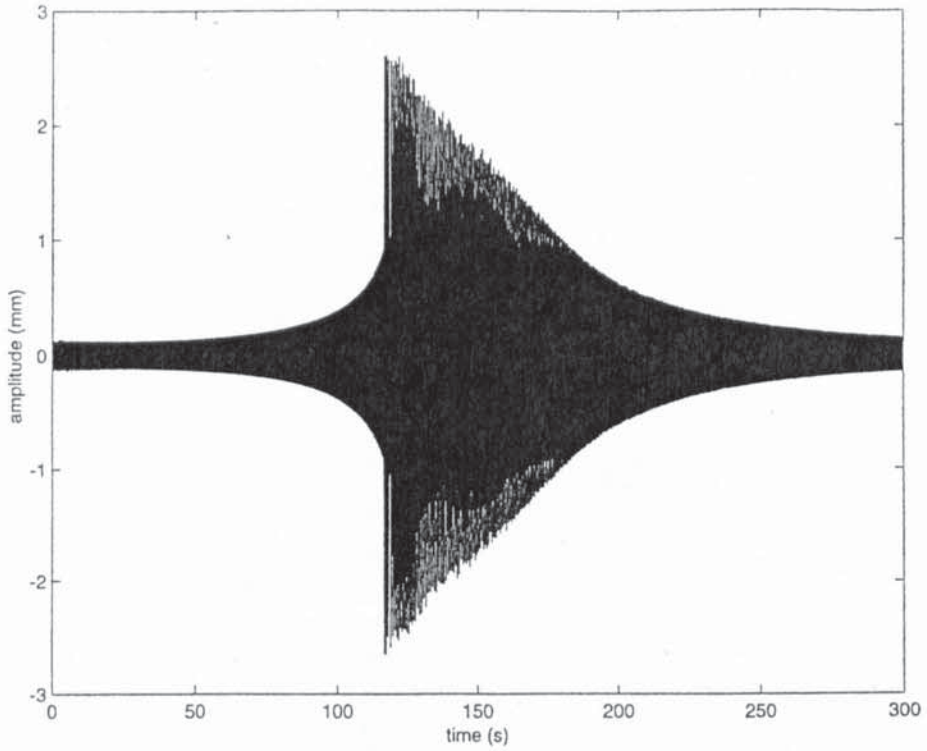

Figure 5.2. The run-up time history

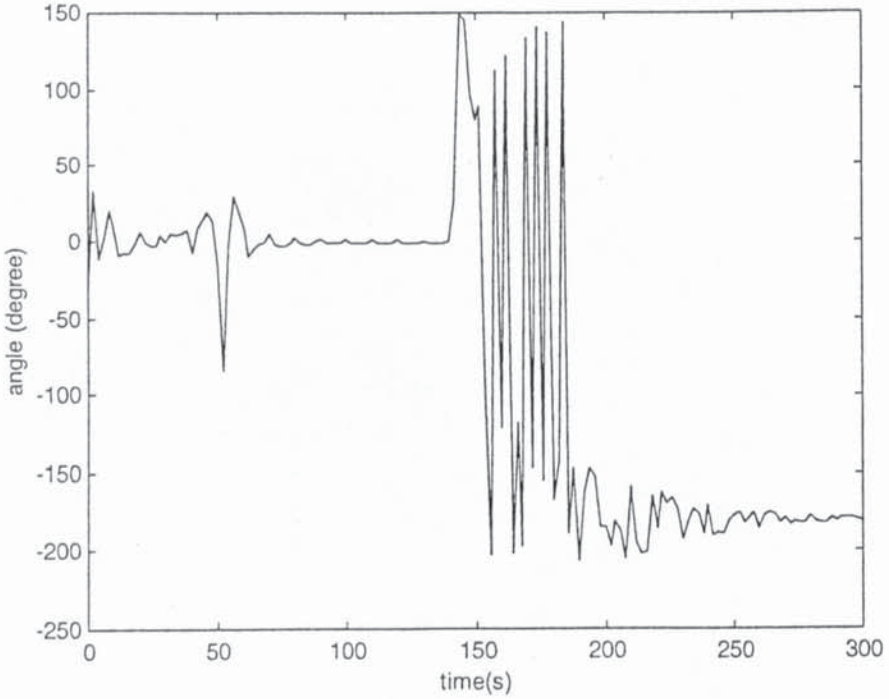

Figure 5.3: The phase angle versus time

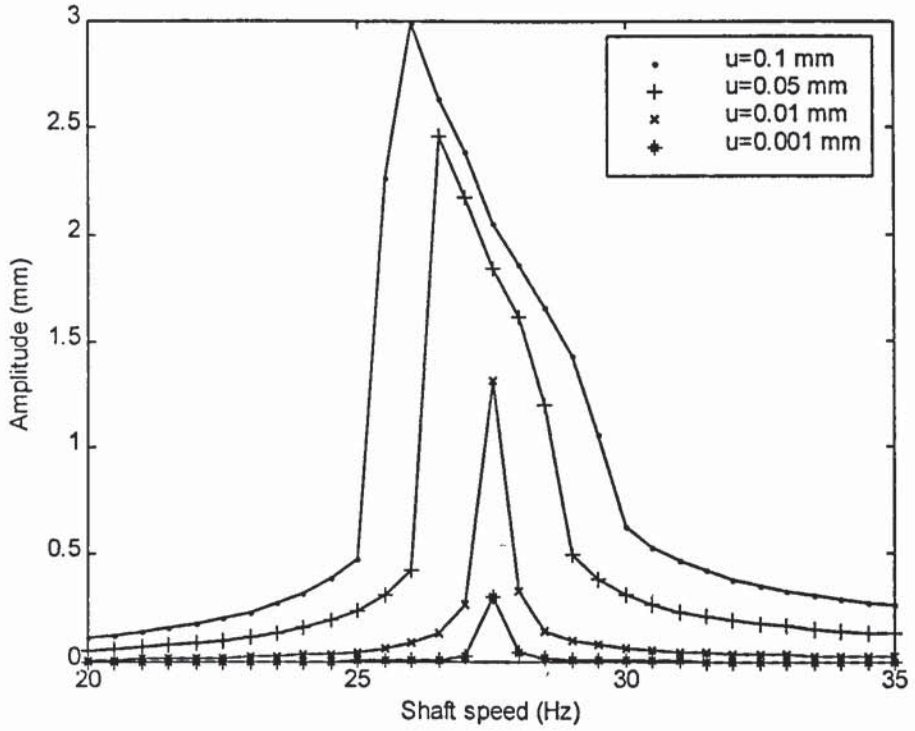

Figure 5.4: Resposnse in the horizontal direction with different unbalance value (unbal=0.001mm,0.01mm,0.05mm and 0.1 mm).

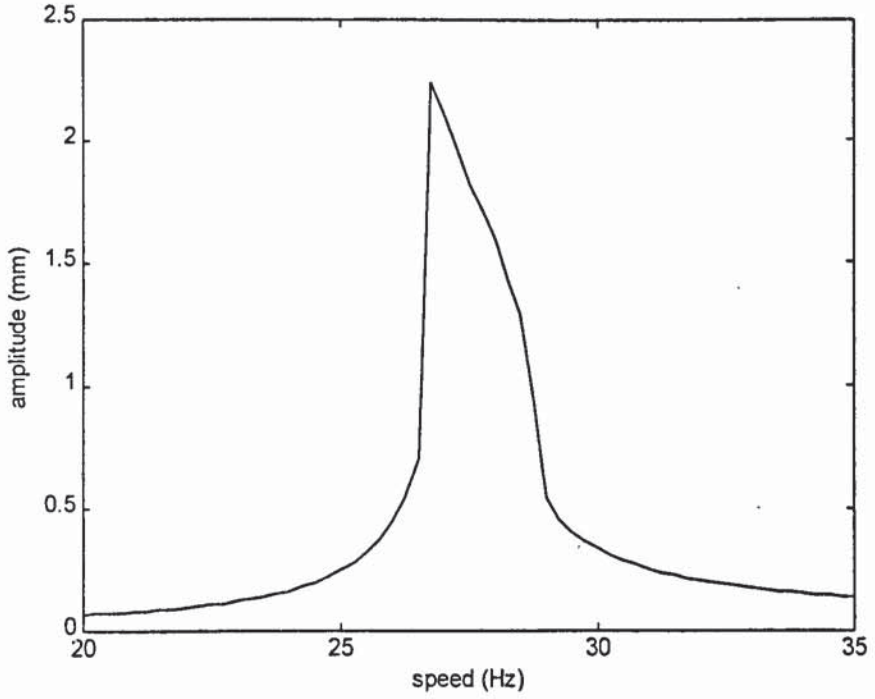

Figure 5.5. Amplitude versus increasing speed (unbal=0.05 mm)

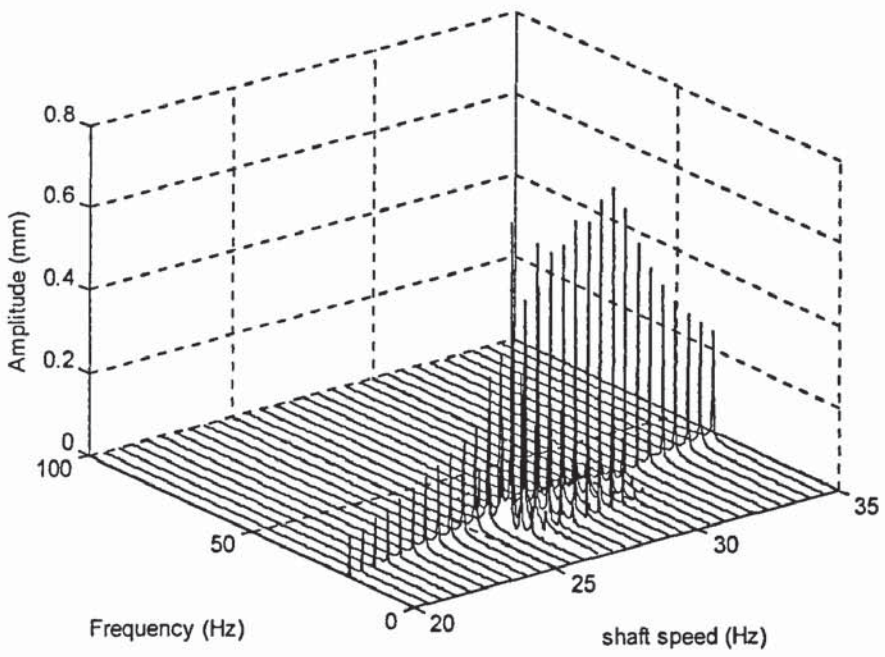

Figure 5.6. Spectral maps (unbal=0.05 mm)

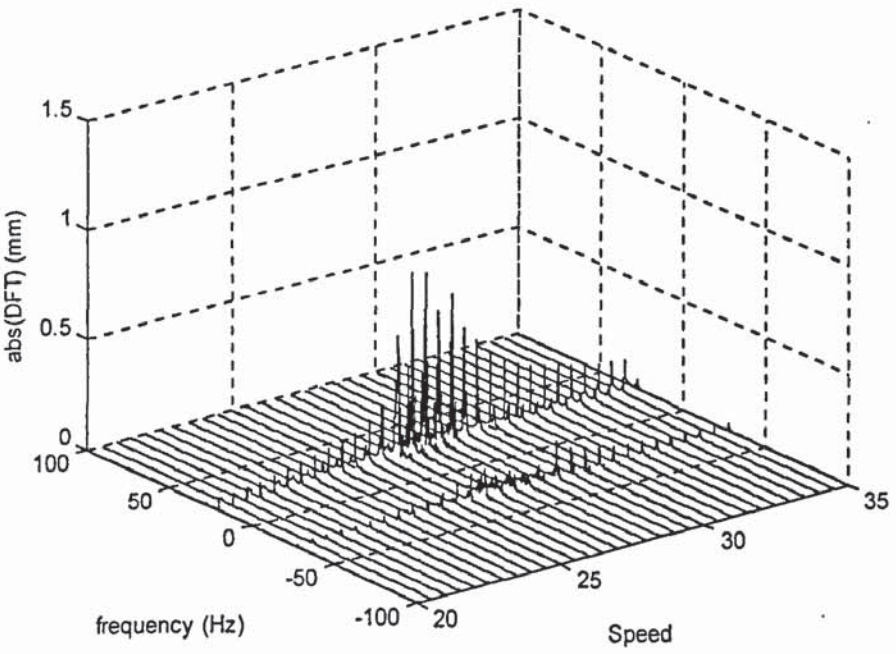

Figure 5.7: Forward-backward whirl of the simulated data.(LHS-forward)

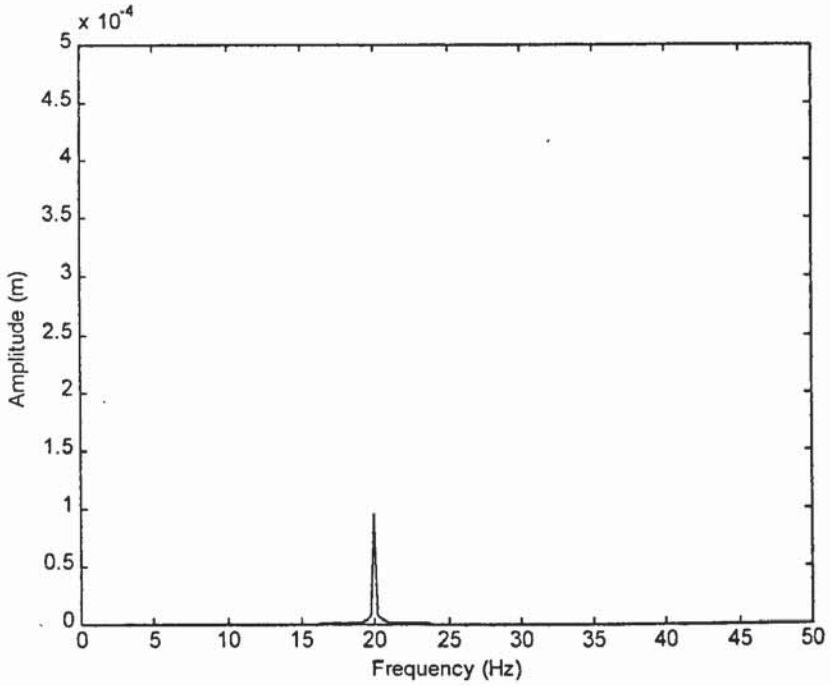

Figure 5.8. Frequency response at 20 Hz.

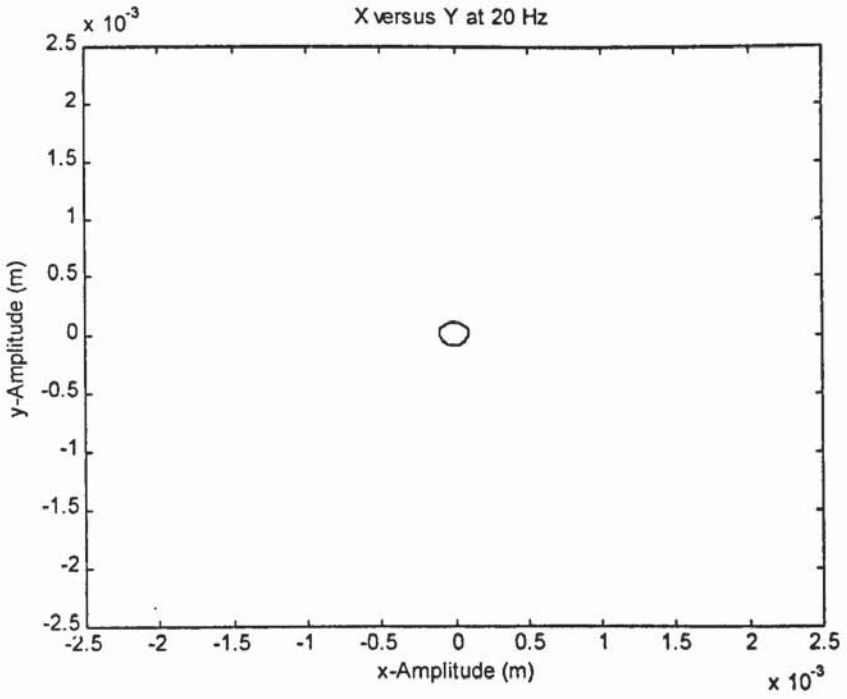

Figure 5.9. Orbit of the response at 20 Hz (1200 rpm)

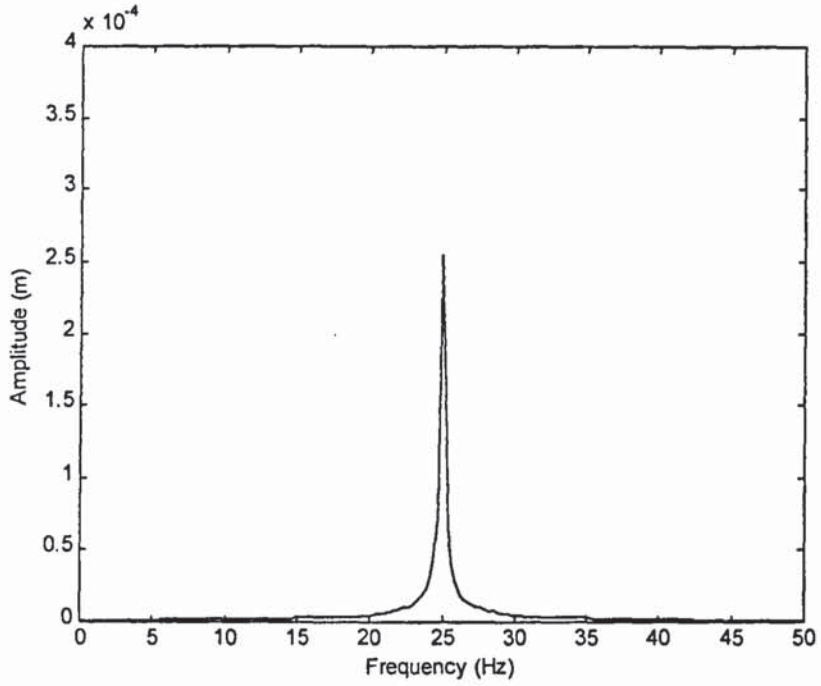

Figure 5.10. Frequency response at 25 Hz.

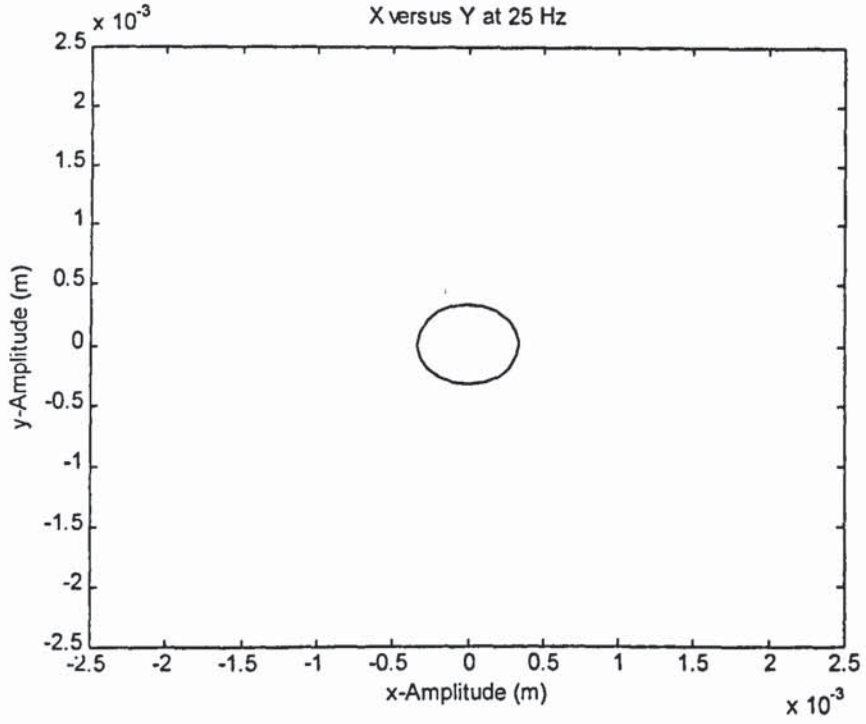

Figure 5.11. Orbit at 25 Hz

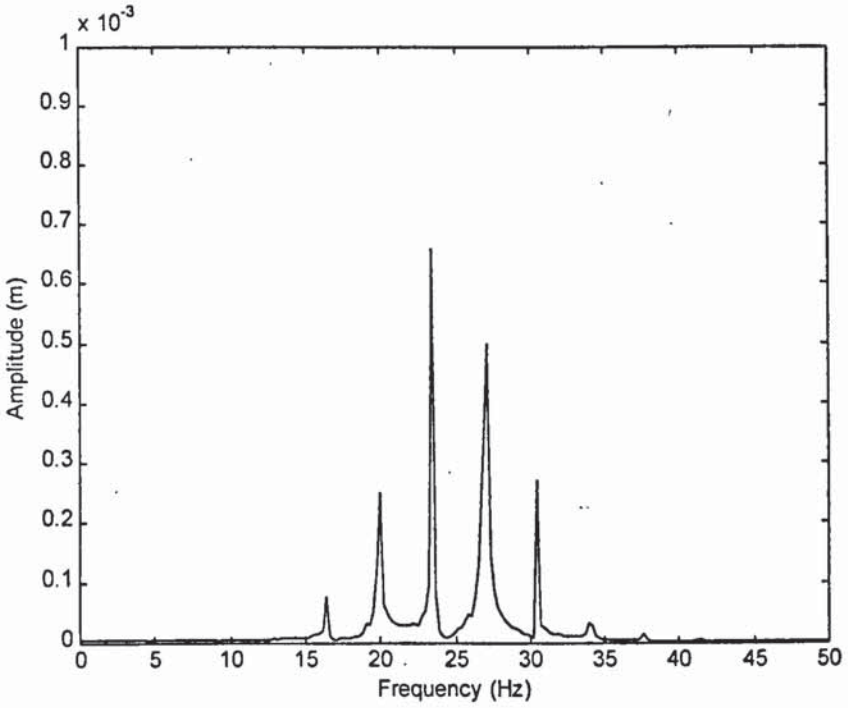

Figure 5.12. Frequency response at shaft speed 27Hz.

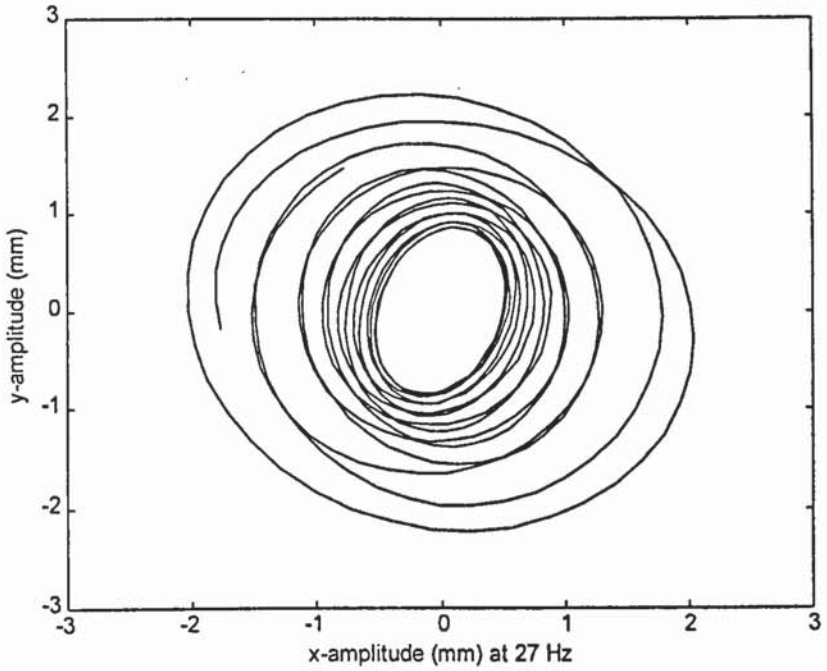

Figure 5.13. Orbit at 27 Hz (1620 rpm)

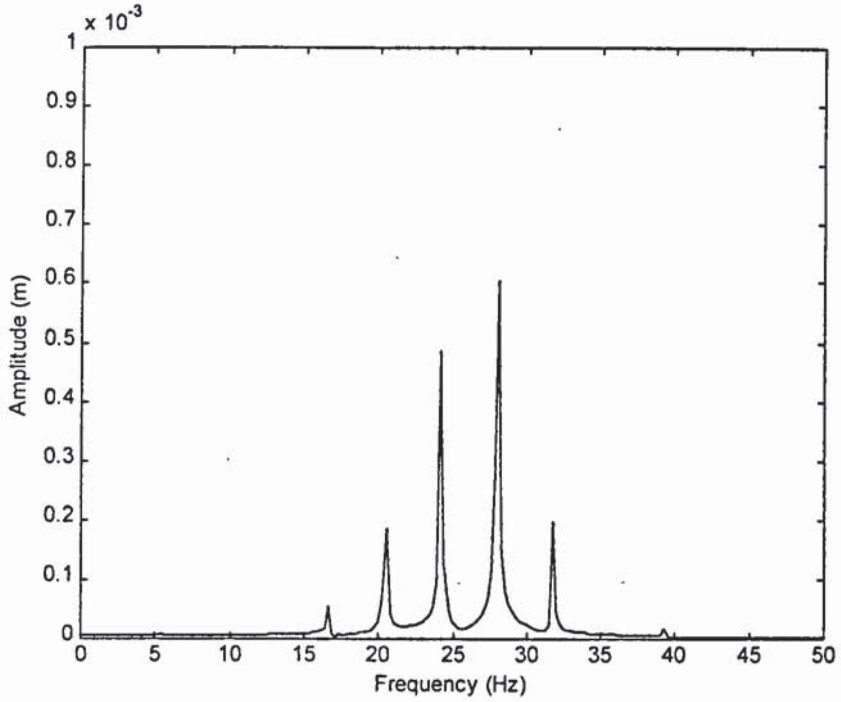

Figure 5.14. Frequency response at 28 cycle/s

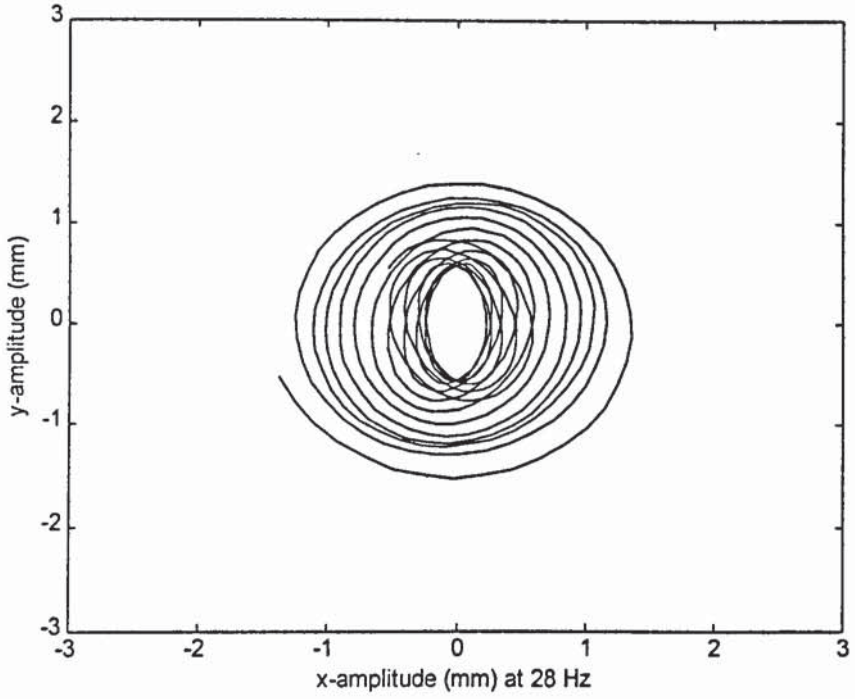

Figure 5.15 Orbit at 28 Hz (1680 rpm)

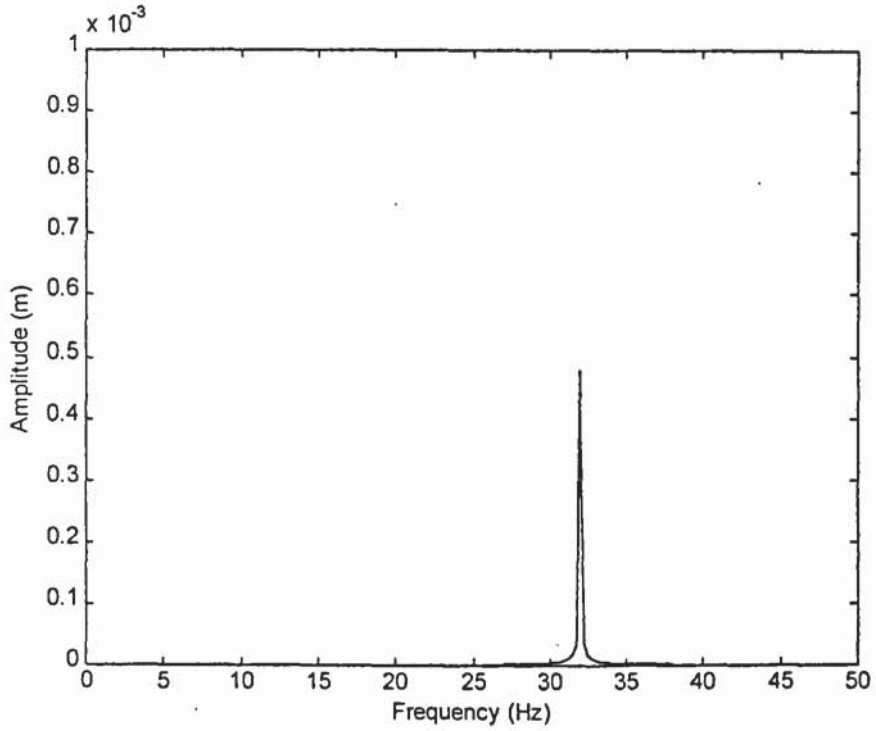

Figure 5.16 Frequency response at 32 Hz

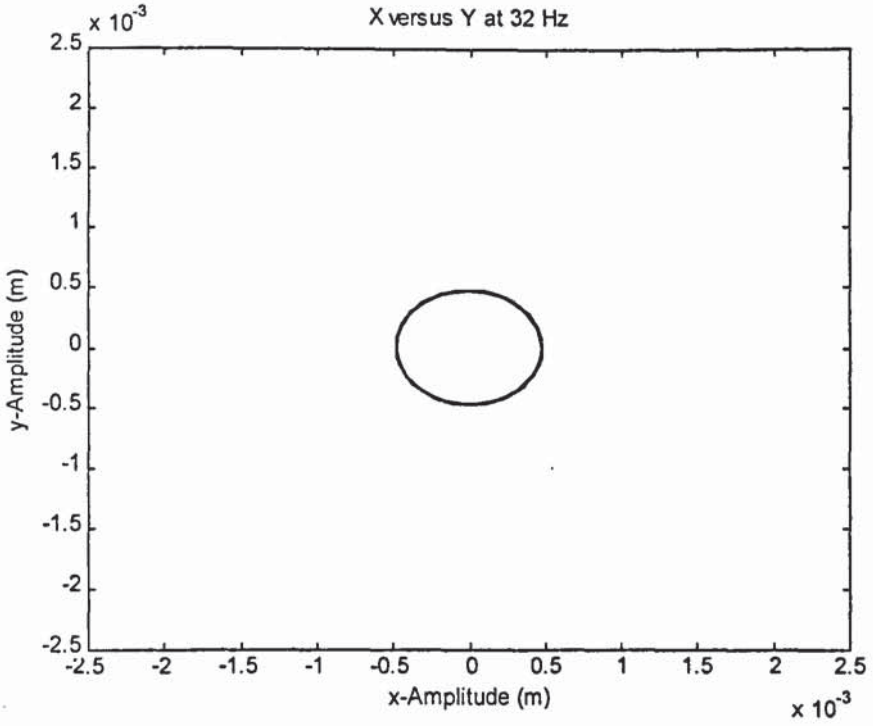

Figure 5.17 Orbit at 32 Hz (1980 rpm)

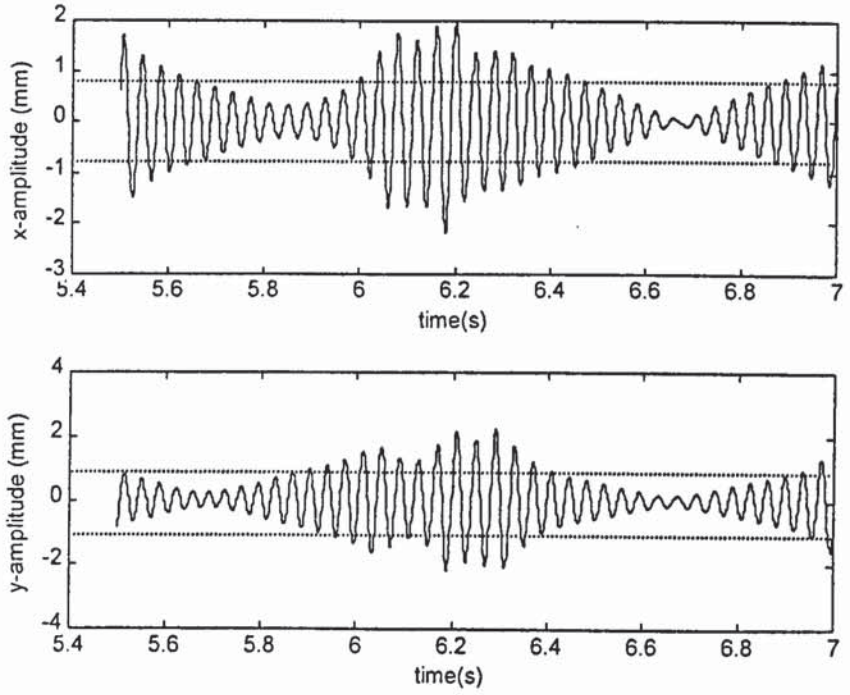

Figure 5.18. Run-up time histories

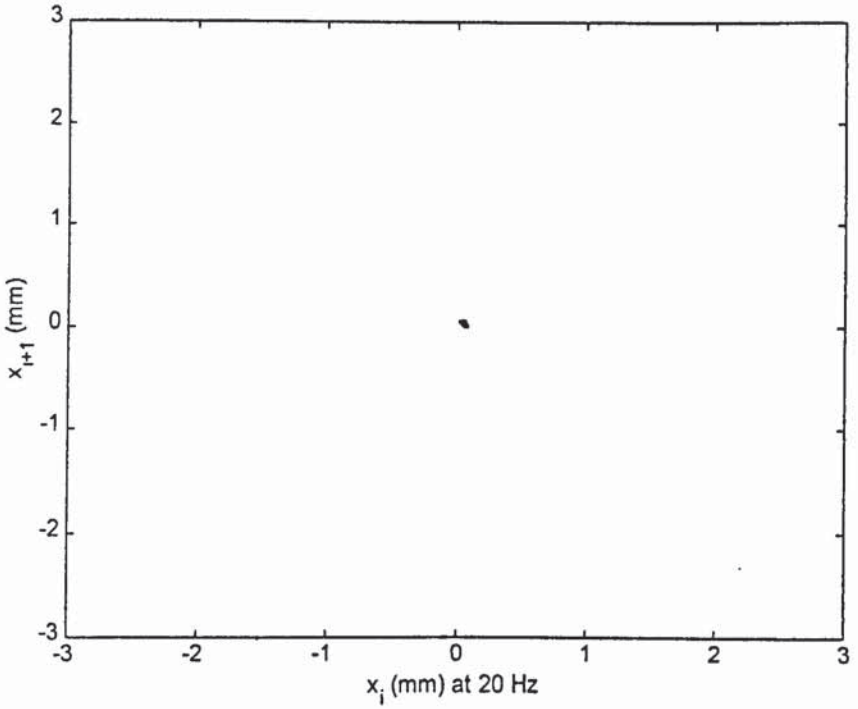

Figure 5.19: Pseudo-phase plot at 20 Hz (1200 rpm) in x-direction

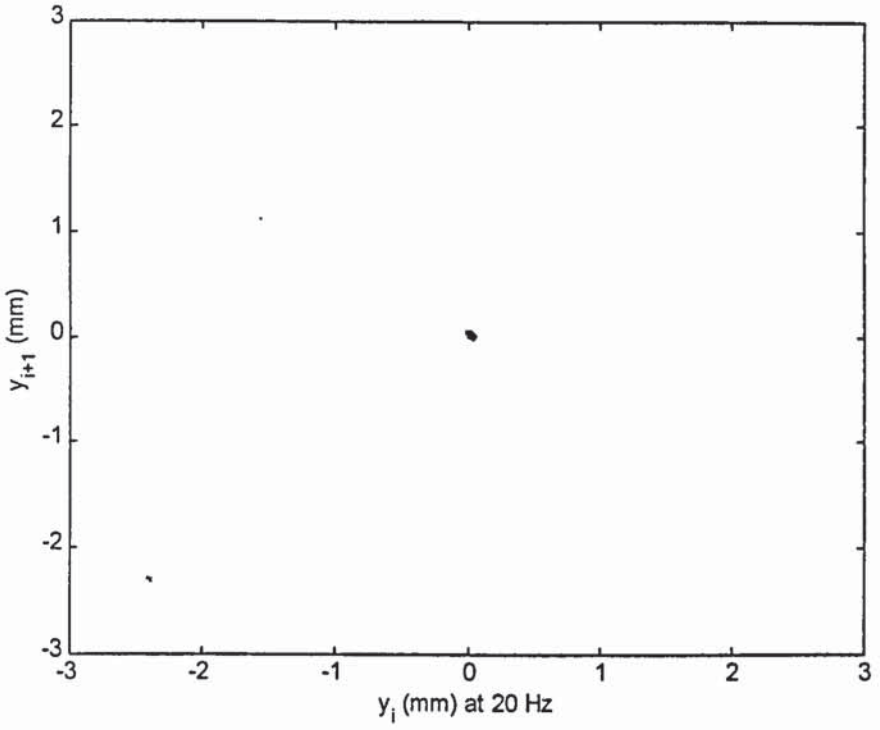

Figure 5.20: Pseudo-phase plot at 20 Hz (1200 rpm) in y-direction

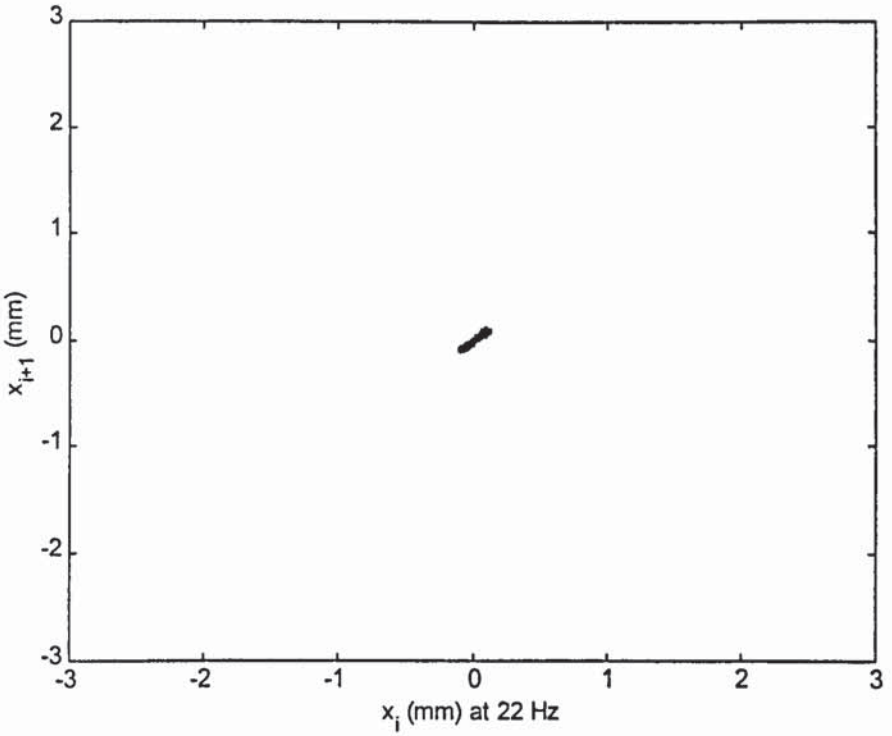

Figure 5.21: Pseudo-phase plot at 22 Hz (1320 rpm) in x-direction

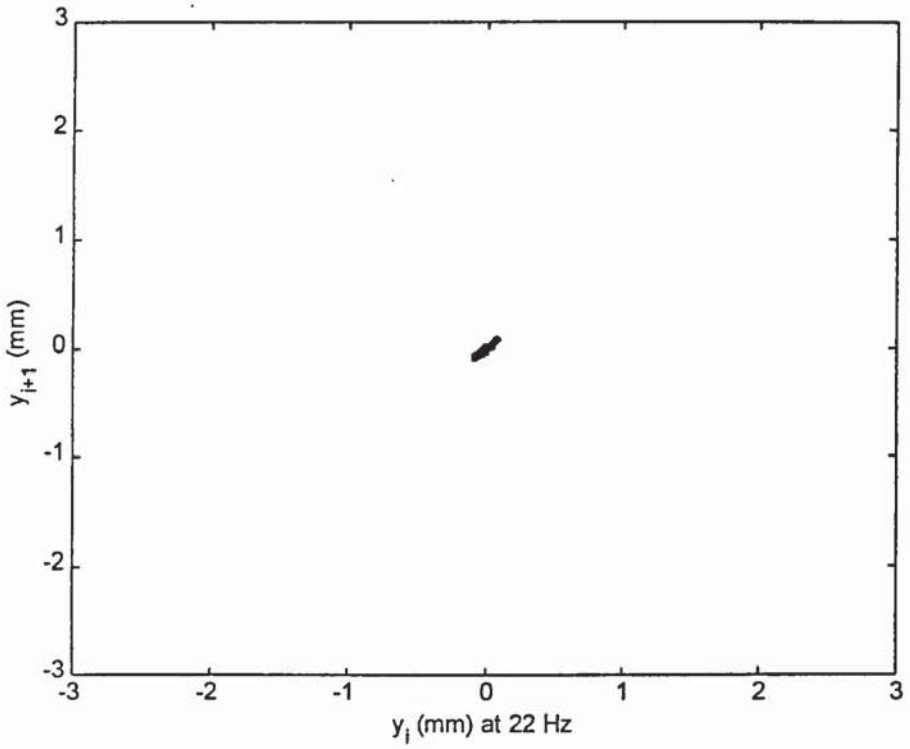

Figure 5.22: Pseudo-phase plot at 22 Hz (1320 rpm) in y-direction

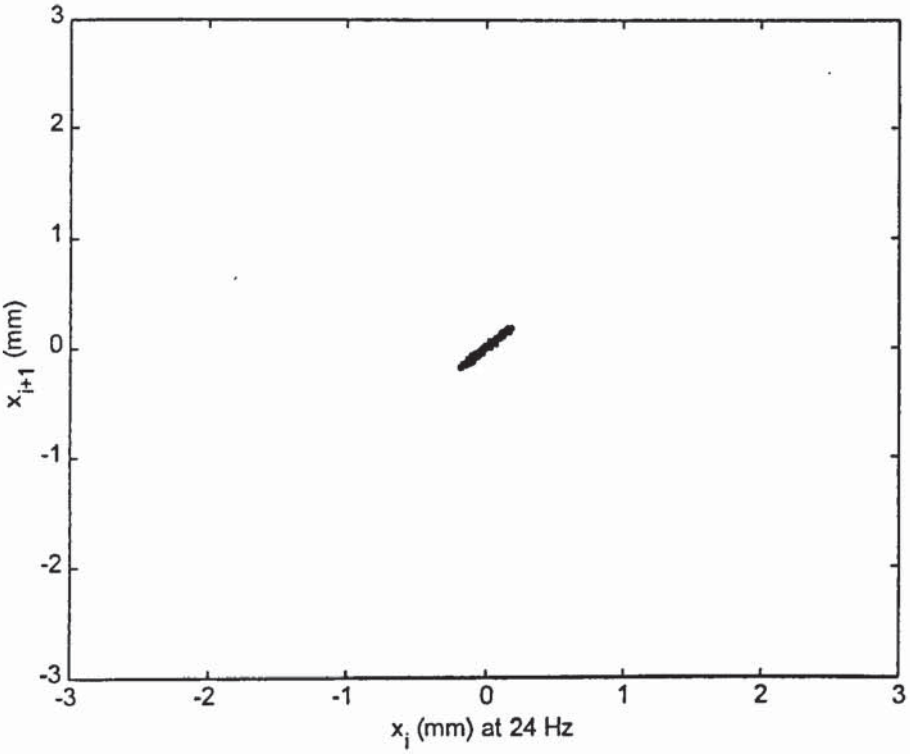

Figure 5.23: Pseudo-phase plot at 24 Hz (1440 rpm) in x-direction

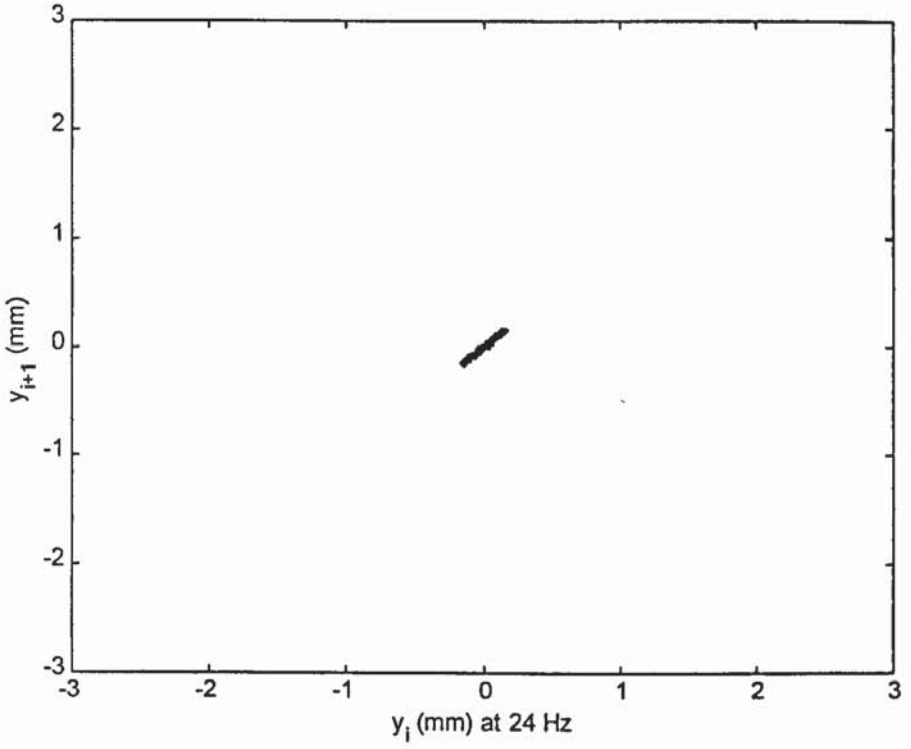

Figure 5.24: Pseudo-phase plot at 24 Hz (1440 rpm) in y-direction

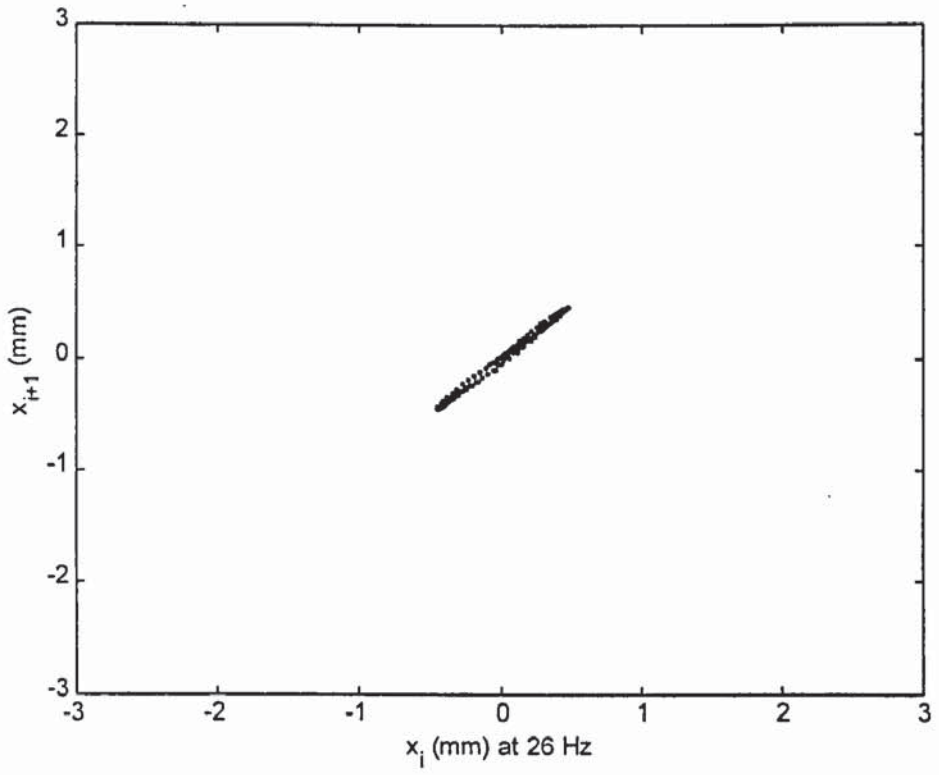

Figure 5.25: Pseudo-phase plot at 26 Hz (1560 rpm) in x-direction

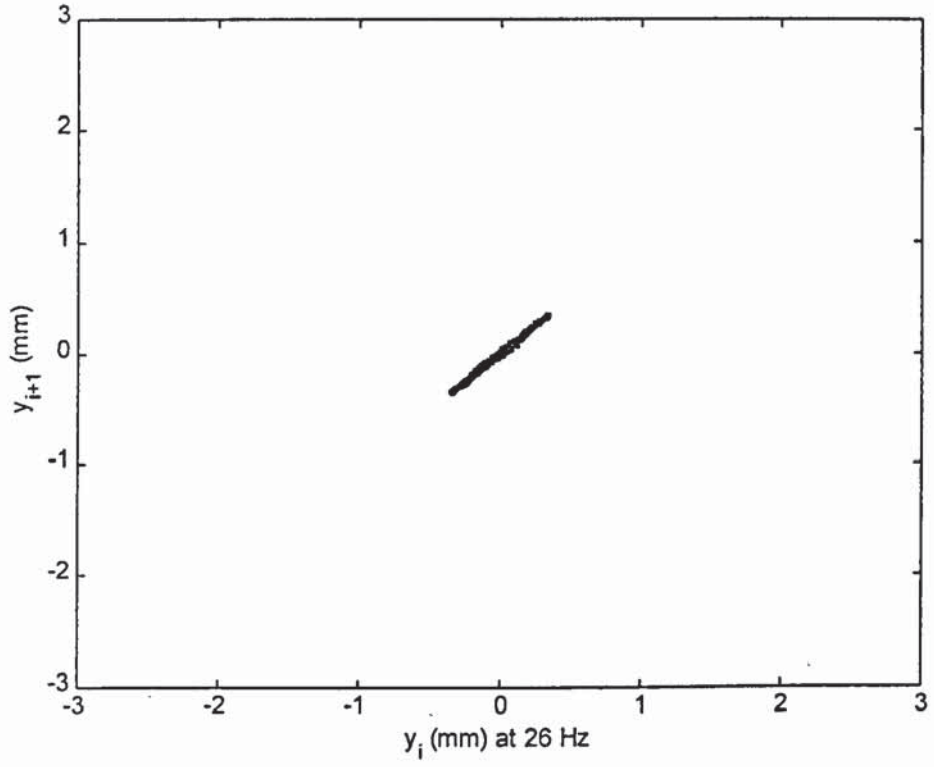

Figure 5.26: Pseudo-phase plot at 26 Hz (1560 rpm) in y-direction

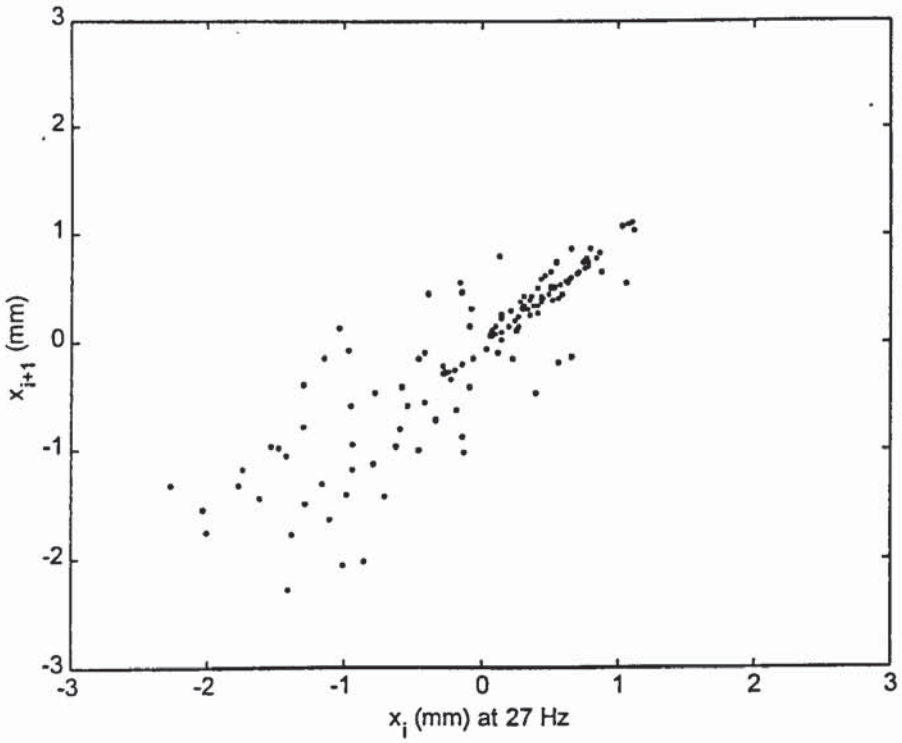

Figure 5.27: Pseudo-phase plot at 27 Hz (1620 rpm) in x-direction

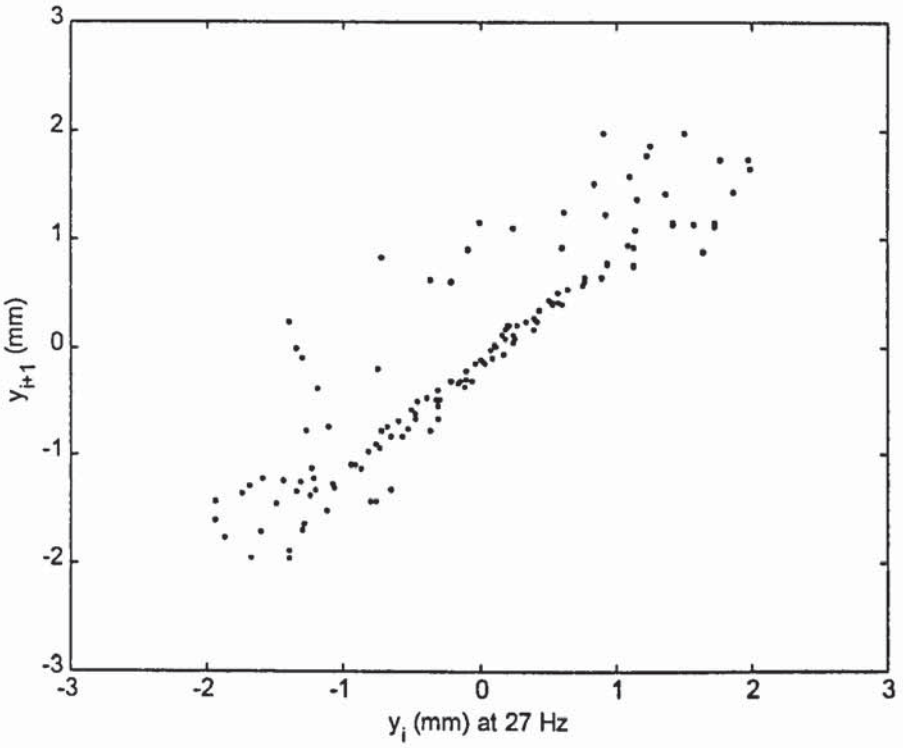

Figure 5.28: Pseudo-phase plot at 27 Hz (1620 rpm) in y-direction

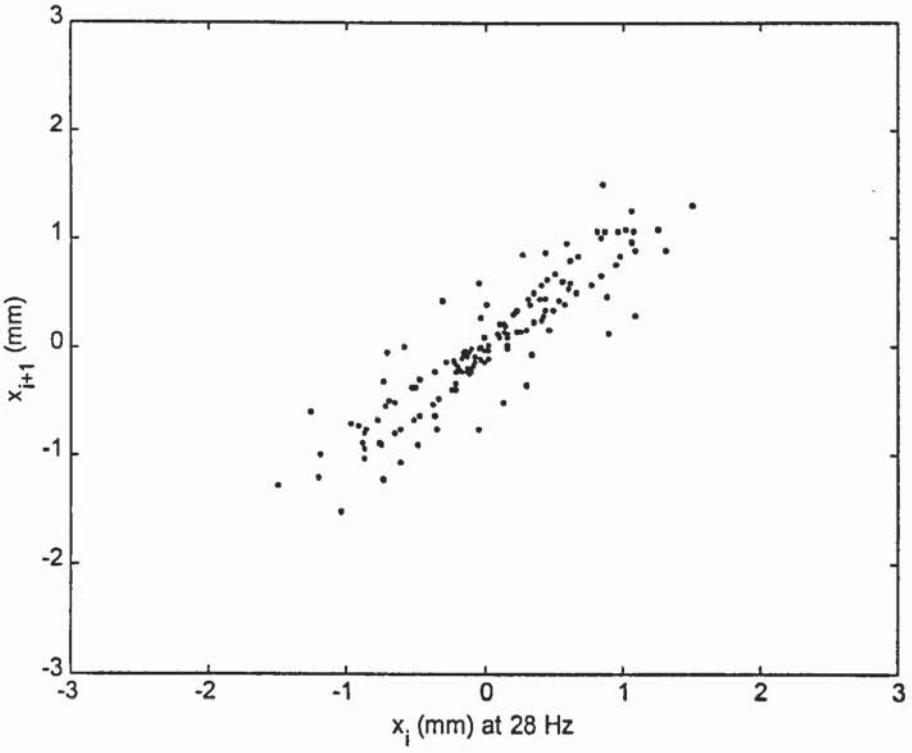

Figure 5.29: Pseudo-phase plot at 28 Hz (1680 rpm) in x-direction

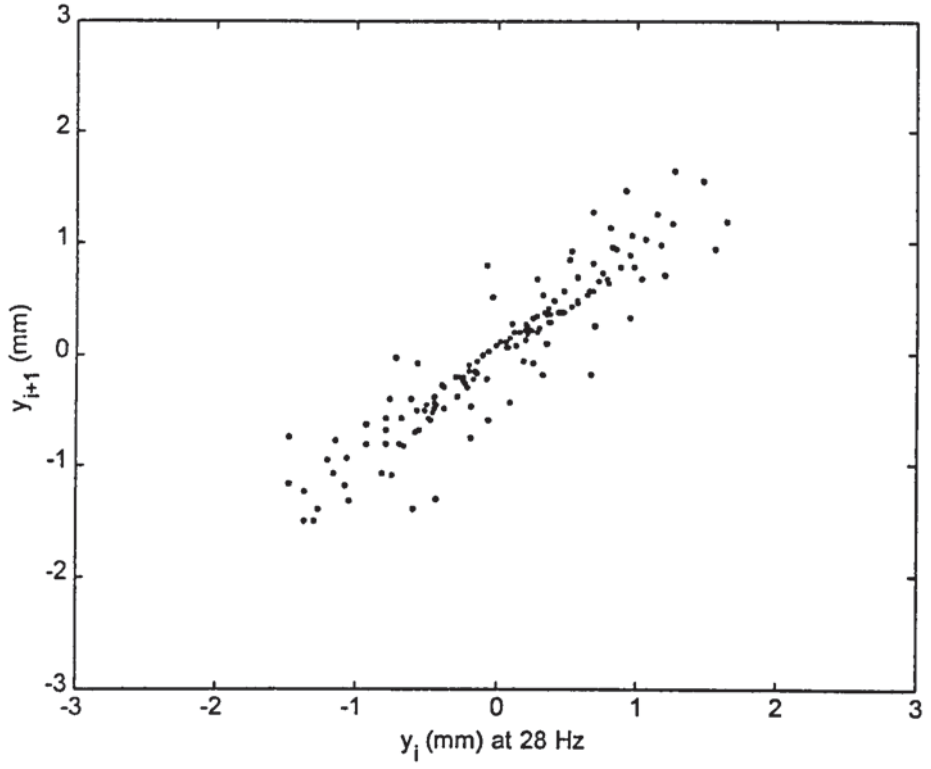

Figure 5.30: Pseudo-phase plot at 28 Hz (1680 rpm) in y-direction

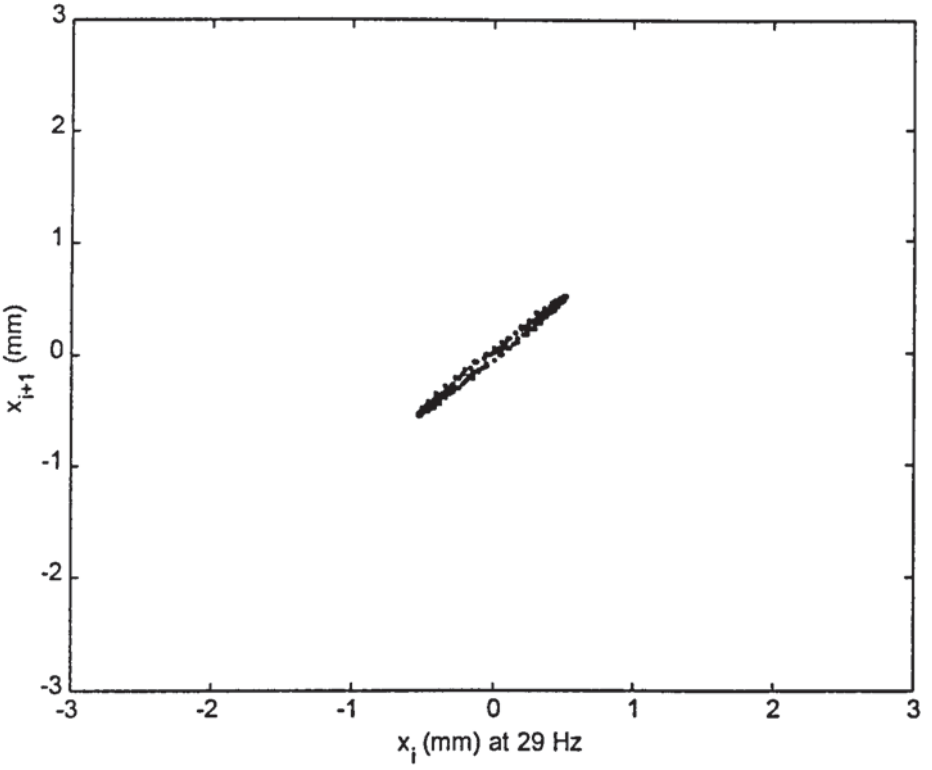

Figure 5.31: Pseudo-phase plot at 29 Hz (1740 rpm) in x-direction

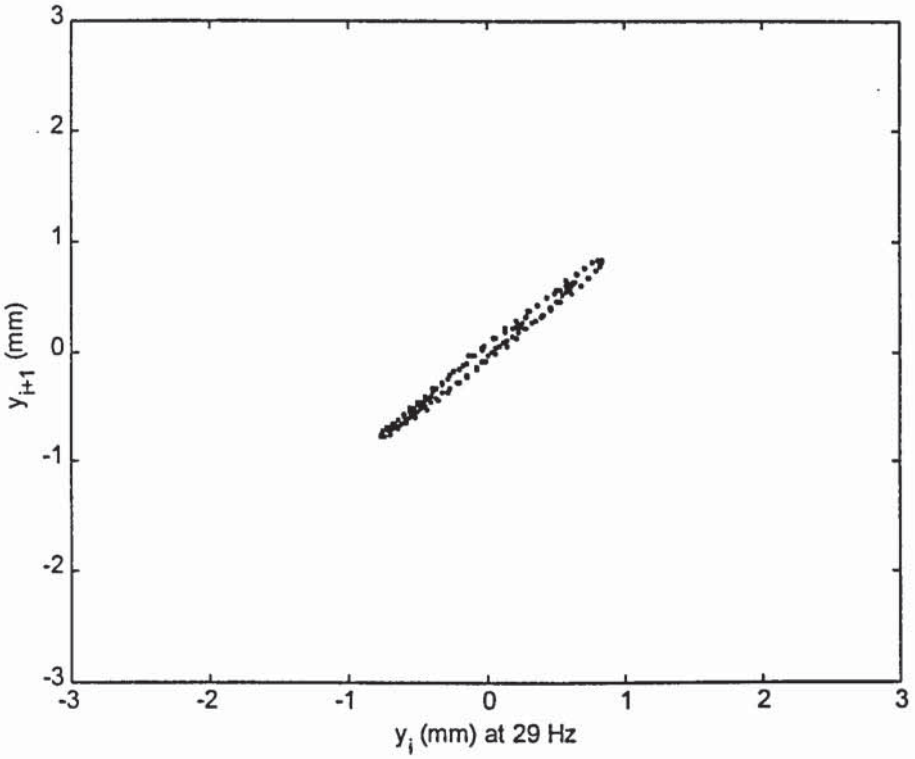

Figure 5.32: Pseudo-phase plot at 29 Hz (1740 rpm) in y-direction

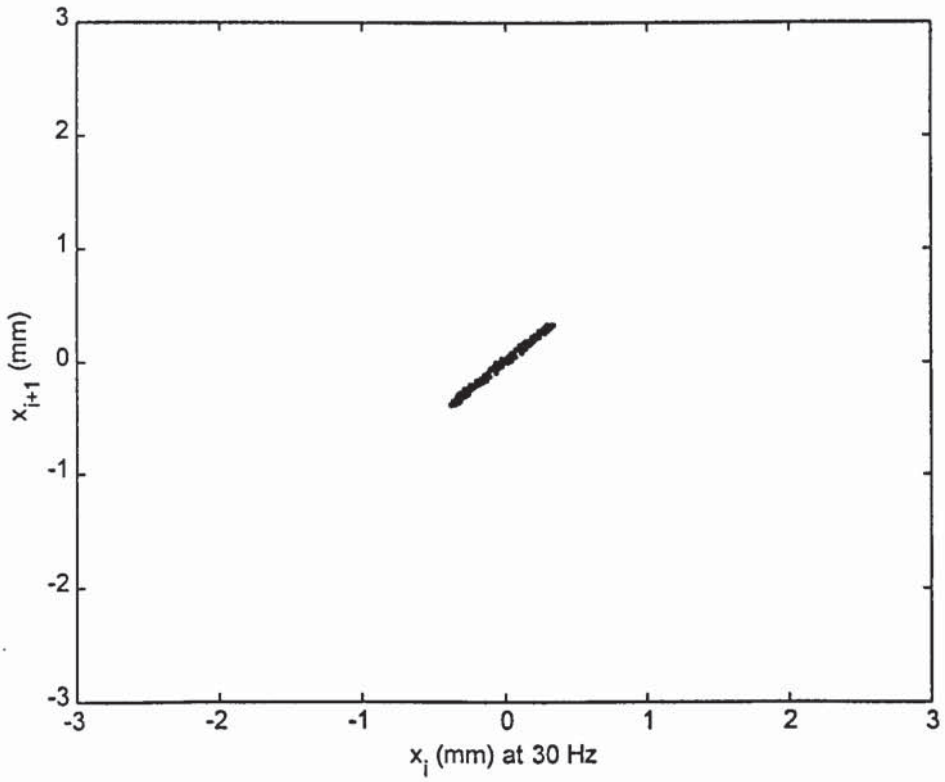

Figure 5.33: Pseudo-phase plot at 30 Hz (1800 rpm) in x-direction

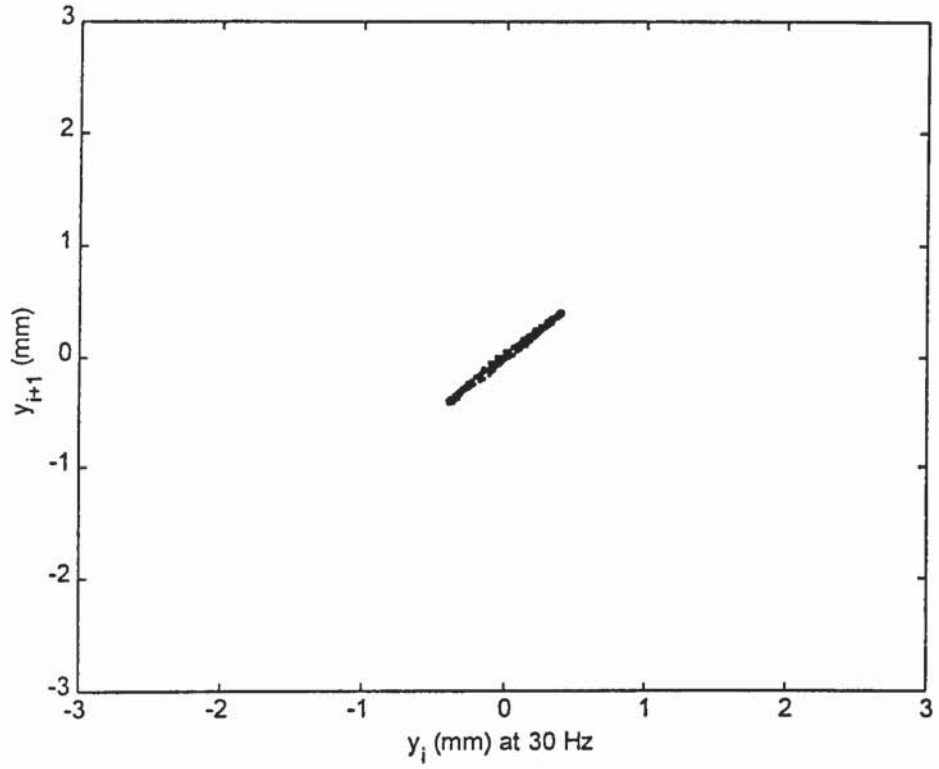

Figure 5.34: Pseudo-phase plot at 30 Hz (1800 rpm) in y-direction

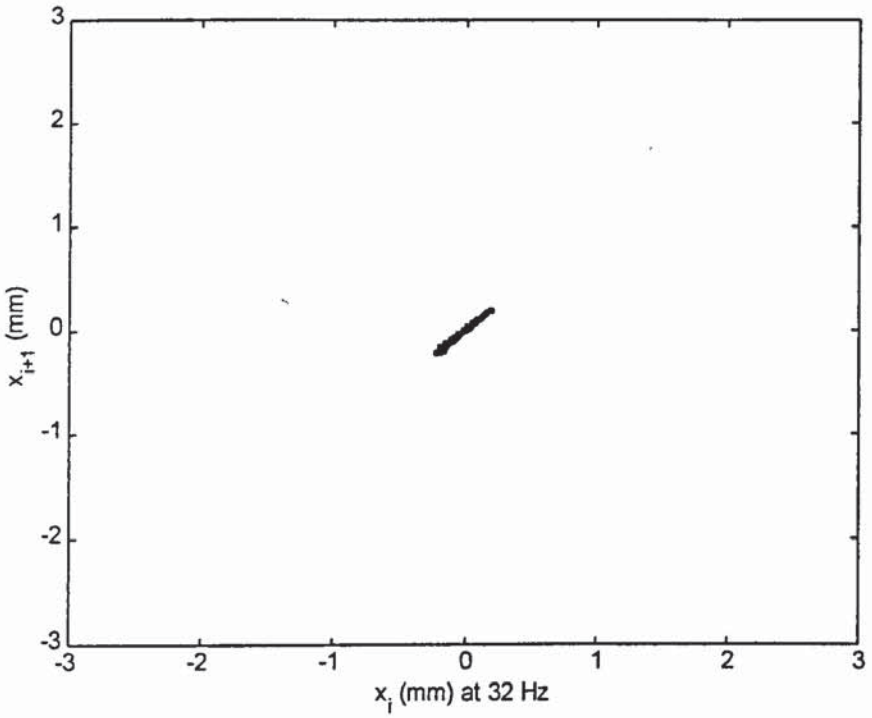

Figure 5.35: Pseudo-phase plot at 32 Hz (1920 rpm) in x-direction

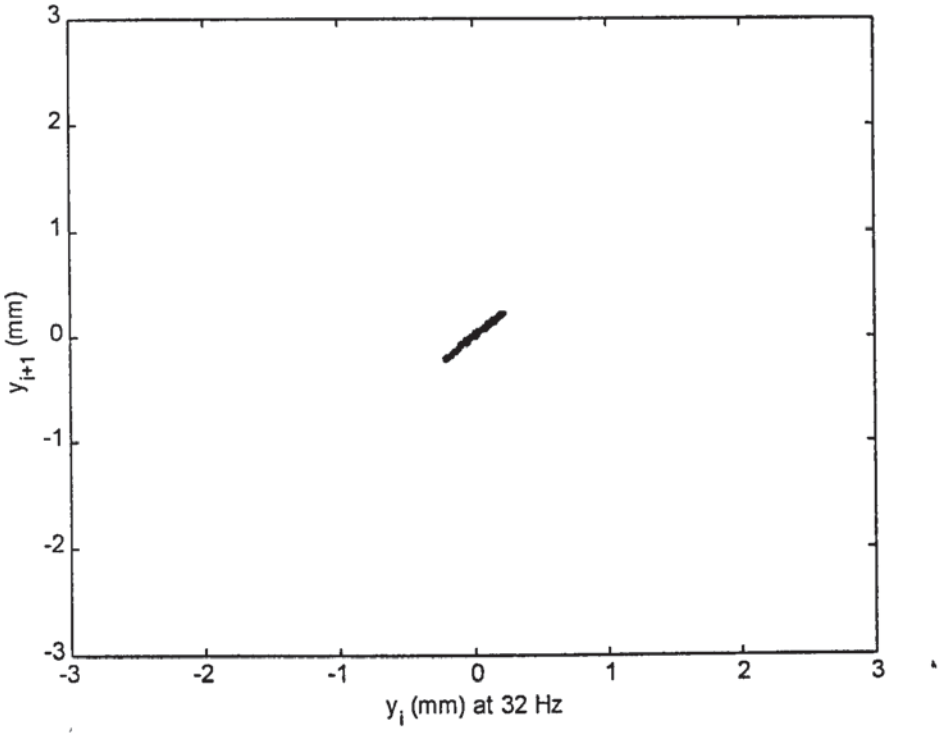

Figure 5.36: Pseudo-phase plot at 32 Hz (1920 rpm) in y-direction

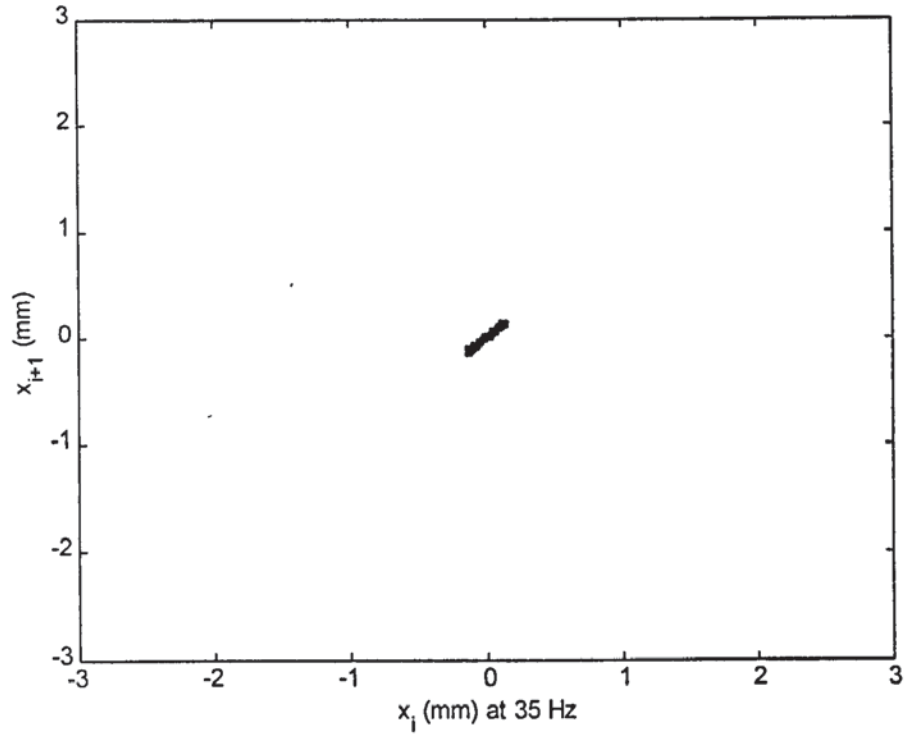

Figure 5.37: Pseudo-phase plot at 35 Hz (2100 rpm) in x-direction

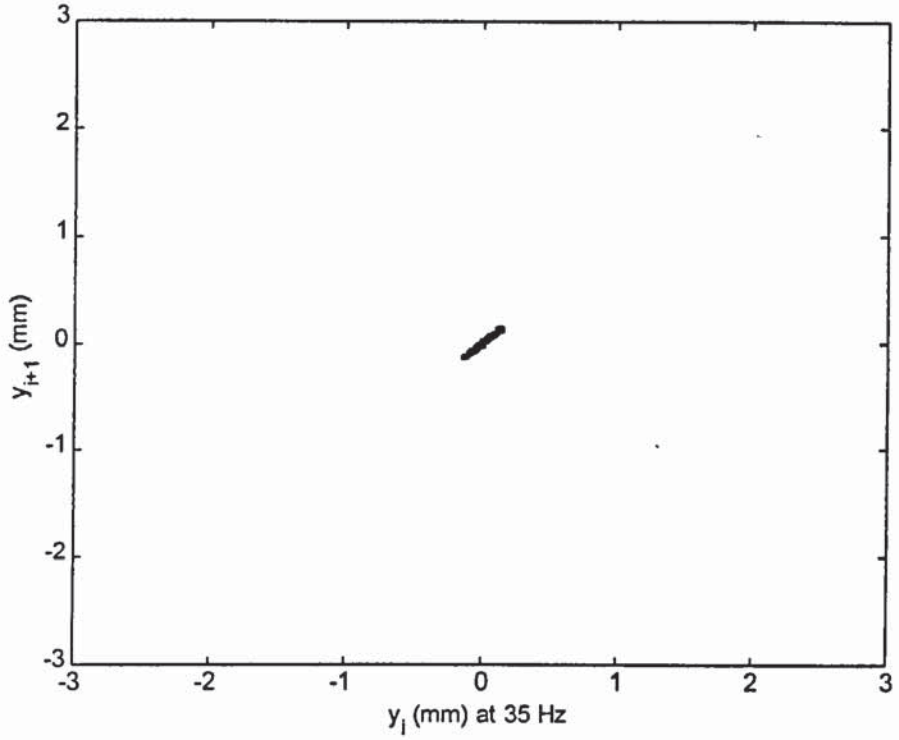

Figure 5.38: Pseudo-phase plot at 35 Hz (2100 rpm) in y-direction

5.3 DISCUSSION ON SIMULATION RESULTS

Figure 5.2 shows the simulation results of the run-up of the model from shaft speed of 20 Hz (1200 rpm) to 35 Hz (2100 rpm) in 300 second. The rate was chosen because it was slow enough to be considered as steady state. Slower rate would take much a larger amount of computer memory. Figure 5.3 shows the phase angle as it passes through the resonance. There is a change of phase at the point where the amplitude passed the threshold value. However, the change of phase is not smooth. This is attributed to the non-periodic motion after the jump effect just before the resonant at 27 Hz. This effect could be described as the opening and closing of the rotor disc.

Figure 5.4 shows the variations in the amplitude with different unbalance force with the increase in the shaft speed. There was a jump occurs as the unbalance value was increased. The curves lean leftward (lower speed). These phenomena take place because of softening effect of the stiffness. It was also noted that the jump only occurs when the magnitude of the deflection is above the threshold value. Figure 5.5 shows the magnitude of unbalance of interest. As the speed reached 27 Hz and the peak of the curve leaned towards left (lower speed). This was expected since the stiffness of the opening disc, shaft and bearing and foundation has a softening effect and the opening disc stiffness is the dominant stiffness.

Figure 5.6 shows the DFT components generated from the data obtained at increments of 0.5 Hz of the shaft speed. Figure 5.6 shows the same data plotted in contour format to distinguish the related peak points. There were sidebands at frequencies range of 26 Hz to 30 Hz. The sidebands could be attributed to the non-periodic nature of the opening and closing of the disc within this frequency range.

Figure 5.7 to Figure 5.17 are the plots of the DFT components and shaft whirl orbits shown at different speeds. At lower speed i.e. 20 Hz (1800 rpm) only the shaft speed was observable and the shaft orbit was relatively small. As the shaft speed increased the amplitude increased and the whirl amplitude also increased. However when it reached resonance and the deflection exceeded the threshold value, there was more that one peak in the DFT and the shaft orbit became unsteady. The time domain plots in the x and y directions are shown in Figure 5.18. After the speed reached 30 Hz (1800 rpm) the unstable whirling becoming stable again.

The plot of the amplitude and velocity in the x and y axes (phase plot) were used to show the phase trajectory of the system. For a sinusoidal excitation the phase trajectory will depict as close circle. However, to make comparison with the experimental result pseudo-phase plot were used instead. Figure 5.19 to Figure 5.38 are plots shown for the x and y directions at different speeds. The plots show the periodicity of the data.

Furthermore, by taking only the point at each cycle at the same position and plotting these points in the amplitude versus velocity diagram will determine the periodicity of the system. At low speed i.e. at 20 Hz the shaft whirl is periodic since the points focus on a single point. As the speeds increases the shaft whirl amplitude increases therefore the points scattered closely along 45° line as in Figure 5.23 and Figure 5.24. This shows that the rotor is still exhibiting periodic motion. At shaft speed close to resonance, the points are widely scattered. This shows that the motion is no longer periodic. Figure 5.25 to Figure 5.30 are the situation where the rotor motion is non-periodic.

The conclusion drawn from the results of the run-up with unbalance is that with increase in speed and maintaining other parameters constant, the vibration amplitude increases as depicted in Figure 5.3. There is sudden jump in amplitude at speed of about 25.3 Hz, before the vibration amplitude reduces again as the speed increases. The amplitude reduces slowly until it drops down at rotor speed of 28 Hz. Comparing with single stiffness system, as in Figure 5.1, the peak is slightly shifted towards the left and the higher amplitude with

broader span. Scrutinising closely in the region between 25 Hz and 28 Hz in the time histories, it is observed that the waveform is modulated, with a clear indication of the change in the stiffness from higher stiffness (k) to lower stiffness (k_1). In physical term the joint appears to open and close within a number of cycles.

The result of the change in unbalance also clearly shows that it increases with the increase in the magnitude of the unbalance. However if we look more closely to the waveform in the time domain we will observe that there is unsteady vibration in the system.

5.4 CONCLUSION

The simulation results presented in this chapter demonstrated the power of the modelling method. The developed simulation tool is sufficiently flexible to investigate turbomachinery of arbitrary geometry. The geometry chosen for the simulation tests is similar to the test rig. This is carried out in order to make the comparison between the simulation results and experimental results. Once the eigensolutions of the structures, including the speed dependency of the modal properties of the rotating part are available, the damping level and a small number of contact parameters are chosen to set up the simulation. From there on the integration of equations of motion is a standard procedure.

Chapter Six

EXPERIMENTAL STUDY

6.0 INTRODUCTION

In this chapter will be discussed the design of the test rig, preliminary testing required to commission the test rig, the sensors and the data acquisition system used.

6.1 TEST RIG DESIGN CONSIDERATION

The purpose of the test was to experimentally validate the data produced from the model of the system. This permits the understanding of the physical system and it can become the basis to assess on the validity of the model. Physical measurements would illustrate whether the predicted phenomena did appear in practice. On a simplified form, the design of the test rig was based on a *Jeffcott* rotor with discs at the mid-span of a light shaft supported by two ball bearings at the ends. The test rig consists of the shaft, rotor disc,

electric motor, supporting bracket and its foundation, flexible coupling and the ball bearing. Detail drawings of the system are shown in the Appendix D

6.1.1 Shaft

Within the limitations of the space and instrumentation, the rotor was designed to compose of a relatively stiff shaft, supported by widely space bearings. The main reason for having a stiff shaft was to minimise the lateral movement due to shaft flexure, although longer shaft will reduce the overall stiffness. A relatively large shaft span was chosen to enable significantly large transverse movement to be recorded. Since the joint was clamped by a weak spring, it was expected that most of the transverse movement of the shaft would be cause by the disc joint opening. The large shaft span would amplify the responses to enable the motion be captured by the transducers. Initially, a mild steel shaft of diameter 16 mm was used. However this shaft had relatively large bow which caused excessive whirling of the shaft. A large balancing mass was required to balance the shaft bow and the unbalance mass of the disc. Therefore to minimise the effect of shaft bow a new straighter shaft was used instead. This was made from silver steel, a material less prone to distortion in manufacture.

6.1.2 Rotor Disc

The rotor disc was made up of two identical half discs which were properly aligned with a spigot. Each piece was machined from single piece mild steel, thus maintaining the homogeneous property. The

discs were held together by equally spaced tension bolts around the disc circumference to give an even compression on the rotor. By measuring the compression of the springs, a good approximation of the clamping force could be determined. Surface roughness plays an important role in defining the joint stiffness and the disc surfaces were machined to be as identical as possible, for excellent contact between the two surfaces. The surface roughness of the rotor disc was limited by the machining tolerances. Since the surface roughness affects the vibration properties of the system, the value of the surface roughness was measured to check for consistency in value. The average surface roughness of both halves of rotor discs are 3.72 μm and 4.18 μm, measured using surface roughness machine. No misalignment occurred when the two surfaces were put together. The bolted rotor disc was located at the mid-span of the shaft. This arrangement minimised the gyroscopic effect due to transverse rotation of the discs. However, it was anticipated that the discs might encounter some slight gyroscopic effect when the discs start to open. The discs arrangement is shown in Figure 6.1.

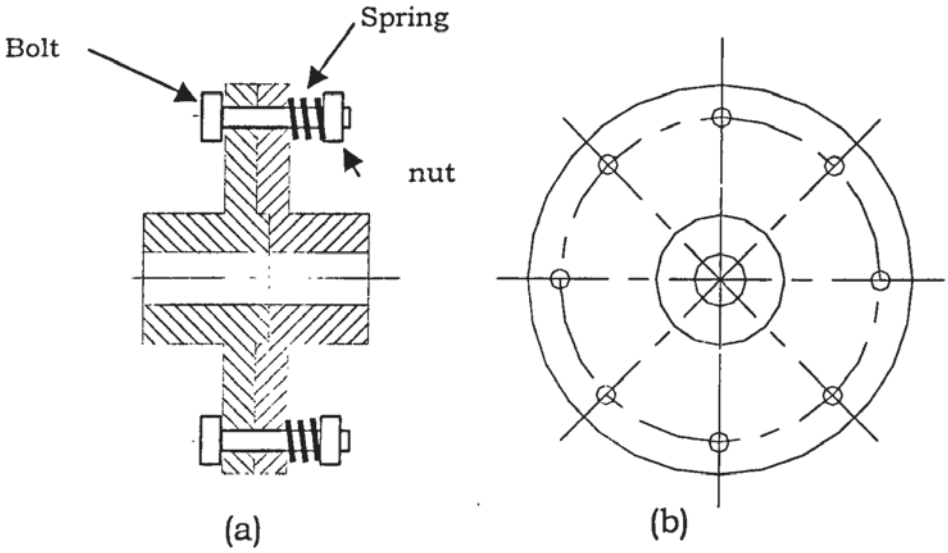

Figure 6.1: Rotor discs assembly

The rotor discs could be clamped together evenly by an axial force created by either a single central bolt or bolts that are placed around its circumference. Due to practical limitations, the bolts were placed around the circumference of the disc (Figure 6.1(a)). However, the disadvantage of this arrangement was that the axial force might not be consistent at all the application points. The additional masses of the bolt and nuts were required to be balanced. Since the aim of this study was to observe stiffness changes, it was critical to exert axial forces that were measurable and so that stiffness would be constant within the range of the movement. Springs of the same stiffness were used to exert the axial force on the rotor. Even forces were applied to each bolt by measuring the compression on each spring and these values were adjusted to be as close as possible. Thus, the unwanted effect of uneven compression was eliminated, as this would have created the unsymmetrical shaft problem. Due to the limitations in the instrument available, the spring compression was measured using a calliper gauge. The springs were selected from a spring catalogue and the spring rates were assumed to be constant and consistent within the experimental range. Springs made of music wire steel with spring rate of 10.63 N/mm with square and grounded ends were selected. To understand the dynamic effect of the joint on the rotor it was necessary to make sure that the joint stiffness was relatively low to give the exaggerated softening effect of the joint.

Another important consideration in the fabrication of the rotor was the effect of the internal damping. This normally occurred in the interface between the rotor disk and shaft. Internal damping was known to have a destabilising effect of rotating machinery and had to be reduced to avoid instability. Therefore, by attaching the rotor discs

to the shaft using split pins and glue, the effect of internal damping was reduced. Apart from that, the clearance between the shaft and the hole was made minimum, to allow effective gluing for good contact between the two surfaces.

6.1.3 Supporting bracket and ball bearing

The rotor shaft system was supported by two ball bearings. Deep groove ball bearings with internal diameter of 15 mm were used to support the shaft. The inner race of the bearing was glued to the shaft to avoid any axial movement between the shaft and bearing. Since clearance always existed between roller and the races in a bearing, to allow smooth movement of the bearing, a small axial pre-load was applied to reduce this clearance. Disc springs were used to apply the small pre-load to the bearing. The pre-load axial force had to be sufficient to avoid any unwanted vibration from the bearing clearance. An unnecessary high pre-load would have effected the transverse movement of the shaft.

Another important feature in the design was that the bearings were attached to the supporting bracket by a plate that was bolted to the supporting bracket. The plate that held the bearing was fabricated to hold the bearing from axial movement by at stopper at the ends and a clamping nut. This was to avoid any clearance between the outer race and the holding plate. The bearings were placed on the supporting frame that was specially designed to hold the bearing in place and would readily be bolted to the rigid foundation as shown in Figure 6.2.

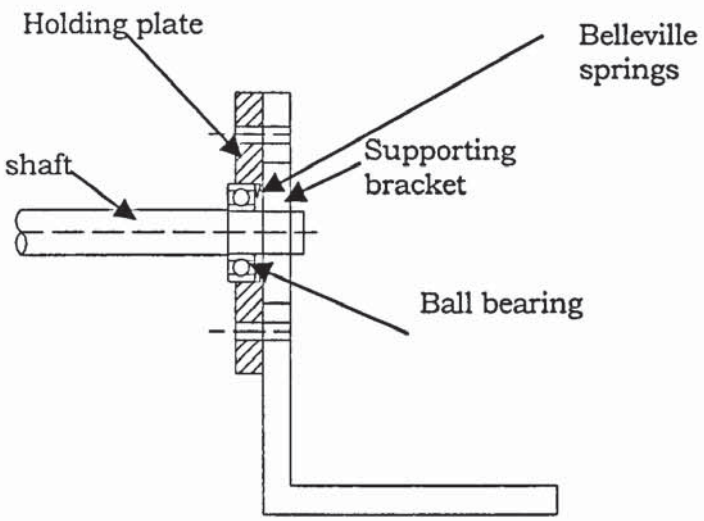

Figure 6.2: Bearing support mechanism

The selection of the ball bearings was not critical since the load that acted on the bearing was relatively small, compared with the bearing rating. However, it was important to select ball bearing taking into consideration that roller bearings create unwanted vibration due to the bearing clearance and this vibration is usually a non-linear vibration. Although its amplitude is small compared with the rotor vibrations, this might generate an unwanted effect in the overall data collected. Applying a small axial force to reduce the clearance reduced this effect. However there was a problem associated with applying the axial force, as a large axial force will hamper the opening of the rotor half. Too large an axial force would decrease the damping value and reduce the resonance frequency of the system.

6.1.4 Motor and Controller

The rotor was driven by a brushless Maxon 250 Watt, D.C. motor that was capable of accelerating the rotor at the desired rate. The main criterion for selection of the motor was its capacity to rotate the system to just above its first resonance with relatively high angular acceleration. Determination of the acceleration was based on the amount of information that was to be accumulated during the acceleration or deceleration. The controller used was an open loop controller where the speed of the motor was directly proportional to the input voltage.

6.1.5 Transducers

The transducers used were non-contacting proximity sensors. To avoid spurious recording of relative motion, they were supported on a rigidly made structure. The sensors produced a linear output voltage directly proportional to the distance between the target and sensing face. The housings are made of an anodised aluminium and the sensing face is ceramic. It had the characteristics of a good linearity and high repeatability. RS M18 analogue output proximity sensors were used. The sensors had a sensing distance range of 2 to 5 mm. with output at 3.5 mm distance equal to 5 V. The sensitivity of the transducers is 2.66 V/mm. Four transducers were used to measure movement in the horizontal and vertical directions.

6.1.6 Coupling

A flexible coupling was used to couple the motor to the shaft. It provided a means of transmitting the necessary torque to drive the rotor and also to isolate the vibrations induced by the rotation of the rotor system. The coupling was chosen to be reasonably flexible and relatively strong in order to withstand the transverse vibrations generated by the system. Since a reasonably high torque was required to run the rotor system at the speed required and to maintain the constant speed, a proper choice of flexible coupling was necessary. For this a bellow flexible coupling with 8 mm hole diameter was selected.

6.1.7 Other considerations and assumptions

In the design of the test rig there were features that were required for the experiment to be successfully conducted. Some of the features of the design are as follows:

- The shaft was straight and rigid to eliminate unnecessary rotor balancing due to shaft bow. Shaft bow will affect the magnitude of imbalance since it axis of rotation is not coincident with the axis of rotation of the rotor-bearing system. Reducing the effect greatly facilitates the balancing process and reduced the error in the experimental results.

- Coupling mechanisms with a facility of measuring the deflection at the centre and moment between the discs. The mechanism allows

the measurement of the opening of the gap due to deflection of the shaft caused by the unbalance force.

- The facility to test with different bolt tensions. Different bolt-axial force can be applied on the rotor, hence giving different restoring force values.

The data for the selected design is given in Table 6.1.

Length(mm)	800
Diameter(mm)	16
Disc diameter (mm)	120
Total discs mass (kg)	2.5
Disc thickness (mm)	10
Hub diameter (mm)	25
Shaft Material: Silver Steel, Density: 7850kg/m^3, E=210 10^9N/m^2	

Table 6.1: Dimensions of the Rotor.

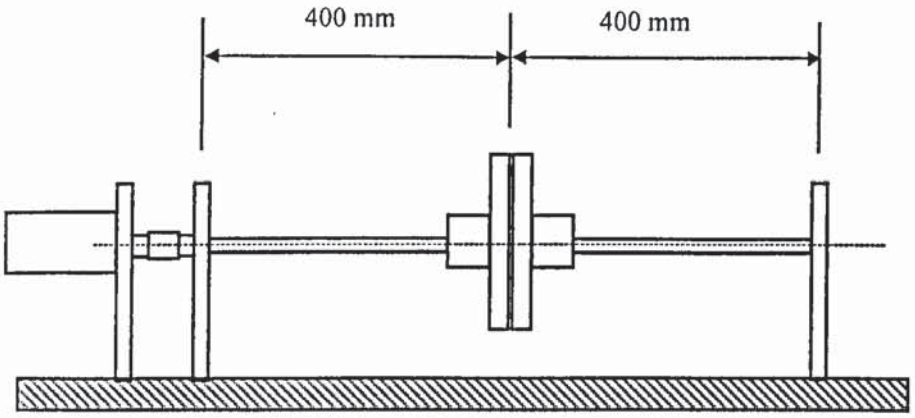

Figure 6.3: Schematic layout of test rig

The set-up of the experimental apparatus is as shown in Figure 6.3. Figure 6.4 shows the photograph of the test rig. The shaft diameter and the mass of the rotor were chosen using analysis based on the Rayleigh method with the assumption that the lowest frequency should lie in the range of 20 to 40 Hz. This method provided the rough estimation on the physical size of the shaft and the rotor disc based on the required system first natural frequency (or resonance). Once the shaft size had been determined the other components of the test rig could be selected.

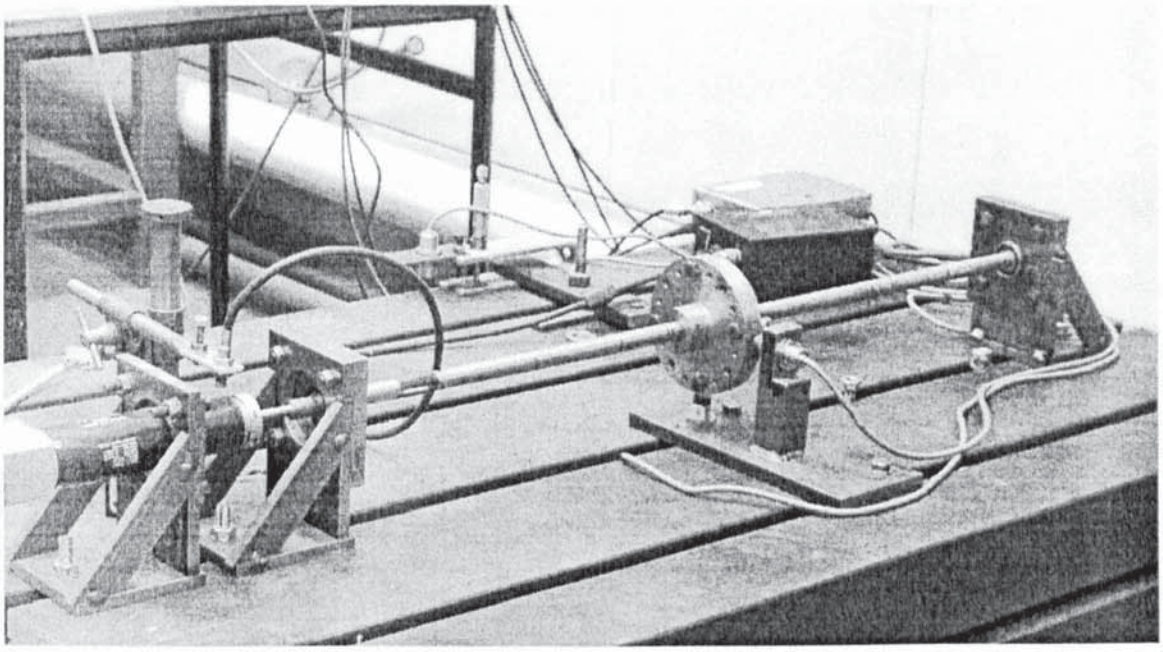

Figure 6.4. Bolted Rotor System

Since the axial load was very small for the system compared to the radial load due to the imbalance mass, the bearings used for the rig were two deep groove ball bearings. With a horizontal arrangement of the rotor axial thrust could be considered negligible. A special thrust bearing would be required for a vertical rotor as the bearing supports

the whole weight of the rotor. To determine of the size of shaft and the weight of the rotor, the critical speed for the system was adjusted to between 25-30 Hz. This was carried out so that during the experimental analysis the rotor speed did not need to be too high. This avoided the unnecessary high speed and at least one critical value was achieved during the experimental study. The rotor size and weight were also important in selecting the right capacity of the driving motor. The motor capacity selection was critical since this would influence the accelerating capacity of the system and affect the range of feasible data that could be acquired for the test rig.

The required motor torque is dependent on the system natural frequency and the required rate of acceleration. Lewis (1945) discovered the relationship between the rate of acceleration and the natural frequency of a system. Acceleration at too lower rate might give an unnecessary large amount of data. Acceleration, at too high a rate might accelerate the rotor to the critical region too quickly and insufficient data might be collected. Lewis formulates the equation below based on the experimental results:

$$q = \frac{N^2}{h} \tag{6.1}$$

Where:

q is a measure of the rate at which the system is accelerated (dimensionless).

N natural frequency of the vibrating system in rad/s.

α acceleration of the system in rad/s^2.

The measure of q represents the rate of system to be accelerated during the experiment. Note that q is inversely proportional to α. From (6.1), q=10 implies an extremely rapid acceleration and q=500 implies a rather slow rate. Based on the inertia of the design a reasonable value of q is 30. With the known mass and moment of inertia of the system the torque capacity of the motor can be determined from:

$$T = I\alpha \qquad (6.2)$$

Where:

T is the torque requires accelerating the system.

I the moment inertia of the system and the motor rotor.

α acceleration required from the above equation.

For the system in consideration, the values of I, N and q are as follows:

$I = 3.2779x10^{-3}\text{kgm}$, $N = 25\text{Hz} = 157\text{rad/s}$, $q = 30$

Using (6.1), we have

$$\alpha = \frac{N^2}{q} = \frac{(157)^2}{30} = 821\text{rad/s}^2$$

Substituting this value into (6.2) we have,

$$T = I\alpha = (3.2779x10^{-3}\text{kgm})x(821\text{rad/s}^2) = 2.691\text{Nm}$$

Based on this calculation a Maxon EC brushless motor with stall torque (starting torque) of 3.017 Nm was selected. It has a power rating of 250 Watts and maximum permissible speed of 10000 rpm.

6.2 MEASUREMENT INSTRUMENTATION

Acquiring data for analysis is the main objective of the whole experimental set-up. In practice measurements are taken with the objective of monitoring, diagnosing, commissioning and quantifying tests (Vance 1988). Measurement plays an important role in vibrations studies and the right selection of the instrumentation and techniques is required for its successful application.

The vibration data is acquired at the locations where the vibrations have the greatest amplitude. Transducers are used to convert the measured quantity, i.e. mechanical response, into electrical signals, which can then be displayed, recorded, plotted or analysed using a computer. The voltage output of most transducers is an analogue signal which is time varying continuous voltage corresponding to the measured quantity. The transducer selection is based on the sensitivity, size, measurement parameter, and the frequency response. It is important to choose a proper transducer for a particular task due to inherent limitations of each transducer (Ehrich, 1992). If the shaft motion is required proximity probes that measure displacement is used. If the bearing housing or structural motion is the best indicator then a seismic transducer sensitive to velocity or acceleration is used.

In rotordynamics two most common measured variables are the vibration and rotor speed. Transducers that are commercially available can be used to measured the vibrations displacement, velocity and acceleration (Vance, 1988). The decision on which types of transducer is best to use depends on the application since the three forms of signal look different. The important factors influencing the decision are the expected range of frequencies and the mechanical mobility (inverse of impedance) of the rotor or structure where the measurement is being made.

Most vibration measurements in rotordynamics are made at the bearings, and the mechanical mobility determines the relative amplitudes of motion between the shaft, bearing and the bearing housing or foundation. Generally, measurements should be made where amplitudes are largest, and if relative motion occurs it should be measured along with the absolute motion of at least one of the parameters.

The velocity and acceleration parameters of the vibration are shifted in phase relative to displacement. Velocity is shifted from displacement by 90° and the acceleration is shifted from velocity by 90° and thus 180° from displacement. The amplitude of the vibration parameters also varies with frequency. For a constant displacement, velocity increases directly proportional to frequency, while acceleration increases with the square of frequency.

Displacement transducers are used to measure the relative motion of the shaft. Non-contacting displacement transducers (also known as proximity probes) produce a high frequency oscillating eddy currents

in the shaft without touching it. As the shaft moves relative to the sensor, the eddy current energy changes, modulating the oscillator. This signal is demodulated, providing an output signal proportional to displacement.

The parameters that are required to be determined are the displacements of the rotor in x and y directions. To measure these displacements two non-contacting displacement transducers (proximity sensors) were used.

6.2.1 Calibration

The issue that is always raised in the usage of measuring instrumentation is how accurate is the measurement. Although the manufacturer always supplements the specification which indicate the operating ranges, there is a tendency that the ranges are non-linear such that it affects the results of the measurements. Calibration is a precaution done to countercheck the reliability of the instrumentation used. Figure 6.5 shows the jig that was used to calibrate the proximity sensors. The calibration was carried out by plotting the relationship between the displacement measured by micrometer (in millimeter) versus displacement measured by proximity sensor (in volts) as shown in Figure A3.

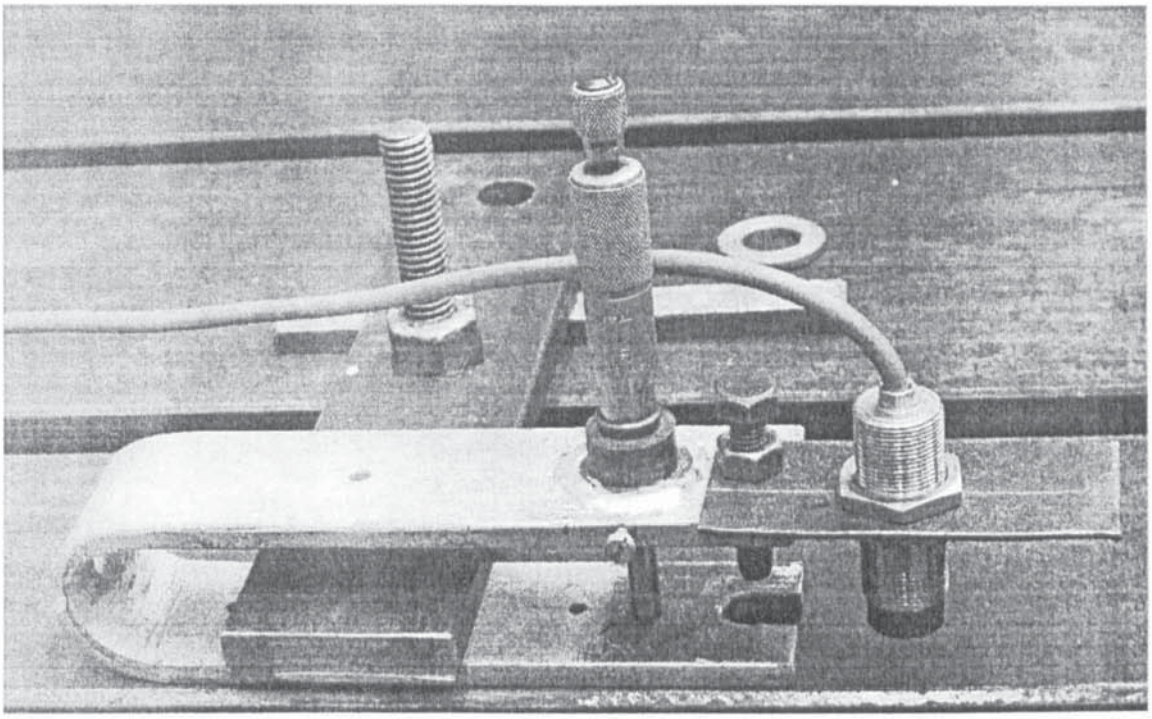

Figure 6.5. Proximity Calibration Gauge

6.2.2 Run-out

Prior to the measurement of the vibration signal it was necessary to ensure that the signals detected were actually from the shaft vibration. The disc surface that is machined may be neither perfectly circular nor concentric with the axis of rotation of the shaft. As a result the output signal from the proximity sensors would indicate vibration when in fact the shaft is not vibrating. This phenomenon is called the mechanical run-out. The vibration signal can also be apparent when the vibration level is zero and there is no mechanical run-out. Inhomogeneity of the shaft material in the form of alloying, or the presence of local residual magnetism or residual stresses caused possibly by machining process, will result in a difference of the material electrical properties at different points on the shaft circumference.

Mechanical run-out can be reduced by correcting the concentricity of the surface of the disc, while various surface treatments can remove the electrical run-out. However, eliminating the possibility of either the mechanical and electrical run-out is achieved by measuring the signal output when the rotor rotates at slow speed and subtracting this from the signal when the vibration is measured.

6.3 STATIC DEFLECTION TESTS

A static deflection test is a simple test carried out to determine the effect of load on deflection of the system. It was carried out in the vertical and horizontal direction with the shaft, bearing and supporting bracket in position. The load was applied by attaching a string on the center disc of the rotor to a crane. The load was measured using a spring balance and the deflection was measured using the proximity sensors. A schematic diagram of the test was as shown in Figure 6.6.

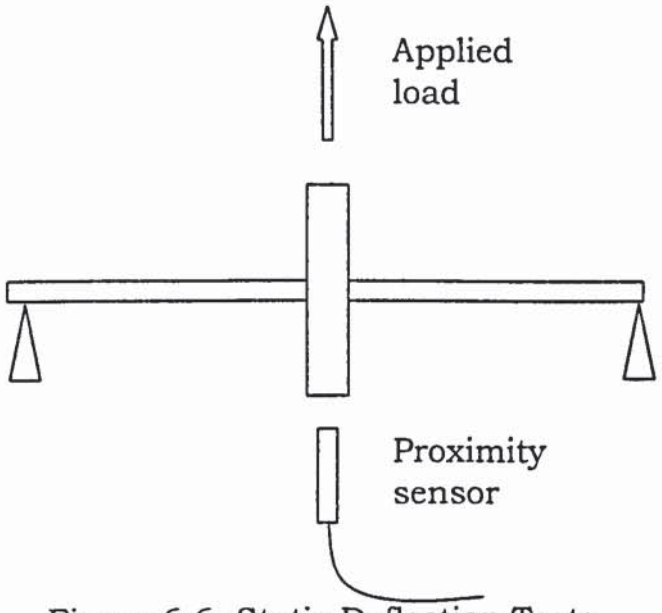

Figure 6.6: Static Deflection Tests

6.4 MODAL TESTS

Useful information can be extracted by using modal tests. Apart from obtaining the natural frequencies and mode shapes of the rotor system, indirectly the results can be used to estimate the stiffness and damping of the system in each plane (Ewins, 1983). The natural frequencies provide approximate information on the values of the critical speeds. The mode shape associated with a natural frequency provides an insight into the deformation shapes when the system is excited at those frequencies.

A modal test on the rotor system was carried out in horizontal and vertical directions using an accelerometer and an impact hammer. By defining equally spaced locations along its shaft and holding the shaft fixed to avoid any unwanted rotation, the accelerometer was positioned at the centre of the of the rotor while the excitation point was varied at different positions along the shaft. Once all the data had been collected from the measurement and excitation points, the natural frequencies, damping ratio and modes shapes were extracted using modal analysis software (SMS-STAR). Furthermore the data can be saved in ASCII format so that it can be used using MATLAB. Figure 6.7 shows the schematic of the experimental set-up.

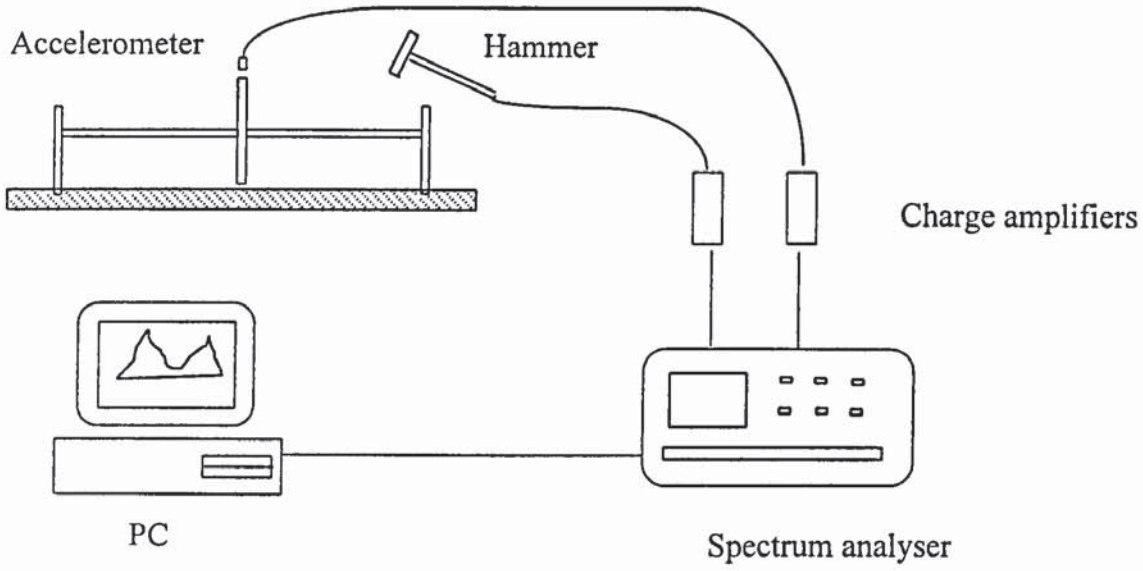

Figure 6.7. Schematic diagram of modal tests

The shaft is described as a series of numbered points where the points are linked with lines forming a wire frame representing the mode shape of the system.

6.5 BALANCING OF ROTORS

One of the fundamental requirements for the smooth operation of rotating machinery is balancing. Perfect balancing means that the axis of inertia of the rotor lies on the spin axis of the rotor. Balancing is a process of attaching masses to the rotor so that the centrifugal forces on the rotor due to the correction masses and inherent unbalance forces are in equilibrium. The art of balancing depends on devising systematic and logical methods for selecting these masses. Of

course, instead of attaching a correction mass to the shaft at an appropriate location, the same balancing effect can be achieved by removing the same size mass from the diametrically opposite side of the shaft at the same axial location.

Balancing procedures have been well established for many years for rigid rotors, although modern developments in automation, instrumentation and computation have produced marked improvements in practice. Much progress, however, has been made in the last thirty years so that routine procedures are now well established (Darlow, 1990).

A well balanced rotor avoids the existence of centrifugal forces and moments that are generated during rotation. The force that is transmitted through the shaft is supported by the bearing and the foundation. In order to lower the chance of failure due to an unbalanced rotor, balancing was required to reduce any excessive unbalance. Unbalance and shaft misalignment are recognised as two major factors that can lead to failure of rotating machinery.

Ehrich (1992) discussed the classification of rotors and their causes of inbalance. In the case of a flexible shaft balancing is required not only to balance the unbalanced mass in the rotor but also to eliminate the effect of deflection on the shaft. This is in contrast with a rigid shaft where there is no deflection in the shaft. In certain cases even the shaft bow makes balancing much more complex. Balancing can be categorised into two broad areas namely (a) balancing done by the manufacturer and (b) in-situ balancing. The first is balancing done by manufacturer on individual components as well as the final assembly,

which normally results in the successful operation of the machinery without further adjustment. The other type is field or in-situ balancing in which the rotor is balanced in its own bearings. Therefore, appropriate instrumentation is required to perform the balancing procedure.

Since the force is rotating at the same speed as the shaft, the vibration amplitude is said to be synchronous. Unbalance can also happen when the principal axis of inertia are misaligned. This results in a rotating couple which contributes to synchronous whirl.

The effect of the synchronous vibration can be reduced significantly by balancing. Balancing is much simpler if the shape of the rotor and shaft is rigid. In some running conditions the assumption of a rigid rotor is applicable, allowing the use of rigid rotor balancing procedures. A rigid rotor is considered as perfectly balanced when a principal axis of inertia passing through the centre of gravity (C.G.) is coincident with the designed axis of rotation or when the measured synchronous vibration in the machine is reduced to zero.

The unbalance force is synchronous with the speed of rotation and increases proportionally according to equation (6.3). Thus

$$F = me\omega^2 \qquad (6.3)$$

The product unbalance mass, m, and the distance of the centre of gravity from the axis of rotation, e, is called unbalance eccentricity (Ehrich, 1992).

$$U = me \tag{6.4}$$

The ultimate requirement of balancing is to reduce this value to zero. At low speeds the response due to unbalance force may be negligible, but at higher speeds the unbalance response can become undesirably high.

Balancing involves placing or removing correction masses on the rotating shaft, so that centrifugal forces due to these masses cancel out the force caused by the inherent unbalance mass, thus cancelling out the vibration. Since, in most cases, it is unlikely that an additional mass can be placed directly in the same plane as the inherent unbalance, special planes, known as balance planes, are often chosen specifically for the purpose of adding weights. This is especially facilitated in larger machines. Balancing is performed on both rigid and flexible rotors and specific methods have been developed to deal with both cases. Rigid rotors are rotors that exhibit no significant deformation, usually due to a low speed of rotation or a high diameter/length ratio. Conversely, flexible rotors are rotors which undergo substantial deformation whilst in operation, due to their long lengths and high operating speeds.

The underlying principle of all balancing techniques is to counteract the unbalance $U = me$, by introducing balancing masses:

$$U_b = -U \tag{6.5}$$

Where the unbalance is assumed to be a vector with N elements, N being the number of balancing planes.

There are many methods of balancing rotating machinery, (Darlow, 1990, Ehrich, 1992), increasing the sophistication to accommodate for the multiplanes, higher speeds, flexible rotors, modular design, to name a few.

The two methods of balancing flexible rotors are the modal and influence coefficient methods. Modal balancing is a procedure whereby the unbalance forces at each mode considered are cancelled out individually. Unbalance planes are chosen and the magnitude of unbalance components is determined, depending on the modes required by the system. Suitable unbalance masses are then chosen to counteract the forces produced by the unbalance components at each mode. Balancing by influence coefficients involves the selection of correction masses so that vibration is reduced to zero at various, specified shaft locations for various constant shaft speed. The actual influence coefficient is the response of the shaft at a given axial point due to a force acting at another (or the same) point along the length of the shaft.

A rigid rotor can be balanced by adding (or removing) correction weights in any two separate planes normal to the shaft [Vance, 1988]. The correction weights are added to translate the C.G. until it lies on the rotational axis and to rotate about the principal axis of inertia passing through the C.G. until it is parallel to the rotational axis.

For flexible rotor rotation at low speeds (speed below the critical speed), the unbalance eccentricity and the shaft displacement are in phase. Under these circumstances, the relative mass-displacement phase angle b is small, and the shaft high spot and heavy spot are said to coincide. With lightly damped rotor, speeds up to 80 percent of the critical speed, there are only a few degrees of phase lag of the displacement vector from the rotor unbalance. As the damping increases, the change in phase below the critical speed becomes pronounced (Ehrich 1992). At any particular speed μ, the relative angular position of the triad of points O, C and M is fixed with respect to each other. Points C and M orbit about origin O with respect to a relative phase angle b, which is speed-dependent (Figure 6.8). There are various methods of balancing for flexible rotors. They include the influence coefficient method, the one-shot balance method, the modal method of balancing without trial weights and the three trial run procedure without phase measurements. Each of these methods has its distinct advantages and disadvantages.

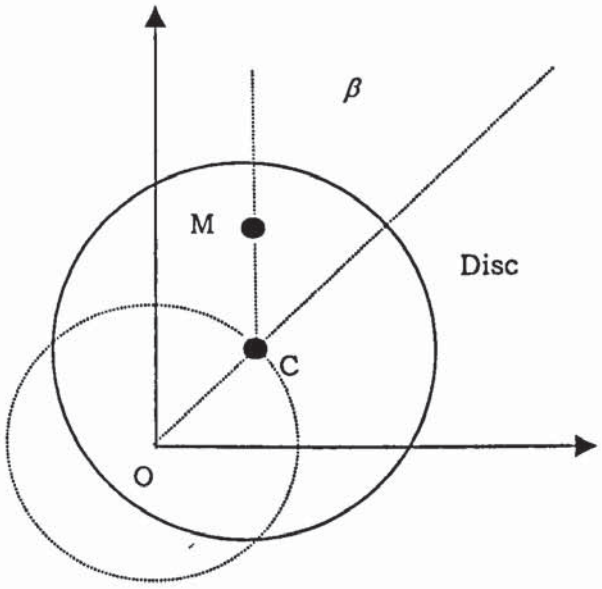

Figure 6.8:- Schematic view of deflected single-mass rotor.

6.5.1. Method of influence coefficients

One of the simplest method uses for balancing is the influence coefficient method. The method requires only a single proximity sensor to measure the vibration amplitude and a keyphasor to determine the phase angle. This can reduce the vibration amplitude at a particular selected speed of rotation. It can be extended to more speeds by maintaining orthogonality between the balancing masses.

The displacements x*(t)* are related to the unbalance, *U*, by the influence coefficients, α,

$$\{x\} = [\alpha]\{U\} \tag{6.6}$$

The goal is to determine α which is required to compute the 'counter-balance'.

$$\{U_b\} = -[\alpha]^{-1}\{x\} \tag{6.7}$$

The initial unbalance, *U*, is unknown and the system response to known perturbations will be used to obtain the necessary information. This is done by attaching a trial mass of known mass to the rotor, causing a different unbalance response U_1.

$$\{x\} = [\alpha]\{U_1 + U\} \tag{6.8}$$

And using the equation above;

$$\{x_1 - x\} = [\alpha]\{U_1\} \tag{6.9}$$

In order to obtain the influence coefficients at different speeds, the test above can be repeated at different speeds. Then the influence coefficients α are given as below:

$$[\{x_1 - x\} \ldots . \{x_n - x\}] = [\alpha][\{U_1\} \ldots . \{U_n\}] \tag{6.10}$$

And α can be determined from:

$$[\alpha] = [X][U]^{-1} \tag{6.11}$$

The mass can be obtained from the above equation.

Balancing of the rotor is carried out by the single-plane balancing technique. For this method, one vibration transducer and one keyphasor transducer are required. Figure 6.9 shows how the required measurements can be made using data acquisition software. The procedures are as follows:

1. Place a single mark on the rotor shaft until the keyphasor (optical type) produces a single mark in one revolution. On the rotor place an eddy current proximity sensor on any position.

2. With the rotor running at a selected speed preferably close to the critical speed, capture the vibration signal and keyphasor signal.

3. Using this information the amplitude and position of the vibration can calculated and the corrective mass should be placed 180° from this position.

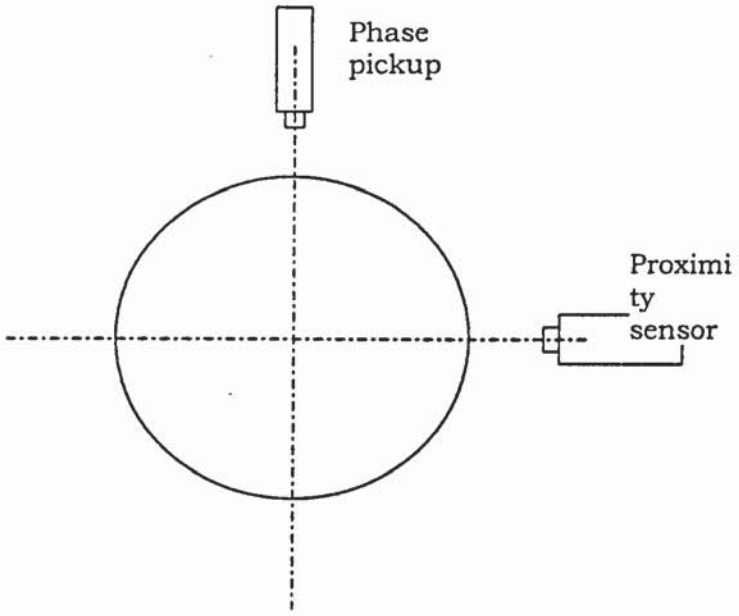

Figure 6.9: Balancing measurements

4. Place the required mass at the position determined before and run the rotor at the same speed as before. The amplitude should reduce considerably.

6.6 FORWARD/BACKWARD DECOMPOSITION FOR ROTATING SHAFTS

A very important feature of the response of rotating machinery is the speed dependency of the response spectrum. Changes of the response with speed of rotation are commonly observed for rotating shafts with discs mounted on them. The unbalance response resulting from the combined effect of very small imperfections and structural asymmetries manifests itself in both the amplitude and the frequency

of the response. Frequencies associated with the natural frequencies of the structure are typically measured on rotors.

Whirling motion of shafts causes the centre of gravity of a shaft cross-section to move in an elliptical orbit (or a combination of elliptical orbits at different frequencies) around the centre of rotation. Backward whirl is usually encountered when the bearings and support structure are anisotropic (Muszyska, 1996, Lee 1993). Hence, separating the whirl response into forward and backward components provides valuable information about the asymmetry of the bearing stiffness in the x and y directions. Under steady-state conditions when the speed of rotation, ω, is constant, and when the only excitation is due to unbalance, the rotor will whirl at a single frequency. The response measured by $x(t)$ and $y(t)$ will have the shape of an ellipse. As shown in Figure 6.11 this ellipse can be decomposed into two opposite directional whirl circles. When there are several sources of excitation or when transient conditions are in effect, each response signal contains many frequencies. For every frequency, there exist forward and backward complex amplitudes (Bucher and Ewins, 1997).

A combined signal is used to separate forward and backward whirl shaft.

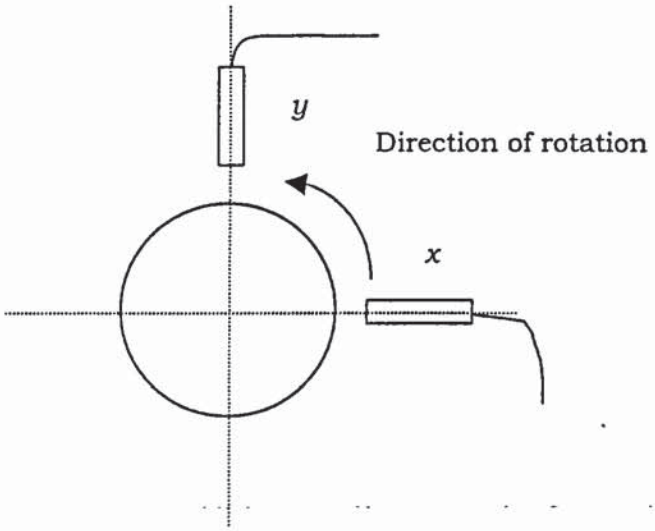

Figure 6.10. Position of two proximity sensors

Combining the response from *x(t)* and *y(t)*, to create a complex signal (as in Figure 6.10).

$$r(t) = x(t) + iy(t) \tag{6.12}$$

we obtain, from a single frequency ω:

$$r(t) = A_f e^{i\omega t} + A_b e^{-i\omega t} + C \tag{6.13}$$

where A_f, A_b are the forward and backward vibration amplitudes respectively and C equals $(x_0 + iy_0)$ and is constant. Applying MATLAB FFT function to equation 6.12, the forward and backward amplitudes can be decomposed.

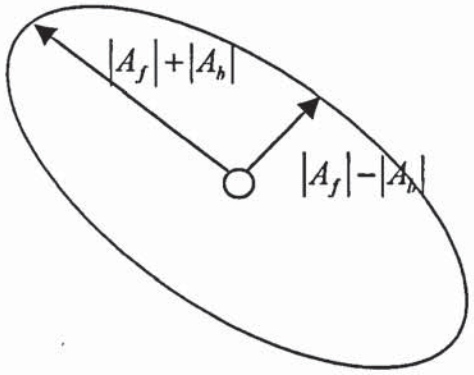

Figure 6.11: Elliptical orbit showing major and minor axes as function of the forward (A_f) and backward (A_b) whirl amplitudes.

6.7 SAFETY AND OVERLOAD PROTECTION

Since the rotor is rotating at relatively high speed, safety becomes an important consideration in the design of a rotor system. Safety considerations here include protection for the operator and the instrumentation used. In this study the rotor is running above the critical speed of the system with loosely tight bolts, leading to opening and closing of the rotor discs and also large lateral deflection in the vertical and horizontal directions. With the unexpected non-linear amplitude movement, there is always a tendency for unwanted accidents to happen, for example the nut becomes very loose or excessive deflection.

As the design of rotor allows for rotation speeds of up to 6000 rpm, appropriate safety precautions were be taken. The kinetic energy contained in the rotor at maximum design speed can be computed with the actual geometry.

$$K = \frac{1}{2}\int v^2 dm \qquad (6.12)$$

To dissipate this energy in the case of an accident, a guard of steel plate was placed on the rotor to avoid any flying object such as nut. The guard is built from a relatively thick plate so that the guard can be left standing by its own weight. This avoids the additional requirement of bolting it to the foundation. The proximity sensors are protected by guard ring, designed to provide restriction on the movement of the rotor before it touches the sensors. The guard ring is made solid bar with a split hole that allows the shaft to pass through with clearance adjusted not to exceed the distance between the transducers and the rotor surfaces. The base of the guard ring is firmly held to the foundation.

The motor is protected from the shaft vibration by the flexible coupling. Apart from connecting the motor to the rotor it also protects the rotor from the unwanted vibration. It has the flexibility of absorbing the transient torsion load to give a steady output.

6.8 DATA ACQUISITION SYSTEM

Another important aspect of the development of the test rig is the data logger. Data loggers are available commercially and depends on

acquisitions speed. The other factor in the selections is looking on the possibility of using the logger for other applications. Since the possible information to be extracted from the test rig will be displacement (2 channels), acceleration (2 channels), keyphasor (1 channel), opening of rotor (1 channel), therefore the minimum of eight channels data logger will the ideal for the applications.

The signal obtained from responses of the rotor system need to be captured in some form that make possible for further analysis. Vibration data can either be analysed directly or recorded for later used after they have been acquired from the transducers. Digital recording device requires analogue-to-digital conversion prior to recording from analogue transducers. Recording data saves acquisition time as well as machine times because many points can be monitored simultaneously for later analysis. Another advantage is that recorded data can be analysed in many different ways without time and environmental constraint apart from the permanent record that is acquired. Figure 6.12 shows the photograph of the data acquisition system.

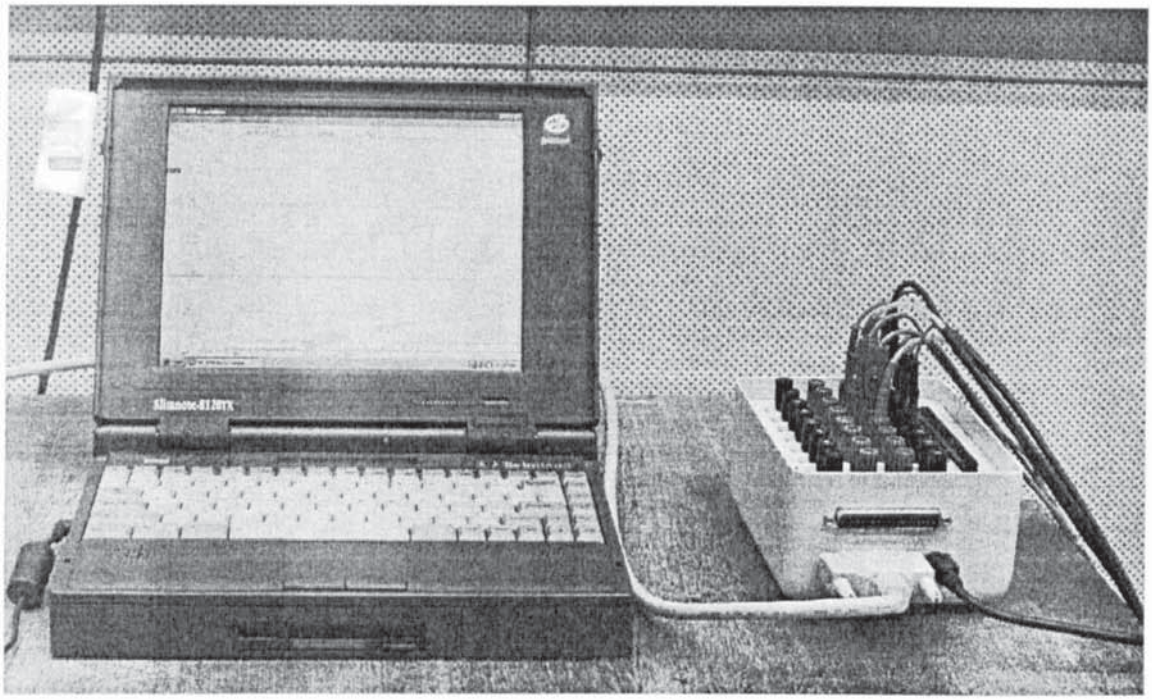

Figure 6.12.Data Acquisition System

The hardware used to capture data for the experiment was a 16 channel Dataq Instruments model DI-200 series. It has a built-in digital to analogue converter that can be attached straight to the parallel port of a PC. It can measure the output voltage from the transducers in the range of –5V to 5V. To acquire the full range of the transducers, which is well above this range, the voltage needs to be steped down. The software used was WINDAQ windows based data acquisition software, which allows real time display of the acquired waveforms to the computer. The software have the pull down menus facilities which allows control on the data acquisition parameters in real time such as sampling rate, numbers of channels enabled, waveform compression, event markers, disk storage and much more. All the waveforms can be saved into a file with 'wdq' extension with size restricted only by the computer space available. Once the data has being captured successfully and saved as a file, using playback

and analysis software the data can be reviewed and analysed using a facility in the software. It also has a built-in file translator that allows the data to be exported and imported in a variety of data acquisition, spreadsheet, and analysis software formats.

In the experiment carried out, three channels were used representing the keyphasor, *x*-amplitude and *y*-amplitude transducers along the horizontal and vertical positions. The data captured is then saved as spreadsheet format. The analysis of the data is next done using written MATLAB script so that the speed, amplitude, phase and other analysis can be carried out.

6.8.1. Sampling rate

The rotor was rotated up to a frequency of about 3000 rpm to be well above the first critical speed. Therefore signal frequencies up to 50 Hz are expected, so the lowest possible sampling frequency possible for each channel to avoid aliasing is 100Hz. However, two samples per cycle are not enough to give a good representation of the signal. So a higher signal is preferable, say 1000 Hz. There is no need for anti-aliasing since the signal generated is quite low.

6.9 CONCLUSION

In this chapter, various considerations in the design of the test rig are discussed. These include the selection of dimensions, motor, coupling, ball bearings; method of bolted rotor section, which allow

the properties of the jointed section to be shown. The balancing of the rotor involved the data acquisition system and transducers used.

Chapter Seven

EXPERIMENTAL RESULTS

7.0 INTRODUCTION

This chapter presents the results from the experimental test carried out as described in chapter 6. Once the experimental rig was successfully designed, fabricated and assembled, the fundamental natural frequency of the system was determined by conducting modal tests. The main purpose of the experiments described in this chapter was to demonstrate the existence of non-linear phenomenon in the bolted joint. In addition, experiments were carried out to prove the validity of the model developed in Chapter 4 and also to demonstrate some of the predicted parameter sensitivities.

7.1 STATIC DEFLECTION TESTS

Static tests were used to determine two important parameters from the test rig. The first parameter was the variation in stiffness with the deflection, as shown in Figure 7.1. This gave the approximate shaft and bearing stiffness before and after the gap opened. Secondly, the value of the threshold can be approximated from this curve. Within

the limitation of the equipment used, the stiffness threshold value with an error of less than 5 percent, was obtained from the curve.

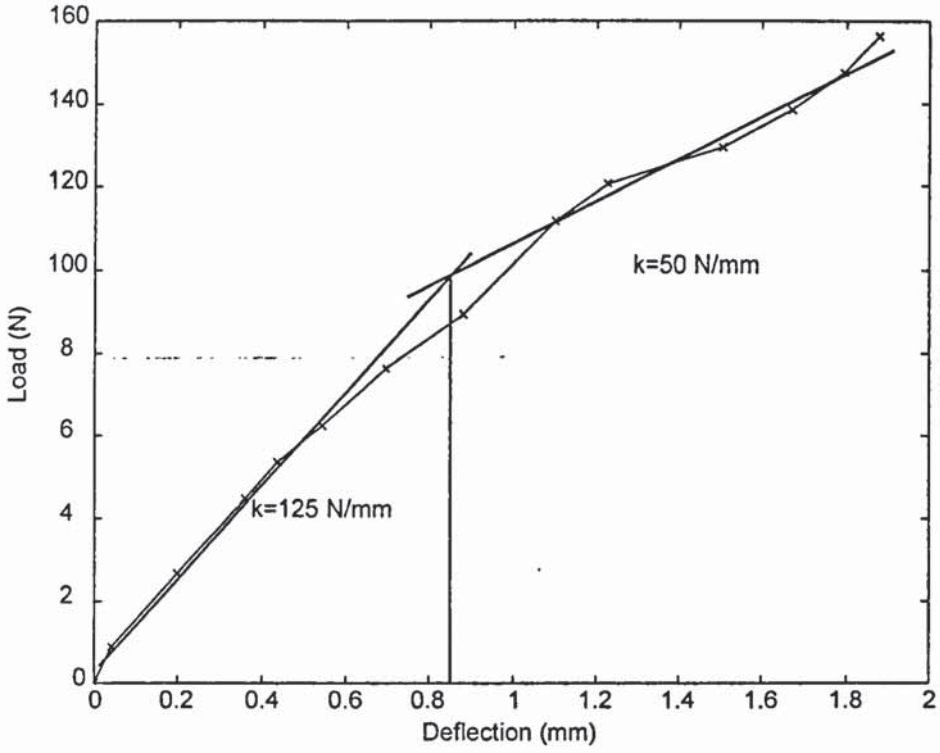

Figure 7.1: Force deflection curve (horizontal direction)

The force deflection test in the horizontal direction (Figure 7.1) indicated that the value of the stiffness of the shaft and bearing and the threshold value, was about 0.7 mm. The straight line showed the close fit of the point produced by experiment. There was a clear change of the stiffness from stiffer value into much softer value. The stiffness of the shaft was much higher than the above stiffness because of the existence of the bearing and foundation stiffness. Figure 7. 2 show the curve of the same test carried out in the vertical direction. There was a difference in the slope and the threshold value which indicated a difference in the stiffness in the vertical and horizontal direction. Figure 7.3 shows the curve when the two curves

was superimposed together. The slope shows that the stiffness in the vertical was larger than the horizontal direction by a factor of 1.3. However after the threshold the difference in the slope was quite small. There was a slight difference in the threshold value due to experimental error in the measurement taken.

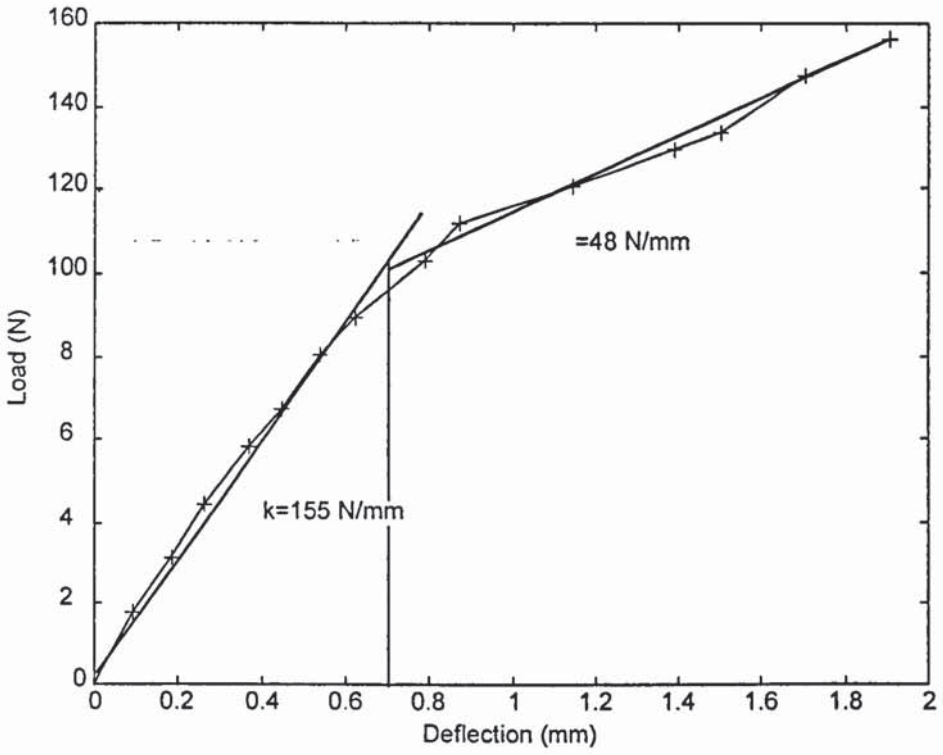

Figure 7.2: Force deflection curve (vertical direction)

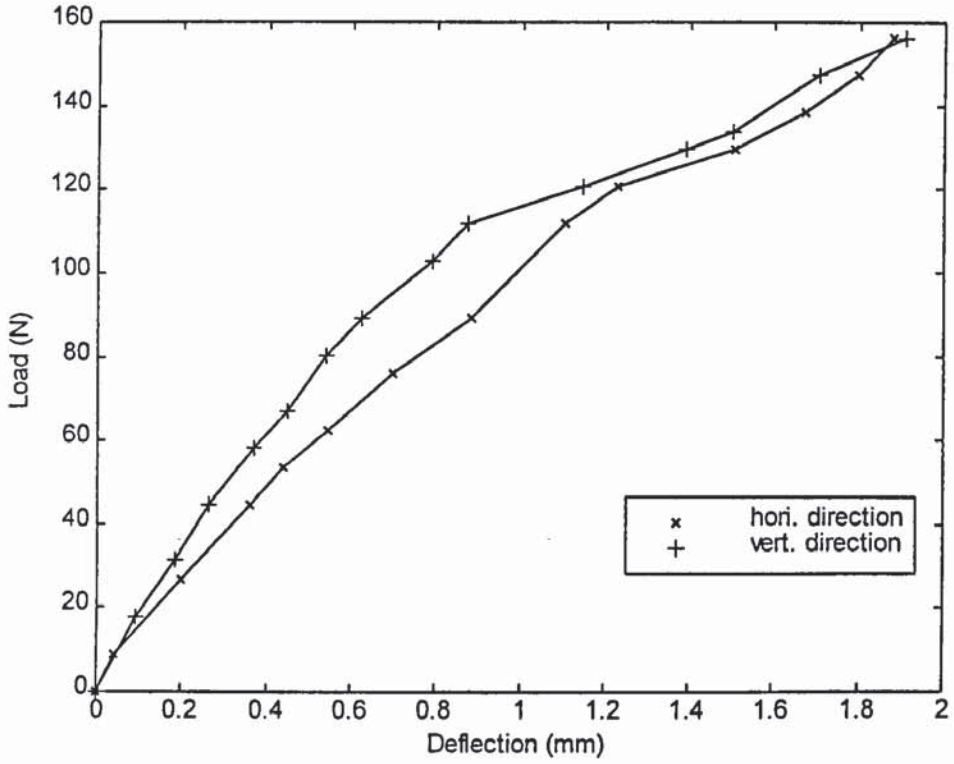

Figure 7.3: Superimposing the vertical and horizontal direction curves.

7.2 MODAL TESTS

A modal test was carried out to determine the system natural frequencies and the mode shapes. Only the natural frequency of the first mode was important because the operating speed only passed through the first critical speed. Modal tests were carried out in the horizontal and vertical directions with the bearings and supports in place to determine the rotor natural frequency and mode shape under these conditions. Since the mass of the system could be calculated, the stiffness of the system in the horizontal and vertical directions can be estimated from the natural frequency. The stiffness obtained was the overall stiffness of the shaft, bearings and the bearing supports since the rotor system is was actual place. The overall

stiffness represented the shaft, bearing and the bracket stiffness connected in series. The shaft stiffness alone was estimated by conducting modal tests in constraints conditions. The foundations were taken to be relatively rigid as compared to the stiffness of the system. Figure 7.4 and Figure 7.5 shows the results of the modal tests in vertical and horizontal directions.

From the modal tests, the natural frequencies for the system are as follows:

No	Horizontal (Hz)	Vertical (Hz)
1	28	32
2	189	195
3	361	392

Table 7.1. Natural frequencies in horizontal and vertical direction

The results of the modal tests can be compared with the tests carried out in the static tests. However, the modal tests only give the stiffness for the initial slope in the static test. Comparing the results in both tests shows that the results are acceptable to 5 percent tolerance.

	Modal Tests	Static deflection tests
Ratio of horizontal to vertical value	$(28/32)^2=0.765$	125/155=0.806

Table 7.2: Stiffness ratio from modal tests and deflection tests.

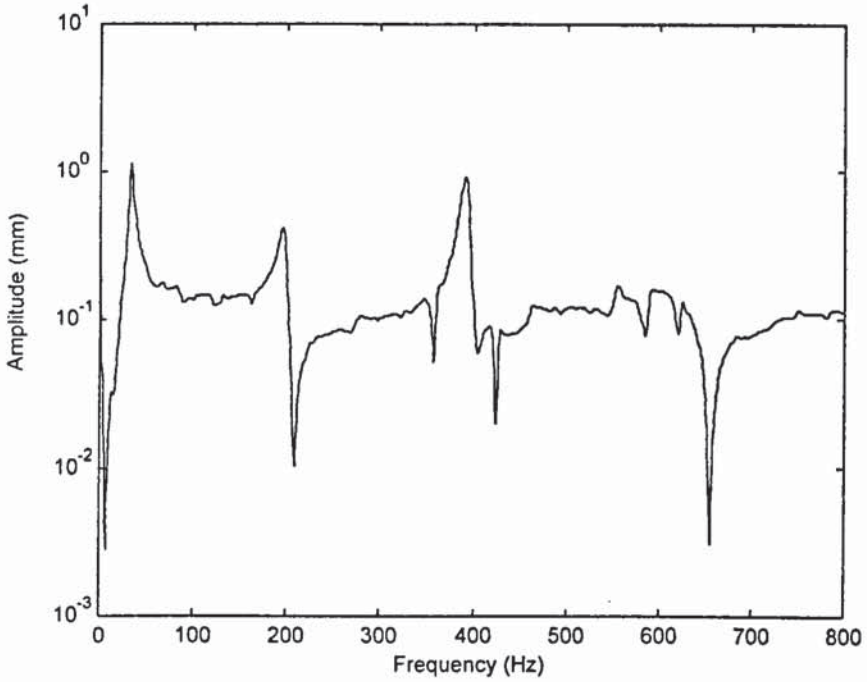

Figure 7.4: Response curve in the Vertical direction.

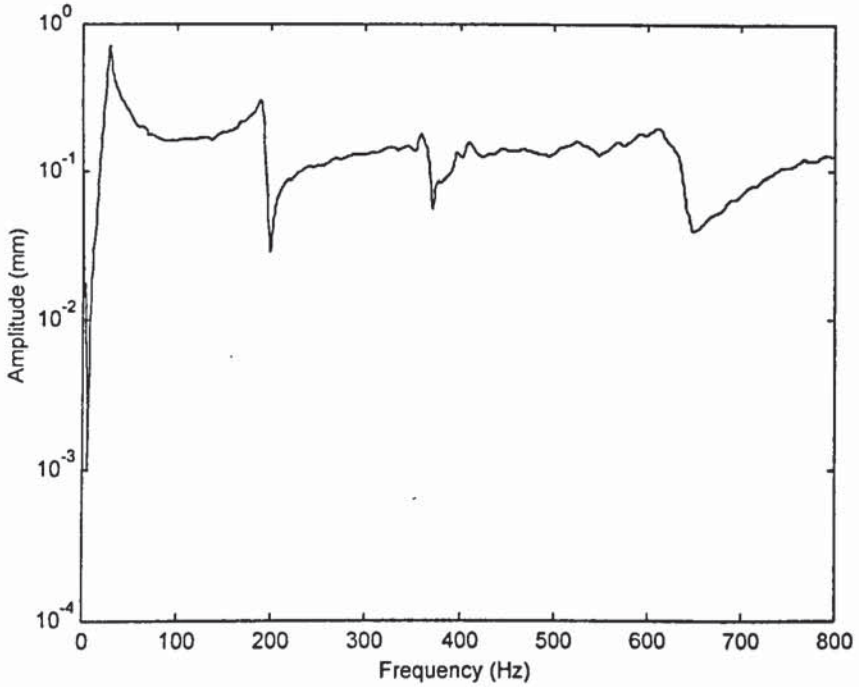

Figure 7.5: Response curve in the horizontal direction.

7.3 BALANCING RESULTS

The unbalance response of the rotor was determined by placing an unbalanced mass on the rotor disc at a position in order to create some deflection, that is, at the place where the unbalance already existed during the fabrication of the components. Large unbalance was added to cause the rotor to deflect beyond the linear deflection range of the rotor. This was to ascertain that the balance results represented the desired speeds which are to be expected from the simulation results.

Only single plane balancing was required to balance the test rig because the rotor could be considered as single lumped rotor and therefore the rotor could be balanced in single plane. The first step was to record the static run-out of the rotor. This was measured at very low speed. The speed chosen was 300 rpm (5 Hz), which was below the resonance and under such conditions the unbalance response was negligible.

The run-out recorded, x_r was

$$x_r = 0.0994\text{mm}\angle -45.08^{\circ} \qquad (7.1)$$

Note that this run-out was –45.08° (i.e. lagging) from the keyphasor position. The next stage was to record the unbalance response at higher speed, preferably at a speed close to resonance. In this exercise the speed taken was 1428 rpm and the unbalance response was.

$$x = 0.5380\text{mm}\angle -30.9^{\circ} \qquad (7.2)$$

After that a small mass was attached at an arbitrary chosen location and again the unbalance response was recorded.
The position of the mass was

$$m = 2.6\text{gm}\angle 22.5^{\circ} \tag{7.3}$$

The new unbalance response, x_1, was

$$x_1 = 0.6091\text{mm}\angle -96.24^{\circ} \tag{7.4}$$

Using the above values the influence coefficient can be obtained. Using equations (6.12), (7.2), (7.3) and (7.4), we have

$$\alpha = 0.2393\angle -170.561^{\circ} \tag{7.5}$$

Therefore the balancing mass for this speed is

$$m = 2.24gm\angle -40.35^{\circ} \tag{7.6}$$

Since there are 8 balancing positions in the rotor, distributed on a 100mm pitch circle diameter, the mass was required to be positioned with a resultant equal to the balancing mass (shown in Figure 7.6).

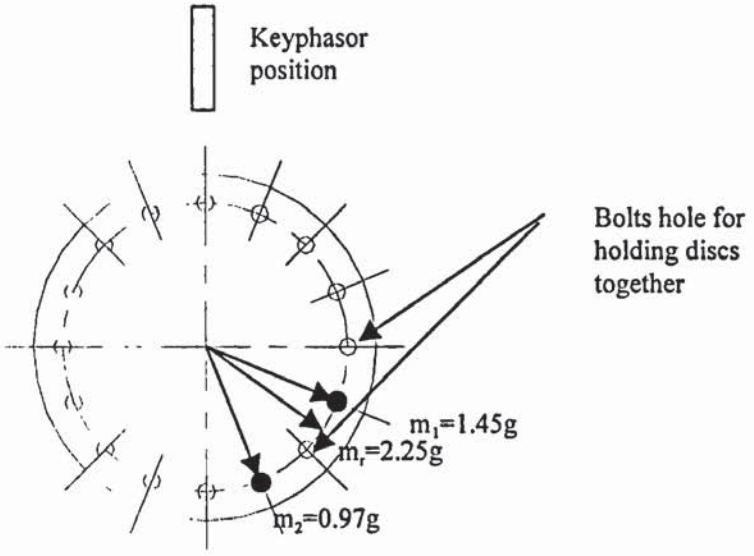

Figure 7.6 balancing mass positions

7.4 TRIAL RUN

A trial run was performed to make sure that the experimental rig was functioning the way it was designed within practical limitations. Since the rig was designed to have a relatively large transverse movement, other effects such as bearing clearance, misalignment and foundation effect could be neglected, thus simplifying the analysis. The transducers used were calibrated to avoid erroneous readings from the sensors. The amount of residual shaft bow was only 0.2 mm peak-to-peak. Figure 7.7 shows the shaft bow curve. Figure 7.8 shows the response taken at very low speed (300 rpm). Comparing with Figure 7.7 suggests that the run-out was very small and can be neglected since most of the response cause by the shaft bow. Note that angular positions in Figure 7.7 and 7.8 are not related to the

same positions on the shaft. There was a phase difference of approximately 150°.

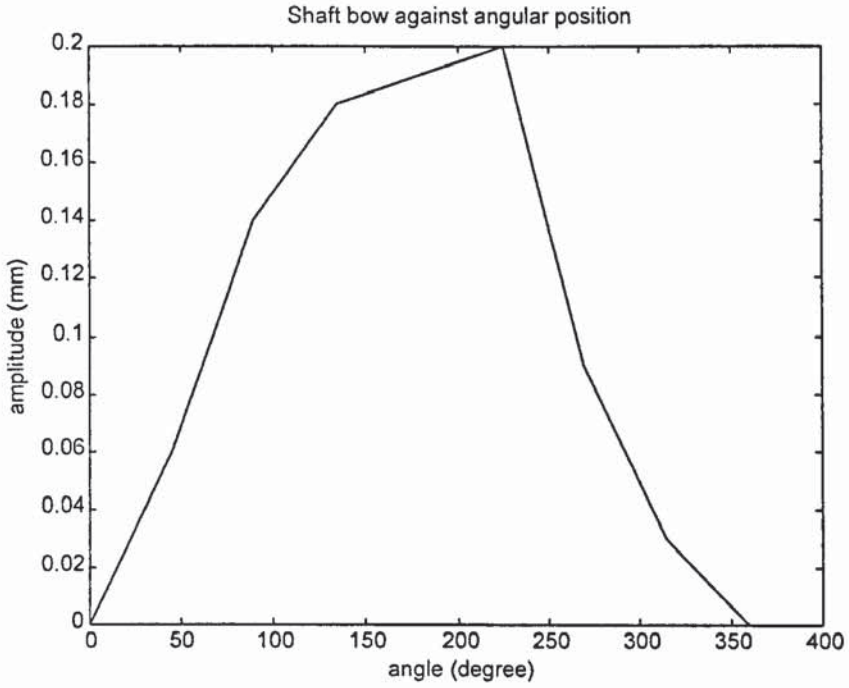

Figure 7.7 Shaft bow (measured using dial gauge)

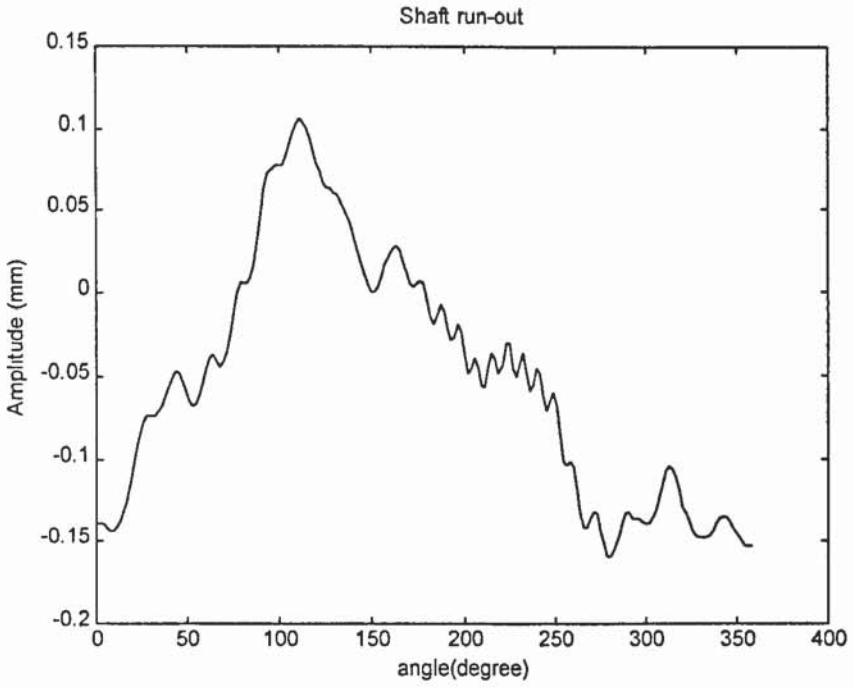

Figure 7.8: Run-out of the proximity sensors.

7.5 TIME HISTORIES

Figure 7.9 shows the time histories from the sensor signals when the shaft was rotated at a speed of 1000 rpm. The first two signals represented the displacement probes in the horizontal and vertical directions whereas the third signal represented the keyphasor output signal. The keyphasor acted as reference point and was also use to determine the speed of the shaft. All the time histories presented use the same scaling to enable quantitative comparisons to be made. The magnitudes of the vibration were measured in volts and had to be converted into displacements (in millimetres) to obtain the actual amplitude of the vibrations. Since the transducers were placed orthogonal to each other, the signals were of 90^0 out of phase to each other.

The linear range of the proximity sensors was 3 mm, and the displacements above this value would not have been correctly displayed. This problem was overcome by putting an additional set of proximity sensors on the opposite side of the existing proximity sensors as shown in Figure 7.10. The proximity sensors were placed off centre to enable a half waveform to be fully captured. To obtain the full waveform of the responses in the vertical and horizontal directions, the responses were combined after subtracting the truncated region of the waveform. The run-out of each sensor was neglected.

Each proximity sensor was capturing the samples at the same rate (i.e 1000 samples per second). As shown in Figure 7.10, proximity sensors P1 and P2 were measuring deflection in horizontal direction. Their mean centre positions were determined at low speed where the full waveforms could be captured. Using the centre positions of each proximity sensor, the waveforms were truncated by setting zero for signal amplitude below the mean centre magnitude after converting the magnitude into millimetres. With two signals truncated below the mean position, the full waveforms were obtained by substrating these signals.

If s_1 and s_2 are signal from P1 and P2, c_1 and c_2 are their mean position obtained at very low rotating speed (i.e. 200 rpm). Converting the magnitude to millimetres we obtained:

$s_{h1} = s_1 - c_1$ and $s_{h2} = s_2 - c_2$ and setting all negative magnitudes to zero, we have the full waveform as:

$s_h = s_{h1} - s_{h2}$

Similarly in the vertical direction, the magnitude of the signal can be obtained as shown in Figure 7.11 and Figure 7.12.

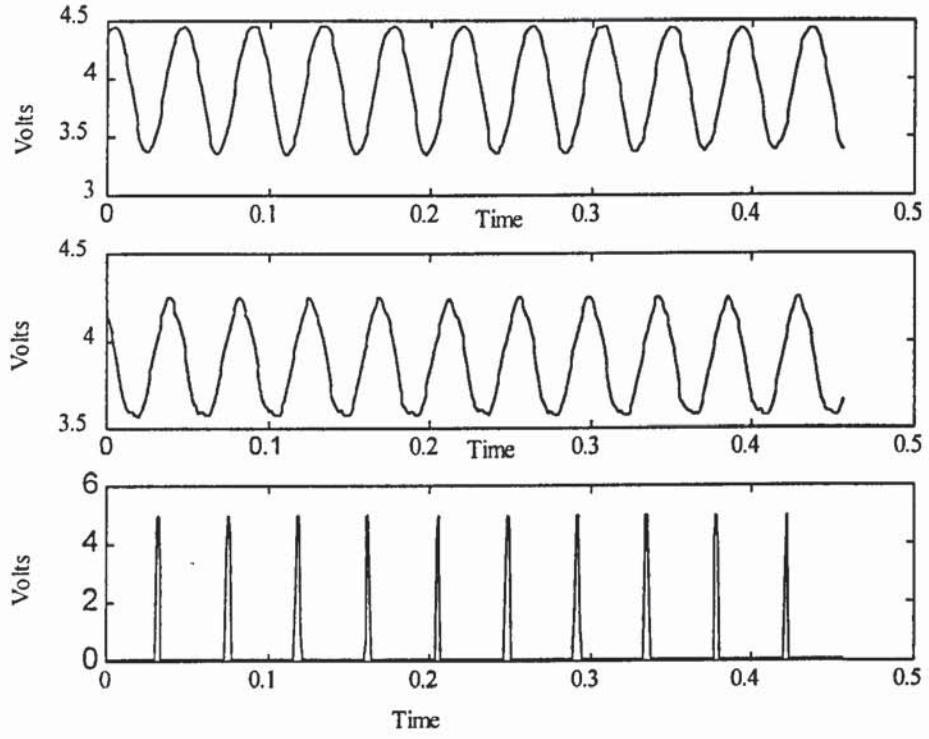

Figure 7.9: The vibration amplitude and the keyphasor signals

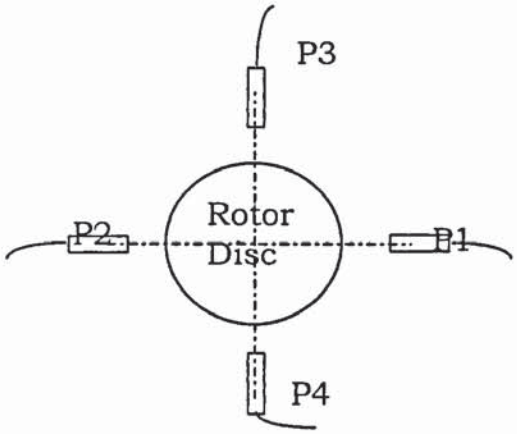

Figure 7.10: Arrangement of the proximity sensors to capture the full waveform when clipping due to out of proximity range.

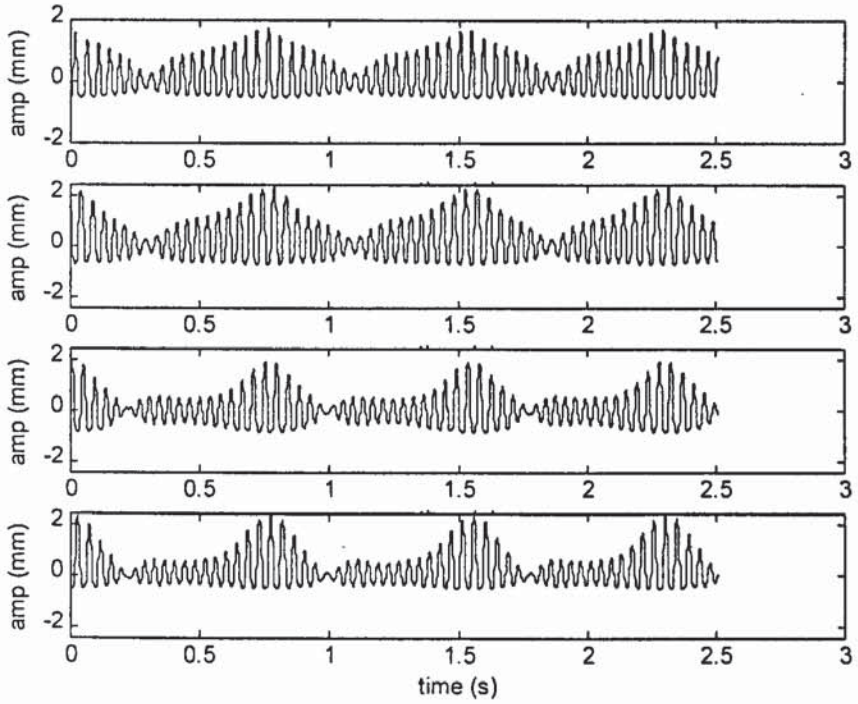

Figure 7.11. Clipping of waveforms on the horizontal and vertical directions

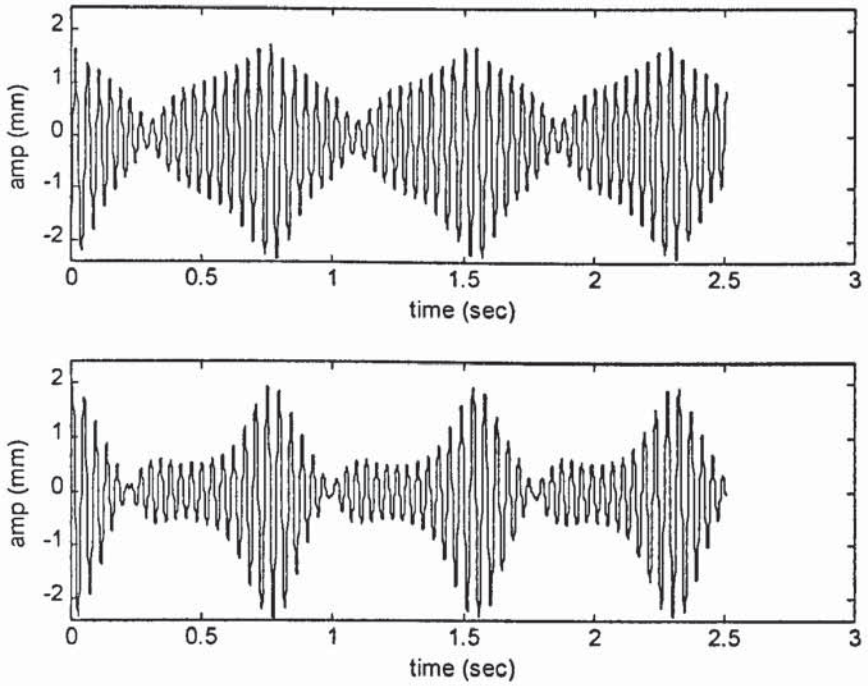

Figure 7.12: Signals after joining two proximities in opposite directions

7.6 RUN-UP AND RUN-DOWN RESULTS

The rotor was run-up from rest to a maximum speed of 2100 rpm and then run-down to rest at the nominal rate of 0.02 Hz/sec (72 rpm/min). The run-up results were produced by extracting the maximum amplitude due to the vibration in the horizontal and vertical directions at different speed increments. This was done by fitting a curve to vibration signal using the least square method for 20 cycles. This method was used to determine the magnitude and the phase angle of the signal from the keyphasor. However when the waveform was non-periodic then only the magnitude of the maximum peak was registered. Obtaining this magnitude with the corresponding speed of the shaft, a graph of the run-up of the system was plotted. Similarly for the run-down, the graph was also plotted to give the indication of the variation of the amplitude with increase or decrease in speed. Figure 7.13 and 7.14 shows the graph of the vibration amplitude versus speed during run-up and Figure 7.15 and 7.16 represent the vibration amplitude during run-down. In each case there are two sets of data plotted with the graph with '+' represent the repetition of the experiment to show that the experiments are repeatable.

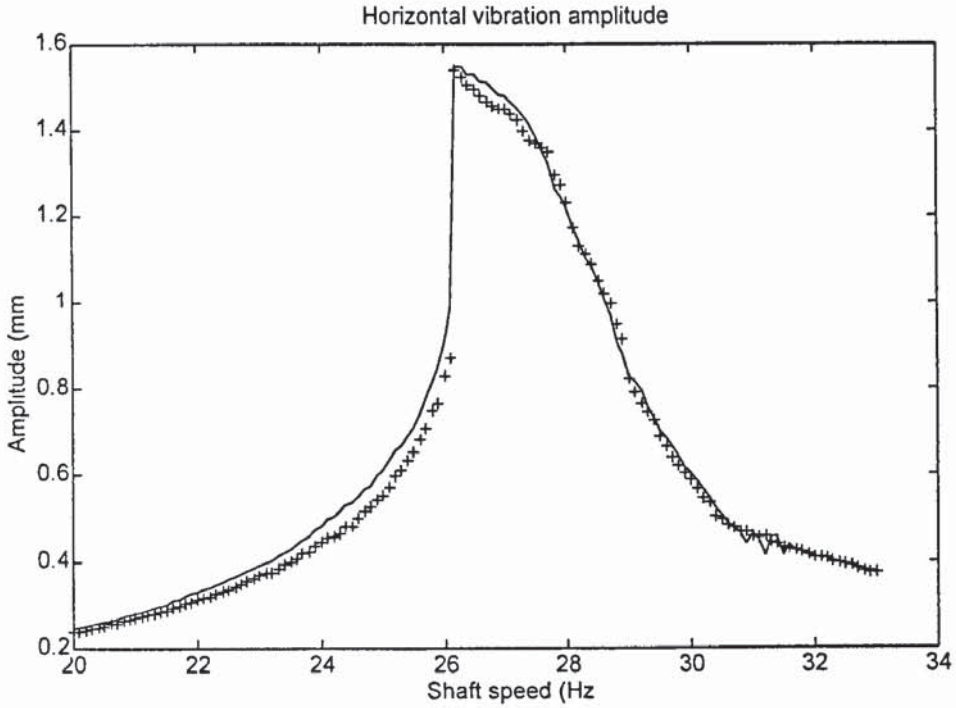

Figure 7.13: Run-up horizontal direction.

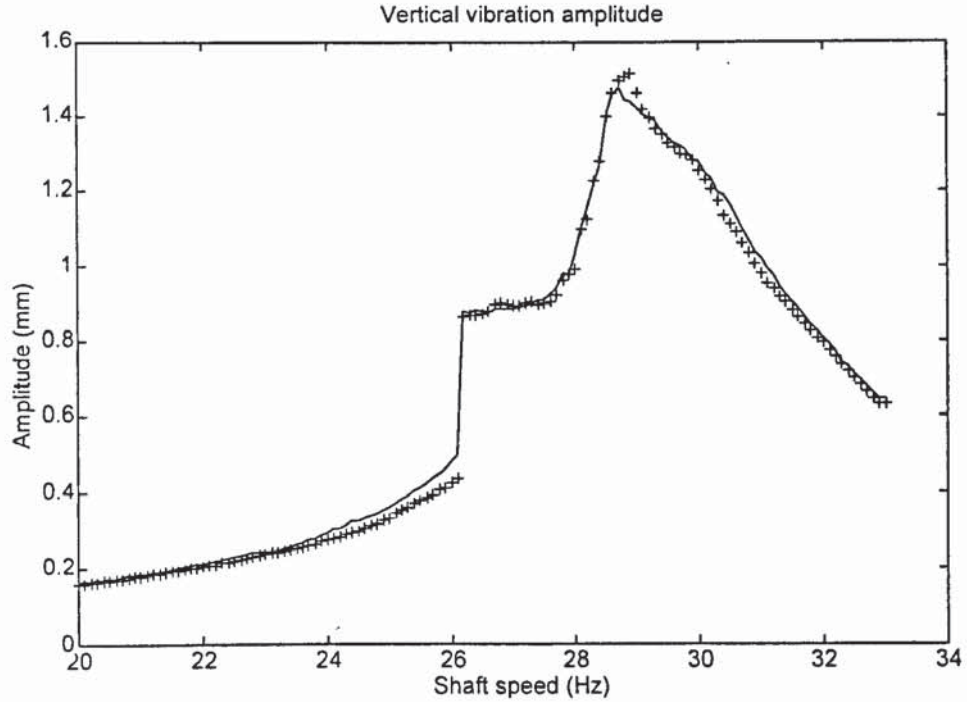

Figure 7.14: Run-up in vertical direction

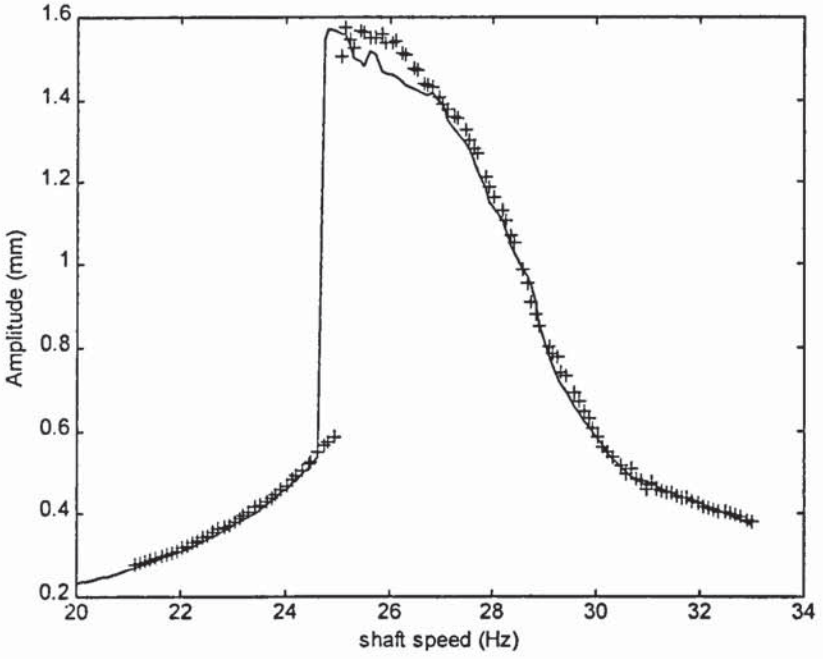

Figure 7.15: Run-down in horizontal direction

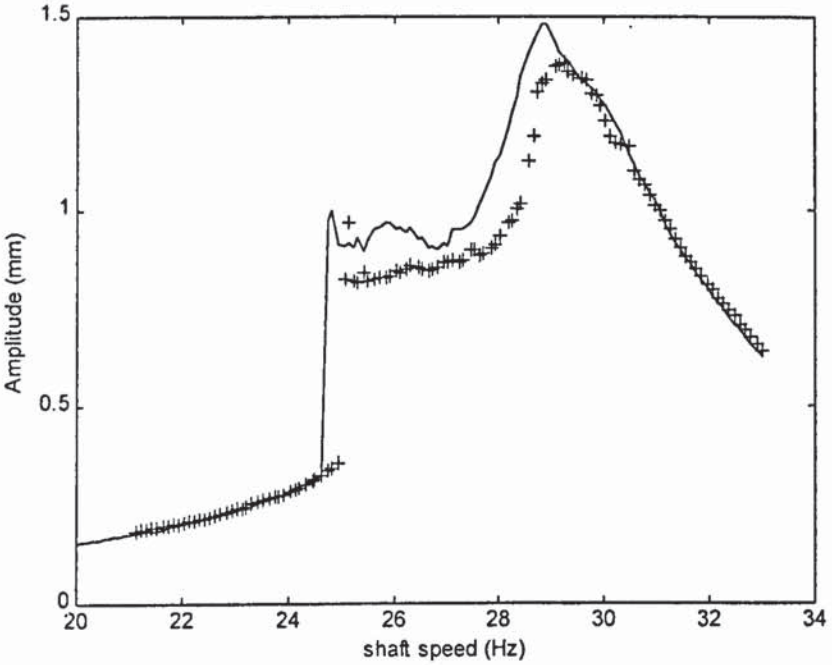

Figure 7.16: Run-down in vertical direction

The above results were produced because there was slight different of the clamping force on the bearing in the vertical and horizontal direction. Modifying the clamping mechanism and applying much lower axial bearing pre-loading force on one end of the bearing produced the results as shown in Figure 7.17 and Figure 7.18.

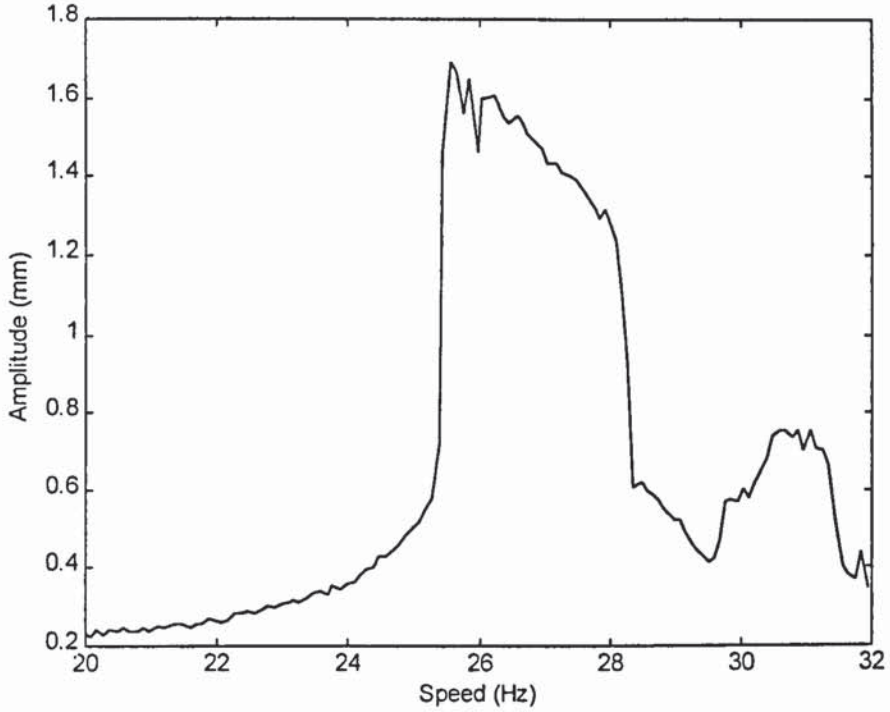

Figure 7.17. Run-up peak value (horizontal)

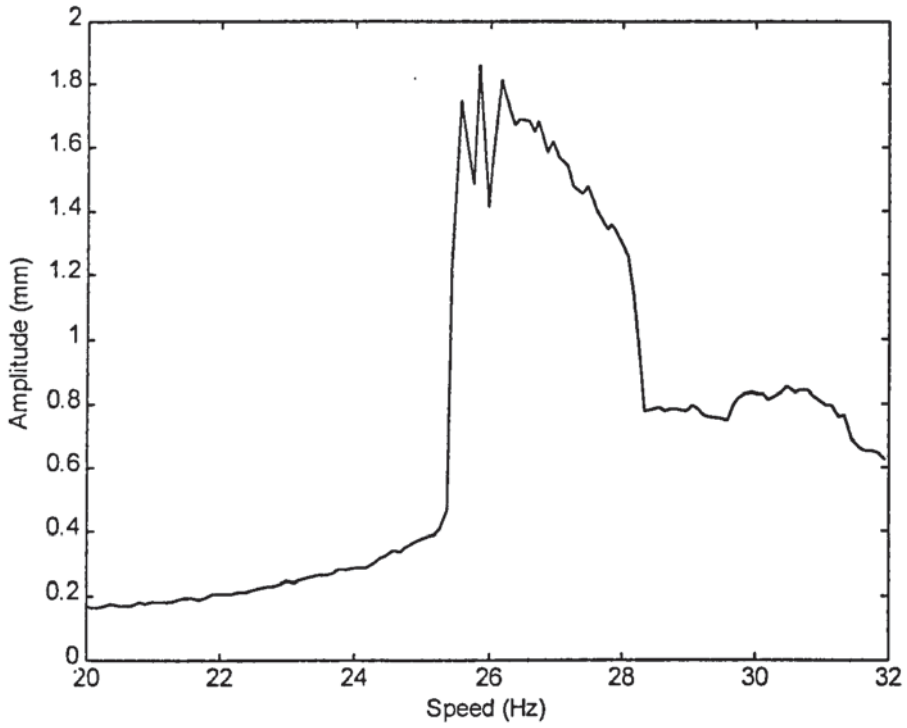

Figure 7.18. Run-up peak value (vertical direction)

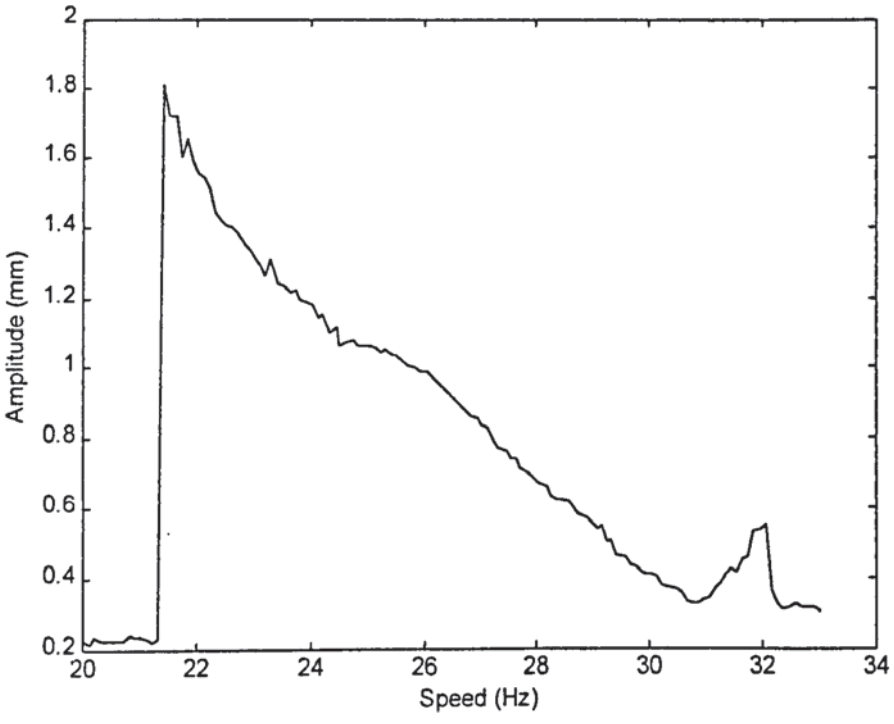

Figure 7.19. Run-down peak value (horizontal direction)

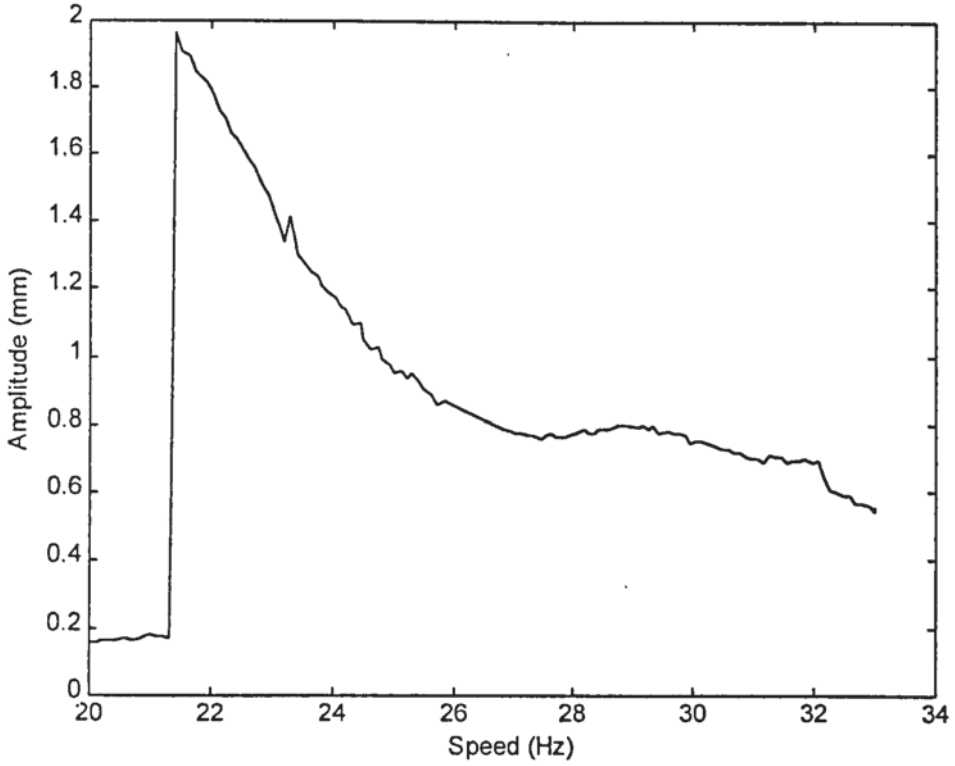

Figure 7.20. Run-down peak value (vertical direction)

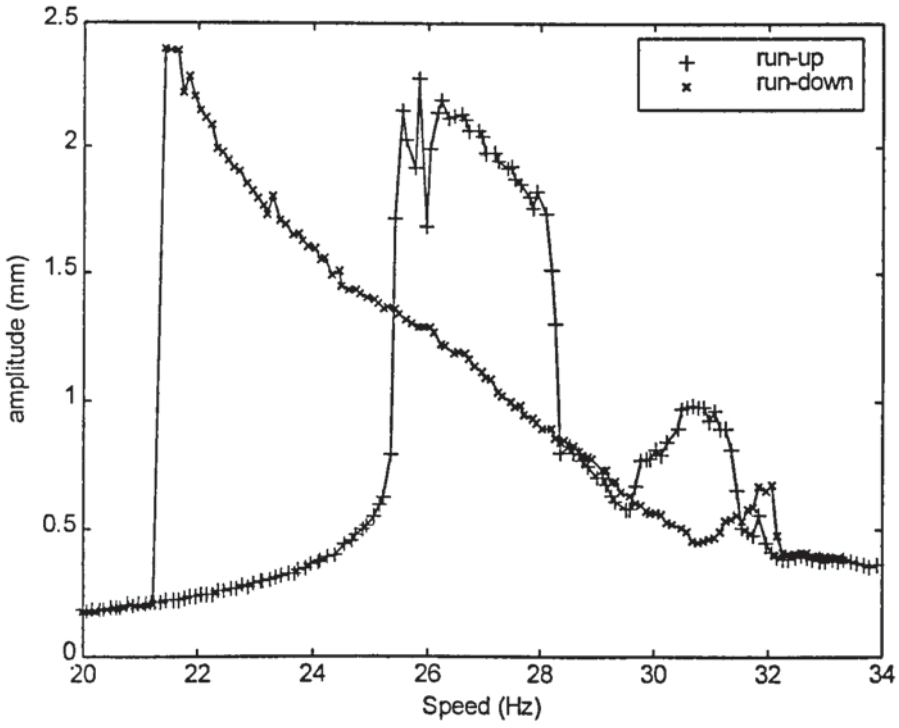

Figure 7.21. Run-up and Run-down (horizontal direction)

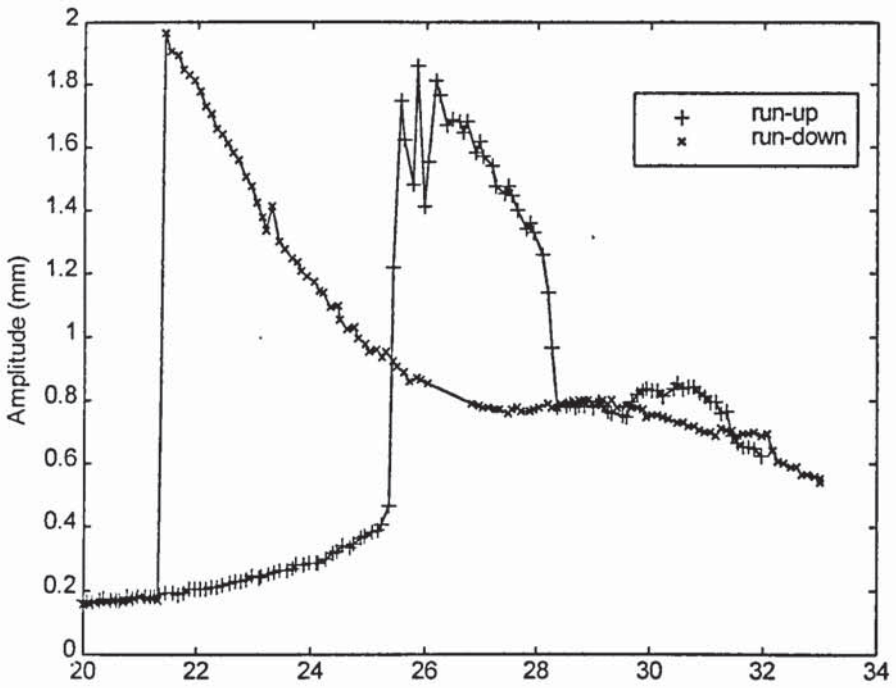

Figure 7.22. Run-up and Run-down (Vertical direction)

7.7 FREQUENCY DOMAIN

In order to provide a better understanding of the results it was necessary to plot the results in the frequency domain. Frequency domain plots showed all the frequencies, which were hidden in the time histories of the waveform. Using MATLAB the time histories can readily be transformed into frequency domain using the function available. The FFT was determined using 1024 equispace data points, with 0.001sec interval over a period of 1.024 sec. The frequency increment used therefore is 0.9765 Hz and the maximum frequency is 500 Hz. An example of the plot is shown in Figure 7.23. where the FFT was taken for the data at speed of 1590 rpm (26.5 Hz). In this example only the range up to 50 Hz is plotted because over the rest of the frequency range the amplitudes were small.

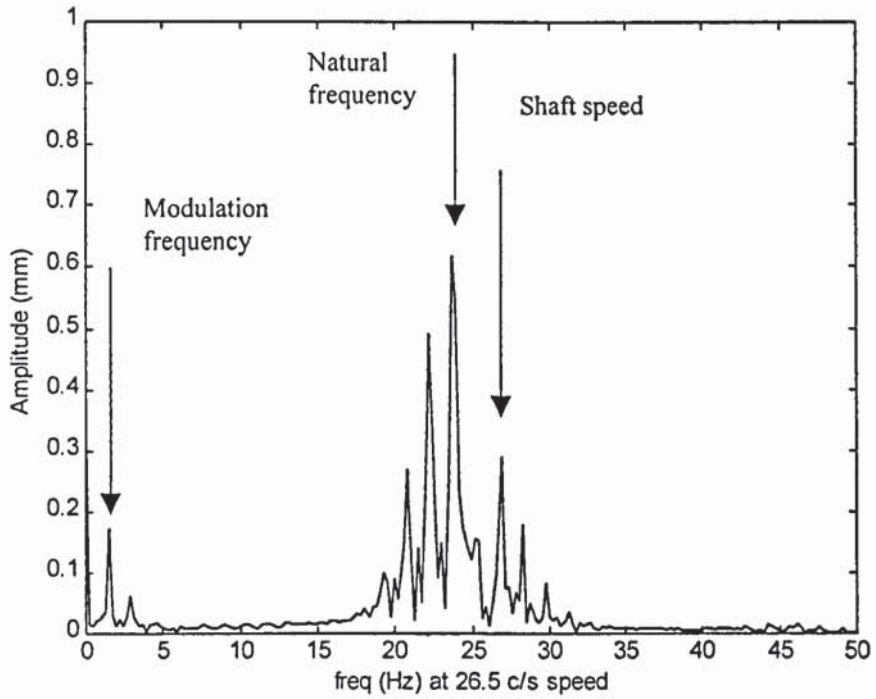

Figure 7.23. FFT diagram of the time histories

7.8 SPECTRAL MAPS OR WATERFALLS PLOTS

The waterfall plot is the plot of the spectra of the rotor response at various machine speeds. The sequence of spectra can be separated by uniform increments of speed. Figure 7.24 shows the experimental spectral plot during run-up of the rotor and Figure 7.25 shows the simulation spectral plot for comparison. Similar comparison was made viewing the plot from the above using contour plots. The plots are as shown in Figure 7.26 and Figure 7.27. Figure 7.28 provides in addition to the frequency content at each speed, clearly separate the forward (positive frequency) and backward (negative frequency) components. Figure 7.29 represents the contour plot of the forward-backward components.

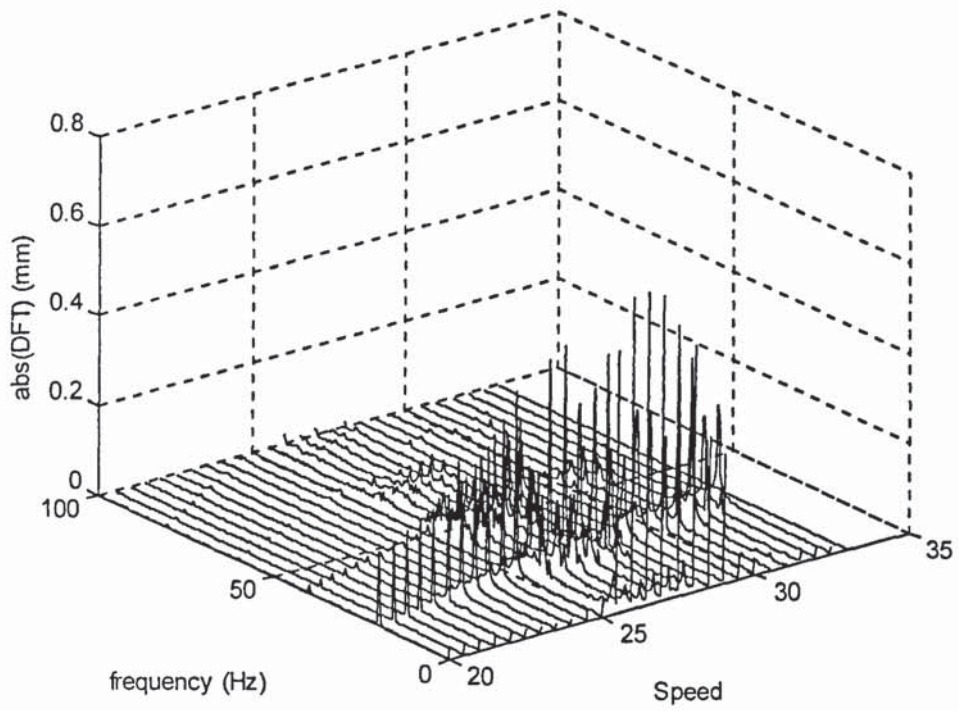

Figure 7.24. Spectra plot of the experimental data

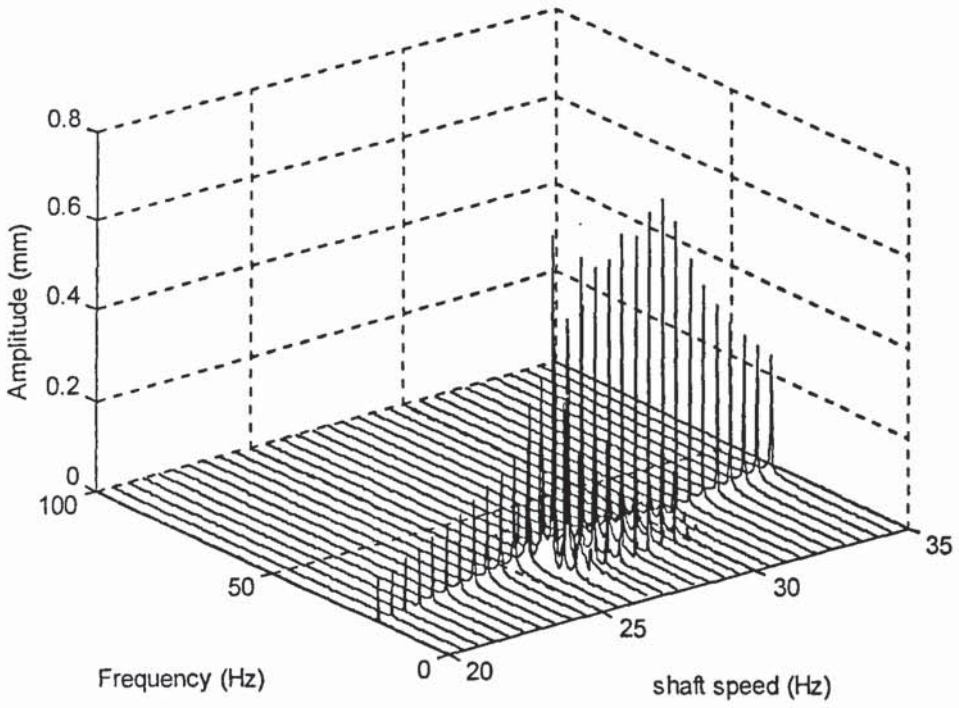

Figure 7.25. Spectra plot from the simulation result.

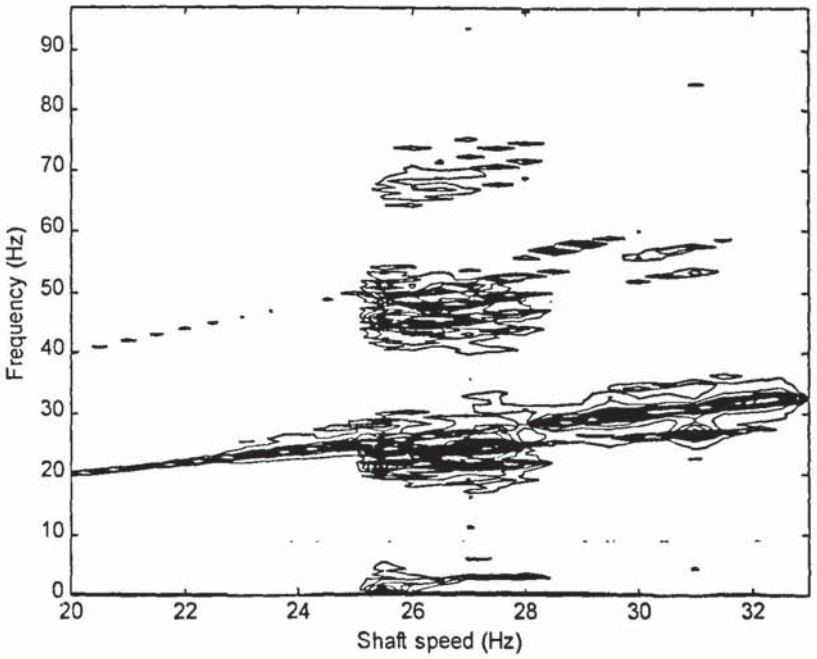

Figure 7.26: The contour plot of the experimental data

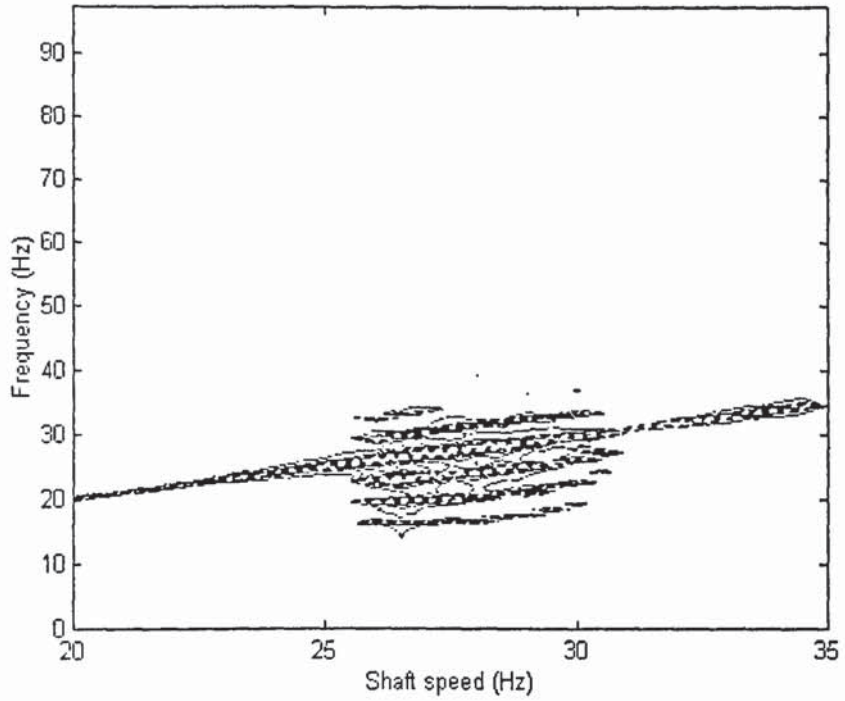

Figure 7.27. The contour plot from the simulation data

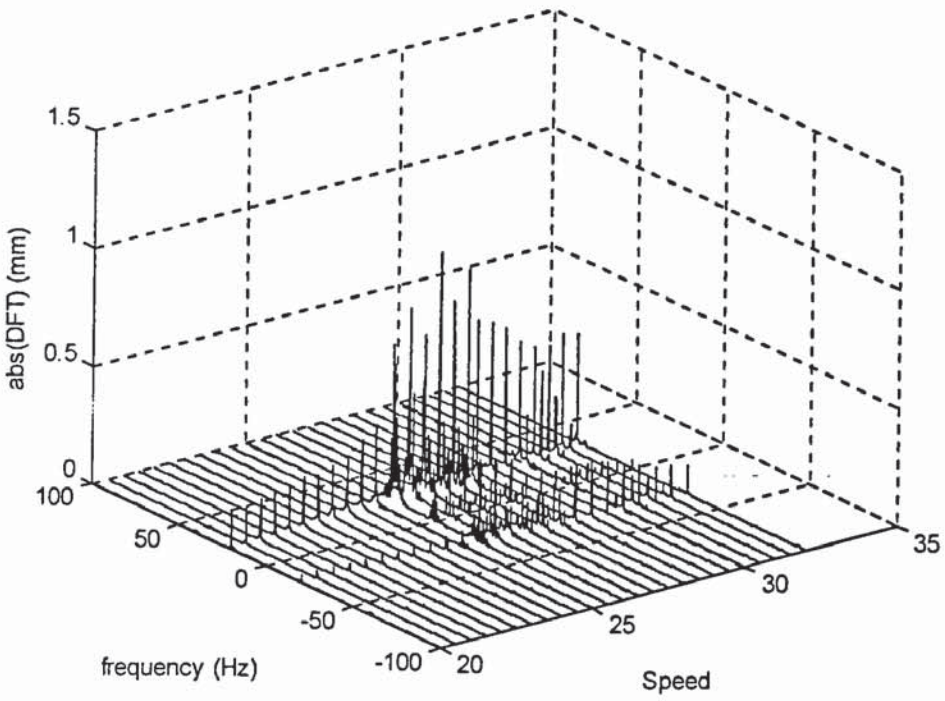

Figure 7.28: Forward-backward whirl diagram using two sensors

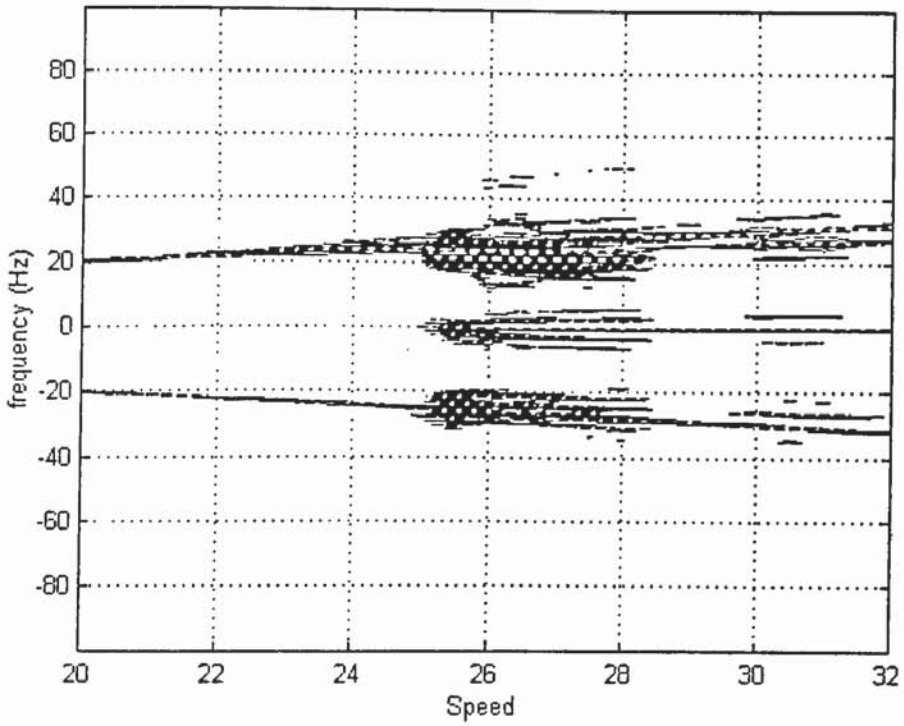

Figure 7.29: Forward-backward whirl contour plot.

Plotting the variation of the frequency response at different speed shows that there was a change in the amplitude with the change in rotor speed. Clearly it depicts that at the position close to resonance of the system in addition to the jump phenomenon there is aperiodic response after the transient of the jump.

7.9 POINCARE'S PLOT

One method of checking whether the result from the system response is chaotic or not is by plotting the amplitude and velocity at an interval of each cycle of the input. For a periodic system the result of the output will be a single point where the value of the response fall on the same region for every cycle. However, for the non-linear system the response may not produce the same point at different cycles. However, for experimental study it is difficult to determine the velocity for each point, therefore a pseudo-phase plot is carried out. Pseudo-phase plot consists of plotting the value of x_i versus x_{i+1} for every cycle (Moon, 1987). Figures 7.30 to Figure 7.37 show the pseudo-phase plot of the experimental data. The data was obtained using 50 points representing 50 cycles. Since the speed increment was slow (0.02 Hz/sec) the 50 cycles used can be assumed to be at constant speed.

Two sets of plots are drawn at each speed to show the different pseudo-phase plots in the vertical and horizontal directions. At slow shaft speeds (20 Hz) (Figures 7.30 and 7.31), the points concentrate on a single position in both directions. This indicates that the rotation is periodic. As the speeds increases to 25 Hz (Figure 7.32 and 7.33) the points are scattered within the focal points along the 45° line. The motion is still periodic but with greater shaft whirl amplitude. At a shaft speed of 28

Hz (Figures 7.34 and Figure 7.35) the points are widely scattered. There is no definite focal point. The motion is non-periodic. After the speed was increased to 32 Hz (Figure 7.36 and 7.37) the focal points appear again. This show that the motion become periodic again but with a greater shaft whirling amplitude.

7.10 ORBITS

Figures 7.38 to Figure 7.42 shows the *x-y* orbit of the shaft whirl at different shaft speeds. The orbit was drawn using 10 cycles to show the shaft movement during these speeds. The plots are to support the information gathered from the pseudo plots in section 7.9.

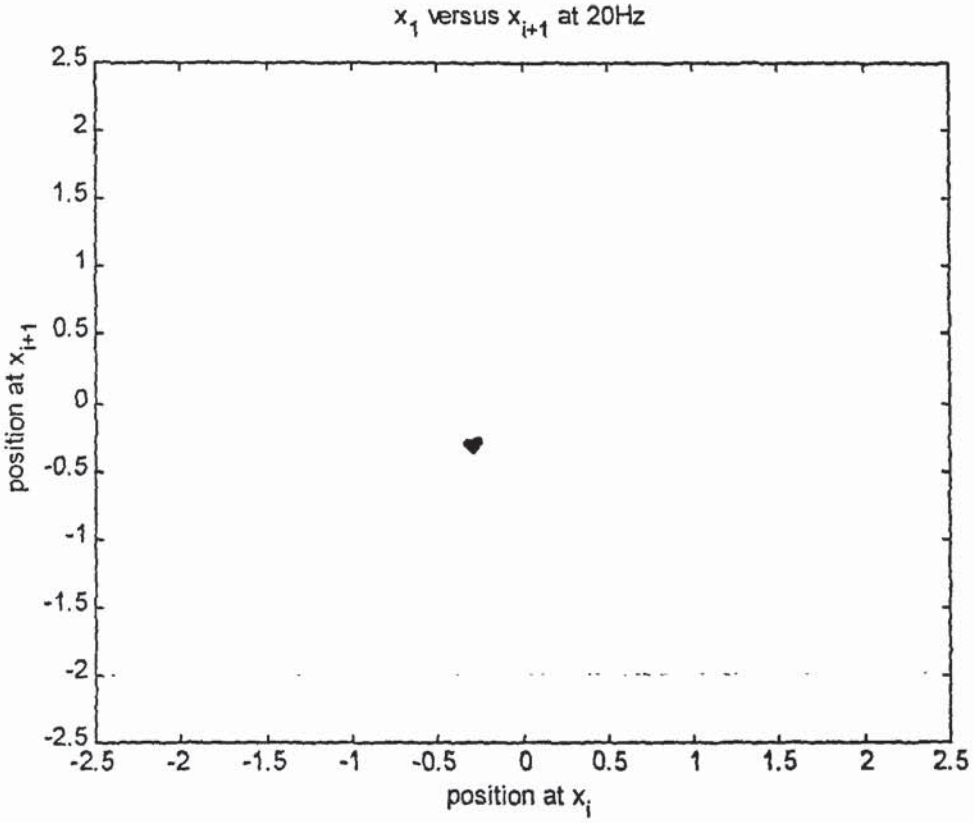

Figure 7.30: Pseudo phase plot at 20 Hz

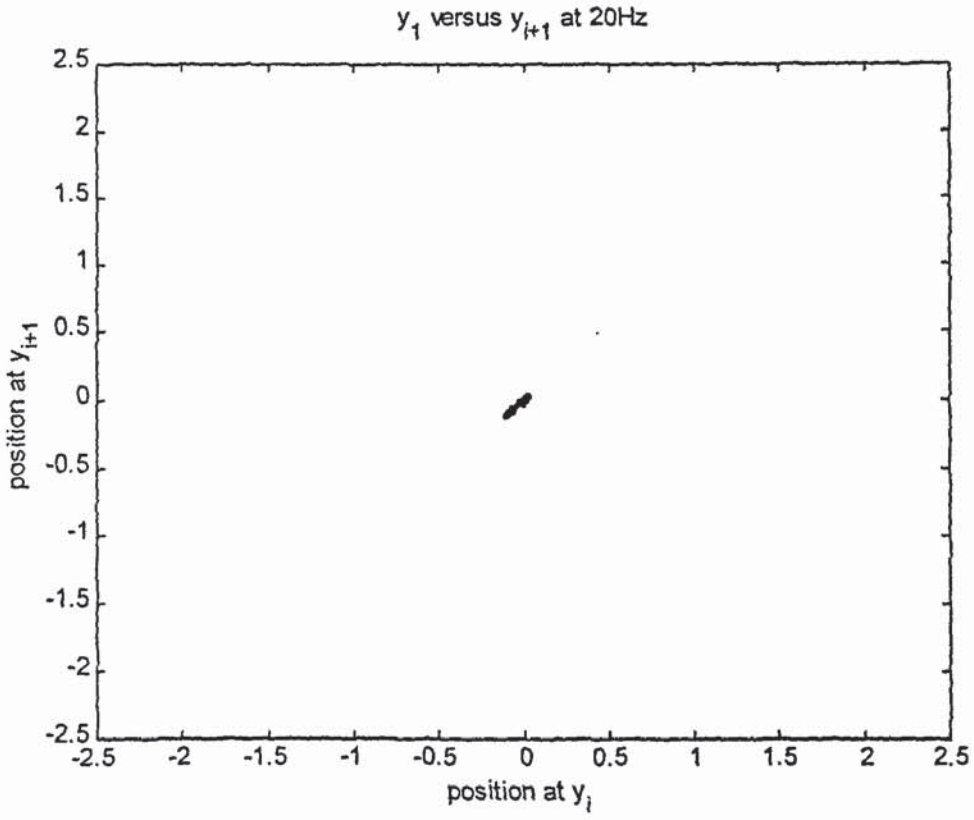

Figure 7.31: Pseudo phase plot at 20 Hz (vertical)

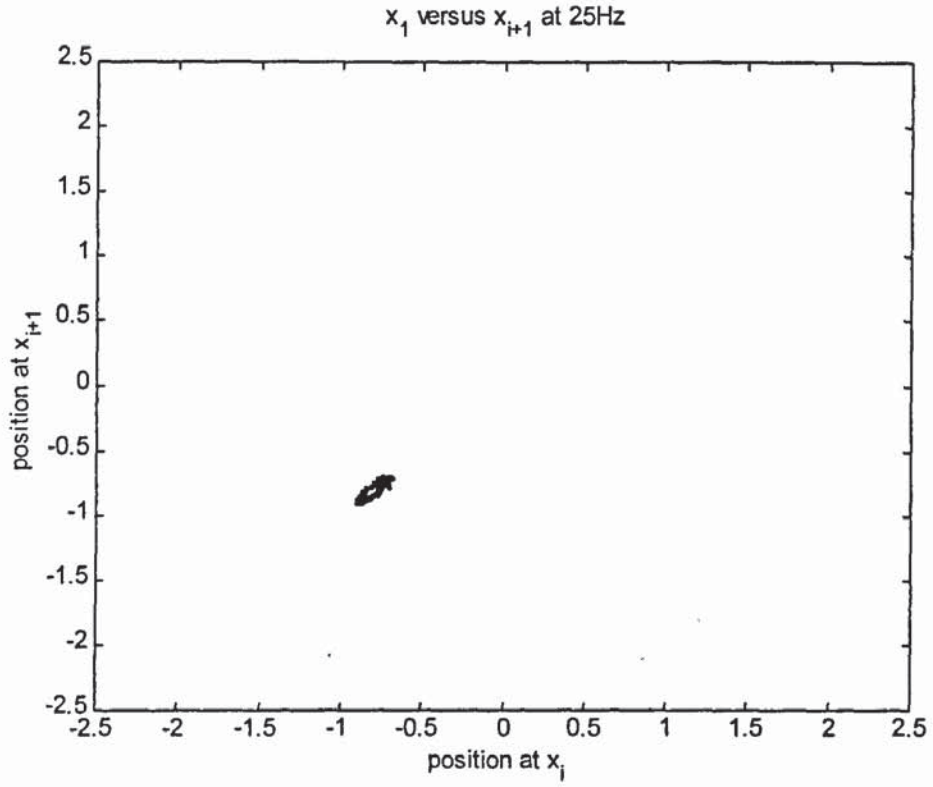

Figure 7.32 Pseudo phase plot at 25 Hz (horizontal)

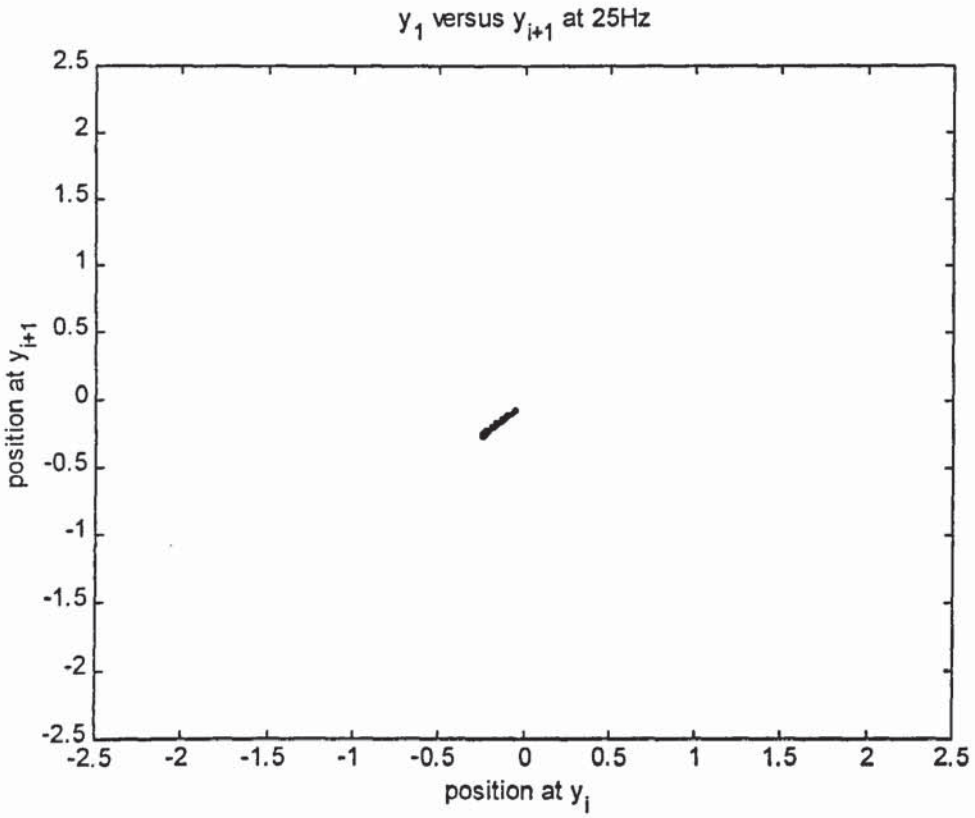

Figure 7.33 Pseudo phase plot at 25 Hz (vertical)

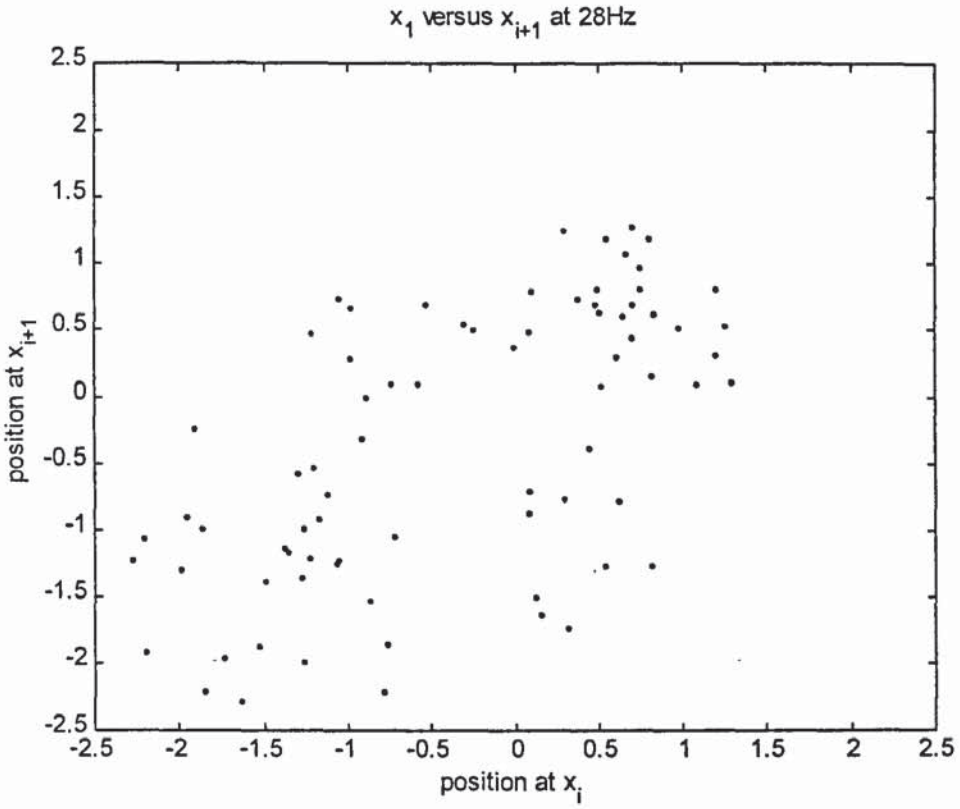

Figure 7.34: Pseudo plot at 28 Hz (horizontal)

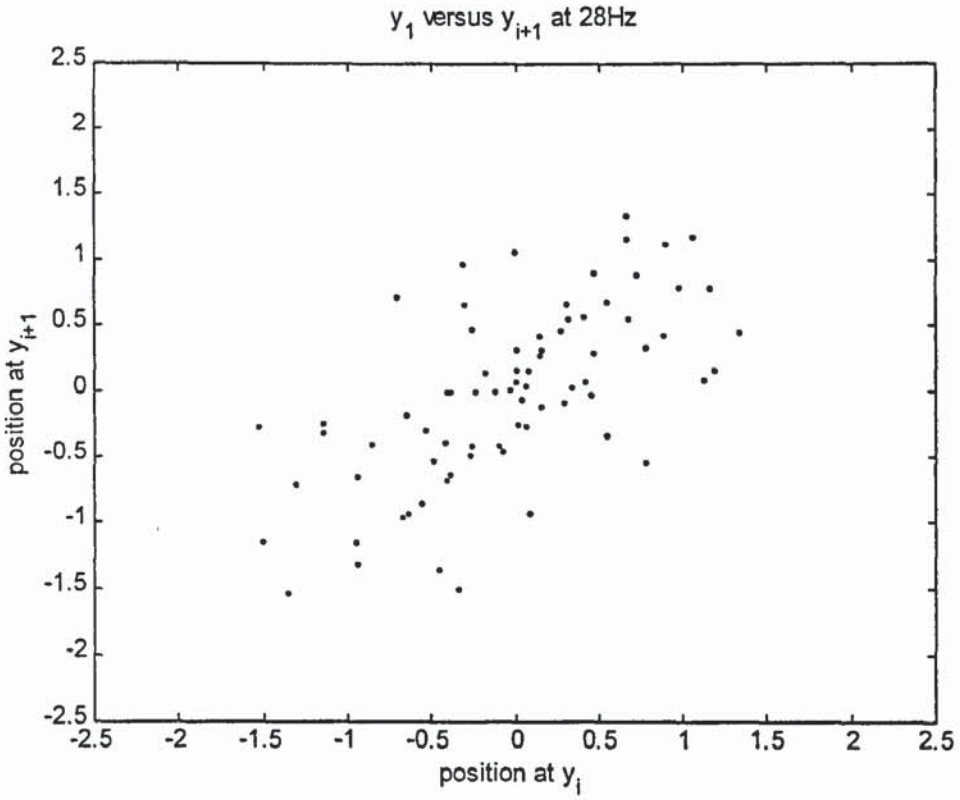

Figure 7.35: Pseudo-plot at 28 Hz (vertical)

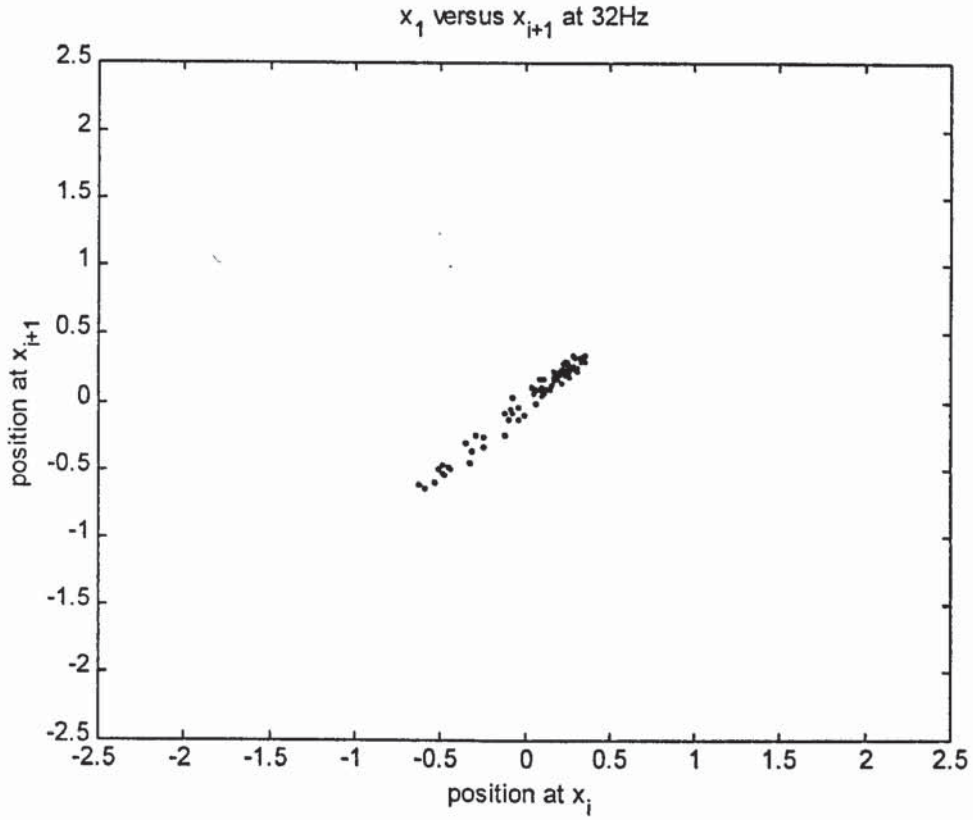

Figure 7.36: Pseudo phase plot at 32Hz (horizontal)

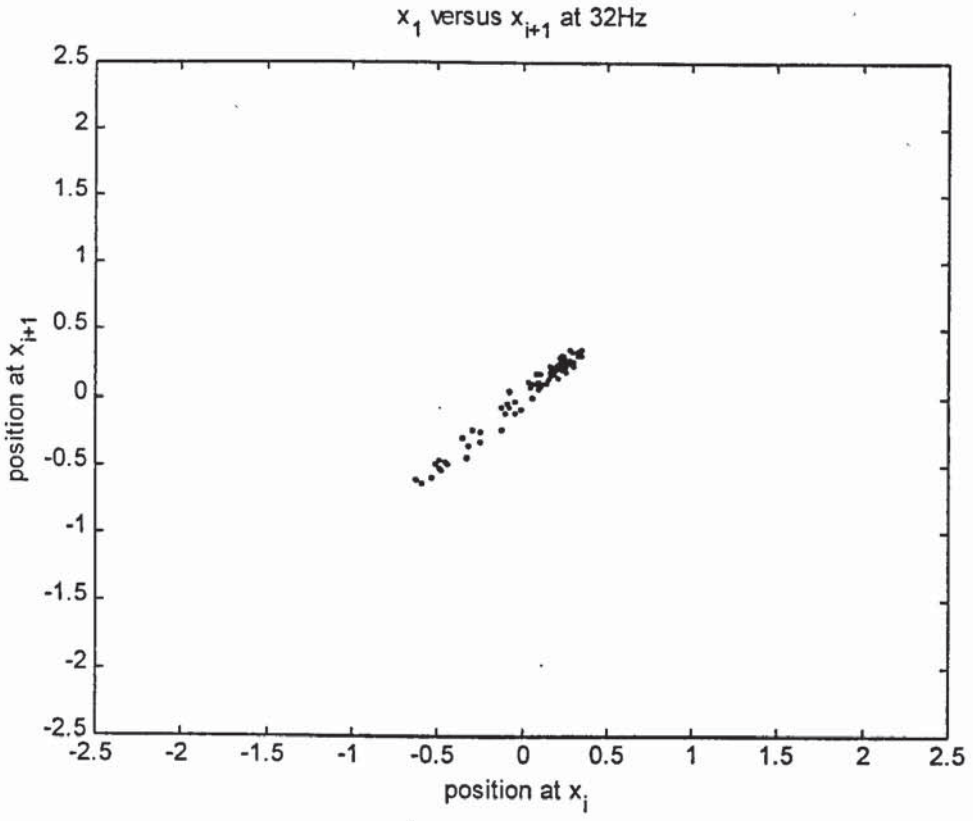

Figure 7.37: Pseudo phase plot at 32Hz (vertical)

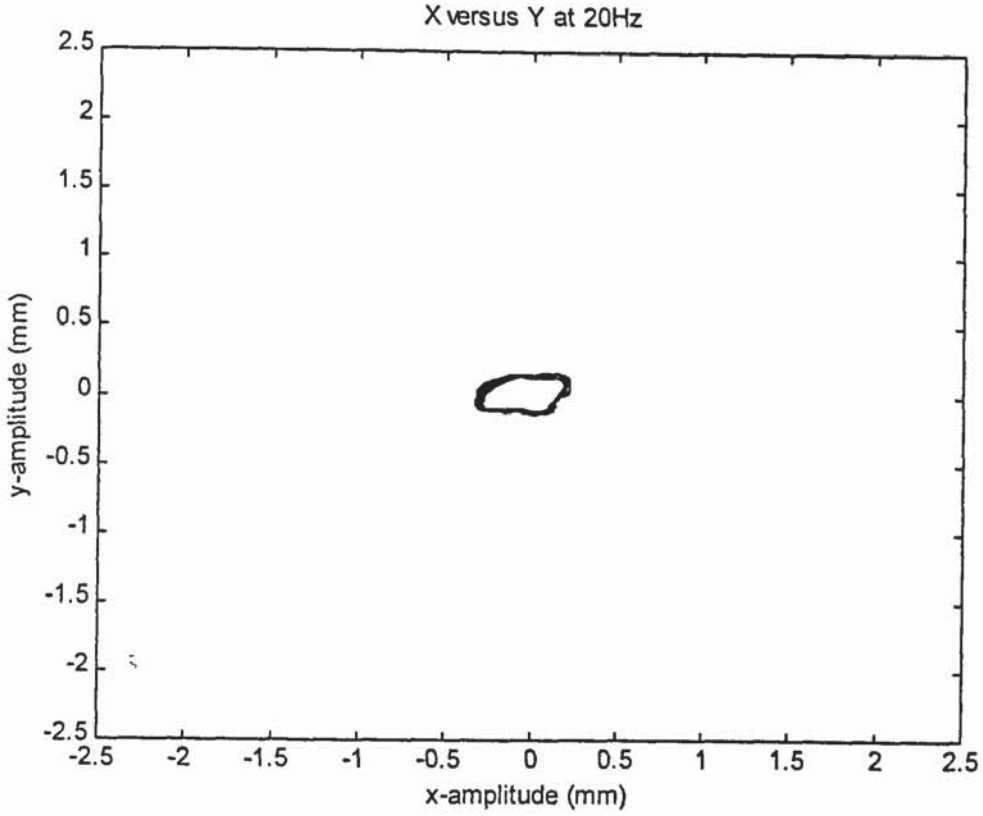

Figure 7.38: Rotor orbit at 20 Hz

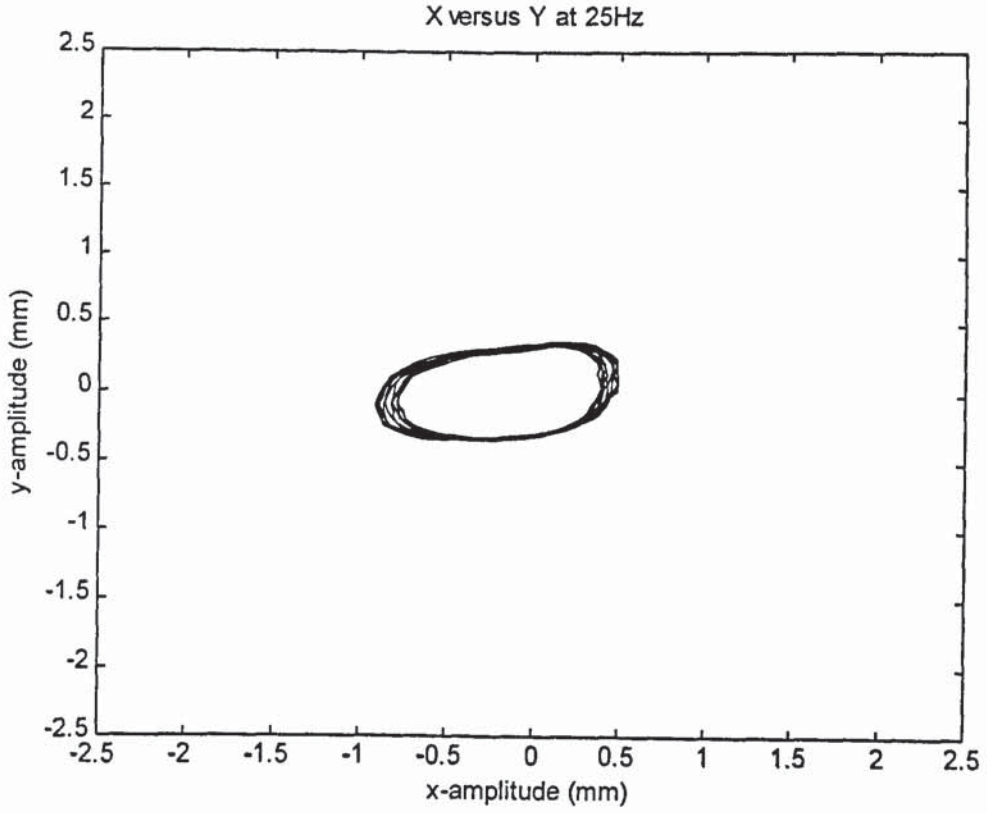

Figure 7.39: Rotor orbit at 25 Hz.

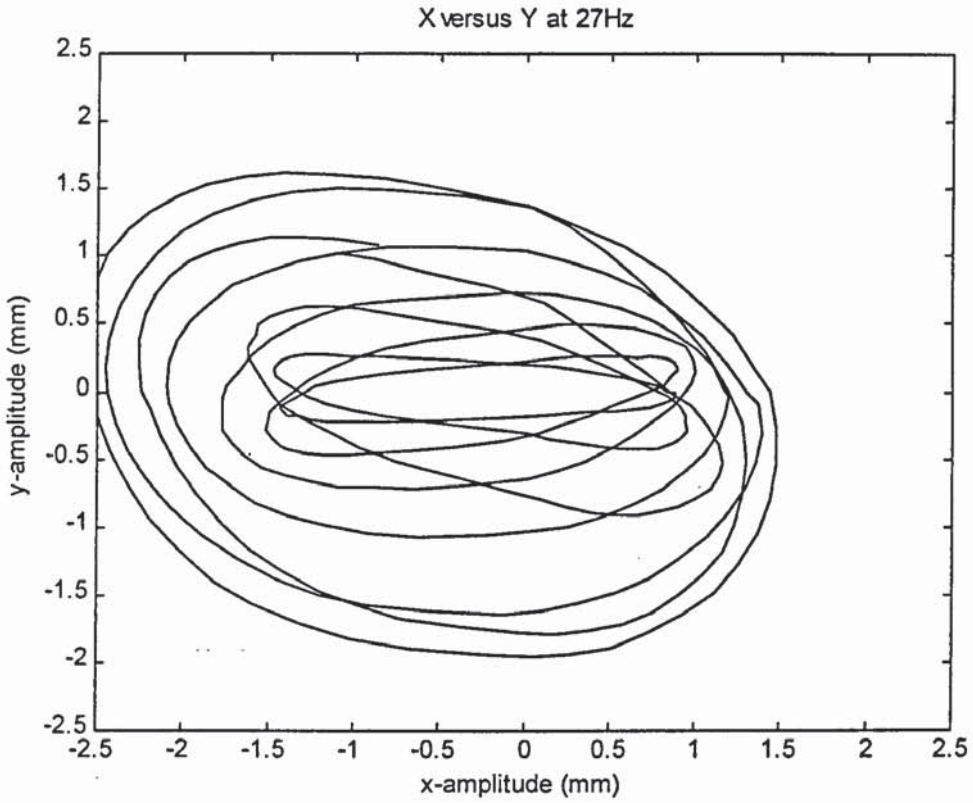

Figure 7.40: Rotor orbit at 27 Hz

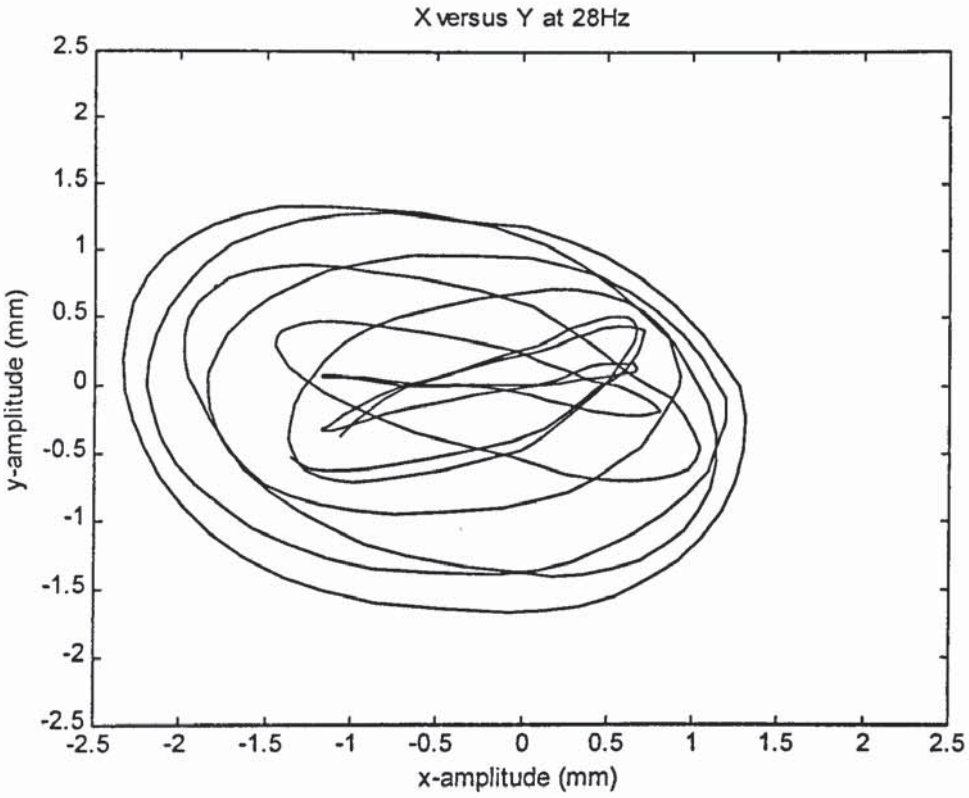

Figure 7.41: Rotor orbit at 28 Hz

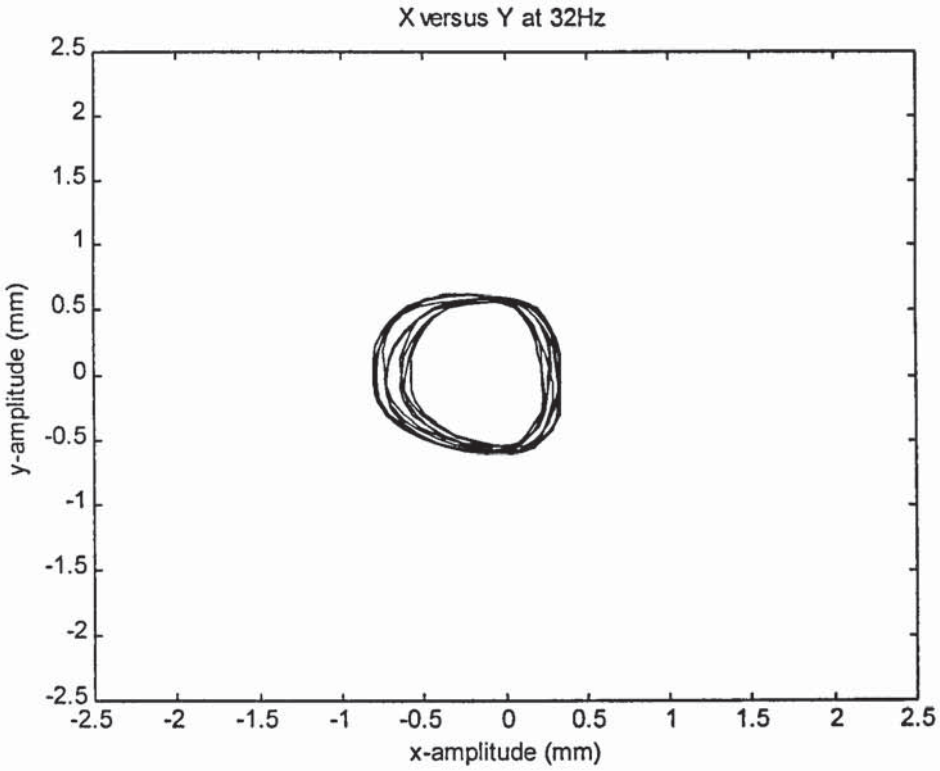

Figure 7.42: Rotor orbit at 32 Hz.

7.10 DISCUSSION OF RESULTS

The static deflection test estimated the stiffness of the system both in the vertical and horizontal directions. The results of the tests carried out in the horizontal and vertical directions are shown in Figure 7.1 and 7.2. There was a slight difference in the overall stiffness between the two directions. The differences could be attributed to the difference in the foundations where the vertical direction was stiffer than the horizontal direction. Figures 7.1 and 7.2 also depicted the change of stiffness from to lower stiffness after a certain threshold value. Visual inspection also indicated that after this value the rotor discs started to open. The threshold value was taken as 0.75 mm. The stiffnesses of the rotor are different from the calculated value using simply supported beam theory. The stiffnesses are the overall stiffness

of the shaft, bearing and foundations. It can be deduced that there are constraints at the supporting ends.

The modal tests gave the natural frequency in the vertical and horizontal directions. As shown in Table 7.1 the natural frequencies in the horizontal and vertical directions are different. These confirm the static tests carried out on the rotor system. Figure 7.4 and 7.5 shows the modal tests responses in the vertical and horizontal directions. Although more than one natural frequencies were obtained, only the first critical speeds were of interest.

Running the test rig slowly through the critical speed with an unbalance force (2.5 gm placed at 50 mm radius from shaft centre) was one form of test conducted on the test rig. Figure 7.5 shows that there was a jump in response during run-up as predicted by the simulation. The amplitude increased gradually as the speed increased until at a speed 25 Hz, there was a sudden increase in the amplitude without increase in speed. This increase in amplitude accounted for the unstable nature of the system at the point where it changed in stiffness. After this point the amplitude gradually decreased until it passed the resonance region.

Another interesting phenomenon observed during run-up, was that the transients effect of the jump did not die away with time but instead it perpetuated for some time along with the increase in speed until about 28 Hz. Closing up the time histories at this point indicated that there was a modulated waveform that indicated there was a closing and opening of the rotor gap, not in one cycle but in number of cycles.

To understand the phenomena further, the Discrete Fourier Transform (DFT) was carried out on the data. The results in Figure 7.6 show the DFT at speed of 26 Hz. This clearly indicated that there were other components present apart from the rotor speed. There were sidebands frequencies that was synchronous with the shaft speed. The run-up spectral map showed the effect of shaft speed of 25 Hz. to 28 Hz. After this region there was also a beating phenomena occurring at about 30 Hz shaft speed. The results were in close agreement with the results obtained from the simulation.

The run-down results showed that the vibration amplitude increased as the speed approached the resonance and continued to increase even after it surpassed the resonance before it suddenly dropped to lower amplitude at speed that was much lower than the original jump during run-up. The pseudo-phase plot (Figure 7.30 to 7.36) shows clearly that at lower speeds i.e. from 20 Hz to 25 Hz, the system was quite periodic in its motion. However from 26 Hz to 28 Hz shaft speed showed there were widely scattered points which indicated that the motion was not periodic. This is similar to the results shown by the spectral maps (Figure 7.7).

7.11 CONCLUSION

In this chapter, results have been reported from a series of experimental tests carried out on the test rig. Firstly, force deflection tests were carried out to determine the stiffness of the shaft and bearing before and after a threshold value when the disc opened. Then, modal tests were carried out to determine the natural frequencies. Finally, a series of run-up and run-down tests were carried out to compare the experimental and the model results.

Chapter Eight

DISCUSSION

8.0 INTRODUCTION

A series of studies were conducted using the simulation and experimental models discussed in the previous chapters. The following discussion is aimed at comparing the predictions of the simulation model with experimentally observed responses. The objective is to obtain an insight into the behaviour of bolted rotor system dynamics due to imbalance.

8.1. MODEL PARAMETERS

Using the data from measurements and calculations, the stiffness, damping, and mass characteristics of the experimental system were identified. The rotor parameters were chosen to match the experimental results. The numerical values are given in Table 5.1. The rotor shaft is slightly bent, and there was imbalance. The comparison of the experimental results and simulation results was made by using the imbalance configuration consisting of an out-of-balance 7.5×10^{-5} kg-m located on the rigid disk.

The theoretical stiffness was obtained by using simply supported beam theory. The value is 70000 N/m (Appendix A.1.2.3). The model validity was supported by finite element model (section 3.4). The experimental force-displacement (Figure 7.1) indicates that the overall stiffness horizontal and vertical directions are 125000N/m and 155000 N/m respectively. Using boundaries of constraint and pinned ends, the stiffness is calculated as 137142 N/m (Appendix A.1.2.3). Therefore, the supporting bracket design and arrangement have a great influence on the stiffness of the system. The mass of the system is taken as the 3.8 Kg (Appendix A.1.2.2) by taking the mass of the rotor and the shaft. This is consistent with the experimental test using modal analysis where the natural frequencies are obtained as 28 Hz and 32 Hz in horizontal and vertical direction respectively. The stiffness of the opening is taken as 50000 N/m based on the opening stiffness obtained from the quasi-static test. The ratios of overall joint stiffness to overall shaft stiffness are 0.3094 and 0.4 respectively in the vertical and horizontal directions. The damping value was determined by logarithmic decrement method. This can also be determined by modal test results. The damping ratio obtained is 0.007, and this value is relatively small. The damping can be attributed to rolling bearing damping since the rotor system is rigid.

8.2 EFFECT OF IMBALANCE

Figure 5.4 and Figure 5.5 shows the series of simulated results from the model with an increase in the imbalance offset magnitude of 0.001mm (0.35 x 10^{-5} kg-m), 0.01mm (3.5 x 10^{-5} kg-m), 0.05mm (7 x10^{-5} kg-m) and 0.1 mm (35 x 10^{-5} kg-m). Figure 7.13 to Figure 7.16 shows the run-up and run-down plot with imbalance value of 7.5 x

10^{-5} kg-m (0.02 mm offset). The response amplitudes increase with increasing imbalance.

Figure 5.2 shows the simulated time histories of the run-up conditions with 0.02 mm offset (7.5×10^{-5} kg-m) imbalance. These plots clearly depicted the backbone curve leaning leftward towards lower speed. There is an unstable region associated with free behaviour of the system independent of the excitation. At lower speed the stiffness of the shaft dominate the response. The vibration amplitude increases with increasing speed until the threshold value, where the system becomes unstable. This jump phenomenon happens when the dominant stiffness is that the joint. The jump is not instantaneous in time but requires a few oscillations to reach the steady-state vibration at the new amplitude. There is also a phase lag of 180° as shown in Figure 5.3. Similar results were shown by Ehrich (1990), using hardening stiffness which showed that the backbone curves lean toward the higher speeds.

The transient responses after the jump are illustrated in simulated result and experiment as shown by Figure 5.18 and Figure 7.12 respectively. There is a close agreement between the model and experimental results. There is an opening and closing (clapping) of the joint within a few oscillations with beat (envelope) frequency of 0.8 Hz interval. This DFT of the signals show that there were equally spaced sidebands of +/-N shaft speed where, N is a fraction of the shaft speed. At 25 Hz, the value of N is 1/5. Since N is not an integer multiple of the speed and therefore it is not due to loosing of the bolts (Goldman 1999). These are shown in Figure 5.12 and Figure 7.12 in the simulation and experiments.

8.3 SPECTRAL PLOTS

Figure 5.8, Figure 5.10, Figure 5.12, Figure 5.14 and Figure 5.16 are the frequency responses at sample speeds of 20 Hz, 25Hz, 27 Hz, 28 Hz and 32 Hz respectively for simulated responses for an imbalance offset value of 0.02 mm. Similarly, Figure 7.23 shows an experimental response of a sample frequency plot at 25.5 Hz with imbalance offset value of 0.02 mm. The experimental and simulated results of the full spectra are shown again below (as depicted in Figure 7.24a and Figure 5.5).

Similarly, the forward-backward whirl components for the experimental and simulation results are shown in Figure 7.29 and 5.5. There is relatively good agreement between the actual and predicted responses, except the peak values, which are very sensitive to damping. At lower speeds, the stiffness of shaft and bearing are dominant. As the speed increases, the joint stiffness becomes dominant. When the whirling amplitude reaches the threshold value of 0.75 mm, an unstable jump occurs.

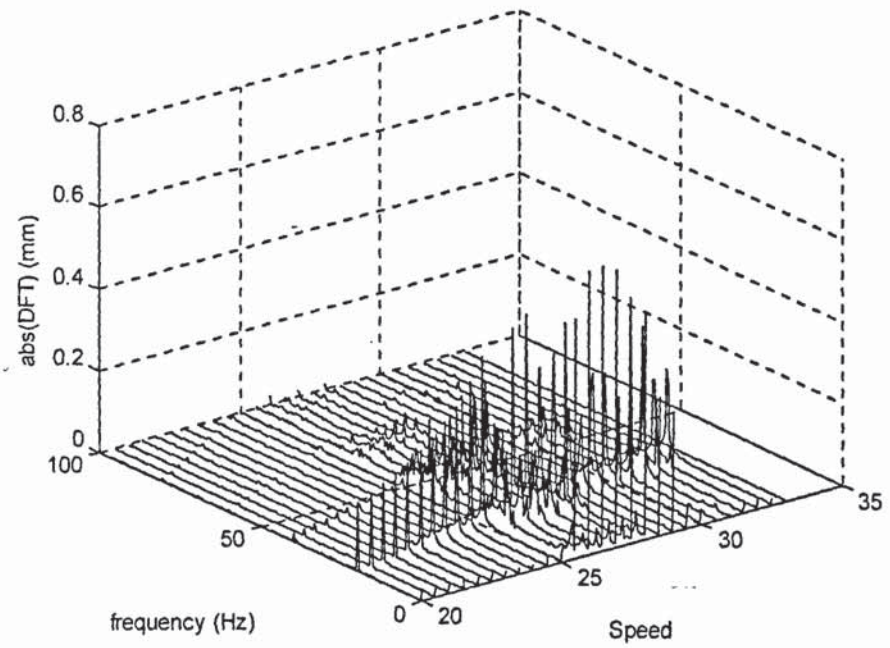

Figure 7.24: Spectra plot of the experimental data

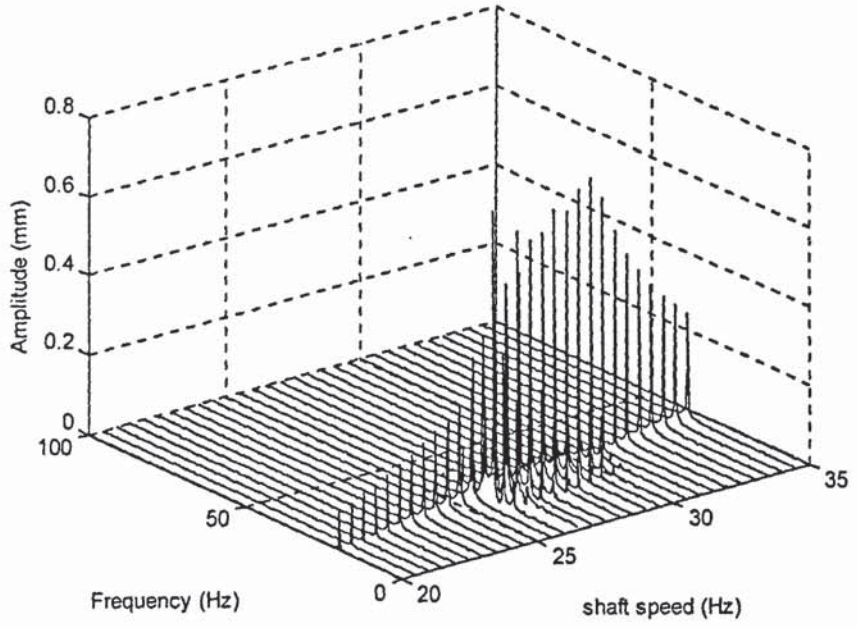

Figure 5.6. Spectra plot from the simulation result.

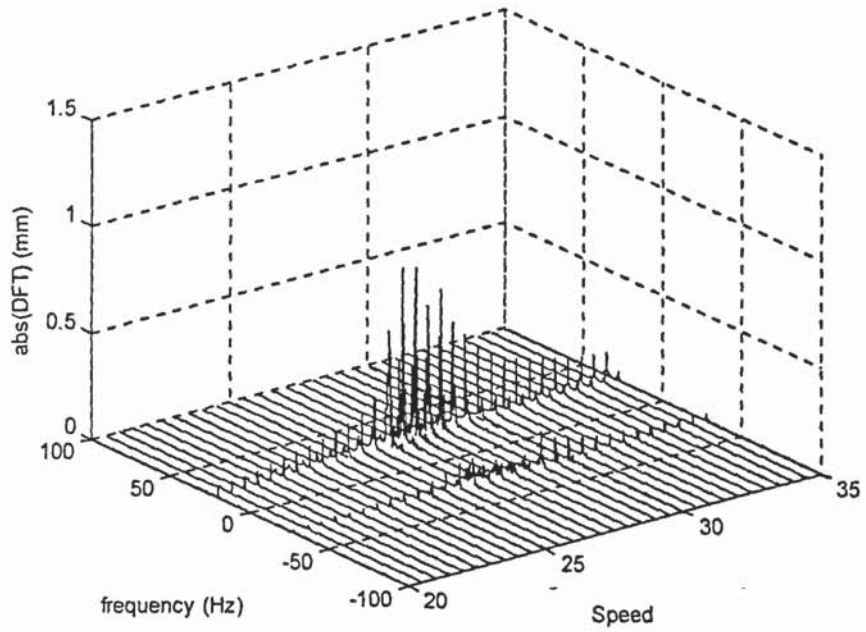

Figure 5.7: Forward-backward whirl of the simulated data.(LHS-forward)

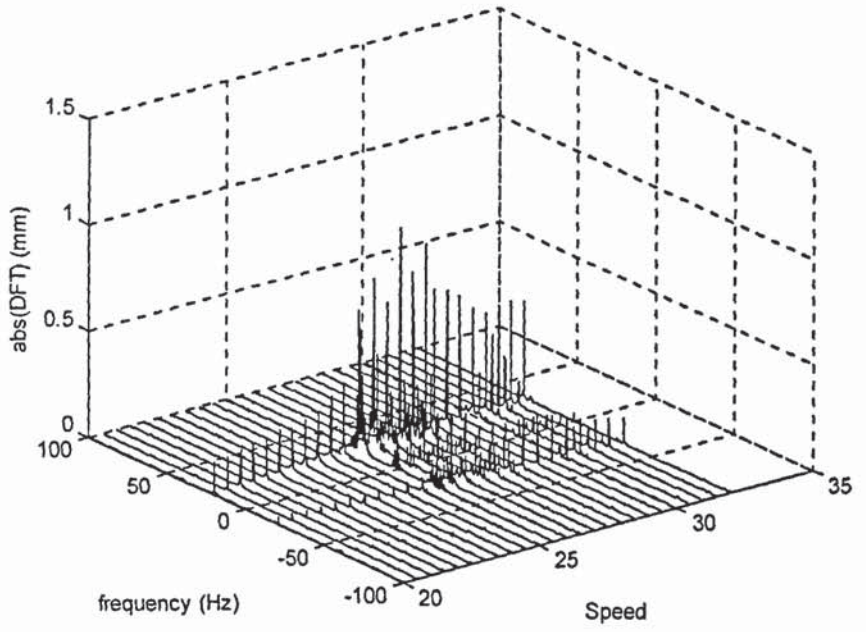

Figure 7.28: Forward-backward spectra diagram of experimental results.(LHS-forward)

The support anisotropy affects the spectrum of rotor/support system natural frequencies. This causes rotor imbalance-related synchronous precessional (orbital) motion to be elliptical rather than circular in a wide rotating speed range. In certain rotating speed regions, the rotor imbalance orbit are precessing backward (Lee, 1993). It can happen that a portion of the rotor precesses while the other precesses backward. Figure 5.7 and Figure 7.28 show the simulation and experimental plots of the simultaneous backward and forward precession of different sections of the rotor. There is a close agreement between both results although the magnitudes are different. This phenomena occur at a rotating speed range of 25 Hz to 30 Hz.

8.4 POINCARE'S PLOTS AND ORBITS

Relatively long time-marching computation is needed to obtain a convergent orbit. Poincare's map was used to investigate the stability of periodic orbits. The numerical data was collected at an interval of each oscillation of period $\tau = 2k\pi \quad (k = 1,2,....)$. Figures of orbits and Poincare's map uses large periods of integration to show whether the system is having bifurcation, quasi-periodic and chaotic motions.

Pseudo-phase plots were used to show the periodicity of the responses (Moon, 1989). Figure 5.19 to Figure 5.38 are the simulated data of the pseudo-phase plots to show the change in the periodic response to quasi-periodic response at 27 Hz and 28 Hz. Referring to Figure 7.30 and Figure 7.37 are the experimental results of similar plots. There is a close agreement with the theoretical results.

Similarly, Figure 5.9, Figure 5.11, Figure 5.13, Figure 5.15 and Figure 5.17 are the samples of orbit plots at shaft speeds at 20 Hz, 25 Hz, 27 Hz, 28 Hz, 32 Hz for simulated response. Figure 7.38 to Figure 7.42 are the orbits for the above speeds.

8.5 EXPERIMENTAL LIMITATIONS

In general, the test rig was used with success to exhibit the desired phenomenon within the limitation of the design. As predicted by numerical simulation, the response of the system driven at speeds other than close to critical speed remain stable in the experiments. At close to resonance the response become unstable, where the jump phenomena occur but were bounded by the structural damping.

There are a few discrepancies in the experimental set-up, which affect the accuracy of the overall results.

(a) There was a slight bend in the shaft (0.2 mm). The bend was probably attributable to the shaft itself and perhaps disk contact surface. Although attempts were made to minimise the bend, the value was still significant for this application. Balancing managed to reduce the vibration level. The vibration amplitude measured is the actual vibration amplitude plus the shaft bend.

(b) The supporting arrangement was giving different stiffness in the vertical and horizontal directions. The shaft was constrained against bending at one end of the rotor. This made the stiffness of the shaft higher than the stiffness calculated using simply supported beam theory.

(c) It was desired that the axial stiffness one end of the bearing was small and the lateral/radial stiffness higher. This arrangement was necessary to allow axial movement when the disk opening happens. Re-modification is necessary to produce the required movement.

(d) The motor controller was not giving a steady rotational speed at lower speed (below 20 Hz). These give an uneven signal due to fluctuating speed. The other limitation was the maximum speed was up to 10000 rpm with no load. Therefore with this speed only the first critical speed was covered.

(e) Proximity sensor range was too small to cover the range of vibration. Although two opposite sensors were used their ranges were only up to 3 mm. This amplitude was considered large enough for most applications, however due to softening effect, the jump sometimes exceed this value. Furthermore it was dangerous to run the rotor at too high amplitudes.

8.6 SIMULINK LIMITATIONS

There are numerous features and blocks in SIMULINK that allows the simulation to be implemented successfully. The performance of the simulations was improved by improving the model design and choice of the simulation parameters. The solver used was ode45 (based on the Runge-Kutta method) with variable step solvers. Ode15s (based on Gear method) was also used at times when ode45 failed to produce stable response. The accuracy of the simulation depended on the

absolute tolerance or relative tolerance. The system seems to converge with the default relative tolerance of 0.001 (0.1%).

There are few issues that hinder the successful implementation of the simulation model:

1. Simulation speed

   Simulation speed depends on a number of factors. The most critical are the speed of the computer used and its memory. Running simulation with barely enough memory will drastically slow down the simulation time.

2. Memory issues

   Apart from the simulation speed a failure encountered was the memory allocation error. This happens due to the large amount of data generated during the simulation process. These involve the time scale setting being to long, tolerance too small and step size too small.

Chapter Nine

CONCLUSIONS AND FURTHER WORK

9.0 INTRODUCTION

In this section, the concluding remarks drawn from simulations and experiments and some areas for further work, which have been highlighted are discussed.

9.1 ACHIEVEMENTS

This work shows that a bolted rotor exhibits certain non-linear characteristic close to system resonance due to unbalance with increases in speed.

9.1.1 Theoretical background

A literature survey was carried on the background to research the topic and the need for research into the subject was established.

The essential theory of bolted rotor was presented. A small order system based on Jeffcott rotor was chosen and the equations were developed. Although in practice the rotor disc comprises more that one disc jointed together by either central bolt or number of bolts along the circumferential position, a simplified model with four degree

of freedom was chosen. This in turn allows a simple test rig to be used to validate the results produced by the model.

9.1.2 Simulations

SIMULINK was used for the simulation with success. The output responses of the system in term of displacements or velocities were acquired.

The results from the simulation predicted the dynamic behaviour of the bolted rotor and in particular predicted the jump phenomenon which occurs when the joint stiffness is dominant.

9.1.3 Experiment

To support the theory and the simulation of the bolted rotor behaviour, an experimental test rig was designed and fabricated. Experiments on the especially built rig demonstrated the occurrence of the jump phenomenon as it passed through the first resonance.

9.1.4 Post processing

The data was analysed from the simulation and the test rig using MATLAB script. The data are represented in time domain and frequency domain representation. Waterfall or spectral plots were used to illustrate the effect of speed increment.

9.2 CONCLUDING REMARKS AND FURTHER WORK

The specific aims and objectives of the thesis have been achieved. This model developed shown the qualitative agreement with the experimental results.

Although an extensive study on the subject of bolted rotor has been carried out, it has revealed that some further development of interest may still be necessary. Areas for further studies are summarised as follows:

- Rotors comprising multiple discs rather that one disc bolted together are those more commonly encountered in practice. Therefore it is felt that having a rotor consisting of more that two disc bolted centrally or on a small PCD will give a better insight into the problem. The balancing will more be demanding. The threshold stiffness value will be from contribution from more that joint.

- The theoretical background developed was based on a single plane Jeffcott rotor with the assumption of rotating frame along the opening of the rotor. The limitation of this assumption is restricted to an isotropic shaft and with the rotor in the middle. For bolted rotors with different stiffnesses in their orthogonal directions, modification to the rotating plane that follows the stiffness plane is made rather than the opening of the rotor. This leads to the equations becoming more complicated.

- The model developed is a simplified model with four degrees of freedom that includes the bearings and their foundation. An

improvement can be made by including the rotational deflection to incorporate rotor that is not placed at the mid-point between the supporting bearing.

- There are a number of limitations in the experimental equipment used. The motor used is a D. C. motor without digital speed encoder, hence the speed cannot be controlled remotely and accurately using a computer. The proximity sensors (range) used has a range that is not large enough to cover the whole range of the deflection. The design of the supporting system needs improvement to eliminate stiffnesses different in the vertical and horizontal directions. The mechanism of the bearing clearance to allow axial sliding movement needs modification to avoid unnecessary constraint to the transverse deflection. These limitations should be overcome in future test rigs.

- The opening or disc movement between the bolted disc is an important parameter to be measured. Due to limitation of the instrumentation the value was determined in relation to the transverse displacement. Since these values are relatively small (magnitude in micrometers), a more sensitive transducer is required to measure this displacement.

REFERENCES:

Adiletta G, A. R. Guido and C. Rossi (1996a), *Non-linear Dynamics*, **10**, 251-269, Chaotic Motions of a Rigid Rotor in Short Journal Bearings.

Adiletta G., A. R. Guido and C. Rossi (1996b), *Non-linear Dynamics*, **11**, 37-59, Non-Periodic Motions of a Jeffcott Rotor with non-linear Elastic Restoring Forces.

Bachschmid, N. and Diana, G. (1984), *IMECH.* C304, 193-197, The Influence of Unbalance on Cracked Rotors.

Benhafsi (1993), PhD Thesis, Aston University, A Parametric Approach to System Identification of Nonlinear Structures.

Bently, D (1974), *ASME paper No. 74-PET-16*, Petroleum Mechanical Engineering Conference, Dallas, TX, Forced Subrotative Speed Dynamic Action of Rotating Machinery.

Bohlen S. and Gaul L. (1987), *5th IMAC*, 86-91, Vibration of Structures Coupled by Nonlinear Transfer Behaviour of Joints: A Combined Computational and Experimental Approach.

Brigham E. O. (1988), **The Fast Fourier Transform and Its Applications**, Prentice Hall International, Inc.

Bucher I. and Ewins D. J. (1997), *Mechanical Systems and Signal Processing*, 11(4), 577-601, Multidimensional Decomposition of Time-Varying Vibration Response Signals in Rotating Machinery.

Burdekin M., Cowley A. and Back N. (1978), *Journal of Mechanical Engineering Science* **20**(3), 121-127, An elastic mechanism for the microsliding characteristics between contacting machined surfaces.

Childs D. W. (1982) *ASME Journal of Energy and Power* **104**, 533-541, Fractional-frequency rotor motion due to nonsymmetric clearance effect.

Childs D. W. (1993), **Turbomachinery Rotordynamics: Phenomena, Modeling and Analysis**, John Wiley and Sons, Inc. New York.

Choi S. K. and S. T. Noah (1992), *Winter Annual Meeting of ASME*, V50, 21-28, Mode Locking and Chaos in a Modified Jeffcott Rotor with a Bearing Clearance.

Choi S. K. and S.T. Noah (1987), *Trans. ASME; Journal of Vibration, Acoustics, Stress, and Reliability in Desigr*, **109**, 255-261, Non-linear Steady-State Response of a Rotor-Support System.

Choy F. K. and Padovan J. (1987), *Journal of Sound and Vibration*, **113**(3), 529-545, Non-linear transient analysis of rotor-casing rub events.

Darlow M. (1992), **High Speed Balancing,** McGraw Hill, New York

Den Hartog, J. P. (1934), Mechanical Vibration,McGraw Hill Book Co, New. York

Dimarogonas A. D. and Paipetis S. A., (1983), *Analytical Methods in Rotor Dynamics*, Applied Science Publishers, London.

Dimarogonas and Papadopoulos (1983), *Journal of Sound and Vibration*, **91**(4), 583-593, Vibrations of Cracked Shafts in Bending.

Dimarogonas, A. (1996), **Vibration for Engineers**, 2nd Editions, Prentice Hall International, Inc.

Dokainish M. A. and Subbaraj K. (1989a) *International Journal of Computers and Structures*, 32, 1371-1386, A Survey of Direct time-integration methods in Computational Structural Dynamics: 1, Explicit Methods.

Dokainish M. A. and Subbaraj K. (1989b) *International Journal of Computers and Structures*, 32, 1387-1401, A Survey of Direct time-integration methods in Computational Structural Dynamics: 2, Implicit Methods.

Dunne F. P. E. and M. Heppenstall, (1990), *Proc. Instn Mech. Engrs.* **204**. 37-42. The Effect of Joints on the Transverse Vibration of a Simple Structure.

Ehrich F.F. (1992), *Trans. of ASME, Journal of Vibration and Acoustics*, **114**, 50-57, Observations of Subcritical Superharmonic and Chaotic Response in Rotordynamics.

Ehrich (1964) *Trans. of ASME, Journal of Applied Mechanics*, 279-282, Shaft Whirl Induced by Rotor Internal Damping.

Ehrich F. F. (1992) **Handbook of Rotordynamics**, McGraw-Hill, Inc, New York.

Ehrich F.F (1991) Jan, *Trans. ASME, Journal of Vibration and Acoustics*, **113**, 50-57, Some observations of Chaotic Vibration Phenomena in High Speed Rotordynamics

Ehrich F.F., (1994), *Proceedings of the 4th Int. Conf. on Rotor Dynamics (IFTOMM)*, 1-6, Rotordynamic Response in Nonlinear Anisotropic Mounting Systems.

Ehrich, F. F. (1988) *ASME Journal of Vibration, Acoustics, Stress and Reliability in Desigr.*, **110**, 9-16, High order Subharmonic Response of High Speed Rotors in Bearing Clearance.

Ewins, (1983), **Modal Testing: Theory and Practice**, John Wiley and Sons Inc., New York.

Flowers G. T., Margithu D. B. and Szasz G.(1998) *Journal of Sound and Vibration* **218**(2), 350-360, The Application of Floquet Methods in the Analysis of Rotordynamic Systems.

Gasch R., (1976), *ImechE*, C178/76, 123-128., Dynamic Behaviour of a Simple Rotor with a cross-sectional Crack.

Gasch R., (1993), *Journal of Sound and Vibration* **160**, 313-332, A Survey of the Dynamic Behaviour of a Simple Rotating Shaft with a Transverse Crack.

Gonsalves D. H., R. D. Neilson and A. D. S. Barr (1995) *Nonlinear Dynamics*, **7**, 451-470, A Study of the Response of a Discontinuity Nonlinear Rotor system.

Goodman L.E. and Brown C. B. (1962), *Trans ASME Journal of Applied Mechanics*, 17-22, Energy Dissipation in Contact Friction: Constant normal and Cyclic Tangential Loading.

Grabowski (1980) *Trans. of ASME, Journal of Mechanical Design*, Vol. **102**, 140-146, The Vibrational Behaviour of a Turbine Rotor Containing a Transverse Crack

Greenwood J. A and Williamson J.B. P (1966), *Proceedings of Royal Society*, Ser. A, 295, 300-319, Contact of Norminally Flat Surfaces.

Gual L., Nckenhorst U., Willner K. and Lenz J.,(1994) *12th IMAC*, 875-881, Nonlinear Vibration Damping of Structures wuth Bolted Joint

Haslinger K. H. (1995), *Journal of Sound and Vibration*, 181, 851-871, Experimental Characterization of Sliding and Impact Friction Coefficients between Steam Generator Tubes and avb Supports.

Hayashi, C. (1964) **Non-linear Oscillations in Physical Systems**, McGraw Hill, London.

Hsu C. S. (1963) *Trans ASME, Journal of Applied Mechanics* **30**, 367-372, On the Parametric Excitation of Dynamic System Having Multiple Degrees of Freedom.

Hsu C. S. (1965) *Trans ASME, Journal of Applied Mechanics*, **32**, 373-377, Further Results on Parametric Excitation of a Dynamic System.

Hsu C. S. (1974) *Journal of Mathematical Analysis and Applications* **45**, 234-251, On Approximating a General Linear Periodic System.

Hu M. -C and Huang S. -C (1998), *Trans ASME; Journal of Vibration and Acoustics* **120**, 551-556, In Plane Vibration and Crack Detection of a Rotating Shaft-Disk Containing a Transverse Crack.

Ishida Y. and K. Hirokawa, (1996), *JSME International Journa*, series C, Vol 39.Vol 2. 225-233, Internal Resonances of a Cracked Rotor (Major Critical speed and speeds in Precritical Range)

Ishida Y. (1991), *JSME International Journa*, **37**(2), C, 237-245, Nonlinear Vibrations and Chaos in Rotordynamics

Ishida Y., Nagasaka I., Inque T. and Lee S. W., (1996), *Nonlinear Dynamics* **11**, 107-120, Forced Oscillations of a Vertical Continuous Rotor with Geometric Nonlinearity.

Jazequel L., Setio H. D. and Setio S.,(1990), *8th IMAC*, Nonlinear Modal Synthesis in Frrequency Domain.

Jeffcott, N. (1919), *Philosophical magazine*, **37**, 304-314, Lateral Vibration of Laded Shafts in the Neighbourhood of a Whirling Speed-The Effect of Want of Balance,

Jordan D. W.and Smith P., (1987), **Nonlinear Ordinary Differential Equations**, Oxford University Press.

Jun O. S., Eun H. J., Earmme Y. Y. and Lee C. –W. (1992), *Journal of Sound and Vibration* **155**, 273-290, Modelling and Vibration Analysis of simple Crack with a Breathing Crack.

Kang Y., Shih Y. –-P and Lee A. –C (1992), *Trans ASME: Journal of Vibration and Acoustics*, **114**, 194-207, Investigation on the Steady State Responses of Asymmetric Rotors.

Kim Y. B and S. T. Noah (1990), *Nonlinear Dynamics* **1**, 221-241, Bifurcation Analysis for a Modified Jeffcott Rotor with Bearing Clearances

Kimball, A. L. (1924), *Gen. Electric Rev.*, **27**, 244-51, Internal Friction Theory of Shaft Whipping.

Kligerman Y. and Gottlieb O. (1998), *Trans. ASME, Journal of Vibration and Acoustics*, 120, 848-853, Dynamics of a Rotating System with a Nonlinear Eddy Current Damper.

Klompas, (1983), *Trans. of ASME, Journal of Enggng for Power*, **105**, 184-191, Unbalance Response Analysis of a Complete Turbomachine.

Kramer, E. (1993), **Dynamics of Rotors and Foundations**, springer, Berlin.

Lee, C.-W, (1993), **Vibration Analysis of Rotor**, Kluver, Dortrecht.

Lewis F. M., (1945). *Trans. of ASME: Journal of Applied Mechanics*, Vibration during Acceleration through a Critical Speed.

Lindfield, G and Penny, J (1999), **Numerical Methods using MATLAB**, 2nd edition, Prentice Hall, Upper Saddle River, New York.

Mayes I. W. and Davis W. G. R. (1984) *ASME, Journal of Vibration, Acoustics Stress and Reliability in Desigr*, **10€**, 139-145, Analysis of Response of a Multi-Rotor-Bearing System Containing a Transverse Crack in a Rotor.

Meirovitch, L., (1986), **Elements of Vibration Analysis**, 2nd Ed., McGraw Hill, New York.

Musako M., Ito Y. and Koizumi T. (1974), *Bulletin of the journal of Mechanical Engineering and Science*, **17**(113), 1494-1501, Horizontal Stiffness and Micro-slip on bolted joint subjected to repeated tangential static loads.

Muszynska A. (1989) *Shock and Vibration Digest* **21**, 3-11. Rotor to stationary element rub-related phenomena in rotating machinery-literature Survey.

Muszynska A. (1996) *The 6th International Symposium on Transport Phenomena and Dynamics of Rotating Machinery*, Honolulu, Hawaii, Dynamics of Anisotropically Supported Rotors

Nayfeh A. H. and Mook D.K., **Nonlinear Oscillations**, Wiley, New York, 1979.

Neilson and Barr (1988), *Proceedings of the I. Mech. E. 4th Int. Conf. on Vibrations in Rotating Machinery.* Scotland, 13-15, 589-598. Response of two elastically supported rigid rotors sharing a common discontinuously non-linear support.

Nelson H. D. (1998) *JSME International Journal* Series C, **41**(1), 1-12, Rotordynamic Modelling and Analysis Procedure: A Review.

Nelson, H. D. (1994), *Proc. IFToMM*, 171-177, Modeling, Analysis and Computation in Rotordynamics – A Historical Review

Newkirk, B. L. (1924) *Gen. Electric Review*, **27**, 169-178, Shaft Whipping.

Parker and Chua, (1989), **Practical Numerical Algorithms for Chaotic Systems**, Springer-Verlag, New York.

Ramirez, R. W. (1985), **The FFT Fundamentals and Concepts**, Prentice Hall, Englewood, Cliffs, N.J.

Rao J.S. (1983), **Rotor Dynamics**, Wiley, New York.

Ren Y. and Beards C.F. (1993), *11th IMAC*, A General Receptance Coupling Technique.

Ren Y. and Beards (1993), *11th IMAC*, 473-378, On the nature of FRF joint Identification Techniques.

Ren Y. and Beards C. F. (1988). *Trans. ASME. Journal of Vibration and Acoustics* Vol. 120, 331-338 Identification of 'Effective' Linear Joints Using Coupling and Joint Identification Techniques.

Ren Y.S. Yang J.M., Zhao Z. L. and Wang Y. H., (1994), Nonlinear Vibration Analysis of Beams with Dry Friction Joint.

Rice H. J. and Xu K. Q., (1996), *Mechanical Systems and Signal Processing*, **10(1)**, 55-63, Linear Path Identification of General Nonlinear Systems.

Sanliturk K. Y. and Ewins D. J., (1996), *Journal of Sound and Vibration*, **193**, 511-523, Modelling two-dimensional friction contact and its Application Using Harmonic Balance Method.

Sekhar A. S. and Prabu B. S. (1994), *Journal of Sound and Vibration* **169**, 655-667, Vibration and Stress Fluctuation in Cracked Shafts.

Shigley (1990), **Mechanical Engineering Design**, John Wiley and Sons, New York.

Shoukry S. N. (1985), *NUMETA 85 Conference*, A Mathematical Model for the Stiffness of Fixed Joints between Machine Parts.

Simon (1992), *Proc. Instn Mech Engrs* **206**, 29-39, Prediction of Vibration Behaviour of Large Turbo-Machinery of Elastic Foundations sue to Unbalance and Coupling Misalignment

Smith D. M. (1933), *Proceedings of the Royal Society of London* **A142**, 92-118. The motion of a rotor carried by a Flexible shaft in Flexible Bearings.

Smith J. M. (1987), **Mathematical Modeling and Digital Simulation for Engineers and Scientists**, John Wiley & Sons.

Soom A. and Chen J. -W. (1986), *Trans. ASME: Journal of Tribology* 108, 123-127, Simulation of Random Surface Roughness-Induced Contact Vibrations at Hertzian Contacts During Steady Sliding.

Tamura A., Iwata Y. and Sato H., (1988), *ImechE* C322, 647-653, Unstable Vibration of a rotor with Transverse Crack.

The Student Editions of MATLAB: Version 4: User's Guide/The Mathworks Inc.: with tutorial by Duane Hanselman and Bruce Littlefield, (1995) Prentice Hall.

Thompson J. M. T, and Stewart, H. B., (1988), **Nonlinear Dynamics and Chaos**, John Wiley and Sons, Chichester.

Timoshenko S. P. and Goodier J. N., (1970), **Theory of Elasticity**, 3rd Ed., McGraw Hill, New York.

Tondl A., (1965) **Some Problems of Rotor Dynamics**, english Translation, London, Chapman and Hall.

Tsai T. C. and Wong Y. Z. (1996), *Journal of Sound and Vibration*, **192**, 601-620, Vibration Analysis and Crack Diagnosis of a Cracked Shaft.

Vance J. M. (1988) **Rotordynamics of Turbomachinery**, John Wiley & Sons, New York

Wauer (1990), *Appl Mech. Rev* ,**43**, no 1,On Dynamics of Cracked Rotors: A literature Survey.

Wu M. -C and Huang S. -C (1988), *Trans. ASME. Journal of Vibration and Acoustics* Vol. 120, 551-556. In-plane Vibration and Crack Detection of Rotating Shaft_Disk Containing a Transverse Crack

Xu and R.D. Marangoni (1994), *Journal of Sound and Vibration* **176**, 663-679, Vibration of a motor-flexible coupling rotor system subjected to misalignment and unbalance, Part 1: Theoretical model and analysis.

Yamamoto (1954), *Memoirs of the Faculty of Engineering*, Nagoya University, On Critical Speeds of a Shaft.

APPENDICES

The appendices provide information and data supplementary to the main text. The data are not critical to the main work that being done.

Appendix 1: Physical Data of the Rotor System

A.1.1. Material Properties

The values used in all calculations are based on most standard text book values (Shigley, 1990):

$E=210.10^{9}Nm^{-2}$

$\rho=7850kgm^{-3}$

$\nu=0.29$ (A1)

A.1.2 Geometry of the structures

A.1.2.1 Rotor Discs

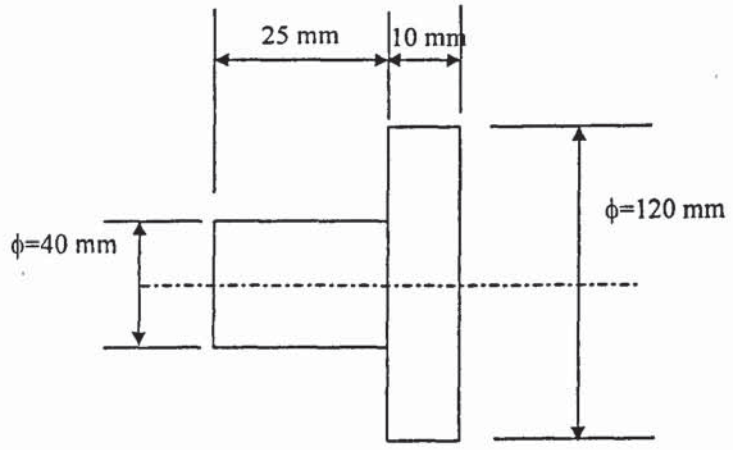

Figure A.1: Half rotor disc.

The rotor disc is made of mild steel with the following dimension

Diameter of disc = 120 mm

Hub diameter =40 mm

Thickness of disc = 10 mm

Thickness of hub=25 mm

Diameter of bolt clamping position = 100 mm

Diameter of bolt = 6 mm

$$\text{Volume of the rotor disc} = \left(\frac{\pi}{4}(0.04)^2 x0.05 + \frac{\pi}{4}(0.12)^2 x0.02\right) = 2.88x10^{-4} m^3 \quad \text{(A2)}$$

$$\text{Mass of rotor disc} = 2.88x10^{-4} x7810 = 2.25kg \quad \text{(A3)}$$

A .1.2.2 Shaft

The shaft was made of silver steel with a diameter of 16 mm.

Length of the shaft = 800 mm

Diameter of shaft for bearing fixing =15 mm

Mass of the shaft (excluding the bearing

$$= \rho\left(\frac{\pi}{4} d^2 l\right) = 7810x\frac{\pi}{4} x(0.016)^2 x0.73 = 1.146kg \quad \text{(A4)}$$

A.1.2.3 Shaft Stiffness

(a) A simply supported beam with a mass at the centre is given by(Shigley, 1990):

$$k = \frac{48EI}{l^3} \tag{A5}$$

(b) A beam with a constraint end and pin beam is given by (Shigley, 1990):

$$k = \frac{768}{7}\frac{EI}{l^3} \tag{A6}$$

Appendix 2: Natural frequency of the a Rotating disc

The estimation of the natural frequency *Jeffcott* rotor is based on the Rayleigh method. By assuming the natural mode of the system known, the corresponding natural frequency can be found by Rayleigh quotient. To obtain the fundamental natural frequency, the method is applicable because most problems a good approximation of the fundamental mode is possible.

$$\omega^2 = \frac{U_i}{T^*} \tag{A7}$$

where

$$T_{\max} = \frac{1}{2}\int_0^l \rho A \dot{y}^2\, dx + \frac{1}{2} M \dot{y}_0^2 \text{ and } U_{max} = \frac{1}{2}\int_0^l EI\, y''^2\, dx \tag{A8}$$

assuming the first fundamental mode shape as:

$$y = \sin\frac{\pi x}{l}\cos\omega t \tag{A9}$$

$$\dot{y} = \omega \sin\frac{\pi x}{l}\cos\omega t \tag{A10}$$

$$\ddot{y} = -\left(\frac{\pi}{l}\right)^2 \sin\frac{\pi x}{l}\sin\omega t \tag{A11}$$

For the maximum value of $\dot{y}$;

$$\dot{y} = \omega \sin\left(\frac{\pi x}{l}\right), \dot{y}_{x=1/2} = \omega$$

$$\ddot{y} = -\left(\frac{\pi}{l}\right)^2 \sin\frac{\pi x}{l}$$

Kinetic energy of the system

$$T = \frac{1}{2}\int_0^l \rho A\left(\omega \sin\frac{\pi x}{l}\right)dx + \frac{1}{2}M\omega^2$$

$$= \frac{1}{2}\rho A\omega^2 \int_0^l \left[\frac{1-\cos(2\pi x/l)}{2}\right]dx + \frac{1}{2}M\omega^2$$

$$= \frac{1}{2}\rho A\omega^2 \left[\frac{l}{2} - \frac{\sin(2\pi x/l)}{2\pi/l}\right]_0^l + \frac{1}{2}M\omega^2$$

$$= \frac{1}{2}\rho A\omega^2 \left[\frac{l}{2}\right] + \frac{1}{2}M\omega^2 \tag{A12}$$

The strain energy (potential) of the system:

$$U_{max} = \frac{1}{2}\int_0^l EI\left(-\left(\frac{\pi}{l}\right)^2\right)^2 \sin^2\left(\frac{\pi x}{l}\right)dx$$

$$= \frac{1}{2} EI\left(\frac{\pi}{l}\right)^4 \left[\frac{l}{2}\right]$$

$$= \frac{1}{4} \frac{EI\pi^4}{l^3} \qquad \text{(A13)}$$

Equating the maximum kinetic energy to the strain energy of the system.

$$T_{max} = U_{max}$$

$$\omega^2 = \frac{\frac{1}{4}\frac{EI\pi^4}{l^3}}{\frac{1}{2}\rho A\left(\frac{l}{2}\right) + \frac{1}{2}M} \quad \text{or}$$

$$\omega^2 = \frac{EI\pi^4}{(\rho Al + 2M)l^2} \qquad \text{(A14)}$$

Calculation of the natural frequency of the system base on the equation A14 above and the value for the rig dimension.

$$\omega^2 = \frac{207x10^9 x3.216x10^{-9} x\pi^4}{(7810x2.01x10^{-4} x0.73 + 2x2.25)x0.73^3}$$

$$= \frac{126653.1}{(1.1463 + 4.5)x0.73^3} = 171.8$$

$$\omega = 27.3Hz \qquad \text{(A15)}$$

Appendix 3: Data of Test Rig

A.3.1 Motor and Controller

The motor used in the experiment is selected based on the necessary torque required to produce an angular acceleration sufficient enough to accelerate the system to enable data to be collected sufficiently. Brushless DC 250W model 136209 Maxon motor was selected with the permissible speed of 10000 rpm and stall torque of 3.017 Nm.

A.3.2 Controller

The motor controller is an open loop controller, therefore the motor speed is directly proportional to the input voltage. The input direction selects the sense of rotation. The control-input disable turns the power stage off. The controller is protected internally against thermal overload.

A.3.3. Data acquisition System

The data acquisition of used to capture data during runup and rundown of the rotor is WINDAQ 200. It consists of a A-D box which with can be directly connected to the parallel port of the computer. It run on the software which will directly capture the waveform of the signal produced by the vibrating component.

A.3.4. Displacement Sensors

The displacement sensors used is the type RS M18 analogue d.c. (13.5-30V) proximity sensors which produce a linear output voltage

directly proportional to the distance between the target and the sensing face. It has a linear range of between 2-5 mm (or 1-9Volt sensing range) with good linearity and repeatability. The sensing surface is made of ceramic to guarantee high accuracy detection and is sensitive to type of metals.

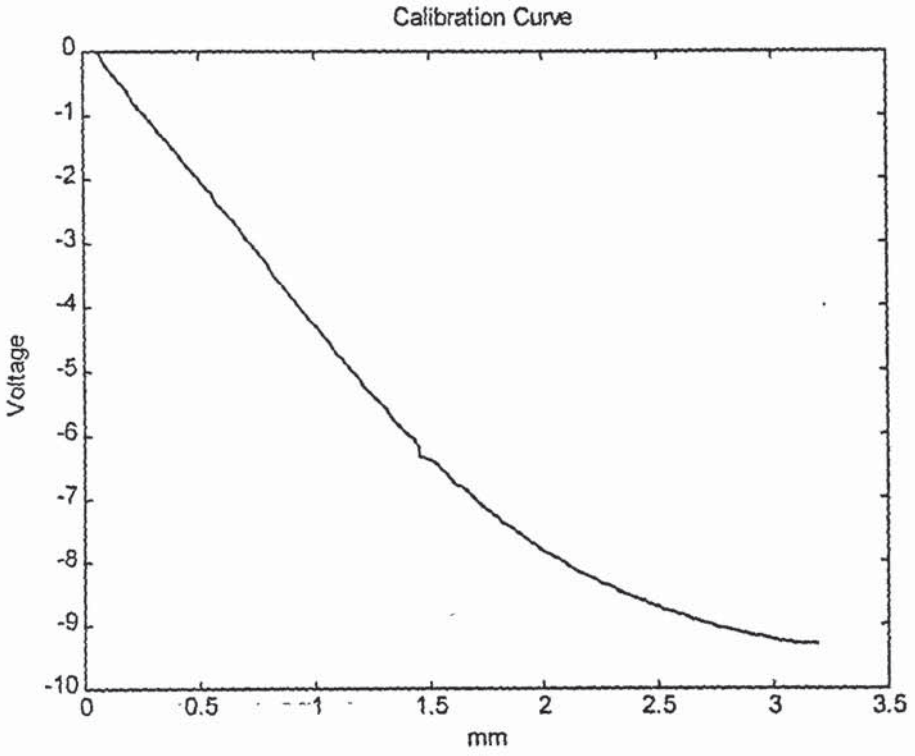

Figure A2 Calibration of small transducer (Bently Nevada).

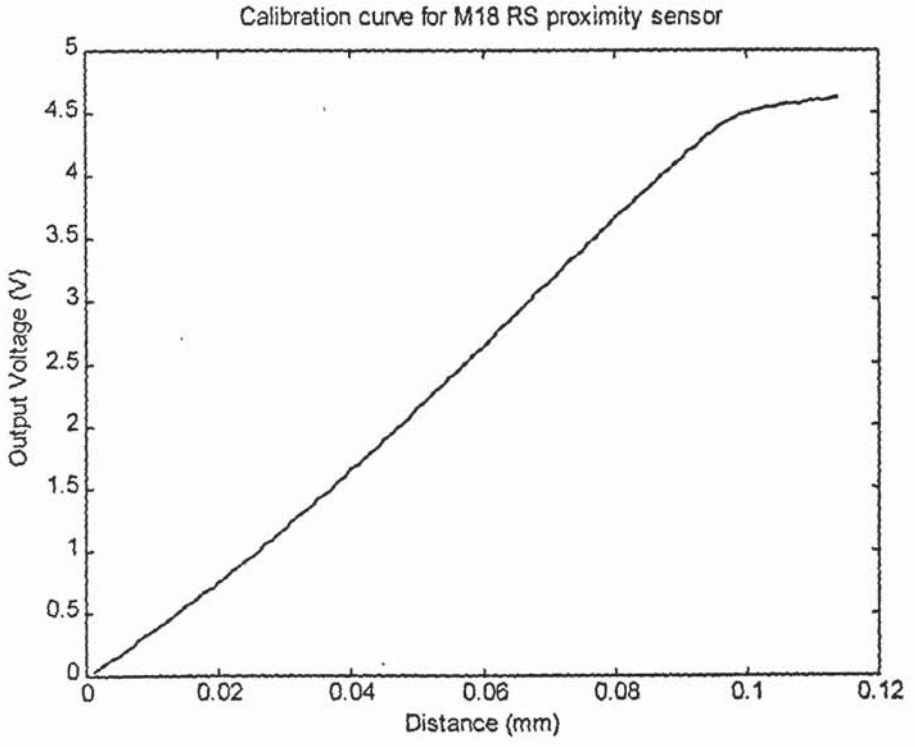

Figure A3: RS M18 proximity sensor calibration curve.

A.3.5 Damping

The damping of the system can be determined by logarithmic decrement method (Dimrogonas, 1996). The vibration signal can be obtained by during an impact test and measuring the amplitude of the vibration. By considering the logarithm of the ratio of the amplitudes of two successive oscillations differing in time by one period $T = 2\pi/\omega_d$, is

$$\delta = \log(x_0 e^{-\zeta\omega_n t} / x_0 e^{-\zeta\omega_n (t+T)}) = \log(e^{\zeta\omega_n t}) = \zeta\omega_n T = \frac{2\pi\zeta}{(1-\zeta^2)^{1/2}} \qquad \text{(A16)}$$

where δ is constant and related to the damping ratio and can be easily determined. For practical application is more convenient to measure the amplitude over a number of cycles. Therefore the above equation become,

$$\delta = \frac{1}{n}\log\frac{X_i}{X_{i+n}} = \frac{2\pi\zeta}{(1-\zeta^2)^{1/2}} \approx 2\pi\zeta \qquad \text{(A18)}$$

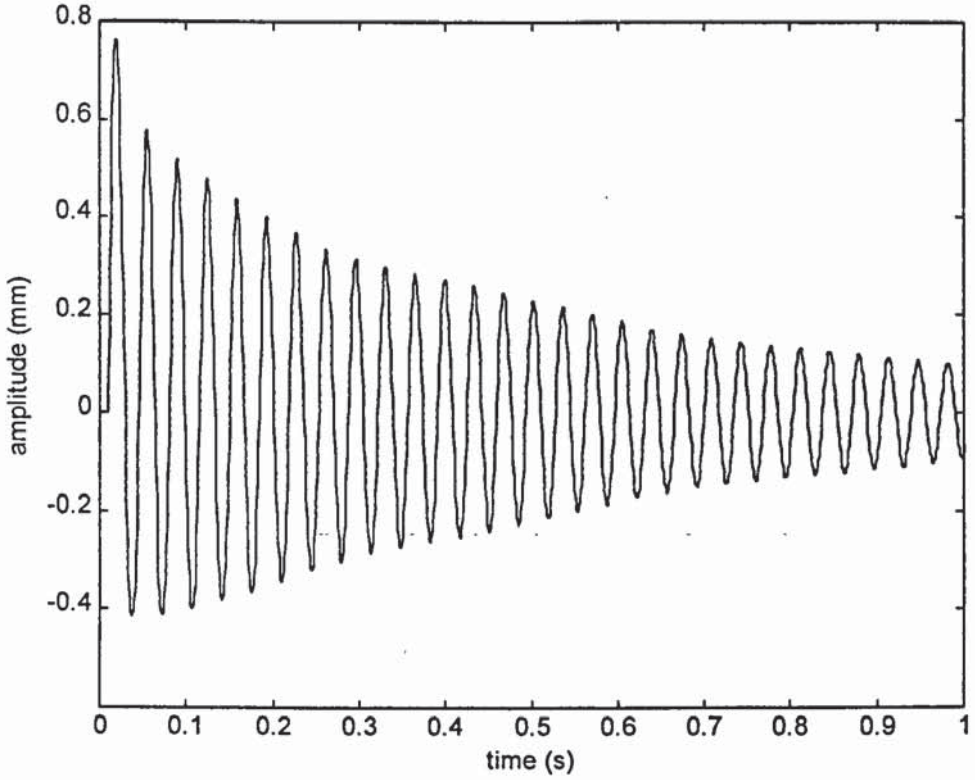

Figure A4: The response due to impact load

Using the vibration signal above the damping ratio is:

$x_i = 0.7629mm$, $x_{i+10} = 0.2875mm$

$$\delta = \frac{1}{10}\log\frac{0.7629}{0.2875} = 0.0423$$

$$\zeta = \frac{\delta}{2\pi} = 0.00675$$

Appendix 4: Simulink Model

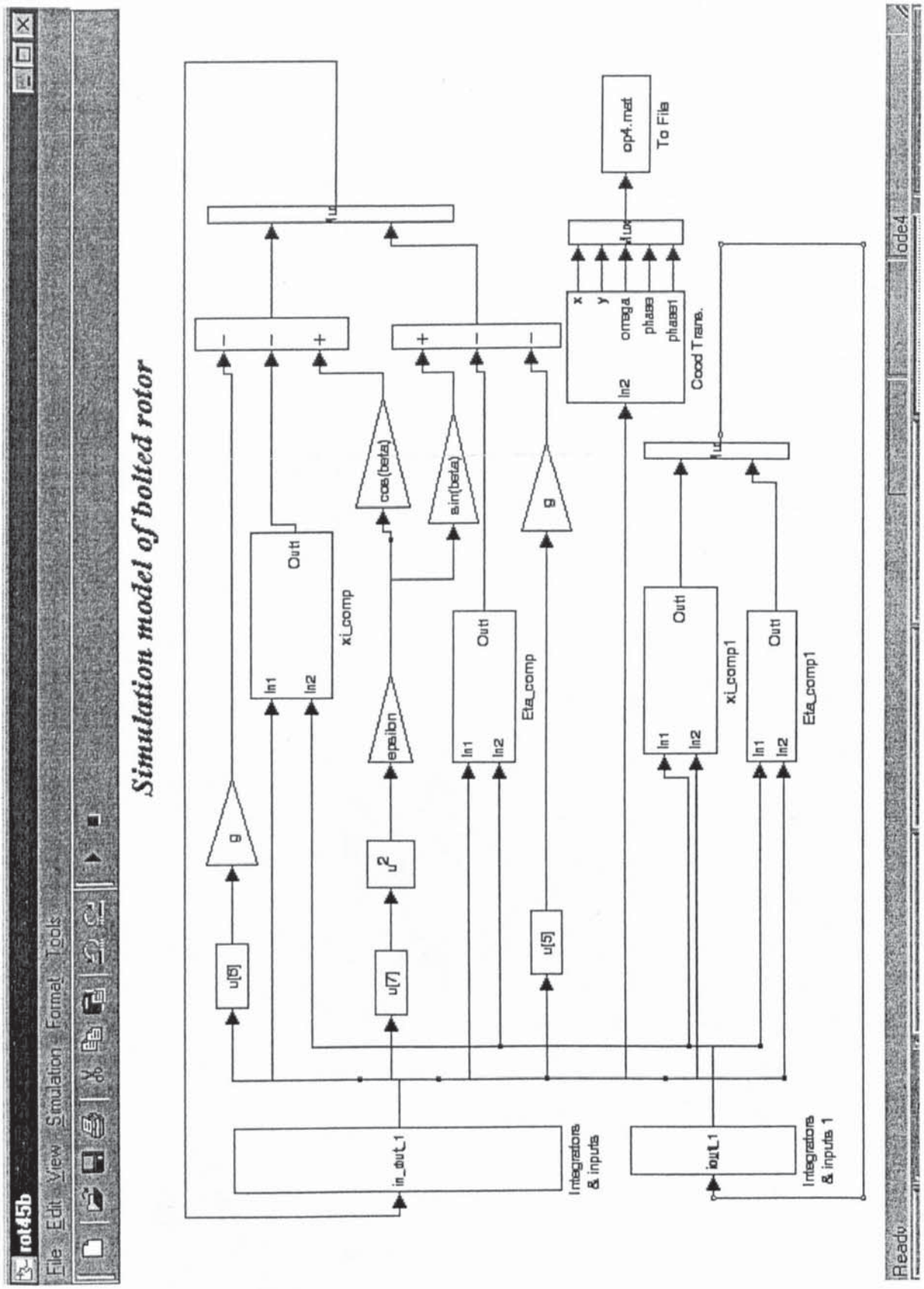

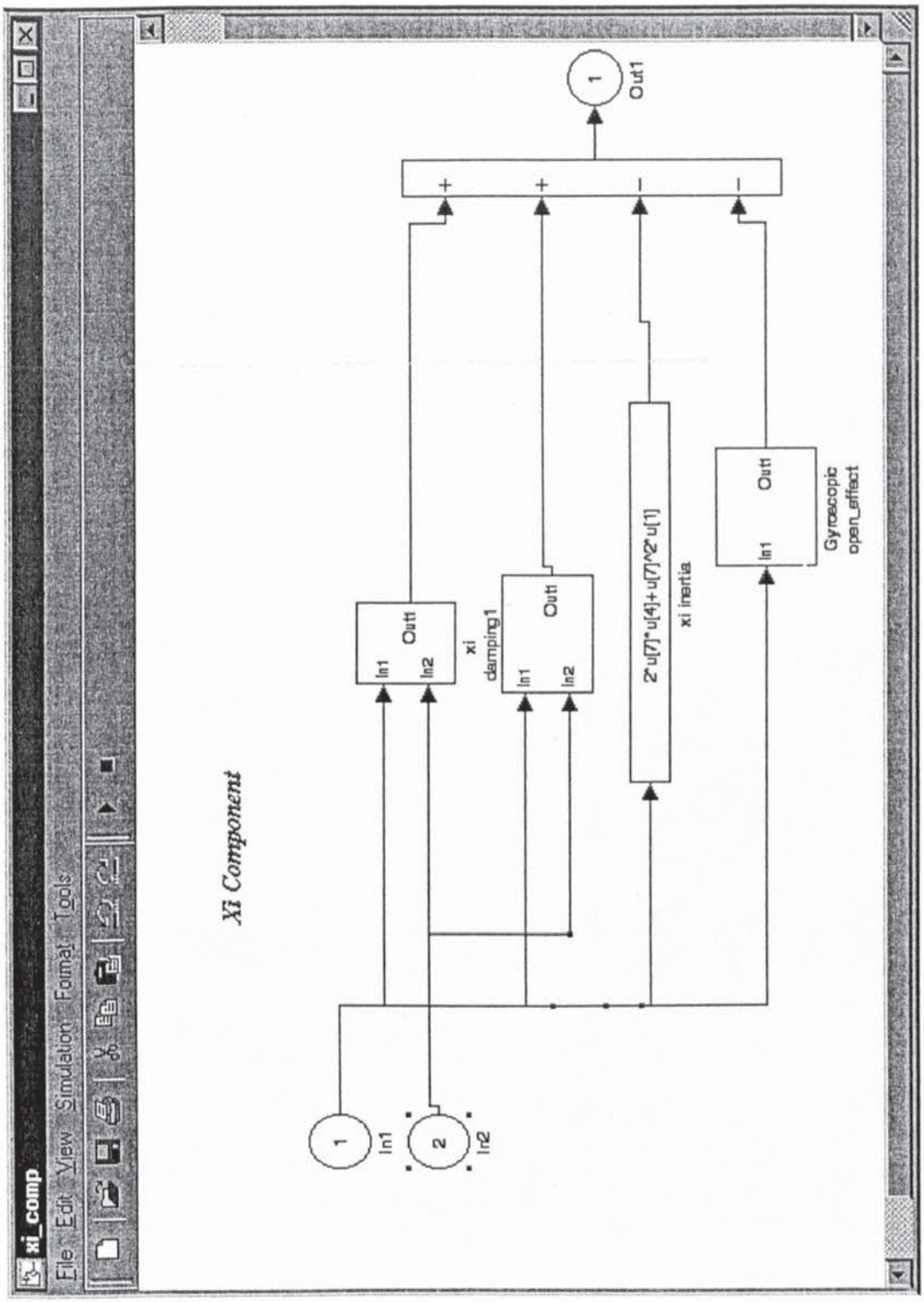
xi_comp
File Edit View Simulation Format Tools
Xi Component
In1
In2
Out1
xi damping1
2*u[7]*u[4]+u[7]^2*u[1]
xi inertia
Gyroscopic open_effect

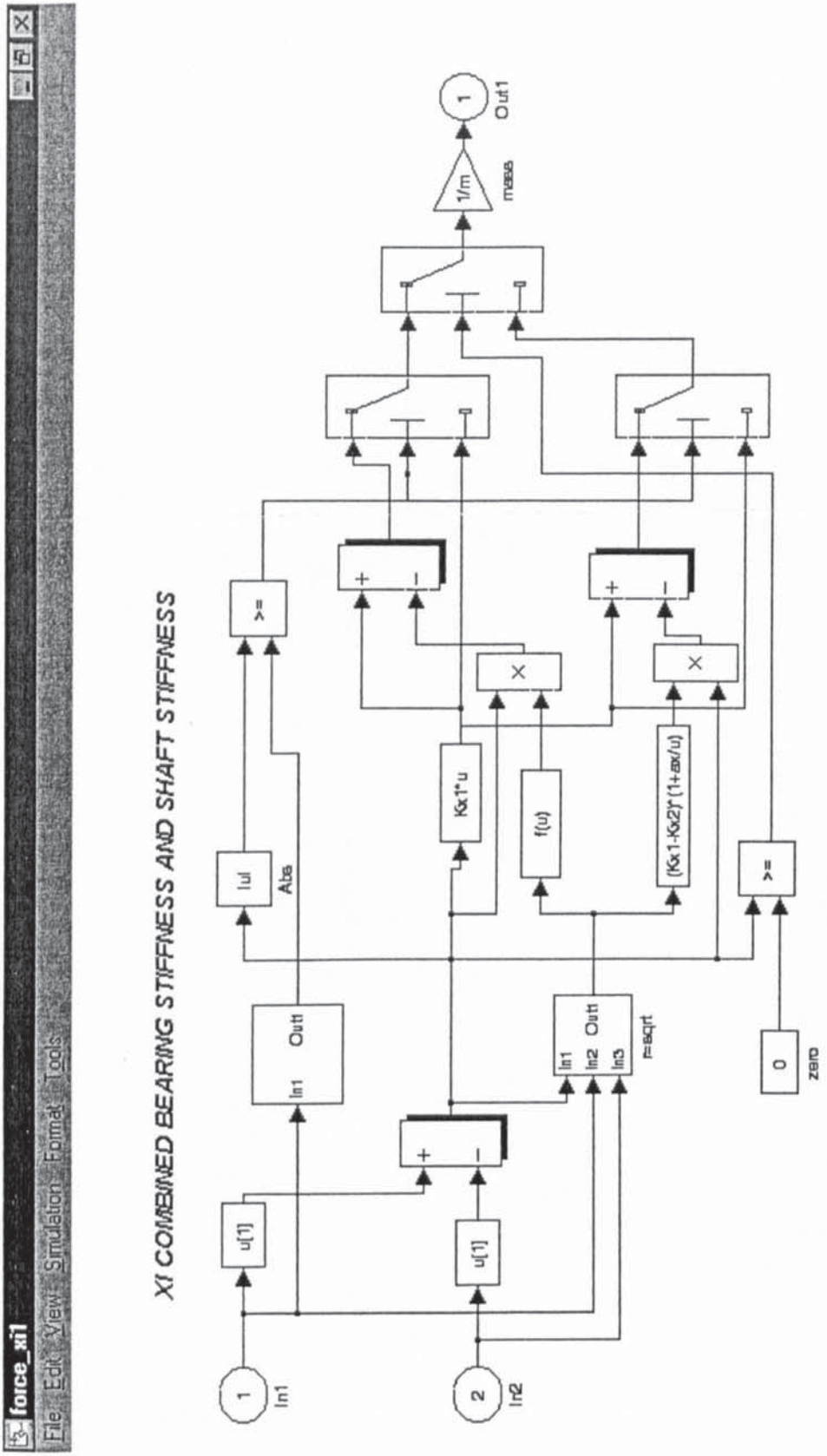
force_xi1
File Edit View Simulation Format Tools
XI COMBINED BEARING STIFFNESS AND SHAFT STIFFNESS
In1
In2
u[1]
u[1]
Out1
In1
|u|
Abs
>=
Kx1*u
f(u)
(Kx1-Kx2)*(1+ax/u)
In1
In2
In3
Out1
=sqrt
>=
0
zero
1/m
mass
Out1

Appendix 5: Test Rig Detail Drawing

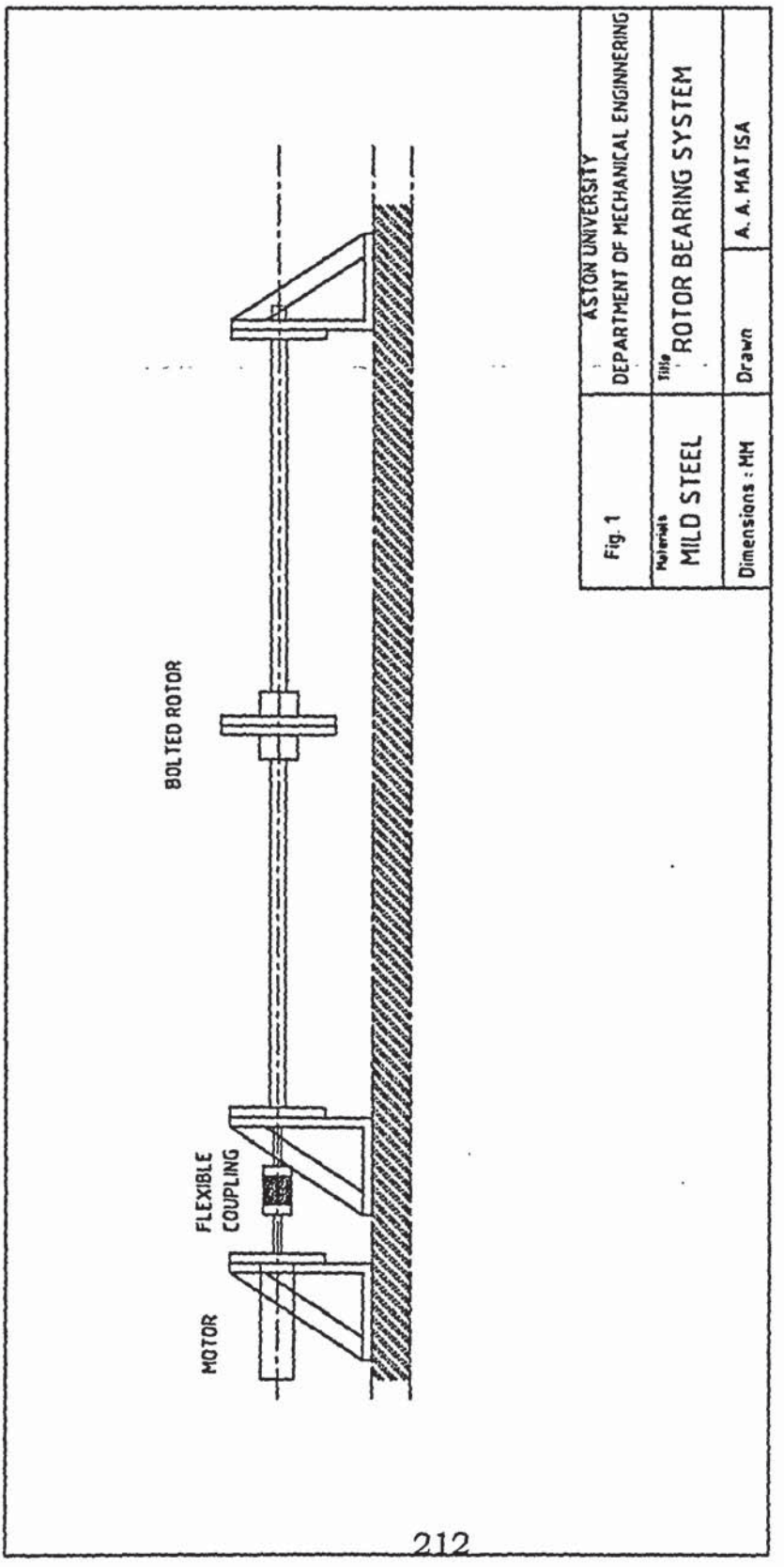

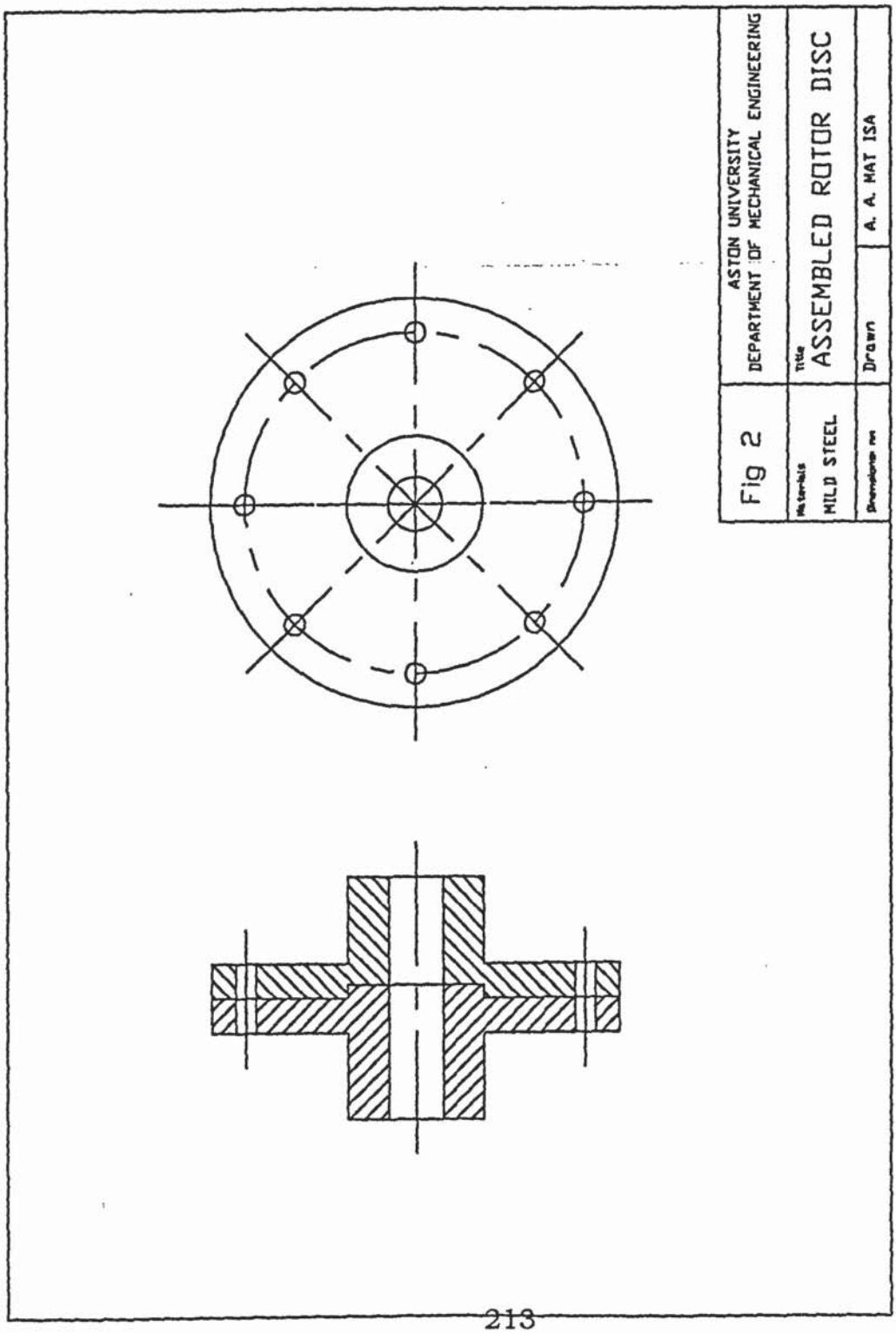
ASTON UNIVERSITY
DEPARTMENT OF MECHANICAL ENGINEERING
Fig 2
Materials
MILD STEEL
Title
ASSEMBLED ROTOR DISC
Drawn
A. A. MAT ISA

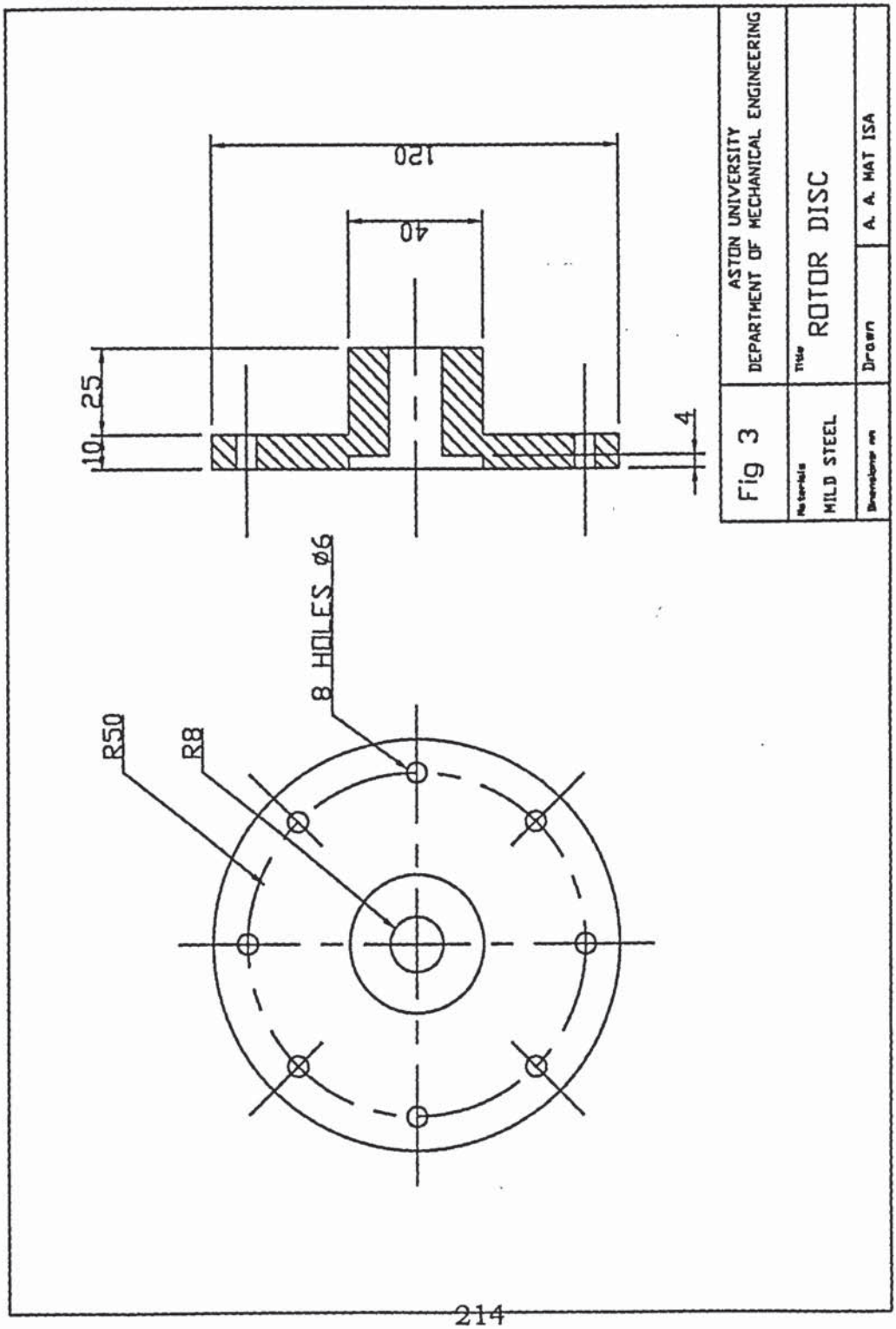
120
40
25
10
4
8 HOLES ø6
R50
R8
Fig 3
ASTON UNIVERSITY
DEPARTMENT OF MECHANICAL ENGINEERING
Title
ROTOR DISC
Materials
MILD STEEL
Drawn
A. A. MAT ISA

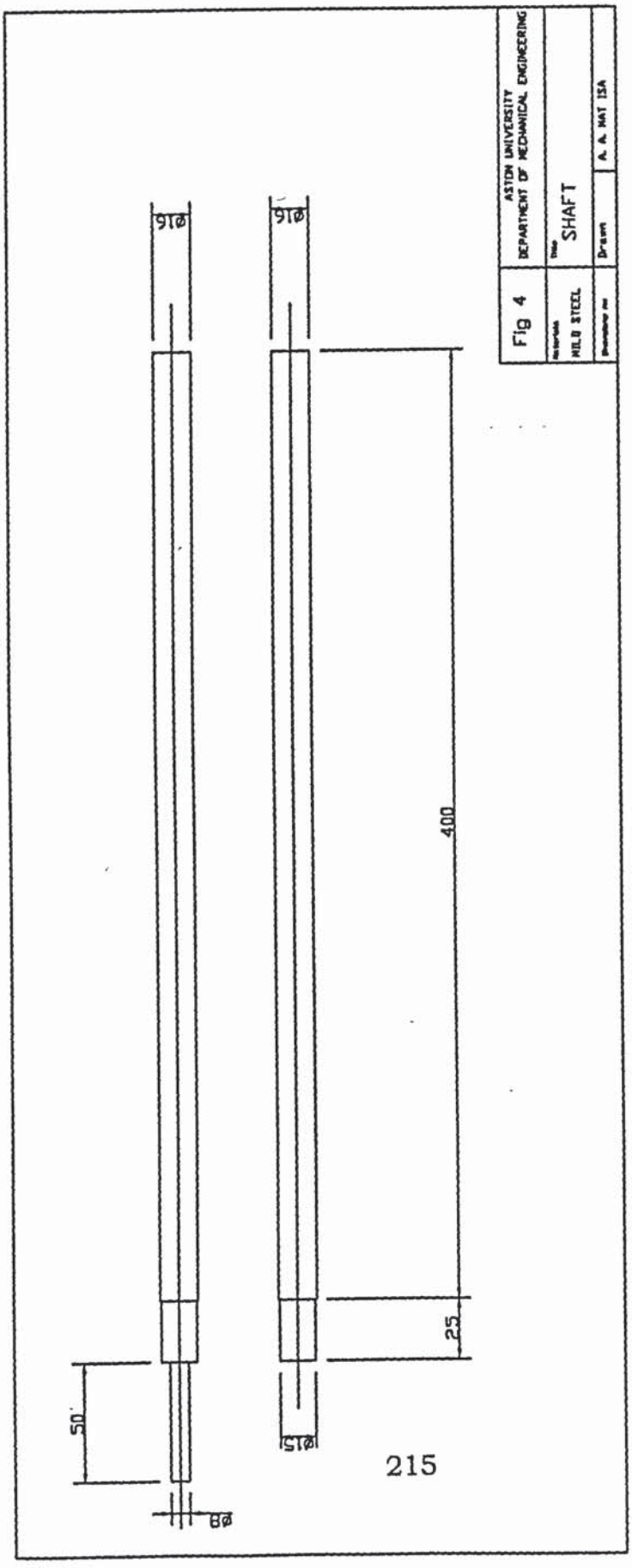
ASTON UNIVERSITY
DEPARTMENT OF MECHANICAL ENGINEERING
Fig 4
Title
SHAFT
MILD STEEL
A. A. MAT ISA
Drawn
ø16
ø16
400
25
50
ø15
ø8
215

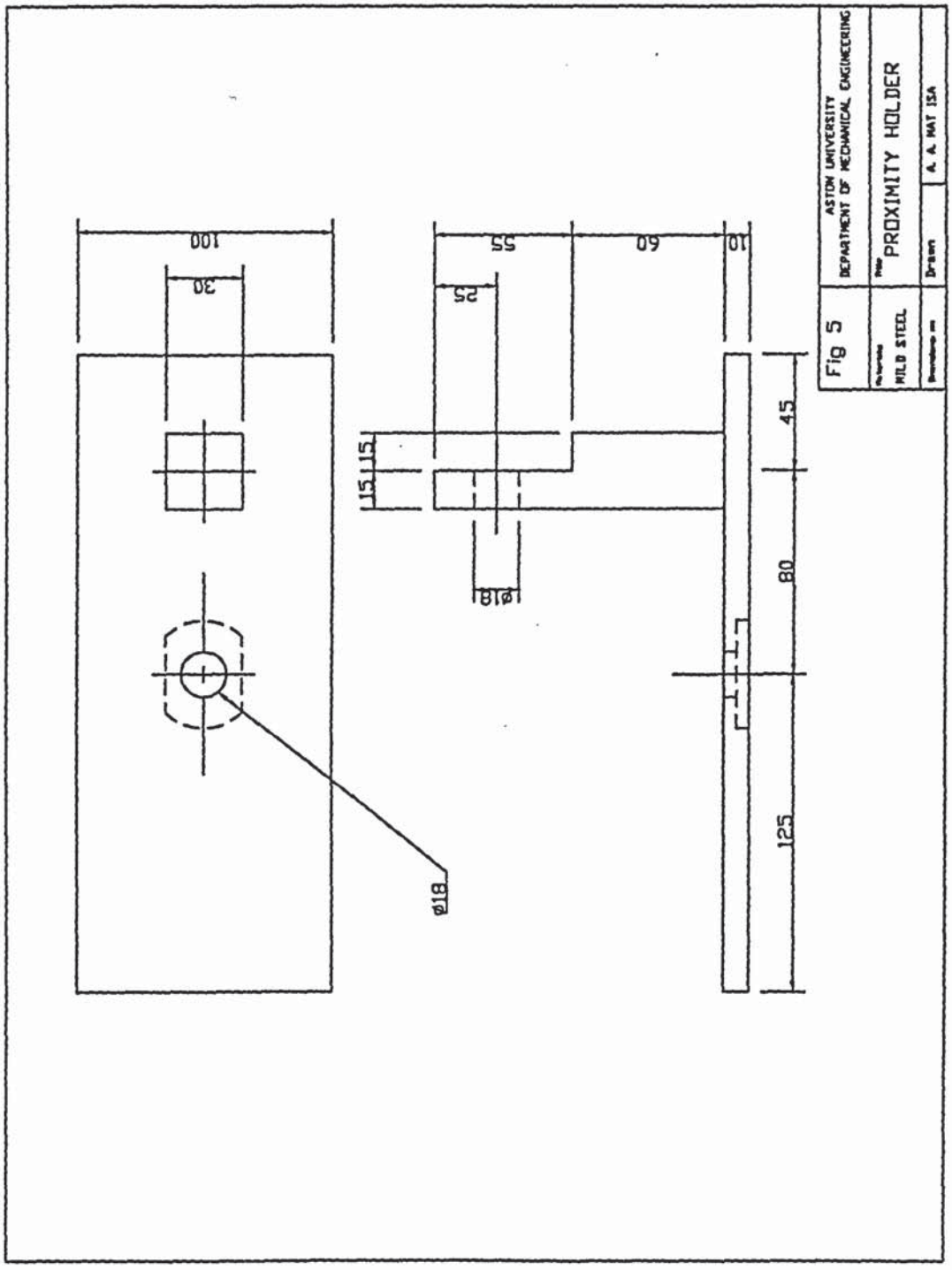
ASTON UNIVERSITY
DEPARTMENT OF MECHANICAL ENGINEERING
PROXIMITY HOLDER
Fig 5
MILD STEEL
A. A. MAT 15A
100
30
55
60
10
25
15
15
45
80
125
ø18
ø18

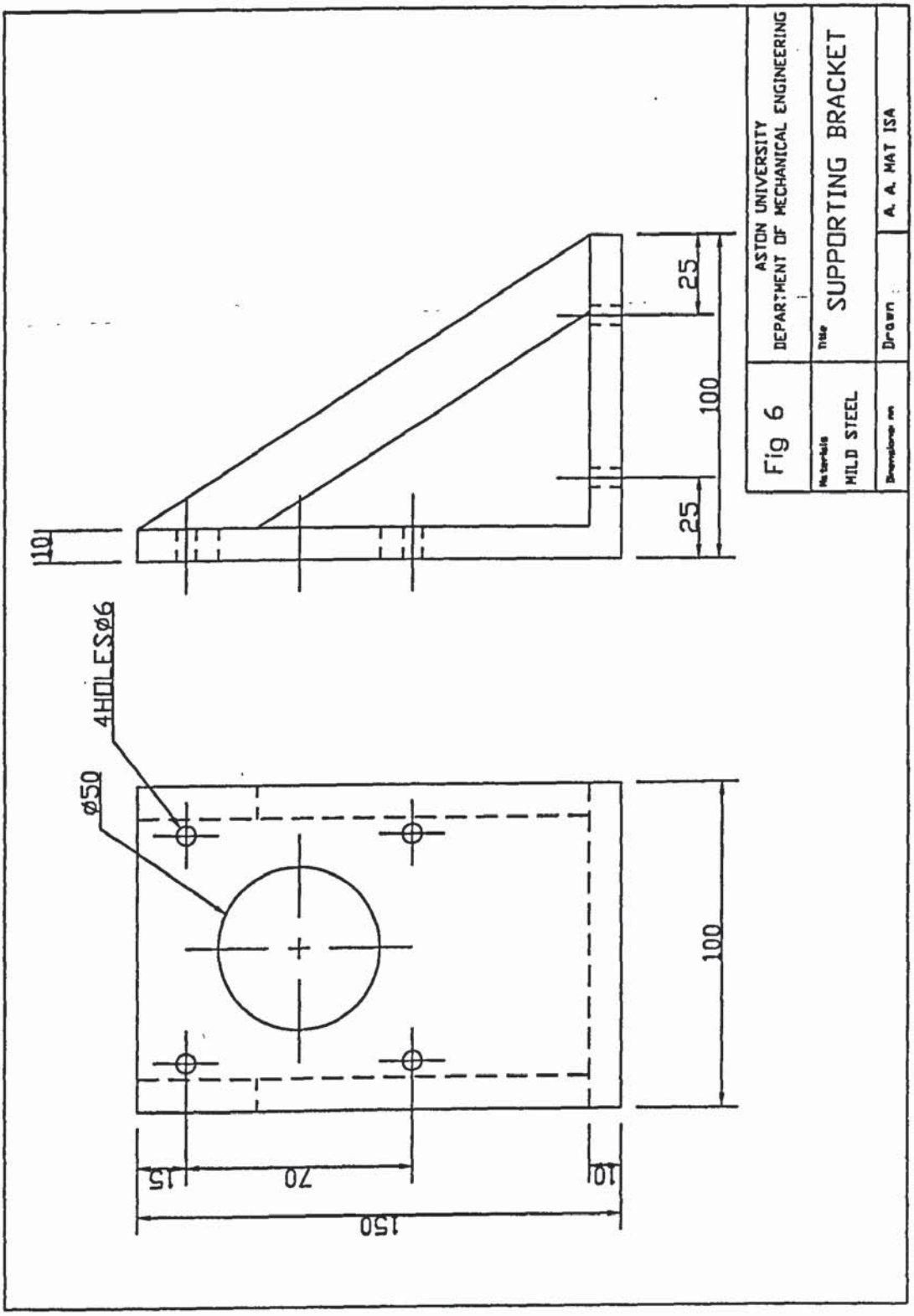
ASTON UNIVERSITY
DEPARTMENT OF MECHANICAL ENGINEERING
SUPPORTING BRACKET
Fig 6
MILD STEEL
A. A. MAT ISA
25
100
25
10
4HOLES ø6
ø50
100
15
70
10
150

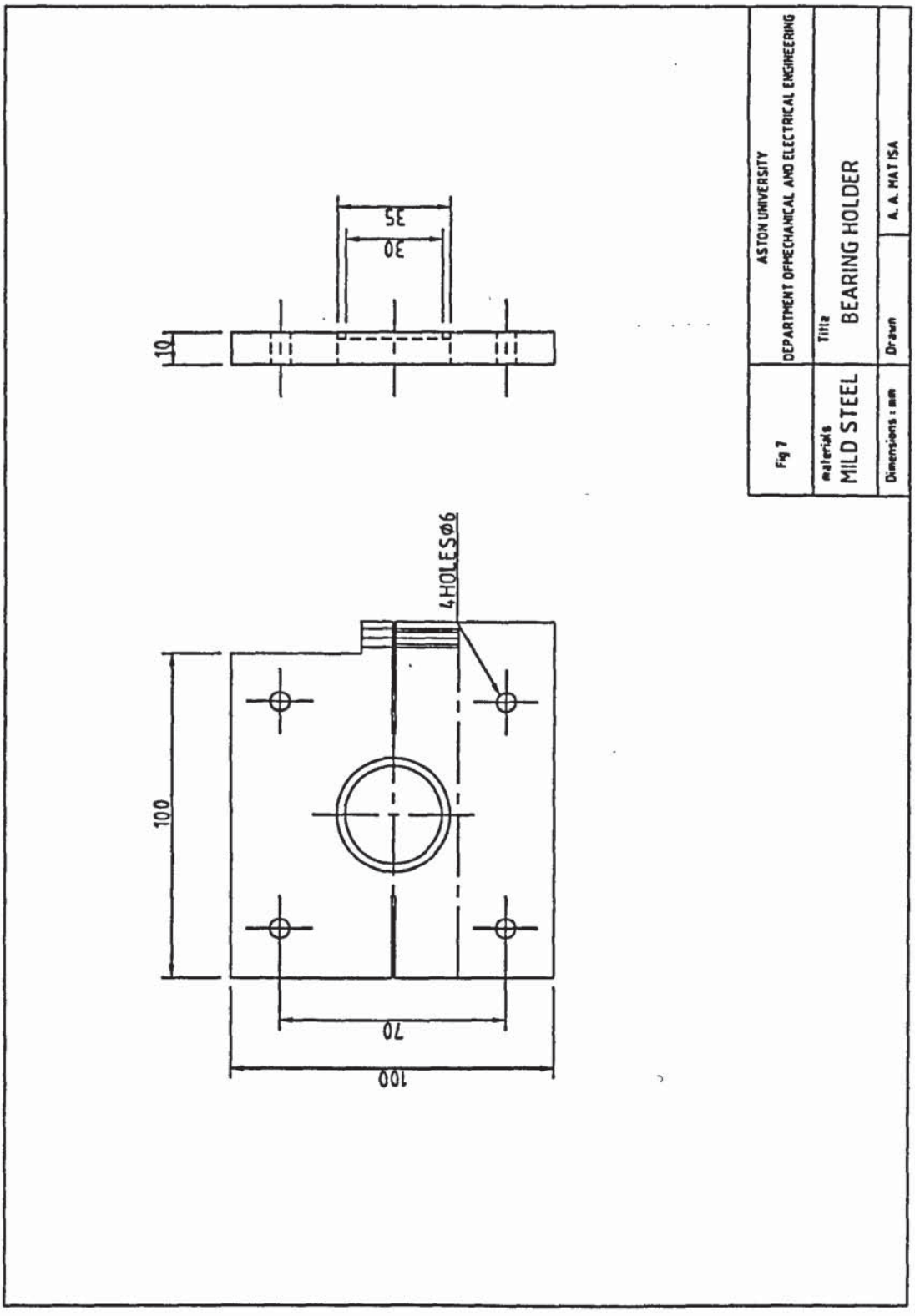
ASTON UNIVERSITY
DEPARTMENT OFMECHANICAL AND ELECTRICAL ENGINEERING
Fig 7
Title
BEARING HOLDER
materials
MILD STEEL
Drawn
A. A. MATISA
Dimensions : mm
35
30
10
4HOLESØ6
100
70
100